Universitat Autònoma de Barcelona

# Molecular genetics of autosomal dominant ataxias: identification and characterisation of two novel spinocerebellar ataxia subtypes

**Marc Corral Juan**

# Molecular genetics of autosomal dominant ataxias: identification and characterisation of two novel spinocerebellar ataxia subtypes

**Marc Corral Juan**

PhD Thesis

2020

Programa de doctorat de Neurociències

Institut de Neurociències

Universitat Autònoma de Barcelona

Universitat Autònoma de Barcelona

# Molecular genetics of autosomal dominant ataxias: identification and characterisation of two novel spinocerebellar ataxia subtypes

PhD Thesis

2020

Programa de doctorat de Neurociències

Institut de Neurociències

Universitat Autònoma de Barcelona

2020


**PhD Candidate**

Marc Corral Juan

**Director**

Dr. Antoni Matilla Dueñas

**Tutor**

Dr. Roser Nadal Alemany

# ACKNOWLEDGMENTS

Sempre parlava en futur de la defensa de la tesi……i ara per fi ja és el present. Han estat anys de feina, molt esforç, d'alts i baixos, de molt aprenentatge i també d'alegries. Per això m'agradaria mencionar a totes aquelles persones, que d'una manera o altra s'han vist involucrades en aquesta etapa de la meva vida.

Primer de tot voldria agrair al Dr. Antoni Matilla per donar-me l'oportunitat de començar, allà cap al 2009, el meu primer contacte professional en el camp de la ciència fins al dia d'avui. Vull agrair-te el teu temps, la teva dedicació, la paciència, els coneixements compartits, i l'exemple que sempre m'has donat de treball, esforç, exigència i tenacitat que evidentment han influït i seran presents en la meva futura carrera científica. Gràcies Toni.

En segon lloc vull agrair a la Dra. Ivelisse Sánchez tots aquests anys compartits. Gracias por compartir tus conocimientos, tus reflexiones, tu visión de la ciencia, tus consejos que me han enriquecido todos estos años y me han hecho mejor científico. Gracias Ivelisse.

M'agradaria agrair també a tots els companys del laboratori, començant per l'Eudald, company de doctorat, amb qui he compartit els bons i mals moments d'aquesta etapa. Ara ens comença una de nova amb tot el que hem après a les espatlles. A per la següent i amb més força. També vull agrair a tots els companys del laboratori actuals, Xavi, Dani, Kerrie, Rafa, i tots aquells estudiants que hi han passat i han posat el seu gra de sorra per fer possible tota aquesta feina realitzada.

Moltes gràcies als pacients i familiars per la seva col·laboració, predisposició i també paciència per a que a poc a poc puguem anar avançant en el coneixement de les atàxies i altres malalties neurodegeneratives amb el clar objectiu de poder oferir-los una millora del seu dia a dia. Vosaltres sou els més forts i els que més exemple doneu.

Agrair a tota la gent que m'ha aportat coneixement científic tots aquests anys començant pel Dr. Víctor Volpini, qui entre congrés i congrés i entre projecte i projecte, compartia amb mi la seva particular visió de la ciència i la genètica. Gràcies Víctor. Agradecer también a todos los colaboradores involucrados de distinta manera en los proyectos realizados todos estos años, al Dr. Dávalos, la Dra. Serrano, el Dr. Álvarez, la Dra. Martínez-Piñeiro, la Dra. Casquero, la Dra. Ispierto, la Dra. Vilas, el Dr. Tolosa, el Dr. Mir, el Dr. Infante y el Dr. Rábano por su colaboración y compartir sus conocimientos clínicos para entender un poco mejor las enfermedades desde el punto de vista clínico.

I would also like to thank you Dr. Laurie and CNAG staff for WES and WGS studies and Dr. Stevanin and all international collaborators for they contribution in these studies. También agradecer al personal del Centro Nacional de Genotipado (CEGEN) por su colaboración en los estudios de ligamiento y al personal de Sistemas Genómicos en los estudios de NGS.

Vull mencionar també als membres del tribunal de seguiment de la tesi, el Dr. Claro, el Dr. Volpini i el Dr. Kulisevsky per tots aquests anys que ens anàvem reunint i compartíeu amb mi el vostre criteri, consell i ànims durant el progrés d'aquest treball. També vull agrair a la Dra. Nadal com a tutora de la tesi pel seu suport durant aquests anys i a la Dra. Guillazo per la seva ajuda en els darrers passos de la tesi.

No em vull oblidar de totes les persones del IGTP amb les que he anat compartint el dia a dia, i han fet els moments difícils més fàcils. Pedro, Pepe, Lucia, Alba, Arce, Eugeni, Gerard, gràcies per els vostres moments d' amistat compartits més enllà de la ciència.

I ja fora de l'àmbit de la ciència a totes aquelles persones que formen part de la meva vida i de les quals sempre he tingut el suport incondicional i per les quals sempre m'he sentit molt estimat. Gracias golondrinos, sabemos que la distancia no es un obstáculo para nosotros y cuando os he necesitado siempre habéis estado allí. Gracias Manolo, Néstor, Tato y Pedro. Gràcies a tots els amics de la universitat, en el seu dia vam fer una pinya que ara ja és indestructible. Rubén, Albert, David, Arturo, Carlos, Jorge, Esteban i Marc.

I sobretot, a la meva família. A tu tiet, l'exemple més gran de força i superació, encara que tu no t'ho creguis. Pel teu amor incondicional, sempre has sigut una persona molt especial per a mi. Has estat el meu àngel de la guarda. Ara em toca a mi ser-ho, i amb molt d'honor. Gran part d'aquesta tesi és per "culpa" teva.

A tota la família Corral i a tota la família Juan, per mostrar-me sempre el vostre suport i ànims i mostrar-me sempre el vostre orgull vers a mi. Y también a toda mi familia turiasonense y amigos, que siempre me habéis hecho sentir como uno más en mi segunda casa. Tampoc em vull oblidar de tots aquells que ja no hi són entre nosaltres.

I evidentment a la meva família. Al meu pare i a la meva mare, gràcies per tot, gràcies per donar-me sempre el suport en tot allò que volgués fer i d'ajudar-me sempre que ho he necessitat. Gràcies per ser com sou, perquè per això jo sóc així i tot el que he aconseguit és en gran part per vosaltres. I gràcies a tu Anna, que encara que siguis discreta, tots sabem que sempre hi ets, amb un cor molt gran. Serà cosa dels gens.....

Y a ti Ángela, gracias por estar a mi lado todos estos años…… y los que nos quedan. Gracias por aguantar mis humores, por tu paciencia, gracias por animarme, por mostrarme tu orgullo hacia mí, como el orgullo que tú me haces sentir y ser para mí un ejemplo de bondad y de persona cada día.

# TABLE OF CONTENTS

# ABBREVIATIONS

ACMG: American College of Medical Genetics and Genomics

AD: Alzheimer's disease

ADCA: Autosomal dominant cerebellar ataxia

ALS: Amyotrophic lateral sclerosis

ATP: Adenosine triphosphate

ATP5H: ATP synthase peripheral stalk subunit D

B2M: β2 microglobulin

BAEP: Brainstem auditory evoked potential

BSA: Bovine serum albumin

CALB1: Calbindin 1

CERAD: Consortium to Establish a Registry for Alzheimer's Disease

CMAP: Compound muscle action potentials

CMCT: Central motor conduction time

CMT: Charcot–Marie–Tooth

CNV: Copy number variation

CRK: CRK Proto-Oncogene

CRKL: Crk-like protein

CT: Computed tomography

DAB: 3,3-diaminobenzidine

DAB1: DAB Adaptor Protein 1

DNA: Deoxyribonucleic acid

Dpf: days post fertilization

DRP1: Dynamin-related protein 1

DRPLA: Dentatorubral-pallidoluysian atrophy

EA: Episodic ataxia

EAAT4: Excitatory amino-acid transporter 4

EEG: Electroencephalography

EKV: Erythrokeratodermia variabilis

EMG: Electromyography

EMQN: European Molecular Quality Genetics Network

ENCODE: Encyclopedia of DNA elements

EP: Evoked potential

ER: Endoplasmic reticulum

ERK: Extracellular-signal-regulated kinase

FYN: Proto-oncogene tyrosine-protein kinase

GAPDH: Glyceraldehyde-3-phosphate dehydrogenase

GEN: Gaze evoked nystagmus

GFAP: Glial fibrillary acidic protein

GSK3β: Glycogen synthase kinase 3 beta

HATs: Histone acetyltransferases

hnRNP K: Heterogeneous nuclear ribonucleoprotein K

Hpf: Hours post fertilization

IDR: Intrinsically disordered region

INAS: Inventory of Non-Ataxia Symptoms

INIs: Intranuclear inclusions

IP3: Inositol trisphosphate

LAMP1: Lysosomal Associated Membrane Protein 1

LANP: Leucine-rich acidic nuclear protein

LC3: Microtubule-associated protein 1A/1B light chain 3

LOD: Logarithm of the odds

MAF: Minor allele frequency

MAP: Microtubule-associated protein

MCP: Middle cerebellar peduncle

MDS: Myelodysplastic syndrome

MEP: Motor evoked potential

MFN1: Mitofusin 1

MJD: Machado-Joseph disease

MNC: Motor nerve conduction

MNCV: Motor nerve conduction velocities

MRI: Magnetic resonance imaging

mtDNA: Mitochondrial DNA

mTOR: Mammalian target of rapamycin

MSA: Multiple system atrophy

MUAP: Motor unit action potential

NCV: Nerve conduction velocity

NGS: Next generation sequencing

NOVA2: NOVA Alternative Splicing Regulator 2

O/N: Overnight

OKN: Optokinetic nystagmus

OMIM: Online Mendelian Inheritance in Man

OMIM #: Descriptive phenotype

OMIM %: Phenotype with unknown underlying molecular basis

OMIM *: Indicates a gene

OPCA: Olivopontocerebellar atrophy

PAN: Periodic alternating nystagmus

PBS: Phosphate-buffered saline

PC: Purkinje cell

PCP2: Purkinje Cell Protein 2

PCR: Polymerase chain reaction

PI3K: Phosphoinositide 3-kinase

PKC: Protein kinase C

PMCT: Peripheral motor conduction times

PP2A: Protein phosphatase 2 A

UPR: Unfolded protein response

Rab5: Ras-related protein Rab-5

Rab7: Ras-related protein Rab-7

RAN: Repeat associated non- ATG

RBP7: Retinol Binding Protein 7

RNA: Ribonucleic acid

RT: Room temperature

SARA: Scale for the assessment and rating of ataxia

SAMD9L: Sterile alpha motif domain-containing protein 9-like

SCA: Spinocerebellar ataxia

SNAP: Sensory nerve action potential

SNC: Sensory nerve conduction

SNCV: Sensory nerve conduction velocity

SNP: Single nucleotide polymorphism

SNpc: Substantia nigra pars compacta

SSEP: Somatosensory evoked potential

SSR: Sympathetic skin response

SWJs: Square wave jerk intrusions

TEM: Transmission electron microscopy

UPS: Ubiquitin-dependent proteasome system

UPR: Unfolded protein response

UTR: Untranslated region

VBM: Voxel-Based Morphometry

VDAC: Voltage-dependent anion channel

VEP: Visual evoked potential

VOR: Vestibulo-ocular reflex

VPS4B: Vacuolar Protein Sorting 4 Homolog B

WES: Whole-exome sequencing

WGS: Whole-genome sequencing

WM: White matter

XBP1: X-box binding protein 1

# ABSTRACT

Spinocerebellar ataxias (SCAs) consist of a heterogeneous group of inherited movement disorders clinically characterised by progressive ataxia variably associated with additional neurological signs such as pyramidal or extrapyramidal signs, ophthalmoplegia, pigmentary retinopathy, dementia or seizures. This clinical heterogeneity is explained by the genetic heterogeneity, with more than 53 loci and 40 genes identified and associated to date.

A cohort of 308 ataxia index cases were included in the present study, finding causative genetic variants in 82 index cases (26.6%), 45 of them previously not described.

During the course of this thesis our group identified a novel SCA37 ataxia subtype and localised its genetic defect to chromosome 1p32. The present study identifies the unstable intronic ATTTC repeat mutation within the 5′-non-coding regulatory region of the Disabled 1 gene (*DAB1)*, as the causative genetic defect of SCA37. Moreover, it describes the clinical-genetic correlation and the first neuropathological findings in SCA37 which reveal that the disease is caused by dysregulation of cerebellar *DAB1* expression with severe loss of Purkinje cells in the cerebellar cortex, and the presence of ubiquitinated perisomatic granules immunostained for DAB1. Importantly, the ATTTC repeat induced *DAB1* RNA switch resulting in the upregulation of reelin-DAB1 and PI3K/AKT signalling in the SCA37 cerebellum.

Last but not least, whole-genome linkage and exome studies were performed in a family from Menorca with seven affected individuals variably presenting with ataxia, nystagmus, dysarthria, polyneuropathy and pyramidal signs with an autosomal dominant inheritance. Variable age at onset ranged from 15 to 50 years. MRI revealed cerebellar atrophy with cerebral demyelination, and neurophysiological studies showed moderate axonal sensory polyneuropathy with abnormal sympathetic skin response predominantly in the lower limbs. The c.1877C>T (p.Ser626Leu) variant in the *SAMD9L* gene was identified as the disease causative genetic defect. The study also demonstrated the mitochondrial location of human SAMD9L protein, with its levels decreased in patients' fibroblasts and evidenced mitochondrial and lysosomal deficits in this novel ataxia subtype. In addition, overexpression of the human mutated *SAMD9L* mRNA revealed impaired mobility and vestibular/sensory functions in zebrafish embryos.

In conclusion, this study identifies the genetic deficits in 26.6% of our ataxia cases, demonstrates the unstable ATTTC repeat mutation within the *DAB1* gene as the underlying genetic cause providing evidence of reelin-DAB1 signalling dysregulation in the spinocerebellar ataxia type 37, and describes a novel spinocerebellar ataxia subtype caused by *SAMD9L* mutation, which triggers mitochondrial and lysosomal dysregulation, pointing to the role of SAMD9L in neurological motor and sensory functions. As a result of this thesis novel insights into the clinical, genetic and physiopathological mechanisms underlying neurodegeneration in spinocerebellar ataxias are identified providing new candidate targets for treatment.

# INTRODUCTION

## 1. Ataxias and cerebellar disorders

Cerebellar damage has been associated with a wide range of movement disorders including incoordination, reduced manual dexterity, postural instability, and gait disturbances. Ataxia is a neurological disease characterised by loss of control of body movement with patients presenting clumsiness, unsteadily walk, slurred speech, and may lose the ability to swallow and breathe normally (1,2). The ataxic movement pattern comes from the discoordination on time and duration of muscle activation or the magnitude and scale of the force produced during voluntary movements where the cerebellum plays a fundamental role. Nonetheless, parkinsonism, dystonia, spasticity, urinary urgency, sleep disturbance, fatigue, or depression are common symptoms for different ataxia subtypes. Ataxia appears due to a neuronal degeneration in the cerebellar cortex, brain stem, spinocerebellar tracts and their afferent and efferent connections. More than 60 different types of hereditary ataxias have been described debuting in childhood or in adulthood (3).

The differential diagnosis of hereditary ataxias includes those acquired, not owing to genetic causes of ataxia such as alcoholism, vitamin deficiency, multiple sclerosis, vascular diseases, oncological diseases. Hereditary ataxias are normally subdivided by type of inheritance; dominant, recessive, X-linked and mitochondrial. The term spinocerebellar ataxia is used for those types of ataxias that present an autosomal dominant inheritance (4).

## 2. Dominant cerebellar ataxias

Dominant ataxias comprise a clinically, genetically, molecularly and neuropathological heterogeneous group of neurodegenerative disorders predominantly characterised by cerebellar dysfunction (1–3). Spinocerebellar ataxias are inherited in an autosomal dominant pattern and include those progressive, congenital or episodic cases with ataxia as the predominant clinical manifestation with patients frequently presenting additional clinical symptoms (**Table 1**). The age of onset of the clinical symptoms is usually between 30 and 50 years of age, although early onset in childhood and onset in later decades after 60 years have been reported for specific subtypes. Prior to the identification of their molecular genetic basis, spinocerebellar ataxias (SCAs) were termed as Marie's ataxia, inherited olivopontocerebellar atrophy, cerebello-olivary atrophy or autosomal dominant cerebellar ataxias (ADCAs) (5). In 1983, Anita Harding proposed a useful clinical distinctive classification for late onset autosomal dominant cerebellar ataxias in four groups, ADCA types I, II, III and episodic ataxias. ADCA type I denotes cerebellar ataxia associated with additional features related to ophthalmoplegia, optic atrophy, dementia or extrapyramidal features. ADCA type II represents cerebellar ataxia associated with pigmentary with or without ophthalmoplegia or extrapyramidal features, and ADCA type III being a pure late onset cerebellar syndrome. The initial classification by Harding also included ADCA type IV presenting mental retardation, myoclonus and

deafness, but later those diseases were classified as mitochondrial cytopathies, and thus were finally not included in Harding's classification of ADCAs (5). Even though, while the number of patients genetically diagnosed and clinically characterised grows, increasing new clinical signs and symptoms are described and associated to different dominant ataxia subtypes.

Some clinical manifestations, when present, may help in their differential diagnosis, as for example, face and tongue fasciculations with ophthalmoparesis and bulging eyes are present in some MJD/SCA3 patients (2). SCA2 patients usually exhibit very slow saccadic eye movements while sensory neuropathy is reported in SCA4, SCA18 and SCA25 cases. Retinopathy in SCA7, epilepsy and seizures in SCA10, action tremor of the hands in SCA12 and SCA27; mental retardation in SCA13 are distinctive differential symptoms. SCA17 cases usually present chorea and dementia while dysphonia and dentate calcification are characteristic of SCA20 patients and myoclonic epilepsy and dementia in some DRPLA cases (2). Even though, while the number of patients genetically diagnosed and clinically characterised grows, increasing new clinical signs and symptoms are described and associated with different spinocerebellar ataxia subtypes.

A number of specific clinical scales have been recently developed to measure the severity of ataxia, and their functional indexes have been shown to be very valuable for neurological assessment methods and therapeutic interventions. Scale for the Assessment and Rating of Ataxia (SARA) is the most widely used because of its proven usefulness, assessing ataxia severity by the assignment scores ranging from 0 (absence) to 40 (most severe) (6,7). In addition, the Inventory of Non-Ataxia Symptoms (INAS) clinical scale has shown useful for the assessment of different symptoms or syndromes including areflexia, hyperreflexia, extensor plantar response, spasticity, paresis, amyotrophy, fasciculations, myoclonus, rigidity, chorea, dystonia, resting tremor, sensory symptoms, brainstem oculomotor signs, urinary dysfunction, and cognitive impairment. Therefore, these recently developed rating scales and SCA functional indexes should be indispensable tools for ongoing and future clinical trials in SCA patients (4).

The identification of at least one affected family member showing mostly all the clinical signs of the disease is indispensable for a precise clinical diagnosis of a specific SCA subtype. This is relevant since the underlying cause of the different ataxia subtypes influences directly in the prognosis of the disease.

Epidemiological data indicate a SCA prevalence of up to 5-7 in 100,000 in some geographical areas, with similar numbers with the prevalence for other uncommon motor neurodegenerative diseases, such as Huntington or motor neuron diseases (4).

## 3. Molecular genetics of dominant cerebellar ataxias

Genetic studies have a great clinical impact in inherited movement disorders including ataxias. Therefore, clinical characterisation of the disease requires a detailed family history, even in apparently sporadic ataxia cases. In 1993 Zoghbi and Orr identified *ATXN1* as the first gene to be associated with an inherited autosomal dominant ataxia, hence denoted as spinocerebellar ataxia type 1 (SCA1) (8). Since then, 53 additional genes or loci have been described associated with different autosomal dominant ataxia subtypes (1,2) (**Figure 4; Table 1**). To date, more than 40 different genes are known to contain the underlying mutations associated with different clinical subtypes, therefore molecular genetics testing is feasible for those dominant ataxias (**Table 2**). Guidelines and best practice procedures and recommendations for the molecular genetics diagnosis of SCAs have been published by advisory committees such as the European Molecular Quality Genetics Network (EMQN) for the quality assurance of molecular genetic testing and internal quality control guidelines (9).

The epidemiological prevalence of each SCA subtype is highly variable as there is a limited number of population studies and heterogeneous molecular genetic approaches in different clinical and genetic diagnostic centres. Most reports described the frequency subtypes based only on genetic studies for polyglutamine repeat expansions in SCAs, which all share a common type of genetic mutation that can be detected by the similar molecular techniques, available in specialized diagnostic genetic centres (10).

The most recent population-based study estimated the average prevalence for dominant spinocerebellar ataxias to be 2.7 patients per 100,000 individuals, ranging from 0 to 5.6 cases per 100,000 individuals (11). It should be noted that the heterogeneity on diagnostic protocols in different specialized diagnostic centres could bias the estimation of the SCAs prevalences (12). The prevalence of different SCA subtypes also differs depending on the geographical region, being SCA3 the most common subtype worldwide, followed by SCA2 and SCA6 (10).

A high prevalence of SCA1 is found in South Africa and Poland (13,14) while in Australia is the most prevalent subtype together with SCA6 (15). SCA2 is the most prevalent subtype in Cuba due to a founder effect (16). Besides, SCA2 together with SCA10 are the most prevalent subtypes in Mexico (17,18), whereas SCA2 is also the most prevalent SCA in Italy, where recently studies reported a few SCA48 families (19). In Canada and the United States SCA3 is the most frequent SCA (17) likewise to Portugal, China and Japan where SCA3 is the most common subtype followed by DRPLA (20). In Brazil SCA3 is also the most prevalent form followed by SCA2, SCA7, SCA1 and SCA10 (21). In contrast, SCA6 is the most prevalent SCA subtype in North England while in countries like Venezuela, Finland and Sweden SCA7 is the most common form (22–24). SCA10 presents a particularly higher prevalence in Peru, Brazil and Mexico, suggesting a founder effect in South America (18). The most recent epidemiological study of dominant ataxias in Spain dates back to 2005

being SCA2 and SCA3 the most frequent genotypes (25). In 2012, SCA36 was described in ataxia families originally from Galicia, where this SCA subtype appears to be the most prevalent form in that geographical region (26).

As previously noted, these epidemiological studies only include the prevalence of SCAs caused by polyglutamine-repeat expanded mutations since they are the most commonly diagnosed and studied SCA subtypes. Therefore, further studies of mutations in other dominant ataxia-associated genes would elucidate the actual frequency of ataxia subtypes. With this regard, a recent European study screening identified *STUB1* variants associated with SCA48 in 30 families from 440 ataxic pedigrees, accounting for a 7% in the cohort (27).

A graphical summary of the distribution and most relevant geographical SCAs according to published data is represented in **Figure 1.**

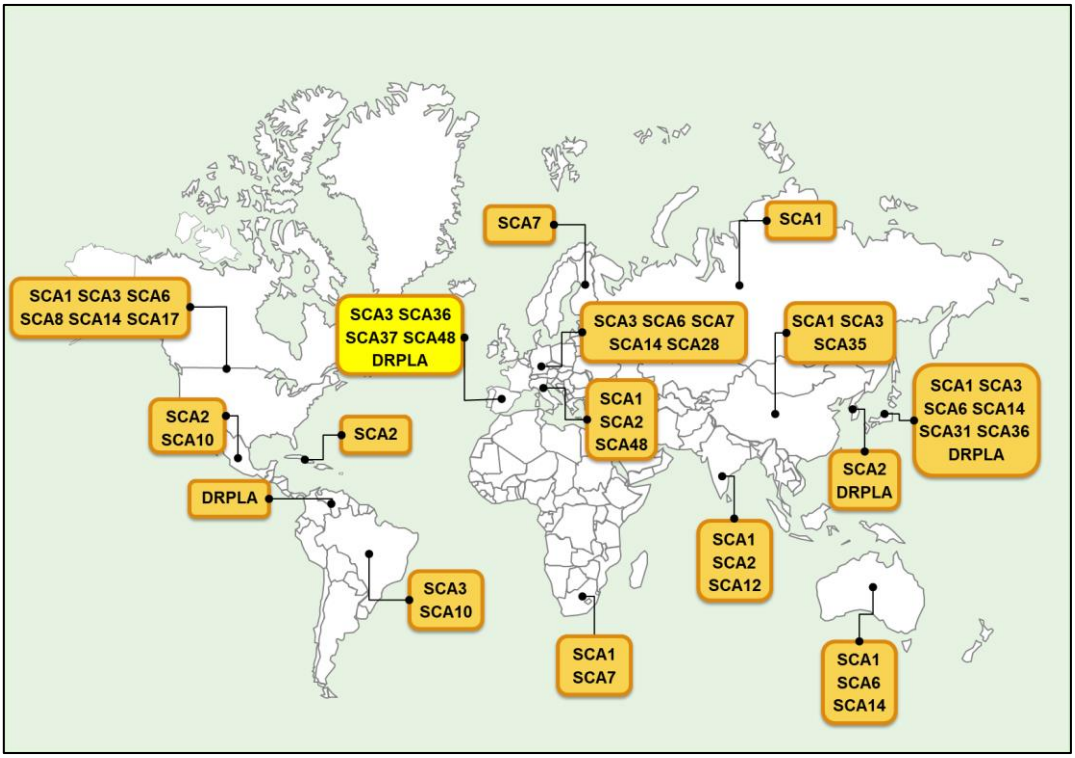


**Figure 1. Geographical distribution of SCAs.** Schematic representation of the global prevalence and relevant spinocerebellar ataxia subtypes by geographical regions. SCA3/Machado–Joseph disease (MJD) is the most common polyglutamine SCA worldwide. SCA36, SCA37 and SCA48 where initially described in ataxic Spanish families (yellow box). Adapted from (10).

## 4. Neuropathology of dominantly inherited cerebellar ataxias

Cerebellar cell degeneration and Purkinje cell loss is a major neuropathological feature in spinocerebellar ataxias. Actually, when the patient shows ataxic symptoms, cerebellar atrophy is

already present in MRI in most cases. Indeed, loss of Purkinje cells and affectation of deep cerebellar nuclei are evident with the remaining cells atrophied or misplaced in the cerebellum (28).

Neuropathological post-mortem studies of dominant ataxias caused by polyglutamine expansions show considerable spatial overlap of neurodegeneration. In contrast, a limited number of neuropathological studies have been reported for the remaining non-polyglutamine expansion associated cases, where brain pathology has been mainly described through MRI (29). Neuropathological alterations described in post-mortem dominant ataxia cases present a global Purkinje cell loss variably accompanied with Bergmann gliosis (SCA1, SCA14 and SCA48), intranuclear inclusions (SCA1, SCA3, SCA7, SCA8, SCA12, SCA23, SCA28 and SCA36), cytoplasmic inclusions (SCA2, SCA6 and SCA31), retinal degeneration (SCA7), hyperphosphorylated Tau (SCA11 and SCA19/22), frontal lobe affectation (SCA19/22), irregular ubiquitin staining (SCA23, SCA28, SCA31 and SCA36) or RNA foci (SCA31 and SCA36) (28,29).

The distribution of neuronal loss in the brains of SCA1, 2, 3, 6, 7, 8 and 17 are summarised in **Figure 2** (29) and the neuropathological studies of these SCA subtypes together with neuropathological reports for SCA4, 10, 11, 12, 14, 19/22, 23, 28, 31, 36, 48, DRPLA and EA4 are included in section 6.

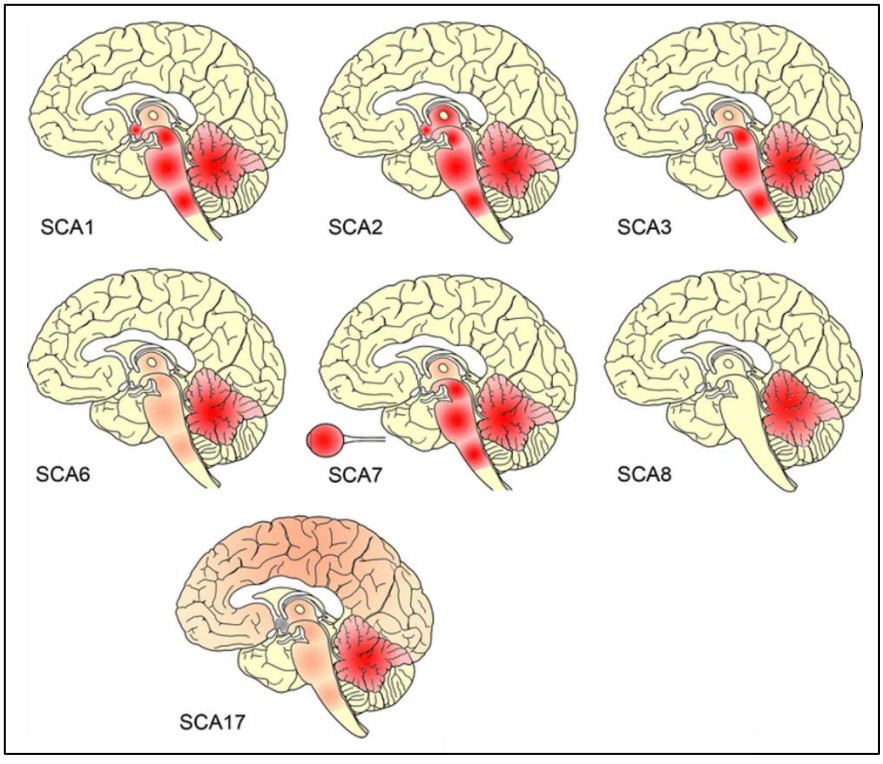


**Figure 2. Distribution of neuronal loss in the brain of patients with SCA1, SCA2, SCA3, SCA6, SCA7, SCA8 and SCA17.** Diagrammatic representation of midsagittal sections through the cerebrum, cerebellum and brainstem of the human brain. The degree of neuronal loss in the cerebral cortex, basal forebrain, thalamus, cerebellum and brainstem is indicated by red (severe) or light red (marked). Adapted from (29).

## 5. Molecular pathogenic pathways implicated in dominant ataxias

Pathological heterogeneity is also characteristic in dominant ataxias regarding to their distinct genetic causes. Brain pathology ranges from relatively pure cerebellar affectation to a broader neurological degeneration involving other parts of the brain, spinal cord and peripheral nerves. Clinical features could vary between patients from different families and even within a family, depending on the type of mutation. Dynamic repeat expansions associated with SCAs (SCA1, SCA2, SCA3, SCA6, SCA7, SCA8, SCA12, SCA17, DRPLA, SCA31 and SCA36) are typically unstable and can change in size between generations, with most of them lengthening upon transmission, with the age at onset and severity of disease symptoms inversely correlating with the length of the glutamine repeat. This phenomenon is known as (clinical and genetic) anticipation. For several repeat expansions in SCAs there is marked parental bias regarding expansion transmission and clinical anticipation (10).

Although causative SCAs mutations presenting with a dominant inheritance pattern were originally thought to result in a dominant toxic gain-of-function, recently several studies have implicated dominant-negative effect, when the activity of the wild-type protein expressed from the healthy allele is affected by the partial loss-of-function of the mutated allele, affecting the pathogenesis of the disease. Thus, even the same mutation could trigger both a dominant gain-of-function and dominant negative effect. Haploinsufficiency has also been described in some cases, mainly associated with nonsense and frameshift mutations or large deletions (30,31).

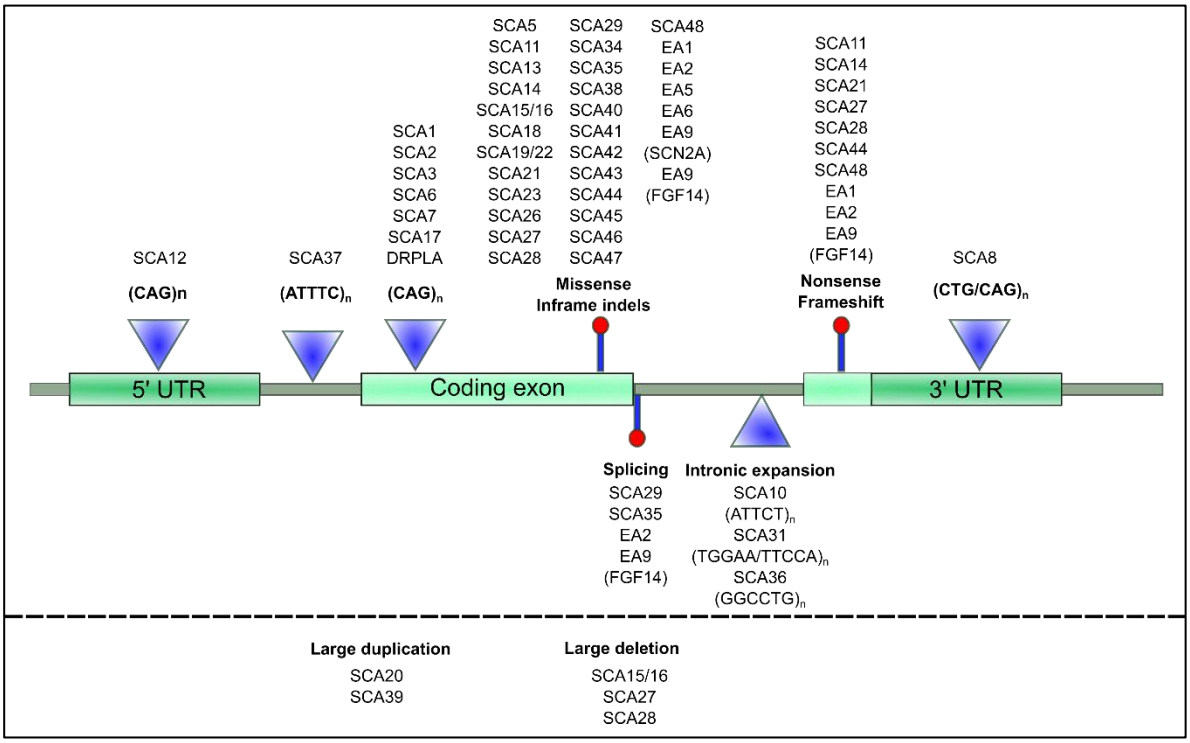


**Figure 3. Types of mutations causing dominant ataxias.** A schematic representation of a gene indicating the ataxia subtype, type of mutation, repeat sequence and location within the corresponding gene.

Molecular alterations leading to neurodegeneration (**Figure 3**) include polyglutamine expansions (SCA1, SCA2, SCA3, SCA6, SCA7, SCA17 and DRPLA), non-coding expansions (SCA8, SCA10, SCA12, SCA31, SCA36 and SCA37), as well as missense, frameshift or splicing mutations, deletions or duplications in genes associated with cytoskeletal proteins (*SPTBN2*, SCA5; *IFRD1*, SCA18), intracellular calcium channels (*CACNA1A*, SCA6 and EA2; *ITPR1*, SCA15; *CACNA1G*, SCA42; *CACNB4*, EA5), protein kinases (*TTBK2*, SCA11; *PRKCG*, SCA14), ion channels (*KCNC3*, SCA13; *KCND3*, SCA19/SCA22; *KCNA1*, EA1), transmembrane proteins (*TMEM240*, SCA21; *TRPC3*, SCA41; *MME*, SCA43), neurotransmitters (*PDYN*, SCA23), protein synthesis (*EEF2*, SCA26), fibroblasts growth factors (*FGF14*, SCA27 and EA9), ATPases (*AFG3L2*, SCA28), fatty acid elongation system (*ELOVL4*, SCA34; *ELOVL5*, SCA38), transglutaminases (*TGM6*, SCA35), Wnt signalling pathway (*CCDC88C*, SCA40), glutamate receptors and transporters (*GRM1*, SCA44; *SLC1A3*, EA6), cell adhesion (*FAT2*, SCA45), lysosomal system (*PLD3*, SCA46), mRNA binding (*PUM1*, SCA47) ubiquitination (*STUB1*, SCA48) and sodium channels potentials (*SCN2A*, EA9) (2).

The characterisation of the cellular and molecular pathways implicated in SCAs neurodegeneration identified common major altered mechanisms in transcriptional dysregulation, protein aggregation and clearance, autophagy, calcium homeostasis, mitochondria defects, toxic RNA gain-of-function mechanisms or apoptosis activation, among others, leading to progressive spinocerebellar dysfunction and neuronal loss primarily cerebellar Purkinje cells (28).

Aggregation and protein misfolding have been described as common toxic gain-of-function mechanisms altered by SCAs polyglutamine expansions, forming nuclear or cytoplasmic inclusions and leading to a neuronal dysfunction, being more severe with a longer number of glutamines in the mutant proteins (28,29). Ubiquitin-dependent proteasome system (UPS) and molecular chaperones also play a pivotal role in the degradation of damaged proteins, thus abnormal accumulation of toxic proteins including those containing polyglutamines would disturb this degradation pathways. Consequently, chaperones associated with endoplasmic reticulum (ER) and the unfolded protein response (UPR) are common activated mechanism in SCAs pathology. The cellular degradation of misfolded proteins is performed by the ubiquitin-proteasome and autophagic-lysosome systems that could also reveal alterations under pathological conditions.

Long polyglutamine stretches have been also described as components of transcriptional regulatory complexes regulating different pathways (32,33). For instance, mutant ataxins alter the expression of histone acetyltransferases (HATs) responsible for the acetylation of histones involved in DNA structure and the regulation of gene expression (34). Furthermore, RNA-mediated toxicity has been found to be a common pathological mechanism shared by different SCA non-coding repeat expansions as SCA8, SCA10 or SCA31 triggering a RNA gain of function (35–37). Alterations in

synaptic neurotransmission have been also described to mediate neurodegeneration in different SCA subtypes as in SCA1, SCA5 or SCA44 (30,38,39).

Cerebellar Purkinje cells are particularly sensitive to calcium levels and fluxes with several genes involved in calcium signalling or homeostasis appearing dysregulated in numerous SCAs subtypes (40,41). Some mutations directly affect genes involved in calcium regulation as occurs in SCA6/EA2, SCA15/16/29, SCA42 or EA5 and other mutations indirectly triggers calcium alterations as in SCA1, SCA2, SCA14 or SCA44 (42). In the same way, mitochondria have also a pivotal role in intracellular calcium homeostasis as well as in mitochondrial apoptotic activated pathways implicated in neuronal apoptosis. Mitochondrial dysregulation by the alteration of cytochrome-c release in SCA3 and SCA7 (43,44), or mitochondrial dysfunction in SCA28 associated mutations in *AFG3L2* gene (45), involved in the formation of protein complexes to ensure protein quality control in the mitochondrial inner membrane, are good examples of mitochondrial deficits in SCA pathology.

Additional molecular pathways have been found specifically altered in different SCAs subtypes as the implication of AKT in ATXN1 (SCA1) phosphorylation (46), the essential role of ATXN2 (SCA2) in RNA processing events (47) or the implication of SPTBN2 protein (SCA5) in vesicle trafficking and glutamate signalling, particularly affecting EAAT4 glutamate transporter, with both pathways dysregulated in SCA5 pathology (48).

Although important advances have been achieved in the molecular field to elucidate the pathology involved in SCAs, most of the implicated mechanism still remain to be described. Thus in the future, as additional SCAs will be identified, other disease proteins and common implicated molecular pathways will be described, elucidating common SCAs mechanisms and facilitating the upcoming efforts to treat them (28).

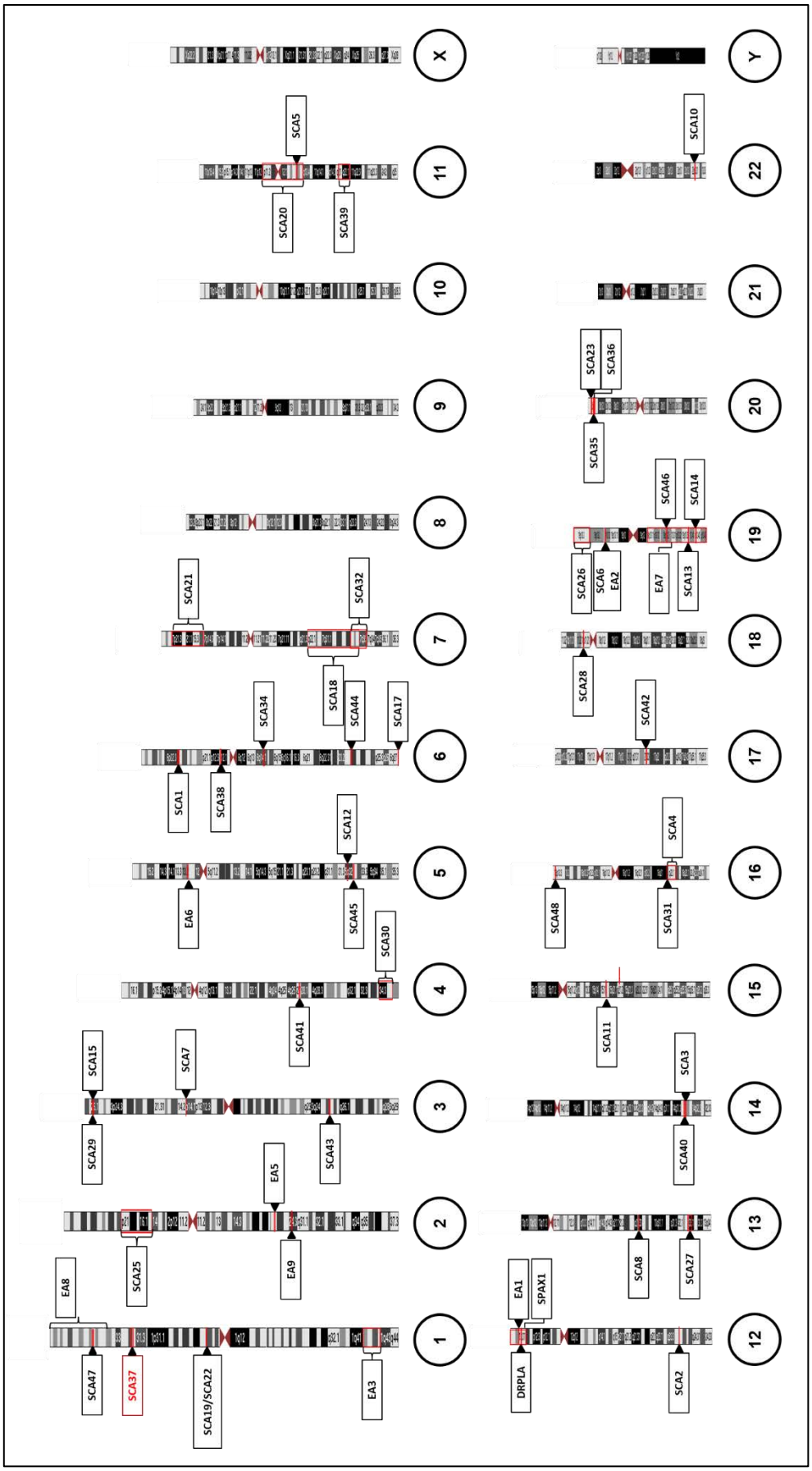


**Figure 4. Ideogram generated with the human genome browser at UCSC (663) showing the chromosomal locations of all dominant ataxia genes identified to date. Adapted from (3).**

**Table 1 Clinical and neuropathological heterogeneities in dominant ataxias.**

| Name | Harding's clinical classification[5] | Average onset | Average duration | Distinguishing clinical features | Eye movement alterations | Neurophy. | MRI | Neuropath. |
|---|---|---|---|---|---|---|---|---|
| SCA1 | Type I | 3rd-4th decade (<10 to >60) | 15 years (10–28), anticipation | Pyramidal signs, peripheral neuropathy | Saccades hypo/hypermetria GEN impaired VOR | MNC, SNC, EP and VEP | Olivopontocerebellar atrophy | Loss of Purkinje cells, neurons of dentate, Bergmann's gliosis, variable loss of granule cells, atrophy of middle cerebellar peduncles. INIs |
| SCA2 | Type I | 3rd-4th decade (<10 to >60) | 10 years (1–30), anticipation | Slow saccadic eye movements, peripheral neuropathy, dementia | Slow and hypometric saccades | MNC, SNC, EP and VEP | Olivopontocerebellar and cortical atrophy | Atrophy of cerebellum, pons, frontal lobe, medulla oblongata, cranial nerves, as well as pallor of the midbrain substantia nigra, cytoplasmic inclusions |
| SCA3/ Machado Joseph disease | Type I | 4th decade (10-70) | 10 years (1–20), anticipation | Pyramidal and extrapyramidal signs, lid retraction, nystagmus, decreased saccade velocity, amyotrophy, fasciculations, sensory loss | Slow and dysmetric saccades, ophthalmoplegia, impaired VOR | MNC, SNC, EP and VEP | Cortical, pontine and spinal cord atrophy | Loss of neurons and gliosis in the substantia nigra, pontine nuclei (in putamen in some cases) as well as nuclei of the vestibular and cranial nerves, column of Clarke and anterior horn. INIs |

| Name | Harding's clinical classification[5] | Average onset | Average duration | Distinguishing clinical features | Eye movement alterations | Neurophy. | MRI | Neuropath. |
|---|---|---|---|---|---|---|---|---|
| SCA4 | Type I | 4th-7th decade (19-72) | Decades | Sensory axonal neuropathy, deafness, may be allelic with SCA31 | Slow saccades, ophthalmoparesis , impaired VOR | SNC | Pure cerebellar atrophy | Atrophy of the cerebellar vermis and the dorsal columns, neuronal loss in Purkinje cell layer and deep nuclei and in the midbrain, pons and the medulla oblongata |
| SCA5 | Type III | 3rd-4th decade (10-68) | >25 years slow progression | Early onset, slow course, first reported in descendant of Abraham Lincoln | Downbeat nystagmus or GEN | Normal | Pure cerebellar atrophy | - |
| SCA6 | Type III | 5th-6th decade (19-71) | >25 years slow progression | Usually pure phenotype, sometimes episodic ataxia, very slow progression | GEN, PAN, impaired pursuit and VOR | Variable results | Pure cerebellar atrophy | Loss of PCs and inferior olives neurons, reactive astrocytes, cytoplasmic *CACNA1A* aggregates |
| SCA7 | Type II | 3rd-4th decade (0.5-60) | 20 years (1–45), anticipation | Visual loss with retinopathy | Pigmentary retinal dystrophy and slow saccades | VEP | Pontine and spinal cord atrophy | Retinal degeneration with loss of photoreceptors and damage to the retinal pigment epithelium, severe neuronal loss in basal ganglia, visual, auditory and somatosensory. Reactive astrocytes are also detectable and |

| Name | Harding's clinical classification[5] | Average onset | Average duration | Distinguishing clinical features | Eye movement alterations | Neurophy. | MRI | Neuropath. |
|---|---|---|---|---|---|---|---|---|
| SCA8 | Type I | 4th decade (1-65) | Normal lifespan | Slowly progressive, sometimes hyperreflexia, decreased vibration sense; rarely, cognitive impairment. | Downward hypermetria | MNC and SNC | Cerebellar and pontine atrophy | Cerebellar atrophy, depigmentation of the substantia nigra, severe loss of Purkinje cells, striking loss of neurons in the pars compacta and the inferior olivary nucleus. Positive 1C2 intranuclear immunoreactivity observed in Purkinje cells and medullar neurons. |
| SCA9 | Type I | 3th decade (21-48) | - | Ophthalmoplegia, dysarthria, pyramidal and extrapyramidal tract signs, weakness, posterior column signs, parkinsonism, phenotype resembling multiple sclerosis | Ophthalmoplegia | Unknown | Cerebellar atrophy and demyelinating lesions on brain | - |
| SCA10 | Type I | 4th decade (12-48) | 9 years | Occasional seizures, most families are of Native American background | Hypometric saccades and GEN | Altered EEG | Pure cerebellar atrophy | Purkinje cell loss, symmetrical atrophy in cerebellar hemispheres |
| SCA11 | Type III | Age 30 (15-70) | Normal lifespan | Usually pure mild phenotype, remain ambulatory | Pursuit impairment, GEN, downbeat nystagmus, saccadic abnormalities | Normal | Pure cerebellar atrophy | Hyperphosphorylated tau |

| Name | Harding's clinical classification[5] | Average onset | Average duration | Distinguishing clinical features | Eye movement alterations | Neurophy. | MRI | Neuropath. |
|---|---|---|---|---|---|---|---|---|
| SCA12 | Type I | 4th decade (8-62) | Slow progress | Slowly progressive, hyperreflexia, subtle parkinsonism, cognitive/psychiatric disorder | Dysmetric saccades, impaired pursuit, and nystagmus | MNC and SNC | Cortical atrophy | Enlarged ventricles, neuritic plaques in the frontal and parietal cortex and neurofibrillary tangles in the subiculum, PC loss, less prominent cerebellar and pontine atrophies, and INIs |
| SCA13 | Type I | Childhood or adulthood | Childhood or adulthood | Mild intellectual disability, short stature | GEN | Normal | Pure cerebellar atrophy | - |
| SCA14 | Type I | 3rd-4th decade (3-70) | Decades (1–30) | Early axial myoclonus | GEN and SWJs | Normal | Pure cerebellar atrophy | Braak II / III neurofibrillary Alzheimer type pathology and mild cerebrovascular disease, several loss of Purkinje cells in hemisphere lobes, Bergmann gliosis |
| SCA15/ SCA16 | Type III | 4th decade (7-66) | Decades (very slow progression) | Pure ataxia, very slow progression, head tremor in Japanese family | GEN and VOR | Normal | Pure cerebellar atrophy | - |
| SCA17 | Type I | 4th decade (3-55) | >8 years | Mental retardation, occasional chorea, dystonia, myoclonus, epilepsy | Hypometric saccades, abnormal pursuit, GEN and impaired VOR | BAEP, MEP an SSEP | Variable cerebrum, brain stem, and cerebellum atrophy | Mild neuronal loss with compaction of the neuropil in the cerebral cortex, mild loss of neurons in the striatum, and moderate loss of PC |

| Name | Harding's clinical classification[5] | Average onset | Average duration | Distinguishing clinical features | Eye movement alterations | Neurophy. | MRI | Neuropath. |
|---|---|---|---|---|---|---|---|---|
| SCA18 | Type I | Adolescence (12-25) | - | Early sensory-motor neuropathy, muscle weakness, atrophy, fasciculation, Babinski response | GEN | SNC | Mild cerebellar atrophy | - |
| SCA19/ SCA22 | Type I | 4th decade (10-51) | Decades | Slowly progressive, rare cognitive impairment, myoclonus, hyperreflexia | Dysmetric saccades | Normal | Mild cerebellar atrophy | Frontal lobe marked widening, cerebellar atrophy, moderate neuronal loss in the substantia nigra, neuronal loss in Purkinje cell layer and torpedoes formation. Hyperphosphorylated tau aggregation in the hippocampal and entorhinal area |
| SCA20 | Type I | 5th decade (19-64) | Decades | Early dysarthria, spasmodic dysphonia, hyperreflexia, bradykinesia, calcification of the dentate nucleus | Hypermetric saccades, GEN, downbeat nystagmus | Normal | Cerebellar atrophy, calcifications of the dentate nuclei, increased inferior olivary T2 signal | - |
| SCA21 | Type I | 6-30 | Decades | Mild cognitive impairment | Impaired smooth pursuit and square wave jerk intrusions | Normal | Pure cerebellar atrophy | - |

| Name | Harding's clinical classification[5] | Average onset | Average duration | Distinguishing clinical features | Eye movement alterations | Neurophy. | MRI | Neuropath. |
|---|---|---|---|---|---|---|---|---|
| SCA23 | Type I | $5^{th}$-$6^{th}$ decade | >10 years | Dysarthria, abnormal eye movements, reduced vibration and position sense | Dysmetric saccades | SNC | Cerebellar and brainstem atrophy | Frontotemporal atrophy, atrophy of vermis, pons, and spinal cord. Neuronal loss in the vermis, dentate nuclei, and inferior olives, demyelination of the posterior and lateral columns of the spinal cord. Ubiquitin INIs in nigral neurons (Marinesco bodies) |
| SCA24 | Unknown | Unknown | Unknown | No published data available | Unknown | Unknown | Unknown | Unknown |
| SCA25 | Type I | 1.5-39 | Decades | Sensory neuropathy | Hypermetric saccades | SNC | Pure cerebellar atrophy | - |
| SCA26 | Type III | 33 (26-60) | Decades | Dysarthria, irregular visual pursuit | Dysmetric saccades, abnormal VOR gain and pursuit | Normal | Cerebellar atrophy sparing the pons and medulla | - |
| SCA27 | Type I | 11 (7-20) | Decades | Early-onset tremor, dyskinesia, cognitive deficit | Impaired saccades and pursuit | Normal | Pure cerebellar atrophy | - |

| Name | Harding's clinical classification[5] | Average onset | Average duration | Distinguishing clinical features | Eye movement alterations | Neurophy. | MRI | Neuropath. |
|---|---|---|---|---|---|---|---|---|
| SCA28 | Type I | 19.5 (12-36) | Decades | Nystagmus, ophthalmoparesis, ptosis, hyperreflexia | Slow saccades, pursuit and OKN impairment | Normal | Pure cerebellar atrophy | Severe atrophy of the upper part of the cerebellar hemisphere, immunoreactivity to ubiquitin and p62 with INIs in brain, cerebellar cortical neurons, and hippocampal, pontine and medullary nuclei neurons |
| SCA29 | Type I | Early childhood | Decades | Learning deficits | GEN and fixation instability | Normal | Pure cerebellar atrophy | - |
| SCA30 | Type III | 52 (45-76) | 8 years | Hyperreflexia | Hypermetric saccades | Normal | Pure cerebellar atrophy | - |
| SCA31 | Type III | 58 (8-83) | >10 years | Normal sensation | GEN | Normal | Pure cerebellar atrophy | Severe loss of Purkinje cells, somatic sprouts with formation of RNA foci and amorphous protein aggregates, containing ubiquitin, synaptophysin and calbindin |
| SCA32 | Type I | Adulthood | Unknown | Variable cognitive impairment, azoospermia | Unknown | Normal | Pure cerebellar atrophy | - |
| SCA33 | Unknown | Unknown | Unknown | No published data available | Unknown | Unknown | Unknown | Unknown |

| Name | Harding's clinical classification[5] | Average onset | Average duration | Distinguishing clinical features | Eye movement alterations | Neurophy. | MRI | Neuropath. |
|---|---|---|---|---|---|---|---|---|
| SCA34 | Type I | Cutaneous signs in childhood, ataxia >40 | Decades | Erythrokeratodermia in childhood. Allelic to Stargardt macular dystrophy 3 and autosomal recessive ichthyosis, spastic quadriplegia, and mental retardation | GEN, ophthalmoplegia, impaired pursuit | Normal | Cerebellar and pontine atrophy | - |
| SCA35 | Type I | Age 43.7 (40-48) | Decades | Hyperreflexia, Babinski responses, spasmodic torticollis | Slow saccades and saccadic pursuit | Normal | Pure cerebellar atrophy | - |
| SCA36 | Type I | Age 52.8 ±4.3 | Decades | Muscle fasciculations, tongue atrophy, hyperreflexia | Impaired pursuit, GEN, supranuclear palsy | Normal | Cerebellar and olivopontocerebellar atrophy | Purkinje cell loss, loss of motor neurons in the hypoglossal nucleus, positive inclusions for ubiquitin and p62 in the cytoplasm of the inferior olivary, RNA foci in neuronal nuclei of the cerebrum, cerebellum, inferior olive, spinal cord and temporal muscle |
| SCA37 | Type III | Age 48 (38-64) | Decades | Slowly progressive pure phenotype, early altered vertical saccades and pursuit | Dysmetric vertical saccades and irregular vertical pursuit | Normal | Pure cerebellar atrophy | - |
| SCA38 | Type I | 39 (34-51) | 41 (20-52) | Usually pure phenotype, slow saccades, few subjects with axonal neuropathy | Slow saccades, GEN | MNC, SNC and EP | Pure cerebellar atrophy | - |

| Name | Harding's clinical classification[5] | Average onset | Average duration | Distinguishing clinical features | Eye movement alterations | Neurophy. | MRI | Neuropath. |
|---|---|---|---|---|---|---|---|---|
| SCA39 | Type I | Infancy | Decades | Spastic ataxia, intellectual disability | Strabismus, saccadic pursuit and horizontal gaze palsy | Neurogenic pattern, prolonged auditory evoked brainstem potentials | Cerebellar atrophy with periventricular white matter hyperintensity | - |
| SCA40 | Type I | 4th decade | Decades | Ocular dysmetria, impaired vertical gaze, hyperreflexia, spastic paraparesis, tremor, dementia | Dysmetric saccades and impaired vertical gaze | Normal | Cerebellar and pontine atrophy | - |
| SCA41 | Type III | 38 | Unknown | Progressive ataxia | Unremarkable | Normal | Mild cerebellar atrophy | - |
| SCA42 | Type I | 9-78 | Decades | Transient diplopia, pyramidal signs, spastic gait | Saccadic pursuit, diplopia, GEN | Altered reflexes | Pure cerebellar atrophy | - |
| SCA43 | Type I | Adulthood (42-68) | Decades | Mild distal lower limb atrophy, hyporeflexia, tremor and peripheral polyneuropathy | Hypometric saccades and GEN | MNC, and altered reflexes | Moderate cerebellar atrophy | - |
| SCA44 | Type I | 5-50 | Decades | Dysdiadochokinesis | Saccadic hypermetria, abnormal pursuit | Normal | Pure cerebellar atrophy | - |
| SCA45 | Type III | Adulthood (>40) | Decades | Slowly progressive ataxia | Downbeat nystagmus | Normal | Pure cerebellar atrophy | - |

| Name | Harding's clinical classification[5] | Average onset | Average duration | Distinguishing clinical features | Eye movement alterations | Neurophy. | MRI | Neuropath. |
|---|---|---|---|---|---|---|---|---|
| SCA46 | Type I | Adulthood (35-69) | Decades | Variable sensory neuropathy at lower limbs | Nystagmus, saccadic dysmetria and pursuit | SNC | Mild cerebellar atrophy | - |
| SCA47 | Type III | Childhood or adulthood | Decades | Slowly progressive cerebellar ataxia and diplopia or delayed motor development with spasticity and epileptic encephalopathy | Diplopia | Normal | Mild cerebellar atrophy with or without enlarged fourth ventricle | - |
| SCA48 | Type I | 40 (23-74) | Decades | Anxiety, deficits in executive function and cognitive-affective symptoms | Dysmetric saccades | Normal | Pure cerebellar atrophy | Massive loss of Purkinje cells in the vermis and major loss in the cerebellar hemispheres, numerous empty baskets, hyperplastic and hypertrophic Bergmann glia and axonal torpedoes in the granular layer |
| DRPLA | Type I | 30 (10-70) | 8 (0-35) | Myoclonus, seizures, choreoathetosis, and dementia | Unremarkable | Normal | Cerebellar and brainstem atrophy | Atrophy and neuronal loss in the globus pallidus (particularly the lateral segment) and dentate nucleus, brainstem, cerebellar and cerebral white matter. Lipofuscin deposits |

| Name | Harding's clinical classification[5] | Average onset | Average duration | Distinguishing clinical features | Eye movement alterations | Neurophy. | MRI | Neuropath. |
|---|---|---|---|---|---|---|---|---|
| EA1 | Episodic | 1st–2nd decade (2–15) | Decades | Constant myokymia, dramatic episodes of spastic contractions and may be associated with epilepsy | Blurred vision | Normal | Normal | - |
| EA2 | Episodic | 2–32 | 8-25 | Paroxysmal recurrent unsteadiness, incoordination, vertigo, and slurring speech | Nystagmus | Normal | Pure cerebellar atrophy | - |
| EA3 | Episodic | 1–52 | Decades | Vestibular ataxia, vertigo, diplopía, tinnitus, and interictal myokymia | Abnormal smooth pursuit, nystagmus | Normal | Normal | - |
| EA4 | Episodic | early adulthood (30-60) | Decades | Recurrent attacks of vertigo, diplopia | GEN | Normal | Normal | Moderate to severe Purkinje cell loss in the vermis with loss of dendritic arborization, depigmentation of substantia nigra, polyglutamine track staining, subtle foci in the flocculus-granular cell layer |
| EA5 | Episodic | Young-adult onset | Decades | Recurrent episodes of vertigo and truncal ataxia | GEN | Normal | Normal | - |
| EA6 | Episodic | Childhood to adulthood | Decades | Progressive ataxia, seizures, and migraine headaches with prolonged alternating hemiplegia | Diplopia, photophobia, nystagmus, hypometric saccades, jerky ocular pursuit | Normal | Could present cerebellar atrophy | - |

| Name | Harding's clinical classification[5] | Average onset | Average duration | Distinguishing clinical features | Eye movement alterations | Neurophy. | MRI | Neuropath. |
|---|---|---|---|---|---|---|---|---|
| EA7 | Episodic | < 20 | Decades | Weakness and dysarthria | Normal | Normal | Normal | - |
| EA8 | Episodic | 1-2 | Decades | Generalized weakness, myokymia, persistent intention tremor and slurred speech | Twitching around the eyes, nystagmus | Normal | Normal | - |
| EA9 (*SCN2A*) | Episodic | Infancy | Decades | Difficulty walking, dizziness, slurred speech, headache, vomiting, and pain | Nystagmus | Normal | Mild cerebellar atrophy, cerebellar edema | - |
| EA9 (*FGF14*) | Episodic | Childhood to adulthood | Decades | Attacks were triggered by fever, nystagmus and/or postural tremor and/or learning disabilities | Nystagmus | Normal | Normal | - |

MEP, motor evoked potential; MNC, motor nerve conduction; Neuropath., neuropathology; Neurophy., neurophysiology; OKN, optokinetic nystagmus; SNC, sensory nerve conduction; SSEP, somatosensory evoked potential; SWJs, square wave jerk intrusions; VEP, visual evoked potential; VOR, Vestibulo-ocular reflex.

## 6. Dominant ataxia subtypes

Forty-three different inherited spinocerebellar ataxia (SCA) subtypes have been described to date. They are conventionally referred as SCAs regardless of whether or not they present with spinal pathology. In addition, the complex form dentatorubral-pallidoluysian atrophy (DRPLA) and eight episodic ataxias (EA) are commonly included.

### 6.1. Spinocerebellar ataxia type 1 (SCA1) [OMIM # 164400]

Clinically, SCA1 is characterised by progressive muscle weakening and ataxia, with difficulties in speech and swallowing. At later stages, symptoms progress to include muscle atrophy, cognitive deficiencies, and bulbar dysfunction leading to respiratory complications, which is the primary cause of death (49). The disease onset usually occurs during the third or fourth decade of life. Patients exhibit cerebellar and brainstem symptoms, but also extrapyramidal signs and peripheral neuropathy. SCA1 electrophysiological studies revealed slow motor nerve conduction velocities (MNCVs) and reduced compound muscle action potentials (CMAPs) amplitudes. There is a high prevalence of electrophysiological evidence for peripheral nerve involvement (96.4%) in SCA1 (50). SCA1 patients also show reduced or absent sensory nerve action potentials (SNAPs) amplitude without decreased sensory nerve conduction velocities (SNCVs) with ulnar nerve alterations (51). Motor unit action potentials (MUAPs) could be increased and brainstem auditory evoked potentials (BAEPs) are often abnormal in SCA1 (52). In motor evoked potentials (MEPs) studies, almost all SCA1 patients presented prolonged central and peripheral motor conduction times (CMCTs and PMCTs) (50). Reduced P40 was found in 75% of SCA1 cases in somatosensory evoked potentials records (53). Abnormal visual evoked potentials (VEPs) have been reported in SCA1 with mainly abnormalities being prolonged latencies of P100 and reduced amplitude of P100 (50).

Oculomotor abnormalities include saccadic dysmetria and reduced speed, although inconstantly observed (54). As a consequence of brainstem involvement, horizontal and vertical ophthalmoparesis may be present (55), as well as gaze evoked nystagmus (56). Square wave jerks (SWJs) and saccadic oscillations, impaired vestibulo-ocular reflex (VOR), and optokinetic nystagmus have also been reported (57).

Structural MRI typically shows olivopontocerebellar atrophy (OPCA) and white matter (WM) atrophy, Voxel-Based Morphometry (VBM) studies reveal atrophy of frontal and cerebellar hemispheric white matter surrounding the dentate nuclei (58). Morphometric analyses of spinal cord area show significant reductions which significantly correlates with scale for the assessment and rating of ataxia (SARA) scores and disease duration in the multiple variable regression analysis (59).

The underlying genetic cause of SCA1 was the first identified to be associated with a specific SCA subtype in 1993 when the presence of an unstable CAG repeat was identified within the *ATXN1* gene

using positional cloning and linkage analysis (8,60). Expansion of the CAG repeat in the *ATXN1* gene is the mutational mechanism in all families with SCA1 examined to date. Normal alleles range from 4 to 39 CAG repeats and the repeat configuration in alleles greater than 21 repeats is interrupted by 1-3 CAT trinucleotides, whereas disease-causing alleles show a perfectly uninterrupted CAG repeat configuration (61,62). The *ATXN1* expansion of 39 or more uninterrupted CAG repeats or 43 or more CAG interrupted repeats in SCA1 patients, results in the highly penetrant, late-onset, and progressive cerebellar ataxia (62,63). Mutable normal (intermediate) alleles ranging from 36-38 CAG repeats without CAT interruptions can result in ataxia without other clinical features of SCA1 and can expand into the expanded range on transmission to offspring (62,64). The penetrance of the expanded mutation is considered to be greater than 95%, but is dependent on age. A woman with 44 CAG repeats with CAT repeat interruptions had an affected father but was herself asymptomatic at age 66 years (65), thus, she may have reduced penetrance. Therefore, alleles of 39-91 uninterrupted CAG repeats are considered abnormal and are likely associated with symptoms (66).

According to an epidemiological study in 2004 SCA1 is the cause of spinocerebellar ataxia in ~3–16% of families with a history of SCA in North America and Europe (67). The highest prevalence of SCA1 is found in Poland (68% of families with SCA), Russia (41%), South Africa (41%), Serbia (34%), Italy (25%) and India (22%).

Neuropathology in SCA1 typically identifies marked atrophy of the cerebellum, brainstem, and frontal cerebral lobe, showing neuronal loss in the cerebellothalamocortical and basal ganglia-thalamocortical loops as well as in the nervous sensory systems (68). Brains may also present damage in oculomotor, ingestion and vestibular associated brain regions and the rest of the so-called precerebellar nuclei. SCA1 brains also show demyelination or atrophy in the cerebellar pedunculus, cranial nerves, and in the somatosensory and auditory tracts. In addition to the primary Purkinje cell damage, they also present astrocyte-GFAP immunoreactivity and neuronal ATXN1 intranuclear aggregation in affected brain regions (68,69).

The *ATXN1* gene is located at 6p22.3 and encodes the 816-amino acid, 87 kDa protein, ataxin-1, which is widely expressed across neuronal and glial populations through-out the central nervous system (70). In humans, *ATXN1* contains nine exons, with the first seven residing in the 5′untranslated region (UTR) and the eighth and ninth encoding the protein-coding sequences (71). The first protein-coding exon carries the CAG repeat tract, which is aberrantly expanded in SCA1 patients.

ATXN1 is a transcription cofactor that interacts with numerous other proteins implicated in gene expression (72). The mutant protein gain a novel toxic function that underlies the pathogenesis of SCA1 (72). Relevantly, the cerebellar leucine-rich acidic nuclear protein (LANP), a member of the inhibitor of histone acetyltransferase complex, interacts significantly stronger with ATXN1 when the number of glutamines are increased (32) while does not vary with the length of the polyglutamine

tract when binding glycolytic enzyme glyceraldehyde-3-phosphate dehydrogenase (GAPDH) (73). In the same direction, the expansion in ATXN1 favours its interaction with the transcriptional repressor protein capicua homologue (capicua) over its interaction with the RNA-binding protein and spliceosome component RBP7. This shift in ATXN1 binding disrupts gene expression and splicing events in vulnerable neurons (74). Studies in mouse models mimicking human pathology (75) and in induced pluripotent stem cells derived from patients with SCA1 suggest that the increase in ATXN1–capicua drives toxicity in the cerebellum through a gain-of-function mechanism (76). Knock-out ataxin-1 mouse models revealed the ataxin-1 role in neurocognitive functions and demonstrated that neurodegeneration in SCA1 is not triggered by a loss-of-function mechanism (77). The toxicity of mutant ATXN1 also depends on its phosphorylation at serine 776, an amino acid that is distant to the polyglutamine expansion (78). ATXN1 engineered to lack serine 776 is no longer toxic, despite still harbouring a polyglutamine expansion. Genetically or pharmacologically inhibiting protein kinase A, the kinase that principally phosphorylates ATXN1 at serine 776, ameliorates disease in a mouse model for SCA1 (79). Moreover, the polyglutamine mutation within Atxn1 alters Pp2a activity modulation even before disease onset in the SCA1 mouse cerebellum and regulates the cerebellar bioenergetics proteome through the GSK3β-mTOR pathway (80,81). In summary, studies of ATXN1 underscore that albeit the polyglutamine expansion in ATXN1 is essential for disease, other motifs within the protein as well as the function of the protein itself influence the toxicity elicited by the polyglutamine mutation.

### 6.2. Spinocerebellar ataxia type 2 (SCA2) [OMIM # 183090]

SCA2 is characterised by a broad group of progressive clinical signs, including gait ataxia, postural instability, cerebellar dysarthria, dysmetria, and dysdiachokinesia. Neuropathy, pyramidal tract involvement, parkinsonism, amyotrophic lateral sclerosis, or pigmented retinopathy may also be observed (82). The age of onset of the cerebellar syndrome in SCA2 is variable, although in most subjects, it appears in the second or third decade of life. CAG repeats in the *ATXN2* gene, explain between 60 and 80% of its variability (83).

SCA2 patients electrophysiology display prolonged distal latency, reduced NCVs, and reduced CMAP amplitudes with absent or reduced SNAP amplitudes and decreased NCV in sensory nerve conductions (50). Large motor unit action potentials (MUAPs) and reduced recruitment in both proximal and distal muscles were also observed in SCA2 patients (84). BAEPs (brainstem auditory evoked potentials) show alteration in SCA2 patients (85) with delayed or absent MEPs (motor evoked potential) (50). The mean P40 wave latency in tibial somatosensory evoked potential (SSEP) appear significantly prolonged (85). Patients additionally display abnormal VEPs with prolonged latencies of P100 and reduced amplitude of P100 (50).

Recently, Pelosi *et al.* suggested that a majority of patients with SCA2 have a sensory neuronopathy and this correlates with disability. A minority of patients have findings consistent with axonal neuropathy (86).

A hallmark of the disease is the severe slowing of ocular movements, observed in about 90% of patients (87). Saccade slowing is correlated with triplet CAG number (88). Hypometric saccades, nystagmus, and square wave jerks intrusions have also been reported (89).

MRI in SCA2 shows typical olivopontocerebellar atrophy. The most prominent finding is the pontine atrophy, with flattening of the inferior part. The degree of olivopontocerebellar atrophy correlates with clinical disability, but not with (CAG)n length. CAG repeats correlated with atrophy of the cerebellum, brainstem, pons, and age of onset. Pontine atrophy correlated with saccade velocities preclinically (90).

In patients with spinocerebellar ataxia type 2, Pulst and collaborators identified a (CAG)n repeat expansion located in the 5-prime end of the coding region of the *ATXN2* gene ranging from 33 to 500 repeats leading to a polyQ expansion in mutant ATXN2 (91)**.** Normal alleles contain 31 or fewer CAG repeats. Mutable normal alleles, previously called intermediate alleles, are not associated with clinical manifestations, but can be meiotically unstable, resulting in expansion of the allele size on transmission to offspring. Full penetrant alleles contain 32 or more CAG repeats without CAA interruption. Alleles of 32 and 33 CAG repeats are considered of "late onset" (after age 50 years). The most common disease-causing alleles are 37 to 39 repeats. Extreme CAG repeat expansion (>200) has been reported (92).

SCA2 has a large worldwide geographical distribution and represents the most prevalent type of the polyQ ataxias in Cuba, India, Mexico, and southern Italy (93). The largest prevalence rates of SCA2 are found in Cuba because of a prominent founder effect, and the highest case frequency is found in the Cuban Holguin province, with 40.18 cases and 182.75 carriers per 100,000 inhabitants (83). Survival studies in SCAs have shown that survival rate in SCA2, as well as prevalence, depends on the geographical location and ethnical groups. Thus, longer survival is found in southern Italy (67 years), whereas in Spanish and Cuban groups, the survival rate is considerably less; 54 and 52 years respectively (93).

Brain damage in SCA2 is similar to SCA1 presenting with atrophy in of the cerebellum, frontal cerebral lobe, pons, medulla oblongata, and cranial nerves as well as depigmentation of substantia nigra (94). Brains also exhibit neurodegeneration in the cortical somatomotor, visual, somatosensory, oculomotor, ingestion-related, vestibular, and precerebellar systems. Furthermore, myelin loss and atrophy may be present in many brain fiber tracts. Some studies reported neuronal ATXN2 intranuclear inclusions occurring in degenerated and spared brain regions (95).

Aggregation, oxidative stress, disturbed cell signalling, dysregulation of calcium homeostasis, abnormal autophagy, and impaired DNA processing all seem to be involved in SCA2 molecular pathogenesis (96).

### 6.3. Spinocerebellar ataxia type 3 (SCA3) [OMIM # 109150]

The neurodegenerative disorder SCA3 was first recognized in the 1970s in several families of Azorean descent as a heritable "ataxia-plus" disorder with overlapping clinical and pathological characteristics. Two of the identified families presenting with this dominantly inherited ataxia were descended from William Machado and Antone Joseph, leading to the disease designation Machado-Joseph Disease (MJD) (97). Symptoms onset in SCA3 typically begins in adulthood between the third to fifth decade of life and progresses slowly with age (98). SCA3 patients exhibit a wide range of progressive motor impairments, including prominent cerebellar ataxia with abnormal gait, impaired balance, limb incoordination, dystonia, spasticity, dysarthria, dysphagia, and oculomotor abnormalities (99). Parkinsonism with or without tremor also occurs in a subset of SCA3 patients (100). Though the severity and rate of decline varies across SCA3 patients, failure in brainstem-associated functions usually leads to death within 10-15 years of symptom onset (101).

Motor nerve conductions display normal or moderately reduced NCVs and reduced CMAP amplitudes in SCA3 patients with reduced SNAP amplitudes, neurogenic damage, abnormal BAEP and MEPs (102). Hotson reported that the P40 was prolonged or absent in 4 out of 7 SCA3 cases (103) and Kondo found abnormal SSEP in all SCA3 patients examined (104).

Ocular movements are often abnormal. Saccades can be slow because of the degeneration of brainstem excitatory and inhibitory burst neurons but velocity can be also normal or increased (54). Saccadic dysmetria, complete ophthalmoplegia, gaze paralysis, vestibulo-ocular reflex and/or gaze-evoked nystagmus have often been reported (105).

MRI studies of presymptomatic patients demonstrated decreases in white matter volume, mainly in the cerebellar peduncles, and also volumetric reduction of the midbrain, spinal cord, and substantia nigra. In early disease stages, atrophy of the cerebellar vermis and hemispheres, pons, brainstem, and the middle cerebellar peduncles were noted. The enlargement of the fourth ventricle is a common neuro radiological finding in SCA3 (90).

In 1993, the genetic mutation causing SCA3 was mapped to chromosome 14q32.1 independently by one group studying the Azorean linked MJD lineages and another European group which had designated the disease SCA3 after discovering that the genetic locus in families exhibiting similar symptoms to SCA1 and SCA2 was distinct from those two previously identified (106,107). In 1994, cloning of the SCA3 and MJD genetic loci identified the same polyQ-encoding CAG trinucleotide expansion, leading to convergence of these diseases into a single allelic disorder, referred to here as

SCA3 (108). The same single locus at 14q32.1 was demonstrated to be responsible for both spinocerebellar ataxia forms (109).

SCA3 brain degeneration is characterised by cerebellar, pons, medulla oblongata and medial cerebellar peduncle atrophy as in the cranial nerves III to XII, with depigmentation of the substantia nigra. Neuronal loss occurs in the cortical nuclei of the somatomotor, sensory, oculomotor, ingestion-related, vestibular and precerebellar brainstem systems (94,110). The dopaminergic, cholinergic, noradrenergic (locus coeruleus) and GABAergic neurotransmitter systems also exhibit neuronal deficits. Reactive astrogliosis is present in the affected brain regions while nuclear inclusions are observed in a large number of grey brain components with up-regulated microglial cells in degenerated nuclei (110).

The CAG repeat expansion in SCA3 resides within exon 10 of the *ATXN3* gene (108). In healthy individuals, this CAG repeat ranges from 12 to 44, whereas in affected individuals the CAG repeat ranges from around 56 to 87 (111). Individuals harbouring CAG repeat lengths ranging from 45 to 55 present incomplete penetrance of SCA3 symptoms (112). As with the other polyQ diseases, the CAG repeat length inversely correlates with age of disease onset and directly correlates with severity of disease (111). Therefore, SCA3 also exhibits anticipation, a phenomenon shared across most polyQ diseases (113).

SCA3 disease is the most common dominantly inherited form of ataxia, affecting approximately 1:50,000-100,000 people (114). While Portuguese SCA3 families have been shown to arise from two independent haplotypes, it has been established that the majority of SCA3 families worldwide result from one intragenic haplotype (115). The greatest SCA3 prevalence reported in East Asian countries include China, Japan and Taiwan, as well as Portugal and Brazil (66).

ATXN3 participates in various ubiquitin-dependent pathways to maintain protein homeostasis. ATXN3 has also been implicated in endoplasmic reticulum-associated degradation, aggresome formation and DNA repair, among other pathways. In all these processes, ATXN3 acts through ubiquitin-dependent functions (99).

### 6.4. Spinocerebellar ataxia type 4 (SCA4) [OMIM % 600223]

The SCA4 phenotype consisted of ataxia with the invariant presence of a prominent axonal sensory neuropathy. Disease onset was typically in the fourth or fifth decade, but age at onset ranged from 19 to 59 years, with a median age at onset of 39 years. Electrophysiological studies identified absent sural sensory responses in twelve SCA4 cases with radial sensory responses absent in 3 cases (116).

By linkage analysis of a Utah kindred with autosomal dominant SCA with sensory neuropathy, Flanigan and collaborators identified a candidate disease locus, termed SCA4, on chromosome 16q

(116). Hellenbroich and collaborators also identified by linkage analysis a German family with autosomal dominant SCA a 3.69-cM candidate region on chromosome 16q22 presenting with cerebellar ataxia with limb dysmetria, dysarthria, and cerebellar atrophy, as well as sensory neuropathy with hypo- or areflexia, decreased sensation, and absent sural sensory nerve action potentials. The mean age at onset was 38.3 years (range 20 to 61), and suggested genetic anticipation (117). Nowadays, the molecular defect remains to be identified.

Macroscopic observation of SCA4 brains revealed atrophy of the cerebellar vermis and the dorsal columns, while microscopical investigation revealed neuronal loss in Purkinje cell layer and deep nuclei as well as in the midbrain, pons and the medulla oblongata (118).

### 6.5. Spinocerebellar ataxia type 5 (SCA5) [OMIM # 600224]

The clinical symptoms of SCA5 progress over time and include incoordination of the extremities, slurred speech, and gait ataxia. The mean age at onset is 33 years and is predominantly an adult-onset ataxia. Cases have presented as early as 5 years with ataxia (119,120). SCA5 is a relatively pure cerebellar disorder, with little brainstem or spinocerebellar tract involvement does not shorten lifespan and has a relatively mild disease course, likely due to the absence of bulbar paralysis in adult-onset patients (121). Downbeat nystagmus or GEN and, more rarely, saccadic dysmetria and saccade slowing constitutes the most common oculomotor abnormalities (122). MRIs in SCA5 patients showed a marked global cerebellar atrophy (121).

By linkage analysis in a large American family with SCA, Ranum and collaborators mapped the SCA5 disease locus to the centromeric region of chromosome 11 (123). In 2006 Ikeda and collaborators identified mutations in *SPTBN2* gene in affected individuals from an 11-generation American kindred descended from President Lincoln's grandparents whose spinocerebellar ataxia mapped to chromosome 11q13, as well as in two additional families (48).

Shotgun sequencing of constructed BAC clones revealed a 39-bp deletion in exon 12 of the *SPTBN2* gene which causes an in-frame 13 amino acid deletion within the third of 17 spectrin repeat domains. A 15-bp deletion in exon 14, also causing an in-frame deletion in the third spectrin repeat, was identified in a French family. Besides, affected members of the German family have a T-to-C transition mutation in exon 7 that causes a leucine-to-proline change in the calponin homology domain, a highly conserved domain that is involved in binding to both actin and dynactin (48). Recently, heterozygous missense variants of *SPTBN2* were described as a frequent cause of congenital cerebellar ataxia (124).

Despite recent NGS diagnostic implementation, *SPTBN2* mutation frequency associated with SCA5 is still unknown.

The molecular mechanisms involved in the pathogenesis of SCA5 include protein stabilization and glutamate signalling pathway and has been suggested that vesicle trafficking may be disrupted (125).

### 6.6. Spinocerebellar ataxia type 6 (SCA6) [OMIM # 183086]

Clinically, SCA6 is characterised by pure cerebellar dysfunction, slowly progressive unsteadiness of gait and stance, slurred speech, and abnormal eye movements with late onset. The range in age of onset is from 19 to 71 years, with a mean age of onset between 43 and 52 years (126).

Electrophysiological studies revealed reduced CMAP and longer latency of wave I and III mean amplitudes in BAEPs from SCA6 patients (127). In contrast, van de Warrenburg and collaborators reported only electrophysiological abnormalities in one 72-year-old patient from seven studied cases (128).

Most SCA6 cases exhibited spontaneous and positional downbeat nystagmus and altered head-shaking nystagmus with ocular movements speed generally preserved (50). Saccades may show variable dysmetria, likely due to impairment of cerebellar fastigial nuclei (129), while ophthalmoparesis is rare (89). Diverse kinds of nystagmus can be encountered in SCA6: downbeat, upbeat, GEN, PAN, and pendular (89,129). The main neuroradiological abnormalities are cortical cerebellar vermis and hemisphere atrophy, with less pronounced atrophy of the pons, middle cerebellar peduncle (MCP), and red nucleus (90).

Zhuchenko and collaborators performed a genotyping survey using polymorphic CAG repeats and DNA samples from patients with late-onset neurogenic diseases and found an expansion of a CAG repeat in the human alpha-1A-voltage-dependent calcium channel gene (*CACNA1A*), which maps to 19p13. In eight families, the CAG repeat expansion of *CACNA1A* gene was identified as the mutation mechanism causing SCA6 (130). SCA6 is only caused by an expanded CAG repeat in exon 47 of the *CACNA1A* gene. This CAG repeat is polymorphic, being in the range of 4–18 in normal alleles, and expanded to 19–33 in individuals with SCA6 (126).

The frequency of SCA patients with SCA6 seems to vary by geographical area, presumably relating to founder effects. SCA6 is the third most common SCA genotype worldwide and represents 10–30% of families with SCA in Germany, the Netherlands, the United Kingdom, Taiwan, Australia, the USA and Japan (131,132).

The pathological alterations in the brain of SCA6 patients are confined to the cerebellum with white matter affectation, being less severe than in SCA1, SCA2, SCA3 or SCA7. Only some areas of the brain related to cerebellothalamocortical motor loops present neuronal loss (133). Additionally, sensory, oculomotor, ingestion-related, vestibular and precerebellar systems could present neuronal

loss. Reactive astrocytes were detected in grey components with cytoplasmic CACNA1A aggregates (134).

While there is some support for the view that SCA6, like many other *CACNA1A* disorders is a channelopathy, the identification of the transcription factor, α1ACT, encoded by a second cistron in the *CACNA1A* gene, a mechanism involving transcription dysregulation mediated by a polyQ-expanded α1ACT protein has become a more likely scenario in the pathogenesis of SCA6 (126).

### 6.7. Spinocerebellar ataxia type 7 (SCA7) [OMIM # 164500]

The hallmark of SCA7 is visual loss due to macular degeneration (pigmentary retinal dystrophy), which leads to progressive and irreversible blindness (135). Other main symptoms of SCA7 are gait and stance ataxia which are often accompanied by dysphagia. Additional symptoms include spastic ataxia, intentional tremors, slow eye movement, ophthalmoplegia, as well as pyramidal signs (136).

Various results were reported from SCA7 patients studies, with some of them showing abnormal electrophysiology (128), while other patients from different studies showed a normal electrophysiological profile (137). Schols and collaborators found that visual potentials recede in SCA7 mainly due to retinal degeneration, and that reduction of P100 occurred in all SCA7 cases (67).

Involvement of the visual system with pigmentary retinal dystrophy is frequent and a typical feature of the disease (138). Saccades can be slow with increased latency, progressing to ophthalmoparesis, though nystagmus has been rarely reported (139).

The main NR findings in SCA7 are pontocerebellar atrophy, with greater involvement of the pons than in the other SCAs. Cerebellar atrophy correlates with disease progression (90). SARA scores are inversely correlated to cerebellar volume, mainly due to atrophy of white matter of the hemispheres, and also some cortical fields (90).

In 1995, Gow and collaborators mapped SCA7 to chromosome 3p14–21.1 in four ataxia kindreds with dominantly inherited ataxia and macular degeneration (135). Using a monoclonal antibody recognizing expanded polyglutamine stretches, Trottier and collaborators also demonstrated a 130-kDa protein in 2 unrelated patients with SCA7 (140). Later, in 1997, David and collaborators identified an expanded CAG repeat in the *ATXN7* gene in 18 patients from 5 families with SCA7. In SCA7 patients CAG repeat size was highly variable, ranging from 38 to 130 repeats, whereas on normal alleles it ranged from 7 to 17 repeats (141). A correlation existed between number of repeats and phenotype; as for 59 or under, the onset is purely cerebellar, while above 59, the disease starts with visual impairment (142).

SCA7 was estimated to account for 1–11.7% of SCAs in diverse populations. The frequency of SCA7 is higher where local founder effects were observed as in Scandinavia, Korea, South Africa and Mexico (143).

SCA7 neuropathology is characterised by the distinctive progressive retinal degeneration with loss of photoreceptors and damage to the retinal pigment epithelium, although brain damage is very similar to SCA1, SCA2 and SCA3 pathology (144). The cerebellothalamocortical and basal ganglia-thalamocortical loops of the somatomotor system together with visual, auditory and somatosensory systems present with severe neuronal loss. This neuronal loss may also be present in the oculomotor nuclei, ingestion-related, vestibular or precerebellar brainstem systems. Myelin loss and atrophy could also be present in cerebellar white matter, corpus callosum, lateral lemniscus, oculomotor and abducens nerves, pontocerebellar and olivocerebellar fibers, trapezoid body, cuneate and gracile fascicles, internal arcuate fibers, and spinocerebellar tracts. Reactive astrocytes were also detectable and retinal cells could exhibit ATXN7 nuclear inclusions (144).

ATXN7 is a component of the SAGA histone acetyltransferase complex. Polyglutamine expansion disrupts the activity of the SAGA histone acetyltransferase, resulting in aberrant chromatin acetylation and marked changes in gene expression (145). Moreover, the interaction S4 subunit of the proteasome complex and the polyglutamine expansion within ataxin-7 alters its protein degradation (146).

### 6.8. Spinocerebellar ataxia type 8 (SCA8) [OMIM # 608768]

Spinocerebellar ataxia type 8 (SCA8) is an autosomal dominant cerebellar ataxia showing progressive, relatively pure cerebellar ataxia. Onset of symptoms range from age 18 to 65, with a mean of 39 years. Gait instability and dysarthria are common initial symptoms. Clinical findings include gait ataxia, nystagmus, cerebellar dysarthria, incoordination of limb, hyperactive tendon reflexes and spasticity (147). Gasser *et al.* reported SCA8 to be associated with sensory or sensorimotor axonal neuropathy (148). Ocular motor examination revealed saccadic dysmetria, more rarely slow saccades or ophthalmoparesis. GEN may be encountered, and fixation is usually disturbed by pendular alternating nystagmus. Diplopia is often complained by patients (149). MRI and CT have consistently shown cerebellar atrophy, specifically in the cerebellar hemisphere and vermis in individuals with SCA8 (150).

In eight pedigrees with autosomal dominant spinocerebellar ataxia, Koob and collaborators identified a CTG repeat expansion in the *ATXN8OS* gene, which was found to be transcribed into an mRNA with an expanded CUG repeat in its 3-prime UTR (151). The corresponding CAG repeat expansion in the 5-prime-to-3-prime orientation of the *ATXN8* template strand was determined not to be translated into a polyglutamine-containing protein. In the largest pedigree, which included affected

members spanning at least four generations, repeat length ranged from 107 to 127 CTG repeats. However, 20 unaffected individuals also carried expanded repeats (151). Although linkage, haplotype and experimental data show that expansions in *ATXN8* cause SCA8, these expansions show reduced penetrance compared with expansions in other SCA disease genes. Thus, some individuals carrying an expansion in *ATXN8* never develop ataxia (152). The CTG repeat expansion in SCA8 is transcribed in both directions, and transcription of the antisense strand of DNA results in a CAG repeat. Although SCA8 is not a polyglutamine disorder, its antisense strand can be translated via repeat associated non-ATG (RAN) translation to generate a polyglutamine-containing protein (10). Normal alleles contain 15 to 50 repeats, expanded alleles contain 71 to more than 1,300 repeats (153).

The SCA8 form of ataxia is thought to account for 2%-5% of autosomal dominant forms of inherited ataxia. The prevalence of the disease is far lower than the prevalence of abnormal ATXN8OS/ATXN8 expansions because of the reduced penetrance of the expanded allele. Most of the expansions found in control groups are either in repeat ranges that are less penetrant or at the lower end of the expansion range (50-100 combined repeats), or are very large expansions (>500 repeats) (153,154).

Described SCA8 neuropathology is characterised by atrophy of the cerebellum, depigmentation of the substantia nigra and a severe loss of Purkinje cells with the remnants presenting atrophy with granular clusters in the cytoplasm (155). There is also a striking loss of neurons in the pars compacta and the inferior olivary nucleus. Positive 1C2 intranuclear immunoreactivity observed in cerebellar Purkinje cells and medullar neurons is attributed to reverse poly-CAG transcription (156).

The bidirectionally transcribed CTG-CAG expansion results in the in vivo accumulation of CUG RNA foci, an ATG-initiated polyGln and a polyAla protein expressed by repeat-associated non-ATG (RAN) translation. Novel toxic SCA8 RAN polySer protein has been described that accumulates in SCA8 patient autopsy tissue. This SCA8 RAN polySer protein accumulates in white matter regions that show demyelination and axonal degeneration. Thus, these data suggest a model in which a novel RAN polySer protein causes white matter abnormalities that contribute to SCA8 and demonstrate that RAN protein levels can be modulated independent of AUG-initiated proteins (157).

### 6.9. Spinocerebellar ataxia type 9 (SCA9) [OMIM % 612876]

Higgins described a large multigenerational American family of British origin with autosomal dominant spinocerebellar ataxia in affected individuals with adult-onset ataxia, sometimes accompanied by ophthalmoplegia, dysarthria, pyramidal tract signs, weakness, extrapyramidal signs, and posterior column signs. Brain MRI of three patients showed cerebellar atrophy (158). No genetic studies have been reported to date for this ataxia subtype.

### 6.10. Spinocerebellar ataxia type 10 (SCA10) [OMIM # 603516]

SCA10 was first described in Mexico in ataxia patients with epileptic seizures (159). In southern Brazil, however, this characteristic is absent, and the main phenotype is pure cerebellar ataxia. Additional symptoms such as ocular dyskinesia, pyramidal signs, cognitive impairment, and behavioural disturbances can be found. Ocular motor involvement is wide with saccades found generally hypometric. GEN is described and fixation may be disturbed by square wave oscillations (160). Neuroradiological imaging revealed predominant atrophy of the cerebellar hemispheres and the vermis (161).

By a genome-wide linkage analysis of a family with SCA, Zu and collaborators identified a candidate 15-cM region, designated *SCA10*, on chromosome 22q13. Anticipation was observed in the available parent-child pairs, suggesting that nucleotide repeat expansion may be the underlying mutagenic mechanism (162). In 2000, Matsuura and collaborators identified an expansion of a pentanucleotide (ATTCT) repeat within intron 9 of the *ATXN10* gene in all affected patients from five Mexican families with SCA10 (163).

The number of $(ATTCT)_n$ repeats commonly found among different populations ranged from 10 to 29, whereas the pathological expanded alleles ranged from 800 to 4500 repeats in affected patients. Furthermore, the intermediate size alleles of repeats 280 to 850 exhibited reduced penetrance (164). The exact prevalence of SCA10 is unknown.

The neuropathological feature in SCA10 is Purkinje cell loss with symmetrical atrophy in cerebellar hemispheres with less vermis affectation (165).

The pathogenic RNA including expanded r(AUUCU) repeats, located within intron 9 of ataxin 10. *ATXN10* mRNA, sequesters proteins including hnRNP K (166). Sequestration of hnRNP K results in aberrant splicing of transcripts, mitochondrial translocation of PKC$\delta$ and caspase-3 activation, leading to apoptosis.

### 6.11. Spinocerebellar ataxia type 11 (SCA11) [OMIM # 604432]

Spinocerebellar ataxia type 11 (SCA11) is characterised by progressive cerebellar ataxia and abnormal eye signs (167). Pyramidal features are seen on occasion. Peripheral neuropathy and dystonia are rare. Six families have been reported to date, one each from the UK, Pakistan, France, Germany, Denmark, and China. Age of onset ranged from early childhood to the mid-40s. Life span is thought to be normal. Oculomotor examination shows pursuit impairment, GEN, or downbeat nystagmus, as well as saccadic abnormalities (168). Brain MRI examination shows mild-to-severe atrophy in both cerebellar hemispheres and the vermis. The brain stem and cerebrum were normal in most individuals (169).

Using a genome-wide linkage strategy in one British family with autosomal dominant cerebellar ataxia, Worth and collaborators defined a 7.6-cM interval in 1999, assigning the disease locus as SCA11, to chromosome 15q14-q21.3 (170). Houlden and collaborators further localised the SCA11 locus to a 5.6-cM region containing 134 genes. They analysed the gene encoding tau tubulin kinase-2, *TTBK2*, and found a 1-base insertion of an adenosine in exon 13. In a second family with pure ataxia, they found a frameshift deletion of 2 bases (GA) in exon 13 of *TTBK2* (171). One missense variant has been recently described in the Chinese population (172). Prevalence is unknown but SCA11 is a rare cause of pure spinocerebellar ataxia.

SCA11 post-mortem neuropathological studies revealed loss of Purkinje and granular cells and neuronal loss in the dentate nucleus together with extensive Tau aggregation in brain (171).

TTBK2 is a serine/threonine kinase, tau tubulin kinase 2, that is essential for initiating the assembly of primary cilia in the embryo and has been hypothesized that the SCA11-associated mutations disrupt the function of TTBK2 in cilia formation (173).

### 6.12. Spinocerebellar ataxia type 12 (SCA12) [OMIM # 604326]

SCA12 is clinically characterised by unusual tremor and a possible later onset of dystonia, subtle parkinsonian features, gait ataxia, and cognitive decline. Age at onset ranges from 8 to 56 years, but the disease usually manifests in the fourth decade of life (174). Gasser and collaborators reported SCA12 to be associated with sensory or sensorimotor axonal neuropathy with reduced SNAP amplitudes (148). Typical oculomotor abnormalities include dysmetric saccades, impaired pursuit, and cerebellar nystagmus (175). Brain imaging typically reveals both cerebral and cerebellar atrophy with relative sparing of brainstem, thalamus, and basal ganglia (176).

In 1999 Holmes and collaborators used repeat expansion detection (RED) to identify an expanded CAG repeat located in the phosphatase 2 regulatory subunit Bβ (*PPP2R2B*) gene in an ataxic proband and other affected family members of an American kindred of German descent (177). The *PPP2R2B* gene encodes a brain-specific regulatory subunit of the protein phosphatase PP2A. and maps to 5q31-q33 (177). SCA12 alleles ranged from 9 to 24 CAG repeats, with 10 CAG repeats being most frequent (60%) (178).

Despite SCA12 is a rare cause of spinocerebellar ataxia worldwide (179), is the second most frequent form of autosomal dominant cerebellar ataxia (16%) in India. Reported Indian cases of SCA12 have been traced back to a common founder endogamous ethnic group, the Agrawals, originating from northern India (180). However, there are several other reports identifying American, Italian and Chinese SCA12 cases (181).

Microscopic observations of SCA12 brains reported neuritic plaques in the frontal and parietal cortex and neurofibrillary tangles in the subiculum. SCA12 brains presented a focal median gliosis in the thalamus with a moderate loss of Purkinje cells in the vermis and cerebellar hemispheres (182). Ubiquitin staining revealed large intranuclear inclusions in morphological normal neurons from substantia nigra pars compacta (SNpc) (182).

The *SCA12* CAG repeat expansion is not thought to encode polyglutamine because the repeat is located in the 5′ untranslated region of the gene. However, this possibility has not been formally ruled out. Alternatively, the repeat might affect the expression of the gene product of *PPP2R2B*, a brain-specific regulatory subunit of protein phosphatase 2A (183).

### 6.13. Spinocerebellar ataxia type 13 (SCA13) [OMIM # 605259]

Spinocerebellar ataxia type 13 (SCA13) includes a distinctive phenotypic spectrum consisting of either non-progressive infantile-onset ataxia and progressive childhood-onset or adult-onset cerebellar ataxia (184). Two different missense mutations in *KCNC3* have been associated with childhood (p.Arg423His) and adult (p.Arg420His) onset (185). Additionally, an small in-frame deletion (p.Pro583_Pro585del) has been related to adult-onset progressive SCA13 with spasticity (186). Gaze evoked nystagmus is the only oculomotor abnormalities described so far in SCA13 phenotypes (187). Neuroimaging shows usually cerebellar hypoplasia for the early-onset subtypes and progressive cerebellar atrophy for the adult onset (188).

By genome-wide analysis of a French family with SCA, Herman-Bert and collaborators found significant evidence for linkage to an 8-cM interval on chromosome 19q13.3-q13.4 (189). Waters and collaborators found linkage to a 4-cM region overlapping with the *SCA13* locus (190) and identified an heterozygous mutation in the *KCNC3* gene in affected members from a Filipino family and a different mutation in a French family (191).

*SCA13* mutations localise to different positions in the protein structure and display allelic heterogeneity with variations in age of onset, progression, and molecular and electrophysiological properties (186).

It has been proposed that *SCA13* mutations impair the firing properties of fast-spiking cerebellar neurons and interfere with the capacity of cerebellar neurons to handle oxidative stress (191).

### 6.14. Spinocerebellar ataxia type 14 (SCA14) [OMIM # 605361]

Spinocerebellar ataxia type 14 (SCA14) is characterised by slowly progressive cerebellar ataxia, dysarthria, and nystagmus. Axial myoclonus, cognitive impairment, tremor, and sensory loss may also be observed. Parkinsonian features including rigidity and tremor have been described in some

families. Findings seen in other ataxia disorders as dysphagia or dysphonia, may also occur in SCA14. The average age of onset is in the 30s, with a range from childhood to the seventh decade. Life span is not shortened (192). Ocular motor examination shows GEN, square wave jerks intrusions, and, occasionally, slow and hypometric saccades (188). Brain MRI in all affected patients showed mild-to-moderately severe cerebellar atrophy and mild cerebral atrophy reported in some elderly individuals (193).

Yamashita and collaborators performed a systematic linkage analysis in a three-generation Japanese family with a locus (SCA14) to a 10.2-cM interval on chromosome 19q13.4-qter (194). In an affected member of an SCA14 family described by Brkanac and collaborators (195), and in two additional ataxia families, Chen and collaborators identified 3 different mutations in the *PRKCG* gene, each of which resulted in a nonconservative missense mutation in a highly conserved residue in C1, the cysteine-rich region of the kinase C-gamma protein (196). Several other studies reported additional missense mutations and in-frame deletions in the *PRKCG* gene with one nonsense mutation recently described in two Japanese patients (197).

SCA14 has a frequency of less than 1% of all autosomal dominant ataxias, and it has been identified in families from Europe, North America, Japan and Australia. (13).

Neuropathology in a SCA14 patient with the missense p.His110Glu mutation revealed Braak II / III neurofibrillary Alzheimer type pathology and mild cerebrovascular disease (198). Several loss of Purkinje cells in all cerebellar hemisphere lobes was present together with Bergmann gliosis.

In vitro experiments on multiple pathogenic missense variants in *PRKCG* demonstrated cytotoxic aggregations in the cytoplasm of primary Purkinje cells and mammalian cell lines, altered kinase activity, impaired ubiquitination, altered substrate specificity followed by cell death (199–202). Takahashi and collaborators suggested that PKCγ could form amyloid-like fibrils in physiological and/or pathophysiological conditions characterizing PKCγ as an amyloidogenic protein (203).

### 6.15. Spinocerebellar ataxia type 15 (SCA15) [OMIM # 606658]

Spinocerebellar ataxia type 15 (SCA15) is characterised by slowly progressive gait and limb ataxia, often in combination with ataxic dysarthria, titubation, upper limb postural tremor and mild hyperreflexia. Onset is between ages seven and 72 years, usually with gait ataxia but sometimes with tremor. Affected individuals remain ambulatory for ten to 54 years after symptom onset. Mild dysphagia usually after two or more decades of symptoms has been observed in members of multiple affected families and movement-induced oscillopsia has been described in one member of an affected family (204). Saccades may sometimes be mildly hypometric. Pursuit and vestibulo-ocular reflex can be impaired. Approximately 80% of affected individuals have GEN (205). Neuroimaging typically reveals atrophy of the rostral and dorsal vermis of the cerebellum. The cerebellar hemispheres may

appear normal or be mildly atrophic. The brain stem and cerebral hemispheres are unaffected (204,206).

Storey in 2001 (207) and Knight in 2003 (208) found linkage to an 11.6-cM region on chromosome 3pter-p24.2. Mutation analysis excluded the *ITPR1* gene from being involved in the pathogenesis of the disorder. Thereafter, Van de Leemput and collaborators identified heterozygous deletions involving the *ITPR1* gene in affected members of three unrelated families with autosomal dominant spinocerebellar ataxia (209), including the SCA15 family of Australian origin used to map the locus by Storey and Knight. Using high-density genome-wide SNP genotyping, Van de Leemput identified a large deletion removing the first three exons of the *SUMF1* gene and the first 10 exons of the *ITPR1* gene. Affected members of two additional families were found to have even larger deletions removing exons 1-44 and 1-40 of the *ITPR1* gene, respectively. Other studies latterly reported missense mutations associated with SCA15/16 (210). Heterozygous missense mutation in the *ITPR1* gene can also cause SCA29, which is distinguished by onset in infancy of delayed motor development followed by nonprogressive ataxia and mild cognitive impairment.

Reported frequencies of the deletion were 1.8% of autosomal dominant SCAs in Germany, 3.2% of all SCAs in Australia, 1.8% of autosomal dominant SCAs in France and 3.3% in Italy. In contrast, *ITPR1* deletion was very rare (0.3% ) in a Japanese cohort of patients (211).

Both loss-of-function and gain-of-function *ITPR1* mutations have been reported resulting in reduced $Ca^{2+}$ or enhanced $Ca^{2+}$ release respectively (212,213).

### 6.16. Spinocerebellar ataxia type 17 (SCA17) [OMIM # 607136]

Spinocerebellar ataxia type 17 (SCA17) is characterised by ataxia, dementia, and involuntary movements, including chorea and dystonia. Psychiatric symptoms, pyramidal signs, and rigidity are common (214). The age of onset ranges from three to 55 years. Individuals with full-penetrance alleles develop neurologic and/or psychiatric symptoms by age 50 years. Ataxia and psychiatric abnormalities are frequently the initial findings, followed by involuntary movement, parkinsonism, dementia, and pyramidal signs. Manganelli's electrophysiological studies found that all seven SCA17 studied were free from signs of peripheral nerve damage presenting abnormal BAEPs with prominent absence of III and IV/V waves (215). Prolonged CMCT was also found in SCA17 cases, but only in the lower limbs and high incidence of severe SSEP abnormalities displaying absence of P14 and P31 waves was reported (215). Ocular motor abnormalities have often been reported as saccadic hypometria, smooth pursuit initiation and maintenance, increased latency and decreased acceleration, GEN, rebound, and downbeat nystagmus (216). Brain MRI showed variable atrophy of the cerebrum, brain stem, and cerebellum (214).

The case reported in 1999 by Koide and collaborators was associated with expansion of the CAG repeat in exon 3 of the *TBP* gene (196). The gene encoded 63 glutamines, far exceeding the range in normal individuals (25 to 42 in Caucasians; 31 to 42 in Japanese). In the families reported by Zuhlke and collaborators expanded (CAG)n alleles of the *TBP* gene ranged between 50 and 55 residues in affected individuals. This expansion may have contributed to the earlier age at onset in the daughter. In the other family, the (CAG)n element was combined with CAA repeats, which had not been described for polyglutamine expansions in other genes (217). The clinical features correlated with the length of the polyglutamine expansion but were not absolutely predictive of the clinical course (214). Fewer than 100 families with SCA17 have been reported worldwide to date.

SCA17 brains show reduced brainstem and cerebellum, with hydrocephalus of the lateral ventricles. Histological studies revealed a reduced cerebellar molecular layer due to the loss of Purkinje cells with empty baskets, axonal torpedoes and unusual dendritic expansions (218). Neuronal loss was also observed in the lower olivary nucleus. The afferent fibers of the dentate nucleus display decreased myelin staining while the efferent fibers are normal. The thalamus exhibited immunoreactivity with ubiquitin, TBP and 1C2 (which stains polyglutamine repeats). Pyramidal neurons from the frontal lobe, and stellate and basket cells from the cerebellar cortex also revealed immunoreactivity to TBP and 1C2 (218).

The TATA- box-binding protein in SCA17, is a key component of the basal transcription machinery in neurons and other cells. Therefore, polyglutamine expansion in this disease protein is likely to perturb the transcriptome in the brain of patients with SCA17 (219).

### 6.17. Spinocerebellar ataxia type 18 (SCA18) [OMIM % 607458]

SCA18 symptoms included features of motor and sensory neuropathy, ataxia, pyramidal tract signs, dysmetria, and muscle weakness (220). Recently, Lin reported a Han Chinese family with SCA18; the family members presented with a slowly progressing gait ataxia, pyramidal tract signs, and peripheral neuropathy (221). Prevalence is unknown albeit SCA18 is a rare cause of spinocerebellar ataxia. In Brkanac *et al*.'s study, SCA18 patients with the mNCV explored, showed normal or mildly slow with occasional prolonged distal latencies with a markedly reduced SNAPs amplitude or no response, and mildly to moderately reduced sNCV (222). GEN is the only oculomotor abnormality so far observed. Examined brain MRIs were normal and did not reveal cerebellar atrophy (221).

By haplotype analysis in a five-generation American family of Irish ancestry, Brkanac and collaborators identified a 14-cM region at 7q22-q32 that segregated with the disorder (222). Latterly in 2009 identified a A-to-G transition at nucleotide 743 that resulted in an isoleucine to valine substitution at codon 172 (p.Ile172Val) in the *IFRD1* gene (220).

No association between identified pathogenic mutations and the molecular pathology triggering the ataxic phenotype has been described to date.

### 6.18. Spinocerebellar ataxia type 19/22 (SCA19/22) [OMIM # 607346]

The SCA19/SCA22 phenotype consists of adult onset and slowly progressive cerebellar ataxia in most cases, frequently with cognitive impairment and variable degree of myoclonus, polyneuropathy, and seizures. Mild parkinsonism has been reported recently in two unrelated French SCA19 families (223). Only 18 SCA19/22 families and sporadic cases of diverse ethnicities have been described to date. Saccades are dysmetric but with normal speed; pursuit are impaired and GEN may occur during gaze-holding (224,225). Brain imaging displayed atrophy of the vermis and in the cerebellar hemispheres, less common cerebral atrophy, and different degrees of white matter hyperintensities (223).

Using a genome-wide screen in the large Dutch ADCA family, Verbeek and collaborators, in 2001, mapped the disorder to chromosome 1p21-q21 (226). Also, by genome wide analysis of a Han Chinese family with ADCA, Chung and collaborators, in 2003, identified a candidate disease locus, termed SCA22 on chromosome 1p21-q23 (225). In 2004, Schelhass and collaborators asserted that the SCA19 and SCA22 loci represented the same disease-causing gene (224). Finally, in 2012, Lee and collaborators identified by exome sequencing a heterozygous 3-bp deletion in the *KCND3* gene, encoding the $K_V$4.3 subunit, in affected members of the previously reported Han Chinese family. The same heterozygous deletion was found in affected members of a French family with autosomal dominant SCA (227).

SCA19/SCA22 neuropathology revealed marked widening of the sulci of the cerebral frontal lobe, enlarged lateral ventricles, pallor of the substantia nigra and atrophy of the cerebellar cortex, moderate neuronal loss in the dopaminergic pars compacta of the substantia nigra. The cerebellar Purkinje cell layer displayed severe neuronal loss with formation of torpedoes in the axons of the remaining Purkinje cells. Neuronal aggregations of hyperphosphorylated tau were identified in the hippocampal and entorhinal areas (206).

Evidence that the mutants instigated anomalous protein biosynthesis and channel gating of KV4.3 was demonstrated by co-expressing $K_V$4.3 wild-type with the disease-related mutants suggesting dominant-negative effects of the mutants on protein biosynthesis and voltage-dependent gating (228).

### 6.19. Spinocerebellar ataxia type 20 (SCA20) [OMIM # 608687]

Spinocerebellar ataxia type 20 (SCA20) is characterised by a slowly progressive ataxia and dysarthria with minor pyramidal signs. Approximately two thirds of those affected cases also display palatal tremor (229). An Australian family of Anglo-Celtic descent is the only family with SCA20 reported

to date (230). Saccades appear hypermetric and pursuit is impaired. Gaze-holding is affected by GEN or downbeat nystagmus, while steady fixation may be disturbed by square wave jerks intrusions (231). Brain MRI showed mild-to-moderate pan cerebellar atrophy and normal cerebrum and brain stem, except for increased inferior olivary T2 signal in those with palatal tremor (230).

By genome-wide linkage analysis, Knight and collaborators identified in 2004 the SCA20 disease locus, in a pericentromeric region on chromosome 11 and noted that the SCA20 candidate region overlaps with the SCA5 locus but detailed molecular analysis in an affected member revealed no pathogenic mutations (232). In 2008, Knight identified a heterozygous 260-kb duplication on chromosome 11q12.2-12.3. The duplicated region was in direct orientation and contains at least 12 genes and being the first spinocerebellar ataxia to implicate a copy number variation (CNV) (229).

No functional studies associated with SCA20 pathology have been reported yet.

### 6.20. Spinocerebellar ataxia type 21 (SCA21) [OMIM # 607454]

SCA21 is characterised by slowly progressive cerebellar ataxia associated with cognitive impairment with an onset in the first decades of life (233).

In 2014, by linkage analysis in a large French family, Delplanque and collaborators found linkage to a 3.58-Mb candidate region on chromosome 1p36.33-p36.32 and identified five missense and one truncating heterozygous mutations in the *TMEM240* gene (233).

A recent study characterised *TMEM240* expression in the cerebellar neuronal network, including neurons of the cerebellar cortex, particularly Purkinje cells and they proposed that TMEM240 may be involved in the organization of the cerebellar network, particularly in synaptic inputs converging on Purkinje cells (234).

### 6.21. Spinocerebellar ataxia type 23 (SCA23) [OMIM # 610245]

The clinical phenotype of SCA23 is highly variable, but its cardinal feature is a late onset, slowly progressive cerebellar ataxia and one patient showed clinical and neuroradiological features similar to multiple system atrophy with predominant parkinsonism (235). Saccades were reported to be dysmetric and with mild reduction of speed. Brain MRIs showed cerebellar vermis and brainstem atrophies (236).

By genome-wide linkage analysis of a large Dutch family in 2004, Verbeek and collaborators identified a candidate disease locus, termed SCA23, on chromosome 20p13-p12.3 (237). Missense mutations in the prodynorphin (*PDYN*) gene were identified in 2010 by Bakalkin and collaborators as causing progressive gait and limb ataxia in four Dutch SCA23 families, including the previously reported family in 2004 (238).

To date, eight SCA23 disease-causing variants in *PDYN* have been identified, six of which lie exclusively within the PDYN Dyn A and Dyn B encoding regions (amino acid residues 207–236) (235). Epidemiological studies corroborate that *PDYN* mutations only account for a small percentage (0.1 %) of European SCA cases (236).

SCA23 neuropathologically revealed cerebrum, cerebellum and brainstem atrophy presenting neuronal loss in dentate nucleus, inferior olive and Purkinje cell layer (237).

Studies in a SCA23 mouse model found pathologically elevated mutant dynorphin A levels in the cerebellum coinciding with transcriptionally dysregulated ionotropic and metabotropic glutamate receptors and glutamate transporters, and altered neuronal excitability (239).

### 6.22. Spinocerebellar ataxia type 24 (SCA24)

Currently none assigned to any locus.

### 6.23. Spinocerebellar ataxia type 25 (SCA25) [OMIM % 608703]

SCA25 phenotype is characterised by cerebellar ataxia with areflexia of the lower limbs and peripheral sensory neuropathy. The age at onset ranged from 17 months to 39 years, although most of affected patients had onset in childhood. Electrophysiological studies revealed normal NCVs in two SCA25 patients, while the CMAP amplitude of one patient's median nerve was mildly reduced. The SNAP was only performed for median nerve and sural nerve, indicating prominent sensory neuropathy. Saccades are hypermetric, of normal speed. Square wave jerk intrusions, GEN, and downbeat nystagmus were reported. Brain imaging showed cerebellar atrophy (240).

The causative SCA25 deficit was mapped to 2p21-p13 in 2005 by Stevanin and collaborators in a large family from South-eastern France (240). To date, the causative mutation has not been yet identified.

### 6.24. Spinocerebellar ataxia type 26 (SCA26) [OMIM # 609306]

SCA26 ataxia is characterised by pure cerebellar signs, including ataxia of the trunk and limbs, dysarthria, and irregular visual pursuit movements (222). Ocular movements show dysmetric saccades, impairment of horizontal and vertical pursuit, and sporadic GEN. MRI showed atrophy of the cerebellum sparing the pons and medulla (222).

By genome-wide linkage analysis of a large family with pure spinocerebellar ataxia, Yu and collaborators in 2005 identified a 15.55-cM candidate disease locus on chromosome 19p13 in affected members of a Norwegian family (241). Molecular studies in the same family in 2012 enabled the

identification of a heterozygous missense mutation in the *EEF2* gene (242). This is the only mutation reported to date.

Functional studies suggested that the mutation disrupted the normal mechanical processes involved in RNA translocation, and indicated that proteostatic disruption causes neurodegeneration (242).

### 6.25. Spinocerebellar ataxia type 27 (SCA27) [OMIM # 609307]

SCA27 cases usually debuts at childhood with all patients suffering from tremor at both hands. Mild unsteadiness and ataxia of the upper limbs begin at age 15 to 20 years. Aggressive outbursts and depression are present in some patients. Some patients also present dyskinesia, mental retardation, and deficits in memory and executive functioning (243). Ocular examination showed dysmetric saccades, disrupted ocular pursuit movements and gaze-evoked nystagmus (243). Two patients showed cerebellar atrophy on MRI (243).

In 2003 Van Swieten and collaborators identified, by combination of genome-wide linkage analysis and whole exome sequencing, a heterozygous frameshift mutation in the *FGF14* gene in a large three-generation Dutch family with 14 members presenting with cerebellar ataxia inherited in an autosomal dominant pattern. To date, nine families and eight single patients with *FGF14* mutations have been reported with a recently interstitial 600 kb deletion identified in SCA27 patients from a Swedish family (244).

Mice models with deletion or knockdown of Fgf14 showed an ataxic phenotype with a reduced number of NaV1.6 channels and a deficit in spontaneous neuronal firing (245,246).

### 6.26. Spinocerebellar ataxia type 28 (SCA28) [OMIM # 610246]

Spinocerebellar ataxia type 28 is characterised by a variable clinical phenotype with slowly progressive unsteady gait, mild cerebellar symptoms, and a variable age of onset from early childhood to the sixth decade (247). Patients with shorter duration of disease prevalently showed cerebellar nystagmus. Those with longer disease duration presented with dysmetric saccades, slow saccades to ophthalmoparesis, palpebral ptosis, pursuit, and optokinetic nystagmus impairment (248). Subjects with SCA28 variably presented with hypometric saccades, saccadic horizontal pursuit, impaired horizontal gaze holding, and superior eyelid ptosis (249). MRI evidenced cerebellar and extraocular muscle atrophies differently contributing to eye movement abnormalities (249).

By genome-wide linkage analysis of a large Italian family, Cagnoli and collaborators in 2006 identified a 7.9-Mb candidate region for the disease locus on chromosome 18p11.22-q11.2 (250). In 2010 Di Bella and collaborators identified five different heterozygous mutations in the *AFG3L2* gene in affected members of five unrelated families with SCA28, including the family reported by Cagnoli et al (251). To date, about 30 different *AFG3L2* variants have been reported in ataxia patients (247).

Cagnoli reported that missense mutations in the *AFG3L2* accounted for around 1.5% of European autosomal dominant cerebellar ataxias (252).

Brain autopsy from a SCA28 patient with a heterozygous deletion of exons 14 to 16 within *AFG3L2* gene revealed severe atrophy of the upper part of the cerebellar hemisphere. In addition, intranuclear inclusions with immunoreactivity to ubiquitin and p62 antibodies were identified in brain and cerebellar cortical neurons, as well as in hippocampal, pontine and medullary nuclei neurons (253).

*AFG3L2* encodes a mitochondrial ATP-dependent metalloprotease (m-AAA protease), which is highly expressed in Purkinje cells and plays a role in protein degradation and regulation of ribosome assembly (251).

### 6.27. Spinocerebellar ataxia type 29 (SCA29) [OMIM # 117360]

Spinocerebellar ataxia type 29 (SCA29) is an autosomal dominant congenital ataxia characterised by early-onset motor delay, hypotonia, and gait ataxia (254). Oculomotor examination showed prevalently GEN and fixation instability (255). MRI showed pure cerebellar atrophy with mainly involvement of vermis (90).

In 2004, by genome-wide analysis of a large kindred with congenital nonprogressive cerebellar ataxia, Dudding and collaborators identified genetic linkage to an 18.9-cM region on chromosome 3p, overlapping with the SCA15 locus (256). By exome sequencing Huang and collaborators in 2012 identified in the same family a heterozygous missense mutation in the *ITPR1* gene. In a Canadian family with a similar disorder they identified a different heterozygous missense mutation (255).

De novo missense variants in *ITPR1*/*SCA29* account for a substantial share of patients with so far unexplained sporadic ataxia, yielding an estimated frequency of 2.5% to 5.5% of sporadic early-onset ataxia in European and North American ataxia families (257).

Ando and collaborators described that SCA29 mutations cause ITPR1 dysfunction by impairing IP3 binding, gating, or carbonic anhydrase-related protein VIII (CA8) mediated regulation. They also suggested that aberrant $Ca^{2+}$ homeostasis could be triggered by abnormal ITPR1 activity contributing to the molecular pathogenesis of SCA29 (254).

### 6.28. Spinocerebellar ataxia type 30 (SCA30) [OMIM % 613371]

The phenotype is characterised by relatively pure, slowly evolving ataxia with mild to moderate dysarthria. In some cases, hyperreflexia at lower limbs was described. At neuro-ophthalmic examination, all patients revealed hypermetric saccades (258). MRI showed pure cerebellar atrophy (90).

By genome-wide linkage analysis in a family presenting with pure cerebellar ataxia, Storey and collaborators identified the SCA30 locus on chromosome 4q34.3-q35.1 (258). To date, the causative mutation has not yet been identified.

### 6.29. Spinocerebellar ataxia type 31 (SCA31) [OMIM # 117210]

SCA31 is a pure cerebellar ataxia, albeit some patients present also with dementia and hearing impairment (259). GEN is the most common eye movement abnormality seen (259). Magnetic resonance imaging showed isolated cerebellar atrophy, most pronounced in the upper vermis (260).

Nagaoka and collaborators in 2000 mapped a locus responsible for what they characterised as a form of pure autosomal dominant cerebellar ataxia to chromosome 16q (261) and Li and collaborators in 2003 identified new polymorphic markers in a restricted area of 16q22.1 of the critical region on eight Japanese families with ADCA type III, including those reported by Nagaoka (262).

In affected patients from 52 unrelated Japanese families with a pure form of cerebellar ataxia mapping to chromosome 16q, Ishikawa identified in 2005 a heterozygous non coding variant in the *PLEKHG4* gene (263).

In 2007 Amino and collaborators identified a Japanese family with autosomal dominant cerebellar ataxia linked to chromosome 16q who did not have the non-coding variant, but carried the common haplotype centromeric to the *PLEKHG4* gene, redefining the disease locus to a 900-kb region (264). Eventually, in 2009 They identified 2.5- to 3.8-kb insertions in all 160 affected individuals from 98 families with SCA31 by Southern blot analysis of the 900-kb critical region (37). PCR amplification followed by sequencing showed that the insertion consisted of a preceding TCAC sequence followed by three pentanucleotide repeat components (TGGAA)n, (TAGAA)n, and (TAAAA)n in all patients tested. The insertions were located within introns of the *BEAN1* and *TK2* genes. The length of the SCA31 insertion was inversely correlated with the age of disease onset (37).

Spinocerebellar ataxia type 31 is the third most common SCA subtype in Japan, and to date only three cases of SCA31 were described in other countries with no SCA31 cases identified in large European and Taiwanese population studies (265).

Neuropathological studies performed in SCA31 patients showed a severe loss of Purkinje cells in the anterior lobe of the cerebellum and dendritic alterations with many somatic sprouts with formation of RNA foci and amorphous protein aggregates, containing ubiquitin, synaptophysin and calbindin (266).

The *BEAN1* transcript of SCA31 mutation was found in SCA31 human brains forming abnormal RNA structures called RNA foci in cerebellar Purkinje cell nuclei. Subsequent RNA pulldown

analysis disclosed that (UGGAA)n binds to RNA-binding proteins and was proposed that TDP-43 binding protein acts as an RNA chaperone against toxic (UGGAA)n (260).

### 6.30. Spinocerebellar ataxia type 32 (SCA32) [OMIM % 613909]

SCA32 is clinically characterised by ataxia, variable mental impairment, and azoospermia in males. There is a broad range of age of onset, particularly among females. Those with onset of ataxia before age 40 years also show cognitive impairment. All affected males were infertile and had azoospermia with testicular atrophy. Brain MRI showed cerebellar atrophy (267).

By genome-wide linkage analysis of a Chinese family with autosomal dominant ataxia and azoospermia, Jiang and collaborators identified linkage to a locus on chromosome 7q32-q33 in 2010 (267). The causative mutation has not been yet identified.

### 6.31. Spinocerebellar ataxia type 33 (SCA33)

Currently, this subtype is pending of assignment.

### 6.32. Spinocerebellar ataxia type 34 (SCA34) [OMIM # 133190]

SCA34 presents with slowly progressive cerebellar ataxia with erythrokeratodermia variabilis (EKV) appearing soon after birth and disappearing with age. Cerebellar syndrome then becomes the predominant feature (268). Brain imaging showed cerebellar and pontine atrophy. In addition, four patients had cruciform hyperintensities (269).

In the initial French-Canadian family, nystagmus was mainly seen. In a Japan family, many patients had GEN (78%), while less commonly, a supranuclear ophthalmoplegia (33%) and impaired smooth pursuit (56%) were observed (188).

By genome-wide linkage analysis Cadieux-Dion in 2014, mapped the candidate region on chromosome 6p12.3-q16.1 and identified by using whole-exome sequencing a missense mutation in the *ELOVL4* gene in affected members of a large French-Canadian family with EKV and ataxia (268).

Since the first identification of *ELOVL4* mutation associated with ataxia, four other families, two of them from Japan and Brazil, were identified to carry missense mutations in the *ELOVL4* gene (270). The Japan variant differed from the Brazilian in the absence of dermatological involvement and the minor severity of ataxia (269).

### 6.33. Spinocerebellar ataxia type 35 (SCA35) [OMIM # 613908]

SCA35 is characterised by gait and limb ataxia, ocular dysmetria, tremor, hyperreflexia and sometimes dystonia. Disease onset ranges from teenage years to late adulthood with a slow

progression. Some cases presented mild mental retardation (271). Patients exhibited dysmetric saccades, sometimes slow, and saccadic pursuit (188). Brain magnetic resonance imaging showed cerebellar atrophy particularly evident in the vermis (272).

By combination of genome-wide linkage analysis and whole exome sequencing of a large Chinese family with autosomal dominant SCA, Wang identified in 2010 an 8.5-Mb locus on chromosome 20p13-p12.2 and a heterozygous missense mutation in the *TGM6* gene. A second unrelated Chinese family with SCA35 was found to carry a different heterozygous mutation (272).

In recent years, another 13 variants were reported in different ethnic groups including Chinese, Asian, European, and Hispanic, but mainly in Asia (273). Although, recent studies identified families with reported *TGM6* variants sharing no feature of SCA35 and demonstrated that the cumulative frequency of *TGM6* reported pathogenic variants is at least 111-fold inflated over disease prevalence indicating a high chance of misdiagnosis or low penetrance (274).

TGM6 wild-type protein mainly localised to the nucleus and perinuclear area, whereas five *TGM6* mutations showed nuclear depletion, increased protein accumulation in the perinuclear area, insolubility and loss of enzymatic function. Aberrant accumulation of these TG6 mutants in the perinuclear area led to activation of the unfolded protein response (UPR), suggesting that specific TG6 mutants elicit an endoplasmic reticulum stress response (275).

### 6.34. Spinocerebellar ataxia type 36 (SCA36) [OMIM # 614153]

SCA36 is clinically characterised by ataxia of late on set with involvement of the motor neuron system, with symptoms similar to amyotrophic lateral sclerosis, and variable severity of tongue atrophy with fasciculation (276). Impaired smooth pursuit and GEN and rarely vertical or horizontal gaze limitation have been observed. Brain MRI shows pancerebellar atrophy, later evolving in to olivopontocerebellar atrophy (277).

By genome-wide linkage analysis followed by candidate gene sequencing and repeat analysis of five Japanese families in 2011, Kobayashi identified a pathogenic heterozygous 6-bp repeat expansion (GGCCTG)n within intron 1 of the *NOP56* gene. Four additional patients with SCA carrying this repeat expansion were identified. The size of expanded alleles ranged from 650 to 2,500 repeats, and there was some evidence for genetic anticipation (276). Garcia-Murias in 2012 confirmed the segregation of the pathogenic expanded GGCCTG repeat in two large kindreds originating from Galicia, Spain (26).

Besides Spain, SCA36 has also been reported in individuals from Italy, France, China, Taiwan, Poland, and the United States (278).

Histopathology studies revealed Purkinje cell loss, especially in the dentate nucleus, and loss of motor neurons in the hypoglossal nucleus in SCA36 Spanish patients (279). In a SCA36 Japanese case neuropathology revealed positive inclusions for ubiquitin and p62 in the cytoplasm of the inferior olivary together with three different types of RNA foci identified in neuronal nuclei of the cerebrum, cerebellum, inferior olive, spinal cord and temporal muscle (280).

Recent functional studies demonstrate that intronic GGCCTG is translated into aggregating dipeptide repeat proteins, including poly(GP) and poly(PR) via repeat associated non-AUG (RAN) translation (278).

### 6.35. Spinocerebellar ataxia type 37 (SCA37) [OMIM # 615945]

During the course of this thesis, by genome-wide linkage analysis of a large Spanish family with late-onset autosomal dominant SCA, our group at the IGTP in collaboration with researchers of IDIBELL in 2013, found linkage to a 0.66-cM interval on chromosome 1p32. Exome sequencing did not identify the causative mutation (281).

Initial clinical information was available for nine affected individuals presenting initial symptoms of increased falls due to gait instability, dysarthria, and clumsiness which appeared at a mean age of 48 years (range, 38-64). Clinical progression was slow, and four patients became wheelchair-bound 10 to 33 years after onset. More variable features included trunk ataxia, dysmetria, and dysphagia. All patients had abnormal ocular movements, consisting mostly of dysmetric vertical saccades and irregular vertical pursuit, and most patients later developed abnormal horizontal pursuit. A few patients had nystagmus. Brain imaging showed cerebellar atrophy with sparing of the brainstem (281).

### 6.36. Spinocerebellar ataxia type 38 (SCA38) [OMIM # 615957]

SCA38 onset ranges between the third and fourth decades. All patients have slowly progressive gait ataxia and some exhibit peripheral axonal neuropathy, *pes cavus* and hyposmia (282,283). Ocular movement abnormalities include slow saccades and GEN. Brain MRI showed cerebellar atrophy (282).

In 2014, by genome-wide linkage analysis in a large Italian family with autosomal dominant SCA, Di Gregorio and collaborators found linkage to a 56.2-Mb interval on chromosome 6p22.2-q14.1 and identified a heterozygous missense mutation in the *ELOVL5* gene (282).

Screening of the *ELOVL5* gene in 456 European probands with SCA identified heterozygous mutations in three additional families and in a French patient with SCA38 (282).

Recently, Gazulla and collaborators reported five members from a Spanish family spanning two generations which developed gait ataxia and intermittent diplopia, presenting with an heterozygous missense variant in the *ELOVL5* gene (284).

Transfection experiments showed that ELOVL5 mutant proteins had a less diffuse ER signal and tended to accumulate in the Golgi apparatus and suggested activation of the unfolded protein response that could lead to apoptosis (282).

### 6.37. Spinocerebellar ataxia type 39 (SCA39)

SCA39 clinical symptoms include cerebellar ataxia, dysmetria, spasticity and dysarthria. Motor impairments from infancy has also been described (285). Electroneuromyography showed a neurogenic pattern and normal conduction velocities. Auditory evoked brainstem potentials were prolonged. In addition to a strabismus, oculomotor signs include saccadic pursuit and horizontal gaze palsy (285).

In 2015, Johnson identified an approximately 7.5-megabasepair duplication on chromosome 11q21-11q22.3 segregating with disease and not found in control individuals. This duplication contained an estimated number of 44 genes (285).

### 6.38. Spinocerebellar ataxia type 40 (SCA40) [OMIM # 616053]

SCA40 clinical features include gait ataxia, wide-base gait, intentional tremor, scanning speech, hyperreflexia, and spastic paraparesis (286). Ocular movement abnormalities included saccadic dysmetria and impaired vertical gaze (188). MRI of the proband's brain showed pontocerebellar atrophy (286).

In 2014, by combination of linkage analysis and whole-exome sequencing, Tsoi and collaborators identified a heterozygous missense mutation in the *CCDC88C* gene in affected members of a family from Hong Kong, China (286).

In 2019 Leńska-Mieciek and collaborators described the first European four-generation Polish family with ataxia, tremor, dementia, and a novel *CCDC88C* gene mutation (287).

Functional studies showed that mutant CCDC88C activated c-Jun N-terminal kinase (JNK) and triggered apoptosis, consistent with a gain of function mutation mechanism (286).

### 6.39. Spinocerebellar ataxia type 41 (SCA41) [OMIM # 616410]

In a 40-year-old man who presented a two-year history of progressive imbalance and gait ataxia, Fogel identified a heterozygous missense mutation in the *TRPC3* gene in 2015 by exome sequencing (288). Brain imaging showed mild atrophy of the cerebellar vermis (288).

In vitro functional expression studies in murine neuroblastoma cells showed that the mutant protein induced neuronal cell death, suggesting a toxic gain-of-function effect (288).

Our group participated in a study that led to evidence showing that the *TRPC3* alternative promoter is a methylation quantitative-trait locus that may be involved in modulating the ataxia phenotype because of an statistical trend for a rare unmethylated homozygous C allele genotype to be present at a higher frequency in idiopathic ataxia patients (289).

### 6.40. Spinocerebellar ataxia type 42 (SCA42) [OMIM # 616795]

Gait instability is the most common manifestation in SCA42, and additional features included dysarthria, saccadic eye movements, diplopia, and nystagmus with some patients presenting pyramidal signs (290). Age of onset is highly variable, although most cases had onset in mid-adulthood. Patients exhibited saccadic pursuit, diplopia, GEN (188). Brain imaging showed cerebellar atrophy of the cerebellar vermis (290).

In 2015, by linkage analysis combined with whole-exome sequencing Coutelier and collaborators identified heterozygous missense mutation in the *CACNA1G* gene in affected members of three unrelated French families (290).

In affected members of two unrelated Japanese families another heterozygous missense mutation in the *CACNA1G* gene were identified in 2017 (291). Recently, Barresi and collaborators described a narrow spectrum of missense mutations in *CACNA1G* and a novel syndrome with infantile-onset cerebellar ataxia (292).

In vitro electrophysiologic studies showed that the mutation results in decreased neuronal excitability and suggested that SCA42 is a channelopathy (290,291).

### 6.41. Spinocerebellar ataxia type 43 (SCA43) [OMIM # 617018]

SCA43 patients presented with cerebellar ataxia, tremor, hyporeflexia and severe peripheral neuropathy (293). Hypometric saccades and inconstant GEN were observed (293). Brain imaging showed moderate cerebellar vermis atrophy (293).

In 2016, by a combination of linkage analysis and whole-exome sequencing, Depondt and collaborators identified a heterozygous missense mutation in the *MME* gene encoding for Neprilysin protein in seven affected members of a large Belgian family (293).

### 6.42. Spinocerebellar ataxia type 44 (SCA44) [OMIM # 617691]

SCA44 patients present with gait ataxia, dysarthria, dysphagia, dysmetria, and dysdiadochokinesis. Some patients had normal reflexes, whereas others showed hyperreflexia and spasticity (30). Variable

ocular movement alterations, mainly saccadic hypermetria and impaired smooth were described (30). Brain imaging showed cerebellar atrophy (30).

In 2017, by whole-exome sequencing, Watson and collaborators identified a heterozygous missense mutation in the *GRM1* gene in affected members of two unrelated families (30). Two additional variants, one missense and one de novo frameshift mutation, were identified in the same study. Biallelic variants in the *GRM1* were previously associated to autosomal-recessive cerebellar ataxia (294).

In vitro functional studies showed that mutations in *GRM1* resulted in a gain of function with excessive mGluR1 signalling and suggested that this would result in increased calcium levels and neuronal excitotoxicity (30).

### 6.43. Spinocerebellar ataxia type 45 (SCA45) [OMIM # 617769]

SCA45 patients were noted to have a relatively pure cerebellar syndrome with limb and gait ataxia, downbeat nystagmus, and dysarthria. Brain MRI shows cerebellar vermis atrophy and hemosiderin deposit on mesencephalon (295).

In 2017, by whole exome sequencing, Nibbeling and collaborators identified a heterozygous missense mutation in the *FAT2* gene in five affected members of a family. A second heterozygous missense mutation was subsequently identified in a sporadic patient (295).

In vitro studies showed that the mutant proteins had significantly increased colocalisation with markers to the Golgi apparatus compared to the wildtype protein, and suggested that the mutations may change cell aggregation and adhesion properties (295).

### 6.44. Spinocerebellar ataxia type 46 (SCA46) [OMIM # 617770]

Affected patients with SCA46 described in 1995 presented with adult-onset sensory ataxic neuropathy with cerebellar signs and variable sensory neuropathy at lower limbs (296). Ocular movement abnormalities included nystagmus, saccadic slowness and dysmetria, and saccadic pursuit (188). Brain imaging did not reveal cerebellar atrophy (296).

In 2017 Nibbeling and collaborators identified by whole-exome sequencing a heterozygous missense mutation in the *PLD3* gene in eight affected members of a family previously described by Van Dijk (295).

In vitro functional expression studies showed that phospholipase D activity of the mutant protein was significantly decreased compared to the wild-type protein (295).

### 6.45. Spinocerebellar ataxia type 47 (SCA47) [OMIM # 617931]

SCA47 late onset ataxic patients developed slowly progressive cerebellar ataxia in their thirties or forties, characterised by gait ataxia, dysmetria, dysarthria, and, in some cases, diplopia (297). Brain imaging showed progressive mild cerebellar vermian atrophy in late onset cases with enlarged fourth ventricle in early-onset patients (297).

By whole exome sequencing in 2018 Gennarino and collaborators identified a heterozygous missense mutation in the *PUM1* gene in affected members of a family. A family member who was unaffected at the age of 80 years, also carried the mutation, indicating incomplete penetrance (297). In the same study, Gennarino *et al.* also reported two unrelated girls with delayed motor development, early-onset ataxia, and short stature with a wide range of neurological alterations and presenting with mutations in the *PUM1* gene (297).

Functional studies demonstrated diverse reduction of PUM1 protein levels consistent with haploinsufficiency (297).

### 6.46. Spinocerebellar ataxia type 48 (SCA48) [OMIM # 618093]

SCA48 is a late-onset cerebellar ataxia associated with gait ataxia, dysarthria, dysphagia, anxiety, deficits in executive function and cognitive-affective symptoms (298). Saccadic dysmetria was the mainly oculomotor abnormality identified. Brain imaging showed selective atrophy of the posterior areas of the cerebellar vermis (298).

In 2018, by combination of whole exome sequencing and linkage analysis, Genis and collaborators identified a heterozygous frameshift mutation in the *STUB1* gene in nine affected members of a multigenerational family from Catalonia (298). Subsequently studies identified 10 *STUB1* pathogenic variants in 10 Italian families (19) and 26 *STUB1* variants in 30 European families (27).

Neuropathological examination showed nearly complete loss of Purkinje cells in the vermis and extensive in the hemispheres with numerous empty baskets, hyperplastic and hypertrophic Bergmann glia and axonal torpedoes in the granular layer. The olive was moderately affected with mild neuronal loss (27).

STUB1 encoded E3 ubiquitin-protein ligase CHIP protein levels were found decreased in the fibroblasts of *STUB1* variant carriers suggesting that the underlying mechanism in SCA48 is haploinsufficiency (27).

### 6.47. Dentatorubral-Pallidoluysian Atrophy (DRPLA) [OMIM # 125370]

DRPLA clinical presentation is frequently heterogeneous with a median onset of 31 years of age. Individuals with younger onsets often present with seizures, and older individuals more commonly present with ataxia and cognitive impairment. The length of the CAG repeat expansion in DRPLA within the *ATN1* gene correlates strongly with age at onset (299).

DRPLA patients exhibit increase of saccadic latency and slow saccades, progressing to palsy. Impairment of smooth pursuit is common, as well as GEN and square wave jerks intrusions (188). Typical MRI findings include cerebellar and brainstem atrophy particularly pontomesencephalic tegmentum (57).

In 1994, Nagafuchi and collaborators mapped the *DRPLA* locus to chromosome 12p by linkage analysis and found that DRPLA patients had an expanded CAG trinucleotide repeat (300). At the same time, Koide identified a candidate gene that contained trinucleotide repeats expressed in human brain and found to show a CAG repeat expansion in 22 individuals with DRPLA (301). Burke *et al.* demonstrated that despite distinct cultural origins and clinical and pathological differences, Haw River syndrome and DRPLA are is caused by the same expanded CAG repeat expansion ranging from 48 to 93 tandem copies in the *ATN1* gene encoding for the atrophin-1 protein (302). Normal alleles range from 6 to 35 CAG repeats. Unstable mutant non-penetrant alleles contain 20-35 CAG repeats and are found in Caucasian populations (299).

DRPLA is most commonly recognised in Japanese population with an incidence of 2–7 per million individuals (299). Within SCA cohorts, the highest frequency of DRPLA is identified among Japanese groups (7–20%), with lower rates in other Asian populations (Singapore, 6%; Korea, 3%). DRPLA is thought to occur at lower rates in non-Asian populations, although these estimates are based on the evaluation of cohorts diagnosed with SCA and may therefore represent an underestimation of DRPLA prevalence. In European populations, DRPLA has a frequency of 0.25–1% in SCA cases of European descent, with higher frequency in Portuguese cohorts (2-4%). In Latin-American SCA cohorts, DRPLA revealed a frequency of 0.14–3.1% (299).

DRPLA is neuropathologically characterised by palladium, subthalamic and dentate nuclei degeneration with moderate red nucleus affection presenting neuronal nuclear inclusion bodies (303). Post-mortem DRPLA brains demonstrated deposition of mutant atrophin-1 protein, from diffuse intraneuronal accumulation to densely packed areas of mutant protein within the nucleus of affected neurons (299).

Invertebrate and cellular DRPLA models revealed lysosomal autophagy and polyglutamine repeat protein accumulation while transgenic mice point to the atrophin-1 role in neuronal proliferation (304–306).

### 6.48. Episodic Ataxia type 1 (EA1) [OMIM # 160120]

Episodic ataxia type 1 (EA1) is characterised by constant myokymia and dramatic episodes of spastic contractions of the skeletal muscles of the head, arms, and legs with loss of both motor coordination and balance. EA1 may be associated with epilepsy. Usually, onset is in childhood or early adolescence (307). Ocular or MRI alterations are absent in EA1 patients (308).

In 1994, using a group of genetic markers from a genomic region on 12p carrying the potassium channel genes, Litt and collaborators demonstrated linkage in four kindreds with episodic ataxia and myokymia (309). In the same year, Browne and collaborators demonstrated mutations in the *KCNA1* gene in four unrelated families with episodic ataxia and myokymia, with a different missense point mutation in each family (310). Although EA1 is the most common diagnosis resulting from *KCNA1* mutations, patients can also exhibit many other types of diseases such as epilepsy, hypomagnesemia, and paroxysmal kinesigenic dyskinesia (308).

Worldwide EA1 prevalence is currently unknown albeit several families have been identified in Australia, Brazil, Canada, Germany, Italy, Russia, Spain, the Netherlands, United Kingdom, and the United States with an estimated prevalence of 1:500,000 (311).

Disease-causing mutations in *KCNA1* are almost exclusively missense mutations that alter highly conserved amino acid residues to disrupt channel function, from the level of expression, assembly, membrane targeting, and ion channel kinetics (311).

Effective treatments with carbamazepine, valproic acid, and acetazolamide have been shown to improve EA1 symptoms (312,313).

### 6.49. Episodic Ataxia type 2 (EA2) [OMIM # 108500]

EA2 is clinically characterised by paroxysmal recurrent debilitating spells of unsteadiness, incoordination, vertigo, and slurring of speech lasting hours to days, with variable progressive ataxia (311). The majority of the EA2 patients present with nystagmus and subtle ocular motor disturbances (314). Brain MRI demonstrated atrophy of the cerebellar vermis (314).

In 1995, Kramer and collaborators demonstrated that a nystagmus-associated episodic ataxia subtype mapped to chromosome 19p (315). Also in 1995, von Brederlow and collaborators found linkage to 19p in two large kindreds with paroxysmal ataxia (316). In 1996, Ophoff and collaborators identified a frameshift and splicing mutations in the calcium ion channel gene *CACNA1A* on 19p13, in two families with EA2. They also described mutations in the same gen associated with familial hemiplegic migraine (317). *CACNA1A* is extensively alternatively spliced where the longest isoform includes the polymorphic CAG region in frame for polyglutamine repeats to cause SCA6 (318).

Over 80 different pathologic mutations have been identified to date within the *CACNA1A* gene, and they typically result in premature truncation of the channel protein via nonsense or frameshift mutations though a number of missense mutations have also been found to be pathologic. Prevalence is estimated less than 1 in 100,000 with 80%-90% estimated penetrance (319,320).

The Cav2.1 P/Q voltage-dependent calcium channel, encoded by the *CACNA1A* gene, is critically important in mediating neurotransmission and is highly expressed pre-synaptically, particularly in the cerebellar Purkinje and granule cells and at the neuromuscular junction (321).

Acetazolamide, 4-aminopyridine, 3,4-diaminopyridine, the potassium channel blocker 4-aminopyridine and chlorzoxazone have proven effective for EA2 (322–324).

### 6.50. Episodic Ataxia type 3 (EA3) [OMIM % 606554]

Episodic ataxia type 3 was clinically described by Steckley and collaborators in 2001 (325). Patients presented with episodic ataxia with vestibular ataxia, vertigo, tinnitus, and interictal myokymia were prominent (325).

In 2005, Cader and collaborators found genetic linkage to a 4-cM region on chromosome 1q42. Although a common haplotype was absent in three affected family members and four unaffected individuals carried the disease haplotype. They suggested that phenocopies and reduced penetrance may explain the inconsistence (326). The defective gene associated with EA3 remains to be identified.

### 6.51. Episodic Ataxia type 4 (EA4) [OMIM % 606552]

EA4 has been used to describe a family with periodic vestibulocerebellar ataxia (PATX) (327). Damj and collaborators in 1996 using linkage analysis ruled out both the EA1 and EA2 loci, but no chromosomal locus has yet been reported (328).

The disorder was characterised by defective smooth pursuit, gaze-evoked nystagmus, ataxia, and vertigo (328). The age of onset ranged from the third to the sixth decade.

Only one EA4 histopathological studied case has been described to date. The brain revealed moderate to severe Purkinje cell loss prominently in the vermis (329). Purkinje cells also displayed loss of dendritic arborization and thickened dendrites and dendritic spines. Depigmentation of substantia nigra was also observed. Polyglutamine track staining was observed with the 1C2 antibody with subtle foci in the flocculus-granular cell layer (329).

### 6.52. Episodic Ataxia type 5 (EA5) [OMIM # 613855]

In 2000 Escayg and collaborators, through candidate gene screening of subjects with episodic ataxia, described a 20-year-old index case with recurrent episodes of vertigo and ataxia that lasted for several

hours. Interictal examination showed spontaneous downbeat and gaze-evoked nystagmus and mild dysarthria and truncal ataxia. The proband's mother had identical episodes of vertigo and ataxia after the age of 30 years as well as longstanding dysarthria and imbalance (330).

Authors found a heterozygous missense variant within *CACNB4* gene. In the same study, investigators identified the same variant in a German family with generalized epilepsy and without ataxia (330).

### 6.53. Episodic Ataxia type 6 (EA6) [OMIM # 612656]

EA6 is characterised by episodic ataxia as well as progressive ataxia, seizures, and migraine headaches with prolonged alternating hemiplegia triggered by mild head trauma and fever (331).

In 2005, Jen *et al.* identified a heterozygous mutation in the *SLC1A3* gene in a 10-year-old boy with episodic ataxia (331). In three affected members of a family with EA6, de Vries and collaborators in 2009 identified a different heterozygous mutation in the *SLC1A3* gene (332)

In cells expressing mutant SLC1A3 protein product, the excitatory amino acid transporter 1, glutamate uptake was reduced suggesting that glutamate transporter dysfunction underlies the disease (332).

### 6.54. Episodic Ataxia type 7 (EA7) [OMIM % 611907]

Kerber and collaborators reported a four-generation family in which seven members had episodic ataxia (333). Onset occurred before age of 20 years, and attacks lasted hours to days and were associated with weakness and dysarthria.

The same authors identified a candidate region on chromosome 19q13 by genome-wide linkage and haplotype analysis (333).

### 6.55. Episodic Ataxia type 8 (EA8) [OMIM % 616055]

By genome-wide linkage analysis of an Irish family with autosomal dominant episodic ataxia, Conroy and collaborators found linkage to an 18.5-Mb locus on chromosome 1p36.13-p34.3 in 2014 (334).

Episodic attacks were characterised by unsteady gait, generalized weakness, and slurred speech. Variable additional features included twitching around the eyes, nystagmus, myokymia, mild dysarthria, and persistent intention tremor (334).

### 6.56. Episodic Ataxia type 9 (EA9) [OMIM # 618924]

There is controversy regarding E9 and its associated gene. In 2019 Schwarz and collaborators described a heterogeneous clinical spectrum of 21 patients presenting with episodic ataxia associated with *SCN2A* mutations (335).

This episodic ataxia subtype was characterised by onset in the first years of life with dizziness, slurred speech, headache, vomiting, and pain. Most patients had neonatal or infantile tonic or tonic-clonic seizures. Some patients had mildly delayed development with speech delay and/or autistic features or mildly impaired intellectual development. Brain imaging showed a stable circumscribed lesion in the left cerebellar hemisphere, but no cerebellar atrophy (335).

In combination with previous reports (336,337), authors concluded that this episodic ataxia subtype occurred throughout mutations in the *SCN2A* gene. OMIM database classified this episodic subtype as EA9 (OMIM # 618924; last update 06/11/2020).

Electrophysiologic studies showed that the p.Ala263Val mutation within *SCN2A* resulted in a 3-fold increase in persistent sodium current and slow inactivation. These findings were consistent with a gain-of-function effect and neuronal hyperexcitability (338).

More recently in 2020, Piarroux and collaborators proposed an episodic ataxia subtype 9 (EA9) linked to *FGF14* in four patients from two families with pathogenic mutations in the *FGF14* gene, previously associated with SCA27 (339). They performed a literature analysis and found previously reported mutations in the *FGF14* gene in eight patients from five families, with phenotypes compatible with episodic ataxia (339).

Authors determined that EA9 present with a variable range of age of onset and triggering factors, particularly fever, variable duration with long-lasting attacks, frequency, and variably associated with chronic upper limb tremor and/or nystagmus (339). Patients present with normal brain MRI and absence of ophthalmological alterations.

Since FGF14 regulates the Cav2.1 presynaptic channels by modulating the current and the vesicular recycling, authors suggested that EA could result from this dysregulation (339).

Therefore, a consensus agreement is pending for the correct classification of these two episodic ataxia subtypes.

**Table 2. Genetic heterogeneity and molecular pathways underlying spinocerebellar ataxias.**

| Name (Locus) | Gene | Protein | Protein function | Type of mutation | Effect of mutation | Molecular pathology |
|---|---|---|---|---|---|---|
| SCA1 (6p22.3) | *ATXN1* | Ataxin-1 | Involved in transcription regulation | (CAG)n | Gain/loss of function | Aggregation, caspase activation, autophagy, $Ca^{2+}$ alterations, glutamate excitotoxicity, transcriptional alteration, mitochondrial impairment, proteosome degradation, neurotransmission deficits, UPR, neurite alterations, (PP2A) activity dysregulation, (PKC) activity deficits |
| SCA2 (12q24.12) | *ATXN2* | Ataxin-2 | Binds RNA/proteins to modify metabolism after stress, and to control calcium ($Ca^{2+}$) | (CAG)n | Gain of function | Dark cell degeneration, aggregation, caspase activation, autophagy, $Ca^{2+}$ alterations, glutamate excitotoxicity, transcriptional alteration, mitochondrial impairment, oxidative stress, neurotransmission deficits, UPR, (PP2A) activity dysregulation |
| SCA3 (14q32.12) | *ATXN3* | Ataxin-3 | Involved in De-ubiquitination and transcription regulation | (CAG)n | Gain/loss of function | Dark cell degeneration, aggregation, caspase activation, autophagy, glutamate excitotoxicity, transcriptional alteration, mitochondrial impairment, oxidative stress, proteosome degradation, neurotransmission deficits, UPR |
| SCA4 (16q22.1) | Unknown | Unknown | Unknown | Unknown | Unknown | Unknown |
| SCA5 (11q13.2) | *SPTBN2* | Spectrin beta chain, non-erythrocytic 2 | Plays an important role in neuronal membrane skeleton. | Missense, in-frame deletion | Loss of function | Disruption of axonal transport and vesicle trafficking, proteosome degradation, neurotransmission deficits, neuronal membrane skeleton defects |

| Name (Locus) | Gene | Protein | Protein function | Type of mutation | Effect of mutation | Molecular pathology |
|---|---|---|---|---|---|---|
| SCA6 (19p13.2) | *CACNA1A* | Voltage-dependent P/Q-type calcium channel subunit alpha-1A | Mediates $Ca^{2+}$ signalling/homeostasis | (CAG)n | Gain/loss of function | Aggregation, caspase activation, autophagy, $Ca^{2+}$ alterations, glutamate excitotoxicity, transcriptional alteration, mitochondrial impairment, neurotransmission deficits, UPR |
| SCA7 (3p14.1) | *ATXN7* | Ataxin-7 | Component of the STAGA transcription coactivator-HAT complex. | (CAG)n | Gain/loss of function | Dark cell degeneration, aggregation, caspase activation, autophagy, transcriptional alteration, mitochondrial impairment, oxidative stress, proteosome degradation, neurotransmission deficits, UPR |
| SCA8 (13q21) | *ATXN8OS* | Ataxin-8 | Unknown | (CTG)n | Gain of function | Aggregation, caspase activation, transcriptional alteration, mitochondrial impairment, neurotransmission deficits, UPR |
| SCA10 (22q13.31) | *ATXN10* | Ataxin-10 | Induces neurogenesis by activating the Ras-MAP kinase pathway | (ATTCT)n | Gain/loss of function | Neurite alterations, transcriptional alteration. |
| SCA11 (15q15.2) | *TTBK2* | Tau tubulin kinase 2 | Key regulator of ciliogenesis; Involved in Tau phosphorylation | Frameshift, missense | Loss of function | Disruption of axonal transport and vesicle traffic and Tau phosphorylation dysregulation |
| SCA12 (5q32) | *PPP2R2B* | Serine/threonine-protein phosphatase 2A 55 kDa regulatory subunit B beta isoform | Regulation of PP2 activity transcription regulation | (CAG)n | Unknown | Caspase activation, glutamate excitotoxicity, transcriptional alteration, oxidative stress, (PP2A) activity dysregulation |
| SCA13 (19q13.33) | *KCNC3* | Potassium voltage-gated channel subfamily C member 3 | Forming a potassium-selective channel | Missense | Gain/loss of function | Potassium channel dysfunction |

| Name (Locus) | Gene | Protein | Protein function | Type of mutation | Effect of mutation | Molecular pathology |
|---|---|---|---|---|---|---|
| SCA14 (19q13.42) | *PRKCG* | Protein kinase C gamma type | Phosphorylate a wide variety of protein targets | Missense, in-frame deletions, nonsense | Gain/loss of function | $Ca^{2+}$ alterations, proteosome degradation, neurotransmission deficits, (PKC) activity deficits |
| SCA15/ SCA16 (3p26.1) | *ITPR1* | Inositol 1,4,5-trisphosphate receptor type 1 | Involved in calcium signalling | Missense, large deletions | Gain/loss of function | $Ca^{2+}$ alterations |
| SCA17 (6q27) | *TBP* | TATA-box-binding protein | General transcription factor | (CAG)n | Gain/loss of function | Aggregation, caspase activation, autophagy, transcriptional alteration, mitochondrial impairment, neurotransmission deficits, UPR |
| SCA18 (7q22-q32) | *IFRD1* | Interferon-related developmental regulator 1 | Involved in NGF proliferative and differentiative pathways | Missense | Unknown | Unknown |
| SCA19/ SCA22 (1p21-q21) | *KCND3* | Potassium voltage-gated channel subfamily D member 3 | Involved in voltage-gated inactivating potassium channels | Missense, in-frame deletion | Loss of function | Potassium channel dysfunction |
| SCA20 (11q12.2-11q13.3) | Unknown | Unknown | Unknown | Chromosomal duplication | Unknown | Unknown |
| SCA21 (7p21.3-p15.1) | *TMEM240* | Transmembrane protein 240 | Synaptic transmembrane protein | Missense, nonsense | Gain of function | Neurotransmission deficits |
| SCA23 (20p13) | *PDYN* | Proenkephalin-B | Preproprotein of ligands for the kappa-type of opioid receptor | Missense | Gain of function | Neurotransmission deficits, glutamate excitotoxicity |

| Name (Locus) | Gene | Protein | Protein function | Type of mutation | Effect of mutation | Molecular pathology |
|---|---|---|---|---|---|---|
| SCA25 (2p21-p15) | Unknown | Unknown | Unknown | Unknown | Unknown | Unknown |
| SCA26 (19p13.3) | *EEF2* | Elongation factor 2 | Catalyses the GTP-dependent ribosomal translocation during translation elongation | Missense | Gain/loss of function | RNA translocation |
| SCA27 (13q33.1) | *FGF14* | Fibroblast growth factor 14 | Interacts with voltage-gated Na+ channels to regulate neuronal excitability | Missense, large deletion, translocation | Loss of function | Disruption of axonal transport and vesicle traffic and voltage-gated Na+ channel dysregulation |
| SCA28 (18p11.21) | *AFG3L2* | AFG3-like protein 2 | ATP-dependent protease | Missense, frameshift, large deletion | Loss of function | Dark cell degeneration, and mitochondrial impairment |
| SCA29* (3p26) | ITPR1 | Inositol 1,4,5-trisphosphate receptor type 1 | Involved in calcium signalling | Missense, in-frame deletion, splicing | Loss of function | $Ca^{2+}$ alterations |
| SCA30 (4q34.3-q35.1) | Unknown | Unknown | Unknown | Unknown | Unknown | Unknown |
| SCA31 (16q21-q22) | *BEAN1* | BEAN1 | Interacts with NEDD4, a ubiquitin-protein ligase | (TGGAA)n | Gain of function | Transcriptional alteration, neurotransmission deficits |
| SCA32 (7q32-33) | Unknown | Unknown | Unknown | Unknown | Unknown | Unknown |
| SCA34 (6q14) | *ELOVL4* | Elongation of very long chain fatty acids protein 4 | Involved in long-chain fatty acids elongation cycle | Missense | Loss of function | Unknown |

| Name (Locus) | Gene | Protein | Protein function | Type of mutation | Effect of mutation | Molecular pathology |
|---|---|---|---|---|---|---|
| SCA35 (20p13) | *TGM6* | Protein-glutamine gamma-glutamyl transferase 6 | Catalyses protein cross-linking and the conjugation of polyamines | Missense, splicing | Loss of function | Aggregation and UPR |
| SCA36 (20p13) | *NOP56* | Nucleolar protein 56 | Involved in ribosomal subunit biogenesis | (GGCCTG)n | Gain of function/Haploinsufficiency | Aggregation and transcriptional alteration |
| SCA37 (1p32) | *DAB1* | Disabled homolog 1 | Interacts with protein kinase pathways to regulate neuronal positioning | (ATTTC)n | - | - |
| SCA38 (6p12.1) | *ELOVL5* | Elongation of very long chain fatty acids protein 5 | Involved in long-chain fatty acids elongation cycle | Missense | Gain/loss of function | Aggregation, UPR and apoptosis |
| SCA39 (11q21-11q22.3) | Unknown | Unknown | Unknown | Chromosomal duplication | Unknown | Unknown |
| SCA40 (14q32.2) | *CCDC88C* | Protein Daple | Involved in non-canonical Wnt signalling | Missense | Gain of function | Apoptosis |
| SCA41 (4q27) | *TRPC3* | Short transient receptor potential channel 3 | Form a receptor-activated non-selective calcium permeant cation channel | Missense | Gain of function | Transcriptional alteration and apoptosis |
| SCA42 (17q21.33) | *CACNA1G* | Voltage-dependent T-type calcium channel subunit alpha-1G | Low-voltage-activated calcium channel | Missense | Gain/loss of function | $Ca^{2+}$ alterations |

| Name (Locus) | Gene | Protein | Protein function | Type of mutation | Effect of mutation | Molecular pathology |
|---|---|---|---|---|---|---|
| SCA43 (3q25.2) | *MME* | Neprilysin | A zinc-dependent metalloprotease that cleaves peptides | Missense | Gain of function | Unknown |
| SCA44 (6q24.3) | *GRM1* | Metabotropic glutamate receptor 1 | G-protein coupled receptor for glutamate | Missense, nonsense | Gain of function | $Ca^{2+}$ alterations and glutamate excitotoxicity |
| SCA45 (5q33.1) | *FAT2* | Protocadherin Fat 2 | Involved in the regulation of cell migration | Missense | Unknown | Aggregation |
| SCA46 (19q13.2) | *PLD3* | 5'-3' exonuclease PLD3 | Exonuclease which digests single-stranded DNA | Missense | Loss of function | Disruption vesicle trafficking and neuronal membrane skeleton defects |
| SCA47 (1p35.2) | *PUM1* | Pumilio homolog 1 | RNA-binding protein that acts as a post-transcriptional repressor | Missense | Loss of function | Transcriptional alteration |
| SCA48 (16p13.3) | *STUB1* | E3 ubiquitin-protein ligase CHIP | Targets misfolded chaperone substrates towards proteasomal degradation | Missense, frameshift, in frame deletion, nonsense, splicing | Gain of function / Loss of function | Transcriptional alteration and proteasome degradation |
| DRPLA (12p13.31) | *ATN1* | Atrophin-1 | Transcriptional corepressor | (CAG)n | Gain of function | Aggregation |
| EA1 (12p13.32) | *KCNA1* | Potassium voltage-gated channel subfamily A member 1 | Mediates transmembrane potassium transport in excitable membranes | Missense, nonsense | Loss of function | Potassium channel dysfunction |

| Name (Locus) | Gene | Protein | Protein function | Type of mutation | Effect of mutation | Molecular pathology |
|---|---|---|---|---|---|---|
| EA2 (19p13.2) | *CACNA1A* | Voltage-dependent P/Q-type calcium channel subunit alpha-1A | Gives rise to P and/or Q-type calcium currents | Missense, nonsense, splicing | Loss of function | Aggregation, caspase activation, autophagy, $Ca^{2+}$ alterations, glutamate excitotoxicity, transcriptional alteration, mitochondrial impairment, neurotransmission deficits, UPR |
| EA3 (1q42) | Unknown | Unknown | Unknown | Unknown | Unknown | Unknown |
| EA5 (2q23.3) | *CACNB4* | Voltage-dependent L-type calcium channel subunit beta-4 | Contributes to the function of the calcium channel | Missense | Unknown | Unknown |
| EA6 (5p13.2) | *SLC1A3* | Excitatory amino acid transporter 1 | Mediates the uptake of L-glutamate and also L-aspartate and D-aspartate | Missense | Gain of function | Glutamate excitotoxicity |
| EA7 (19q13) | Unknown | Unknown | Unknown | Unknown | Unknown | Unknown |
| EA9 (13q33.1) | *FGF14* | Fibroblast growth factor 14 | Interacts with voltage-gated Na+ channels to regulate neuronal excitability | Missense, nonsense, splicing | Loss of function | Unknown |
| EA9 (2q24.3) | *SCN2A* | Sodium channel protein type 2 subunit alpha | Mediates the voltage-dependent sodium ion permeability of excitable membranes | Missense | Gain of function | increase in persistent sodium current, slowed inactivation, increased cell membrane excitability |

HAT, histone acetyltransferases; NGF, nerve growth factor; UPR, unfolded protein response.

## 7. Therapeutics

Currently limited effectiveness has been obtained for drug treatment of cerebellar ataxias, being primarily supportive care the most applied therapy. Nonetheless, there are several emerging clinical and preclinical studies candidates to become potential therapies for autosomal dominant cerebellar ataxias (340).

For instance, acetazolamide and gabapentin have been shown to produce some benefits regarding ataxic symptoms in SCA6 (341). In addition, riluzole, a glutamate release inhibitor, has been shown to improve function in patients with ataxia as measured by SARA scores. It mostly affects axial domains by improving speech and gait. Side effects of riluzole include mild liver enzyme increases and transient vertigo but it is generally well tolerated (342,343). Moreover, recently there is an ongoing clinical trial with troriluzole, a prodrug formulation of riluzole, as a potential treatment for excessive glutamate mediated neuronal transmission, to examine its effect on slowing disease progression (ClinicalTrials.gov Identifier: NCT03701399). Therefore, Longer studies and disease-specific trials are needed to confirm whether these findings can be widely applied in clinical practice for the treatment of SCAs.

Likewise, valproic acid (VPA), an histone deacetylase inhibitor clinically used to treat bipolar and seizure disorders, tested in SCA3 patients, improved SARA measures of locomotor function, with some adverse effects (344). Also in SCA3 patients, varenicline improved SARA scores for gait, stance, and rapid alternating movements as well as the timed walking test after 4 weeks, but a high dropout prevented the completion of the study (345). SCA3 dystonia and spasticity symptoms have been successfully treated with botulinum toxin although caution and small dosage are recommended (346). Furthermore, amantadine and dopaminergic and anticholinergic drugs have been used to alleviate tremor, bradykinesia, or dystonia in SCA2 and SCA3 (347–349) while restless legs and periodic sleep leg movements symptoms have been shown to ameliorate using dopaminergic agonists or clonazepam (350–352).

A retrospective study also demonstrated that patients with SCA who took coenzyme Q10 had better SARA scores, suggesting that may have disease-modifying effects albeit requires further randomized placebo-controlled trials (353). Lithium has shown neuroprotective benefits in preclinical models of polyglutamine disorders and therefore has been used for the treatment of some SCA subtypes (354,355).

Recently, the treatment of a small cohort of SCA38 patients with docosahexaenoic acid has been shown to be beneficial (356).

β-blockers, benzodiazepines or chronic thalamic stimulation have been shown to ameliorate intention tremor (340); magnesium, quinine, or mexiletine could alleviate muscle cramps (357); while

piracetam proved efficient for several clinical symptoms such as myoclonus, vertigo, dyslexia, dementia or cognitive decline, and improved gait ataxia at high dose (358–360).

Additionally, preclinical studies with citalopram rescued neuronal dysfunction in SCA3 *C. elegans* model, and reduced ataxin-3 neuronal inclusions and astrogliosis, improving motor symptoms in SCA3 mouse models and providing rationale evidence for future clinical trials (361). Other preclinical studies in SCA animal models are based on gene therapy, which knock down the expression of the mutated protein with specific antisense oligonucleotides (ASOs) targeting the mutated gene. These studies hold promise as disease-modifying therapies (362–364). Small hairpin RNA silencing mutant *ATXN3* intraventricular injected has shown to improve motor symptoms in SCA3 mouse models (365). In addition, the delivery of microRNA against the toxic gene product in SCA6 mouse models, also improved the motor performance and Purkinje cell degeneration (366).

Since the identification of acetazolamide as preventive treatment for frequent ataxia episodes in episodic ataxias, it has been the main treatment for EA, especially EA2, reducing the duration and severity with minimal side-effects (367). For those patients who do not respond or are intolerant to acetazolamide, the 4-aminopyridine alternative treatment has shown reduction in downbeat nystagmus (368). Low-dose benzodiazepines may also be useful to minimize symptoms of severe vertigo and nausea, allowing patient to recover from the debilitating ataxia and migraine headache symptoms (311).

Until a successful pharmacological treatment is found, leading to improving the quality of life and survival in patients with ataxia, rehabilitation therapies have shown effectiveness for improving welfare. Physiotherapy is currently being used as an effective alternative treatment in combination with daily autonomous training of the gait and stance, improving ataxic symptoms (369,370). The therapist also counsel patients and family about the impact of the disease in every day's life and possible physical and sensory treatments and their real expectations. Those physical therapies include aerobic fitness, biomechanical assessment and counseling to preserve independence and mobility aided by support devices. Physiotherapy may be complemented with interactive video games, home balance exercise, or partnered dance as some studies suggested (371,372). Furthermore, treatment of the dysphagia and dysarthria requires speech and language therapies to prevent swallowing problems and to improve speech intelligibility (340).

## 8. Zebrafish models for dominant spinocerebellar ataxias

Zebrafish cerebellar development, differentiation and functionality reaches maturity during embryonic and larval stages, with Purkinje cells developing fast and emerging already at 56 hours post-fertilization (hpf). Zebrafish Purkinje cells electrophysiological characteristics are present at 7 days post-fertilization (dpf) allowing them to control visual stimuli driven eye or swimming

movements and also involved in motor learning. Therefore, zebrafish provides a highly valuable model for cerebellar neurodegenerative diseases to gain insights into how pathogenic molecular defects correlates with anatomical, physiological and behavioural deficits (373,374).

There are a few studies using zebrafish as a disease model of dominant spinocerebellar ataxia. For instance, *atxn1a* and *atxn1b* genes were identified in zebrafish as homologs of human *ATXN1* (375), and similar study investigated the expression of *ataxin3*, the ortholog of *ATXN3* in SCA3, creating two transgenic zebrafish lines with 23Q and 84Q (376). Recently, Inactivation of *atxn7* through antisense oligonucleotides or genome editing showed ocular malformation in zebrafish resembling that in SCA7 (377). In the same way, a SCA13 zebrafish model has been modelled by a genetic system for tuneable Purkinje cell-specific transgene co-expression to manipulate and monitor cerebellar Purkinje cells (374).

Therefore, zebrafish is a potential model for demonstrating the causal relationship between mutation and pathological deficits in the SCAs and also offers a useful tool to explore and develop future therapies.

# OBJECTIVES

The main objectives of this thesis were to further increase our knowledge of the genetic, epidemiological and physiopathological underlying mechanisms in spinocerebellar ataxias (SCAs). In particular, a previously undescribed cohort of 308 index cases with dominant cerebellar ataxias were studied with the aim of identifying and characterizing their causative genetic and molecular defects.

The specific objectives were:

1. To estimate the prevalence of gene variants across a cohort of 308 cases with dominant cerebellar ataxia.

2. To identify novel SCA subtypes and characterise their molecular genetic defects associated with SCA37.

    2.1. To further characterise the SCA37 subtype identified during the course of this thesis, to identify the underlying genetic defect, determine its prevalence, and describe the genotype-phenotype correlations.

    2.2. To study and characterize the SCA37 neuropathology and the underlying cellular and molecular mechanisms of cerebellar neurodegeneration in this specific ataxia subtype.

    2.3. To study a novel SCA subtype in a five-generation Spanish family (M-SCA) from the Balearic island of Menorca, to identify the underlying genetic defect and describe the genotype-phenotype correlations.

    2.4. Last but not least, to characterise the M-SCA underlying physiopathology in human fibroblasts cell lines from patients and in a novel zebrafish disease model.

# MATERIALS AND METHODS

## 1. Ethics

This study was conducted according to the ethical principles for medical research involving human subjects according to the Declaration of Helsinki.

Informed consents were obtained for all individuals included in the study, which were approved by the ethical board of the University Hospital Germans Trias i Pujol (HUGTiP) in Badalona, the University Hospital Virgen del Rocio in Seville, or the Fundación CIEN in Madrid and local ethics committees.

## 2. Cohort of patients and relatives with autosomal dominant ataxias

A total of 308 ataxia index cases, 47 at risk, and 38 healthy relatives were included in the study, all referred by collaborating neurological or neuropediatric services, presenting with ataxia as a primary clinical sign and cerebellar atrophy by magnetic resonance imaging, were examined by at least one neurologist and DNA samples were obtained and genetically studied. Anamnesis from medical histories were used when available to refine clinical and genetic correlations. Autosomal dominant inheritance was assumed based on positive familial history or clinical signs compatible with a defined SCA subtype. Segregation studies were performed when familial DNA was available. Genetic diagnosis and counselling were provided when available.

### 2.1. SCA37 families

Detailed clinical data from the AT-901 SCA37 family was previously reported (281). We later identified a second pedigree with the SCA37 phenotype linked to the same locus (AT-9012 family). Family AT-9012 was assessed following the same clinical protocol applied to Family AT-901. Clinical information was obtained from 27 SCA37 members, whereas 18 were clinically examined, five affected and 13 healthy. Two additional pedigrees (AT-59 and AT-90) from the same area in the south of Spain with 10 affected patients with a similar clinical phenotype and three asymptomatic relatives were identified and included in this study. Once the SCA37 causative mutation was identified, three additional index cases from the total of 308 ataxia index patients were genetically studied because of their common geographical origin.

#### 2.1.1. Cerebellar volume and mid-sagittal vermis relative diameter quantification

To quantify cerebellar volume, we used the CERES algorithm (378) to calculate the percentage of the cerebellar volume relative to the total intracranial volume on T1-weighted 1.5 T MRI images from five SCA37 patients (patients III:8, IV:1 and III:1 from family AT-90; and patients IV:4 and IV:5 from family AT-901). Normal boundaries were used from 30 age- and gender-matched controls (age range: 24–75 years) randomly selected from the open access IXI dataset previously reported (378).

To quantify the mid-sagittal vermis relative diameter, the total posterior cranial fossa diameter was measured in a linear segment from the posterior commissure to the opisthion and the largest sagittal diameter of the cerebellum parallel to the previous linear segment in three patients (patients IV:4 and IV:5 from family AT-901; and patient III:6 from family AT-90) and three asymptomatic subjects carrying the SCA37 mutation (Subjects V:3 and VI:2 from Family AT-901, and Subject IV:8 from Family AT-9012). The ratio of the cerebellar vermis diameter over the total posterior cranial fossa diameter was calculated (379) and compared to 16 age and gender-matched controls.

### 2.2. M-SCA family

Clinical examination was performed in a family from Menorca with 17 members, six healthy and 11 affected, nine of them with a detailed neurological exam. The SARA scores (7) were assessed for six ataxic patients (III:7, IV:2, IV:6, IV:8, IV:14 and V:1). Affected patients were further investigated using an enhanced clinical protocol, including electrocardiograms, echocardiograms, audiometric tests, nerve conduction studies, magnetic resonance imaging of the brain, evoked potentials, during follow-up visits. All the studies were performed in the absence of medication treatment.

#### 2.2.1. Cerebellar volume quantification

Cerebellar volume was quantified as described above on T1-weighted 1.5 T MRI images from five M-SCA patients (Patients IV:2, IV:6, IV:8, IV:14 and V:1).

#### 2.2.2. Electrophysiological studies

Six patients from the M-SCA family (III:7, IV:2, IV:6, IV:8, IV:14 and V:1) underwent nerve conduction, EMG as well as SSEP studies. In three patients, we could also assess autonomic nervous system. All neurophysiological studies were performed by means of TruTrace® EMG system (DEYMED Diagnostic, Hronov, Czech Republic) and conducted according to standard methodology (380). The protocol included nerve conduction studies, F-waves, electromyography (EMG), autonomic nervous system test and somatosensory evoked potentials (SSEPs). Motor nerve conduction studies included bilateral deep peroneal and posterior tibial nerves and sensory nerve studies included bilateral sural, superficial peroneal and median (digit II) and ulnar (digit V) sensory nerves. F waves were studied for median, tibial and deep peroneal nerves. EMG study was also performed from anterior tibial muscle. Sympathetic skin response (SSR) and the R-R period were selected to assess sympathetic and parasympathetic autonomic nervous system, respectively. Bilateral tibial nerve SSEPs were recorded on Erb point, cervical spinal cord (C7) and scalp (Cz'/Fz according to 10-20 International System).

## 3. Genetics and genomics studies

### 3.1. Analysis of known SCA repeat expansions

Fluorescent PCR analysis to study the SCAs 1, 2, 3, 6, 7, 10, 12, 17, 31, 36 and DRPLA associated genes were performed using primers and PCR conditions as described in **Supplementary Table 1**. Large pathogenic expansions in ATXN10 (SCA10) and *NOP56* (SCA36) were discarded by repeat-primed PCR (276,381).

### 3.2. Specific gene sequencing by Sanger and NGS

Traditional Sanger sequencing and PCR amplicon NGS on Miseq Illumina, were used for the analysis of the 5% of the ataxia cohort samples to identify conventional missense, nonsense, splice site, small deletions or insertions mutations in specific ataxia genes. For PCR amplicons NGS libraries were prepared using the following standard protocol as described in the Nextera XT DNA Library Prep Kit (Illumina, Inc., San Diego, CA). For each amplicon PCR product, 5 µl were loaded into one well of a 96-wel SequalPrep™ Normalization Plate (Thermo Fisher Scientific, Waltham, MA) for amplicon purification and normalization. Eluted PCR amplicons for each DNA sample were pooled and 1 ng DNA (5 µl) was tagmented using Nextera transposome at 55 °C for 5 min and the reaction stopped with the addition of 5 µl of Neutralize Tagment Buffer. After completion of the tagmentation reaction, libraries were amplified and required indexes and adapters sequences added for sequencing cluster generation. Next, single-sided bead purification to clean up libraries. The quality of the libraries was analysed using Agilent Technology 2100 Bioanalyzer using a High Sensitivity DNA kit (Agilent Technologies, Santa Clara, CA) and normalised using Nextera library normalization reagents. Finally, normalized libraries were denatured and diluted to the final loading concentration required for Miseq sequencing system (Illumina, Inc.).

### 3.3. Targeted gene panels sequencing

Three different versions of custom DNA target enrichment hybridization probes depending on the known genes associated with ataxia at the time of the study were used (**Supplementary Table 2**). Targeted exons were captured using SureSelect Capture Library reagents (Agilent Technologies) following Agilent protocols and recommendations. The quality and the quantity of the library were analysed in TapeStation 4200, High Sensitivity assay (Agilent Technologies). Library was sequenced by paired-end sequencing (100 x 2) in Illumina HiSeq 2500 sequencer (Illumina, Inc.). Phred was used to calculate quality values (382). A specific custom pipeline was implemented for the bioinformatics analysis. Briefly, Burrows-Wheeler Aligner (383) and 'in-house' scripts were used to map the reads against the human reference genome version GRCh38/hg38. Variant calling was performed using a combination VarScan (384) and GATK (385). 'In-house' scripts were developed

to combine and filter variants. Identified variants were annotated using the Ensembl database (386). Variants were filtered out, prioritized and classified to obtain a list of variants with a minor allele frequency (MAF) ≤0.01 in 1000 Genomes 1000 Genomes (http://www.ncbi.nlm.nih.gov/variation/tools/1000genomes/), Exome Variant Server (EVS) (http://evs.gs.washington.edu/EVS/), ExAC Browser (http://exac.broadinstitute.org/), gnomAD (387), the variant position in the gene, the variant effect and the pathogenesis prediction by four different prediction algorithms (Condel, SIFT, PolyPhen2 and Mutation Taster) (388–391). Sequencing was considered satisfactory when mean coverage for panel and exome studies per patient was >100x, with > 95% of bases covered more than 20x. When required, an extended panel version was applied for genes associated with neurological diseases presenting overlapping clinical signs. Pathogenicity criteria was assessed using previously criteria from Coutelier and collaborators (392) from their panel study on patients with dominant cerebellar ataxia, adapted from the American College of Medical Genetics and Genomics (ACMG) guidelines for pathogenicity classification (393) which not perfectly suited for rare diseases (393).

### 3.4. Familiar and population genetic studies

For SCA37 studies DNA samples were obtained from 70 individuals, 31 affected and 39 healthy or asymptomatic, from seven independent SCA37 families, and 96 DNA samples from our cohort of ataxia patients. DNA was extracted with the Chemagen Magnetic Separation Module I automated system (Perkin Elmer, Waltham, MA) from peripheral blood. Whole-genome sequencing studies were performed in two SCA37 patients (Patients IV:9 and V:9) from the AT-901 family. Two SCA37 linked SNPs identified by WGS, rs79992829 and rs146472695, both with a low minor allele frequency (MAF) of 0.0056 were useful for the identification of three additional SCA37 pedigrees (AT-9012, AT-59, and AT-90) from our cohort of ataxia kindreds. The genetic haplotypes were determined using genetic markers on 1p32 region (**Supplementary Table 3**). All members from the seven SCA37 pedigrees were genotyped for the ATTTC expansion by PCR Sanger sequencing with the Big Dye Terminator v3.1 cycle Sequencing Kit (Thermo Fisher Scientific) (**Supplementary Table 3**).

For M-SCA genetic studies DNA samples were obtained from seven affected and six unaffected relatives. Furthermore, 80 genomic DNA samples from the Menorca population (kindly provided by Dr. Eduardo Tolosa, Neurology Service, Hospital Clinic, Barcelona) were analysed to study *SAMD9L* variant frequency.

### 3.5. Linkage and haplotype analysis

As previously described, twelve SCA37 relatives, six healthy and six affected, from the AT-901 family were included in the initial genetic linkage study that used the Infinium HumanLinkage-12

Genotyping Bead Chip (Illumina, Inc.). The panel included 6,609 single-nucleotide polymorphism (SNP) markers with an average gap of 441 kilobases and 0.58 cM across the genome. Genotypes were assigned using the Bead Studio genotyping module software (Illumina, Inc.), and linkage was analysed using Merlin (394). Penetrance was set to 80% for all participants. To confirm linkage and refine mapping, 10 affected and 23 healthy relatives of the pedigree were further genotyped for microsatellite markers located on chromosome 1 and for SNPs using the Genome-Wide Human SNP Array 6.0 (Affymetrix, Santa Clara, CA), which contains 906,600 SNPs. Two-point and multipoint genetic linkage analyses were then performed with the MLINK and LINKMAP modules (both version 5.10), respectively, from FASTLINK (version 4.1P) (395). For the multipoint analysis, we used the framework maps from the Marshfield Medical Research Foundation (396), deCODE Genetics (397), and Généthon (398).

For M-SCA linkage studies, eleven relatives, five healthy and six affected, were included in the initial genetic linkage study performed in collaboration with the Centro Nacional de Genotipado (CEGEN) using the Illumina Infinium HumanOmni5 Chip (Illumina, Inc.). The panel included more than 4,000,000 markers with an average gap of 680 base pairs across the genome. Genotypes were assigned using the BeadStudio genotyping module software (Illumina, Inc.), and initial non-parametric and parametric linkage were analysed using Merlin 1.1.2 (394). Two-point and multipoint genetic linkage analyses, were performed with MLINK and LINKMAP modules (version 5.10), from the Quiklink compilation (version 16) of the LINKAGE program (395,399). We used informative SNPs within the candidate region and their allele frequencies as the genetic markers. SLINK simulation program (400) was used to validate the expected maximum LOD score that could be obtained with this pedigree in 1,000 replicates.

An affected-only analysis was implemented, which bases the linkage analysis solely on the genotype marker status of the seven affected individuals in the pedigree, and considers that the disease could initiate either with cerebellar atrophy on MRI, nystagmus or hyperreflexia as initial signs.

### 3.6. Whole exome sequencing analysis

SCA37 whole-exome sequencing (WES) was performed with DNA samples from two affected relatives (IV:4 and V:9 from AT-901). DNAs were enriched using SureSelect All Human Exome v.2 (50 Mb) target enrichment technology according to the manufacturer's protocol (Agilent Technologies). The enriched DNA was paired-end sequenced on an ABI SOLiD v4 (Life Technologies, Carlsbad, CA). Reads were mapped against the reference human genome (UCSC hg19) with Bioscope v1.3 (solidsoftwaretools.com) using default parameters. Variant and indel calling were performed with a combination of the Genome Analysis Toolkit (385) and SAMtools v0.16 (401). Based on the hypothesis that the mutation underlying this rare familial disease was not present in the general population, known variants were discarded from further analysis based on the information

from the Ensembl v62 database (402), which hosts data from the most important Human variation resources such as 1000 Genomes, dbSNP, HapMap or gnomAD among others. Then, variants not shared by both patients were filtered out. Synonymous changes were identified and filtered from the variant list using the CONsensus Deleteriousness score of missense SNVs (Condel) (388). Candidate genes were prioritized based on potentially damaging variants, as previously described (403).

For studies of the M-SCA family, whole-exome sequencing (WES) was performed with genomic DNA obtained from peripheral blood of patients IV:2 and IV:14 in collaboration with the National Centre for Genomic Analysis (CNAG) in Barcelona. Exome capture was performed using Nimblegen SeqCapEZ Exome V.3 (Roche, Basel, Switzerland) for 64 Mb according to the manufacturer's protocol. Paired-end, 100 bp long reads were generated on a HiSeq2000 platform (Illumina, Inc.). Read alignment was performed using GEM (404) to Hs37d5 genome, allowing for up to four mismatches when necessary, followed by local-realignment with GATK 3.1-1 (385). Variant calling was performed using Samtools 0.1.19 (401). Identified variants were annotated using SNPEff (405), Annovar (406) and dbNSFP (407) where appropriate. Variants with a minor allele frequency ≥1% in genetic databases including the Exome Aggregation Consortium, 1,000-Genomes Project, dbSNP and gnomAD were excluded from further analysis. The genetic heterogeneity model proposed by Ng et al (403) was applied in order to identify potential candidate genes. Candidate variants were assessed for their computationally predicted pathogenicity by SIFT (408), PolyPhen-2 (409), Condel (388), FATHMM (410), MutationAssessor (411), MutationTaster (391), Provean (412), and CADD (413), and prioritized in accordance with the clinical characteristics shared by affected individuals. Segregation of candidate variant was confirmed by Sanger sequencing.

### 3.7. Whole Genome sequencing (WGS)

Whole-genome sequencing studies (WGS) were done in two SCA37 patients (IV:9 and V:9) from the AT-901 family with a non-PCR protocol to a median depth of ≥35 in the National Centre for Genomic Analysis (CNAG). Alignment with the GEM aligner and variant calling was performed with SAMtools (401). Structural variants were analysed using a combination of SAMtools, BAMtools (414), Velvet v1.2 (415), Breakdancer (416), SVseq2 (417) and GASV (418). Repeat Masker (419) was used to identify repetitive DNA elements within the *SCA37* region such as simple repeats, long interspersed nuclear elements (LINEs), short interspersed nuclear elements (SINEs), and long tandem repeats (LTRs).

### 3.8. R-based algorithm for DNA variant interpretation

VariantSweeper®, a novel in house R-based algorithm that generates a ready-to-report table was designed and implemented for DNA variant interpretation in NGS studies. This algorithm reports gene annotation, nucleotide change, chromosome location, exon or intron identification, variant's

reference in the Ensembl database (420), genotype, allele frequency, protein change, pathogenicity index combining Condel (388), SIFT (408) and PolyPhen (409) in silico predictions, related publications, frequency of each variant in our database, variant coverage, and affected protein domains.

**4. Fibroblasts and cell lines cultures**

Fibroblasts from M-SCA patients IV:14, V:1 and two age and gender matched controls were cultured from skin biopsies. Fibroblasts and SH-SY5Y neuroblastoma cells used tot test SAMD9L constructs were cultivated in Easyflask T75 with filter (Thermo Fisher Scientific) with Dulbecco's modified Eagle medium (Thermo Fisher Scientific) supplemented with 10% of Fetal bobine serum (Thermo Fisher Scientific), and 1% of Penicillin-Streptomycin-Glutamine (Thermo Fisher Scientific).

**5. Generation of SAMD9L constructs**

The coding region of SAMD9L cDNA was amplified by PCR using *Pfu*I polymerase (Promega, Madison, WI) and patient's white blood cells cDNA as template. The resulting fragment was then subcloned in frame into the pCS2 expression vector (421).

The pCS2-SAMD9LWT construct included 5'-CCGCCACC-3' Kozak sequence previous to cDNA SAMD9L constitutional ATG. To introduce the c.1877C>T (p.Ser626Leu) point mutation, in vitro mutagenesis was performed using PCR and specific primers (**Supplementary Table 4**). The sequences of pCS2-SAMD9LWT and pCS2-SAMD9L.S626L were confirmed by Sanger DNA sequencing.

**6. Cell transfection**

Both pCS2-SAMD9LWT and pCS2-SAMD9L.S626L DNA constructs were transfected using lipofectamine in to SH-SY5Y cells according to instructions provided by the manufacturer (Thermo Fisher Scientific) to test SAMD9L constructs. Transfected cells were incubated with the vector and lipofectamine mixture for 4 h in OPTIMEM (Thermo Fisher Scientific) and growth for 48 h in Neurobasal medium (Thermo Fisher Scientific) with B27 supplement and penicillin-streptomycin either on 6 well plate or flask.

**7. Neuropathology**

Post-mortem brains were studied from two clinically and genetically confirmed SCA37 relatives (Subjects IV:9 and IV:10) from the large previously reported AT-901 SCA37 Spanish pedigree (281) and one gender- and age-matched control brain with no medical history of neurological disease. Brain samples were processed according to a common post-mortem protocol followed by the Spanish Banco de Tejidos de la Fundación CIEN (BTCIEN, Madrid, Spain). Briefly, rapid neuropathological autopsy

was performed upon call by the donor's proxies. Immediately after extraction, the right half of the brain was sliced and frozen, while the left half was fixed by immersion in phosphate-buffered 4% formaldehyde for at least three weeks. A full neuropathological study was performed on the left half brain after fixation. Cervical spinal cord was also assessed. All sections were stained with haematoxylin-eosin (H&E) for anatomical orientation and pathological assessment of neurodegeneration. Representative cerebral tissue sections from SCA37 patients were immunostained with the anti-tau antibody for cytoskeletal changes related to Alzheimer's diseases (AD) or other known human tauopathies (422). The AD-related cortical cytoskeletal pathology was classified on these tau-immunostaining sections based on the CERAD (423,424) and Braak staging system (425). Brain beta-amyloidosis was assessed according to previous proposed procedure (426). In addition, selected cerebral, cerebellar, and brainstem tissue sections were immunostained with an affinity-purified alpha-synuclein antiserum to visualize inclusions related to Parkinson's disease or other human synucleinopathies (427,428). Immunostaining for ubiquitin was used to identify any abnormal protein deposits and for TAR DNA-binding protein 43 (TDP-43) to recognize either primary or secondary TDP-43 pathology. Calbindin-D28K immunolabelling allowed investigation of cerebellar Purkinje cells and their neurite processes. Phospho-neurofilament immunostained cerebellar basket cells and their filaments. For immunocytochemistry and immunofluorescence, sections were deparaffinised in Clearene (Leica Biosystems, Wetzlar, Germany), hydrated in 100% and 96% ethanol, and dd$H_2O$. Immunocytochemistry sections were then immersed in 3% hydrogen peroxide in methanol for 30 min to block endogenous peroxide activity. Next, slides were rinsed and microwaved in Lab Vision™ citrate buffer for heat-induced epitope retrieval (pH 6.0 10 min) (Thermo Fisher Scientific), cooled down at room temperature (RT), and rinsed in phosphate buffered saline (PBS) with 0.1% Tween. Non-specific binding was blocked for 1 h with SuperBlock Blocking Buffer (Thermo Fisher Scientific). Primary antibodies used were anti-Calbindin-D28K (EG-20; Sigma-Aldrich, St. Louis, MO), anti-DAB1 (PA5-62538; Thermo Fisher Scientific), anti-human neurofilament protein (clone 2F11; Dako; Agilent Technologies, Santa Clara, CA), anti-GFAP (Z0334; Dako; Agilent Technologies), anti-Ubiquitin (Z0458; Dako; Agilent Technologies) and anti-SAMD9L (25173-1-AP; ProteinTech, Rosemont, IL). After adding primary antibody diluted in Lab VisionTM Antibody Diluent OP Quanto (Thermo Fisher Scientific), sections were incubated overnight at 4 ºC. Sections were then rinsed in 0.1% Tween in phosphate-buffered saline (PBS) before incubation with secondary biotinylated rabbit anti- mouse IgG (H + L) Superclonal™, biotinylated goat anti-rabbit IgG (H + L) Superclonal™ antibody (Thermo Fisher Scientific) or secondary fluorescent, Alexa Fluor® 594 donkey anti-rabbit or Alexa Fluor® 488 goat anti-mouse (Jackson ImmunoResearch, West Grove, PA), for 1 h at room temperature and rinsed with 0.1% Tween in PBS. For immunohistochemistry studies, slides were incubated for 30 min with Ultra-Sensitive ABC Peroxidase Standard Staining Kit (Thermo Fisher Scientific) and rinsed with 0.1% Tween in PBS

followed by a 30-min incubation with 3,3-diaminobenzidine (DAB) and stable peroxide substrate buffer. Sections were washed in water and incubated for 5 min with DAB enhancer (Dako; Thermo Fisher Scientific), counterstained with haematoxylin and eosin, dehydrated, cleared, and mounted. For immunofluorescence, a 10-min incubation with Hoechst was performed for nuclear staining. Visualization was performed using a Carl Zeiss Axio Scope 2 or an Axio Observer Z1 microscope coupled with a LSM710 ZEN confocal module and processed with ZEN imaging software (Zeiss, Oberkochen, Germany). The molecular layer thickness was measured and 200 Purkinje cells from the cerebellar vermis and hemisphere regions were counted on calbindin-stained sections from each SCA37 patient and one control. For each cerebellar region three independent measurements were taken from a total of 17 images with the ImageJ software (429).

**8. Cell culture immunofluorescence**

For immunofluorescence, cultured cells on coverslips were quantified, washed and permeabilised after which they were incubated overnight at 4 °C with primary antibodies. Following a washing step, coverslips were incubated with secondary antibodies (3% BSA in 1x PBS) for 45 min at RT. Finally, a 10 min incubation with Hoechst was performed for nuclear staining. For staining of mitochondria with 100 nm MitoTracker™ Red CMXRos (Thermo Fisher Scientific) was diluted in DMEM prior to addition to cells for 45 min at 37°C in 5% $CO_2$ atmosphere. After the incubation period, cells were washed three times in cell culture media prior to fixation in 4% paraformaldehyde/PBS at room temperature for 20 min and permeabilized and blocked in 0.2% Triton X-100/PBS for 1 h before primary antibody incubation when applicable. Visualisation was performed using a Carl Zeiss Axio Scope 2 or an Axio Observer Z1 microscope coupled with a LSM710 ZEN confocal module (Zeiss) and processed using ImageJ (429) and analysed using JACOP and Coloc2 plugins.

**9. SDS-PAGE and immunoblotting**

Proteins were extracted from human cerebella by homogenization in RIPA lysis buffer containing 50 mM Tris-HCl pH 7.4, 150 mM NaCl, 0.5% Na Deoxycholate, 0.1% SDS, 1% Triton, 50 mM NaF, 5 mM $NaVO_3$, 2 mM EDTA and protein inhibitor cocktail (Roche). Protein concentration was determined using the DC-BioRad protein assay (BioRad, Hercules, CA). One hundred and fifty micrograms of protein sample were mixed with 4X protein loading buffer (125 mM Tris-HCl pH 6.8, 50% glycerol, 4% SDS and 0.2% (w/v) Orange G) (LI-COR, Lincoln, NE) with 10% DTT, separated by electrophoresis at constant 20 mA, transferred onto PVDF membranes with a trans-blot turbo transfer system (BioRad) at 25 V (1 A) for 30 min and blocked with casein for 60 min.

For Reelin immunoblotting, samples were lysed using a Polytron homogenizer (Kinematica Inc, Luzern, Switzerland) for 40 sec on ice with lysis buffer containing 50 mM HEPES pH 7.5, 150 mM NaCl, 1.5 mM $MgCl_2$, 1 mM EGTA, 10% glycerol and 1% Triton X-100 containing protein inhibitor

cocktail (Roche) and phosphatase inhibitors (10 mM $Na_4P_2O_7$, 200 μM $Na_3VO_4$ and 10 mM NaF), and ultra-sonicated for 40 sec at 4 ºC. Twenty micrograms of protein sample were resolved by 6% SDS-polyacrylamide gel and transferred onto nitrocellulose membranes at constant 30 V O/N. Membrane was blocked for 60 min and incubated with primary anti-reelin (MAB5366 clone 142; Millipore Sigma, Burlington, MA) for 90 min.

Primary antibodies used were beta-actin (AC15; Sigma-Aldrich), pan anti-AKT (#4691; Cell Signalling, Danvers, MA), anti-phospho-AKT (Ser473) (#9271; Cell Signalling), anti-Calbindin-D28K (EG-20; Sigma-Aldrich), anti-DAB1 (PA5-62538; Thermo Fisher Scientific), anti-GFAP (Z0334; Dako; Agilent Technologies), anti-PI3 Kinase p85 (05-212; Merck, Kenilworth, NJ), anti-reelin (MAB5366 clone 142; Millipore Sigma), anti-SAMD9L (25173-1-AP; Proteintech), anti-beta-actin (AC15; Sigma-Aldrich), anti-LC3 (NB100-2220; Novus Biologicals, Centennial, CO), anti-LAMP1 (H4A3; Developmental Studies Hybridoma Bank, Iowa City, IA), anti-DRP1 (sc-271583; Santa Cruz, Dallas, TX), anti-MFN1 (sc-166644; Santa Cruz) and anti-GAPDH (G9545; Sigma-Aldrich). Infrared-dye conjugated secondary antibodies anti-mouse IRDye® 800CW and anti-Rabbit IRDye® 700CW (LI-COR) were used. Signals were detected and analysed with Odyssey analyser software (LI-COR).

## 10. RNA expression studies

### 10.1. Analysis of human *DAB1* gene expression

Total RNAs were obtained from cerebellar vermis and hemispheres from SCA37 Patients IV:9 and IV:10 of Family AT- 901, and an age-matched control using RNeasy® Mini Kit (Qiagen, Hilden, Germany). RNA integrity was measured using the RNA ScreenTape assay (Agilent Technologies). cDNAs were synthesized from 1 mg total RNA with PrimeScript RT reagent Kit (Takar Bio Inc., Kusatsu, Shiga, Japan). Partial transcript fragments were analysed by standard PCR conditions with exon-specific primers (**Supplementary Table 3**). PCR amplicons were purified and sequenced by Sanger. To quantify the expression levels, cDNAs were mixed with SYBR® Green PCR master mix (Applied Biosystems; Thermo Fisher Scientific, Waltham, MA) and specific primers. GAPDH was amplified as an internal control. Cycles and analysis were performed on the LightCycler 480 (Roche) and relative cDNAs fold-changes were normalized to *GAPDH* cDNA and calculated using the $2^{-\Delta\Delta CT}$ method (430). ENCODE *DAB1* RNA sequence reads were compared on BAM files from Purkinje cells from a 6-year-old male child and a 20-year-old adult male (431).

Aligned data were sorted and indexed using SAMtools (401). Read counts for DAB1 RNA were analysed with HTseq (432) using *GAPDH* reads counts to normalize and compare intersample differential expression. RBPmap (433) and PROMO (434) algorithms were used to identify putative

splicing and transcription factor binding sites in the human *DAB1* gene RNA and DNA sequences, respectively. The gene structure image was generated with GSDS 2.0 (435).

### 10.2. Analysis of human *SAMD9L* expression

Total RNAs were obtained from fibroblast samples from patients IV:14 and V:1 of the M-SCA family and two age-matched control using RNeasy Mini Kit (Qiagen). RNA integrity was measured using RNA Screen Tape assay (Agilent Technologies). cDNAs were synthesised from 1 µg total RNA with PrimeScript RT reagent Kit (Takara Bio Inc.). To quantify the expression levels, cDNAs were mixed with SYBR® Green PCR master mix (Thermo Fisher Scientific) and specific primers (**Supplementary Table 4**) for a partial product which includes partial exon 4 and 5 to avoid amplification of DNA contamination. *GAPDH* was amplified as internal control. Cycles and analysis were performed on the LightCycler 480 (Roche) and relative cDNAs fold changes were normalised to *GAPDH* cDNA and calculated using the $2^{-\Delta\Delta CT}$ method (430). ENCODE *SAMD9L* RNA sequence reads were compared on BAM files from adult cerebellar Purkinje cells, adult granular and pyramidal cells, 6-years-old child cerebellum, and cerebellar and spinal cord human embryos (435).

## 11. Mitochondrial studies

### 11.1. Mitochondrial DNA mutation load and lesion quantification

Sequencing of the mtDNA genome from fibroblasts samples from IV:14 and V:1 M-SCA affected patients and two age-matched controls, was performed using the Illumina MiSeq platform (Illumina, Inc.). Enrichment of the entire mtDNA was performed by nine long-range PCR (**Supplementary Table 5**) using LA Taq DNA polymerase with GC Buffer I (Takara Bio Inc.) and 100 ng of total genomic DNA. Library preparation was performed by the Illumina Nextera XT kit (Illumina, Inc.) according to the manufacturer's instructions. Four indexed DNA libraries were equimolarly pooled and sequenced in a single lane of 1 MiSeq flow-cell using paired 150 nt reads. Reads were mapped to the revised Cambridge Reference Sequence (rCRS; GenBank ID NC_012920.1) using the MiSeq Reporter (Illumina, Inc.), which uses a Burrows-Wheeler Aligner (BWA) (383) and the Genome Analysis Tool Kit (GATK) (385) for variant calling of single nucleotide polymorphisms (SNPs) and short indels. Heteroplasmy levels were calculated by the read depth of variations vs. reference nucleotides for all nucleotide positions. Quantification of mtDNA copy number and depletion was performed by qPCR using primers for two short D-LOOP and MT-CO3 mtDNA regions and a nuclear *GAPDH* gene region (**Supplementary Table 5**) in combination with TB Green Premix Ex Taq II (Takara Bio Inc.). Mitochondria DNA lesions were quantified using an adapted version of the long-run qPCR technique for DNA-damage quantification (LORD-Q) method previously described (436), calculating 10kb lesions using amplification efficiency from standard curve based on Ct values. In the adapted version, TB Green Premix Ex Taq II (Takara Bio Inc.) reagent was used for the

amplification of the long 3,723 bp mtDNA instead of the combination of an independent fluorescent dye with a Hot Start Taq.

### 11.2. Determination of ATP content

The ATP content in two patient's fibroblasts from IV:14, V:1 M-SCA affected patients and two age-matched controls was measured with ATPlite Luminescence ATP Detection Assay System (Perkin Elmer) according to manufacturer's instructions. The luminescent intensity was measured in quadruplicate wells with the microplate reader Varioskan® Flash (Thermo Fisher Scientific). The results are expressed as relative ATP levels compared to controls after normalizing for protein concentration.

## 12. Computational protein structure prediction and protein-protein interaction (PPI) network analysis

Sequence alignments against NCBI_Conserved_Domains (CD)_v3.16, PDB_mmCIF70_4_Feb, Pfam-A_v32.0 and SMART_V6.0 domain and structural databases were performed using HHpred (437), a highly sensitive profile-profile protein homology search method. Microtubule binding motifs, were predicted using MAPanalyzer (438), a microtubule-associated protein prediction. PredictProtein (439), DisEMBL (440), InterPro (441) and MobiDB-lite (442) were used for intrinsically disordered regions (IDRs) prediction. NetPhos 3.1 (443) and NetworKIN (444) servers were used to predict serine, threonine or tyrosine phosphorylation sites. hSAMD9L (NP_001290425.1) reference protein was used. Protein–protein functional network interaction multi-protein analysis was performed using the STRING database (445).

## 13. Transmission electron microscopy (TEM)

Fibroblasts from patient IV:14 and one age and gender matched control were growth as described earlier fixed in 2.5% glutaraldehyde, 2% paraformaldehyde in 0.1M phosphate buffer (pH7.4) for 2 h at 4ºC and processed as previously shown (408). Briefly, cells were post-fixed in 1% phosphate saline buffered osmium tetroxide containing 0.8% $KFeCN_2$ and dehydrated through an ethanol series before clearing in propylene oxide, and embedded. Ultrathin sections were stained with uranyl acetate and lead citrate and examined in an EX-electron microscope (model JEM1200; JEOL, Akishima, Tokyo, Japan) at 80 kV. Pictures were acquired using either 12K or 30K magnification. The length and the total number of autophagosomes, mitochondria, lysosomes and autolysosomes were counted and divided by the cytoplasmic area using TEM observation and Fiji software in at least 10 fibroblasts sections. Values from affected fibroblasts were compared and relativized to control fibroblasts.

## 14. Zebrafish ataxia model

All applicable international, national and/or institutional guidelines for the care and use of animals were followed. Animal procedures were approved by the Ethics Committee on Animal Experimentation of the Germans Trias i Pujol Research Institute (IGTP). Zebrafish studies were conducted in collaboration with Zeclinics.

### 14.1. Zebrafish embryo preparation and microinjection

Adult wild-type heterozygous zebrafish (*Danio rerio*; AB background) were maintained in animal facility at 27 ºC on a light cycle of 12 h light, 12 h dark. Zebrafish embryos, obtained in a cross between wild-type AB individuals, were collected in E3 1x medium Petri dishes. The wild-type and mutant human *SAMD9L* sequences were cloned into $PCS2^{+}$ downstream of an SP6 promoter containing a 3'polyA signal. Plasmids were amplified by transformation of *Escherichia coli* HST08 competent cells, digested with *Not*I restriction enzyme, synthesized using mMessage mMachine SP6 Transcription Kit (Thermo Fisher Scientific) following manufacturer's instructions and resuspended in RNAse-free water.

Fertilized embryos were microinjected into one-cell stage embryos with 1 nl of wild-type or mutant human *SAMD9L* mRNA at 25, 50 and 100 ng/µl. Embryos were grown at 28 ºC and 2 h post injections non-fertilized eggs were discarded. 24- and 96-hours post fertilization (hpf) survival and teratogenesis were scored.

### 14.2. Zebrafish behavioural study

Five days post fertilization (dpf) larvae were injected with 100 ng/µl of wild-type or mutant human *SAMD9L* mRNA or GFP mRNA. Dead embryos were discarded. Locomotion and response to visual and physical stimuli were traced and analysed by the EthoVision XT 12 software (Noldus, Wageningen, Netherlands) and the DanioVision (Noldus) device for thirty-two zebrafish embryos from each injected condition. To detect changes in the larvae locomotion deviations from the stereotyped behaviour characterised by motility in the dark phase and reduce motility in the light phase, larvae underwent 50 min dark/light alternating environments of 5 min each one. This experiment was replicated with 10 min of alternating light-dark/light cycles. Distances travelled (mm) during each minute and head turns were measured.

## 15. Statistical analysis

Statistical analyses were performed using SPSS 21.0 (IBM Corp., Armonk, NY) with significance set at $P<0.05$. Data between samples were analysed using the Shapiro-Wilk test to assess for normal distribution followed by the parametric t-test or alternatively with the non-parametric Mann-Whitney

U-test. Spearman's rank correlation was used to estimate the contribution of the repeat expansion size and gender on disease age of onset.

### 15.1. Statistical analysis for zebrafish studies

Behavioural time series statistical data were analysed using two-ways repeated mixed-effects ANOVA followed by post hoc comparisons with the Tukey HSD (honestly significant difference test) for groups of data with equal variances. Total distance travelled and the number of turns were analysed using one-way mixed-effects ANOVA followed by post hoc comparisons with the Tukey HSD for groups of data with equal variances. Those values that did not meet normality or equal variances criteria were individually tested with non-parametric test Mann–Whitney U test. Statistical significance was defined as $P<0.05$. SEM denotes for standard error of the mean.

# RESULTS

# Chapter I: Relative frequency of dominantly inherited ataxias in our cohort of ataxia patients.

### 1.1. Prevalence of SCAs in our cohort of ataxia cases

A total of 308 Spanish ataxia index cases were included in the present study first for the detection of polyglutamine expansions by PCR, and when negative, DNAs were sequenced by NGS either for multigene panel or whole-exome sequencing (WES) analyses, with the implementation of a novel R-based algorithm. This study revealed 59 different causative genetic variants in 74 index cases (24%) and nine at-risk relatives, with 54 index cases presenting mutations in one of 16 dominant ataxia genes (**Figure 5; Table 3**). Of the 59 identified variants, 37 (62.7%) were located in 16 genes previously associated with dominant ataxia (**Figure 6**). Expanded repeat expansions were identified in 21 index cases (6.81%) while all others 53 positive index cases (17.2%) presented conventional mutations identified by NGS sequencing. The most frequently mutated gene was the *ATXN3* (24.07%) identified in 13 index patients. Next in frequency were genetic defects of the *CACNA1A* gene (SCA6 and EA2 cases) (11.11%) with six variants identified in eight patients from six independent families, the *ITPR1* gene (11.11%) with seven variants identified in seven index patients (one of them, P28, carrying another likely pathogenic variant in the *PRKCG* gene), and *ATXN2* repeat expansions (9.26%) in seven patients from five independent families. Four index patients presented variants in the *AFG3L2* gene (7.41%) segregating with the disease in four related individuals, and four different variants in the *TGM6* gene (7.41%) were identified in four other patients. Also, three index cases presented variants in the *PRKCG* gene (5.56%), one of them segregating with the disease. Three variants in the *STUB1* gene (5.56%), two missense variants in the *SPTBN2* gene (3.70%) and two in the *KCNC3* gene (3.70%) were found in seven independent cases. Additionally, variants in six other dominant ataxia genes (*ATXN1*, *IFRD1*, *KCND3*, *PDYN*, *CACNB4* and *SLC1A3*) were found in individual cases. The remaining 20 cases were classified as carrying likely or possibly causative variants in genes not corresponding to previously associated dominant ataxia genes.

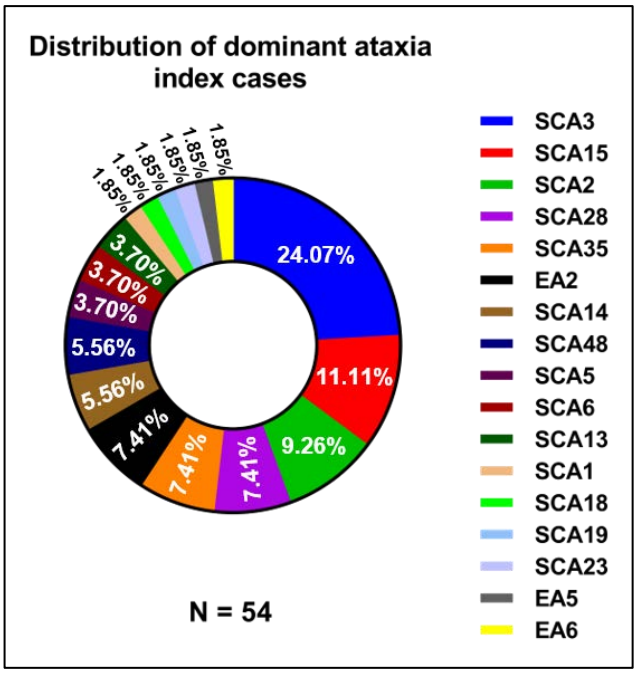


**Figure 5. Distribution of dominant ataxias identified in our ataxia cohort.** Expanded mutations in SCA6 and point mutations in EA2 localises in the same gene (*CACNA1A*).

**Table 3. Relevant variants identified in 83 affected patients from our ataxia cohort.**

| Ped. | Patient | Disease | Gene | Type of mutation | Genotype | Mutation | ACMG classification | Pubmed Ref. |
|---|---|---|---|---|---|---|---|---|
| AT-01 | P1 | SCA1 | *ATXN1* | Expansion | Het | (CAG)49 | Pathogenic | 8358429 |
| AT-02 | P2 | SCA2 | *ATXN2* | Expansion | Het | (CAG)40 | Pathogenic | 8896555 |
| AT-02 | P3 | SCA2 | *ATXN2* | Expansion | Het | (CAG)40 | Pathogenic | 8896555 |
| AT-03 | P4 | SCA2 | *ATXN2* | Expansion | Het | (CAG)38 | Pathogenic | 8896555 |
| AT-03 | P5 | SCA2 | *ATXN2* | Expansion | Het | (CAG)36 | Pathogenic | 8896555 |
| AT-04 | P6 | SCA2 | *ATXN2* | Expansion | Het | (CAG)37 | Pathogenic | 8896555 |
| AT-05 | P7 | SCA2 | *ATXN2* | Expansion | Het | (CAG)36 | Pathogenic | 8896555 |
| AT-06 | P8 | SCA2 | *ATXN2* | Expansion | Het | (CAG)38 | Pathogenic | 8896555 |
| AT-07 | P9 | SCA3 | *ATXN3* | Expansion | Het | (CAG)68 | Pathogenic | 7874163 |
| AT-08 | P10 | SCA3 | *ATXN3* | Expansion | Het | (CAG)68 | Pathogenic | 7874163 |
| AT-09 | P11 | SCA3 | *ATXN3* | Expansion | Het | (CAG)69 | Pathogenic | 7874163 |
| AT-10 | P12 | SCA3 | *ATXN3* | Expansion | Het | (CAG)71 | Pathogenic | 7874163 |
| AT-11 | P13 | SCA3 | *ATXN3* | Expansion | Het | (CAG)64 | Pathogenic | 7874163 |
| AT-12 | P14 | SCA3 | *ATXN3* | Expansion | Het | (CAG)62 | Pathogenic | 7874163 |
| AT-13 | P15 | SCA3 | *ATXN3* | Expansion | Het | (CAG)66 | Pathogenic | 7874163 |
| AT-14 | P16 | SCA3 | *ATXN3* | Expansion | Het | (CAG)67 | Pathogenic | 7874163 |
| AT-15 | P17 | SCA3 | *ATXN3* | Expansion | Het | (CAG)66 | Pathogenic | 7874163 |
| AT-16 | P18 | SCA3 | *ATXN3* | Expansion | Het | (CAG)69 | Pathogenic | 7874163 |
| AT-17 | P19 | SCA3 | *ATXN3* | Expansion | Het | (CAG)66 | Pathogenic | 7874163 |
| AT-18 | P20 | SCA3 | *ATXN3* | Expansion | Het | (CAG)70 | Pathogenic | 7874163 |
| AT-19 | P21 | SCA3 | *ATXN3* | Expansion | Het | (CAG)72 | Pathogenic | 7874163 |
| AT-20 | P22 | SCA5 | *SPTBN2* | Missense | Het | c.1766C>A (p.Ala589Asp) | Likely Pathogenic | - |
| AT-21 | P23 | SCA5 | *SPTBN2* | Missense | Het | c.6763C>T (p.Leu2255Phe) | Likely Pathogenic | - |
| AT-22 | P24 | SCA6 | *CACNA1A* | Expansion | Het | (CAG)21 | Pathogenic | - |
| AT-23 | P25 | SCA6 | *CACNA1A* | Expansion | Het | (CAG)22 | Pathogenic | - |
| AT-24 | P26 | SCA13 | *KCNC3* | Missense | Het | c.1603G>A (p.Val535Met) | Pathogenic | 25756792 |
| AT-25 | P27 | SCA13 | *KCNC3* | Missense | Het | c.2251G>A (p.Ala751Thr) | Likely Pathogenic | - |
| AT-26 | P28 | SCA14 | *PRKCG* | Missense | Het | c.448T>G (p.Cys150Gly) | Likely Pathogenic | - |
| | | SCA15 | *ITPR1* | Missense | Het | c.2311A>G (p.Met771Val) | Likely Pathogenic | - |
| AT-27 | P29 | SCA14 | *PRKCG* | Missense | Het | c.254G>A (p.Cys85Tyr) | Likely Pathogenic | - |
| AT-28 | P30 | SCA14 | *PRKCG* | Missense | Het | c.254G>A (p.Cys85Tyr) | Likely Pathogenic | - |
| AT-28 | P31 | SCA14 | *PRKCG* | Missense | Het | c.254G>A (p.Cys85Tyr) | Likely Pathogenic | - |
| AT-29 | P32 | SCA15 | *ITPR1* | Frameshift | Het | c.4864delG (p.Asp1622MetfsTer29) | Pathogenic | - |
| AT-30 | P33 | SCA15 | *ITPR1* | Missense | Het | c.799A>G (p.Thr267Ala) | Pathogenic | - |
| AT-31 | P34 | SCA15 | *ITPR1* | Missense | Het | c.4218C>G (p.His1406Gln) | Possibly causative | - |
| AT-32 | P35 | SCA15 | *ITPR1* | Missense | Het | c.2935G>A (p.Val979Met) | Possibly causative | - |
| AT-33 | P36 | SCA15 | *ITPR1* | Missense | Het | c.4429G>A (p.Val1477Ile) | Possibly causative | - |

| Ped. | Patient | Disease | Gene | Type of mutation | Genotype | Mutation | ACMG classification | Pubmed Ref. |
|---|---|---|---|---|---|---|---|---|
| AT-34 | P37 | SCA15 | *ITPR1* | Splicing | Het | c.3660C>T* | Possibly causative | - |
| AT-35 | P38 | SCA18 | *IFRD1* | Missense | Het | c.4C>G p.Pro2Ala) | Pathogenic | 28601596 |
| AT-36 | P39 | SCA19 | *KCND3* | Missense | Het | c.1193C>T (p.Pro398Leu) | Pathogenic | - |
| AT-37 | P40 | SCA23 | *PDYN* | Frameshift | Het | c.658_659delGT (p.W220GfsX33) | Pathogenic | 23471613 |
| AT-38 | P41 | SCA28 | *AFG3L2* | Missense | Het | c.1996A>G (p.Met666Val) | Pathogenic | 21595125, 20725928 |
| AT-38 | P42 | SCA28 | *AFG3L2* | Missense | Het | c.1996A>G (p.Met666Val) | Pathogenic | 21595125, 20725928 |
| AT-38 | P43 | SCA28 | *AFG3L2* | Missense | Het | c.1996A>G (p.Met666Val) | Pathogenic | 21595125, 20725928 |
| AT-38 | P44 | SCA28 | *AFG3L2* | Missense | Het | c.1996A>G (p.Met666Val) | Pathogenic | 21595125, 20725928 |
| AT-39 | P45 | SCA28 | *AFG3L2* | Missense | Het | c.31C>T (p.Arg11Trp) | Likely Pathogenic | - |
| AT-40 | P46 | SCA28 | *AFG3L2* | Missense | Het | c.386C>G (p.Ser129Cys) | Likely Pathogenic | - |
| AT-41 | P47 | SCA28 | *AFG3L2* | Nonsense | Het | c.847C>T (p.Arg283Ter) | Pathogenic | - |
| AT-41 | P48 | SCA28 | *AFG3L2* | Nonsense | Het | c.847C>T (p.Arg283Ter) | Pathogenic | - |
| AT-42 | P49 | SCA35 | *TGM6* | Frameshift | Het | c.1523delG (p.Gly508AlafsTer4) | Pathogenic | - |
| AT-43 | P50 | SCA35 | *TGM6* | Nonsense | Het | c.835G>T (p.Gly279Ter) | Pathogenic | - |
| AT-44 | P51 | SCA35 | *TGM6* | Splicing | Het | c.990-1G>C | Pathogenic | - |
| AT-45 | P52 | SCA35 | *TGM6* | Missense | Het | c.926G>A (p.Ser309Asn) | Likely Pathogenic | - |
| AT-46 | P53 | SCA48 | *STUB1* | Frameshift | Het | c.823_824delCT (p.Leu275AspfsTer16) | Pathogenic | 30381368 |
| AT-47 | P54 | SCA48 | *STUB1* | Missense | Het | c.292T>A (p.Phe98Ile) | Likely Pathogenic | - |
| AT-48 | P55 | SCA48 | *STUB1* | Missense | Het | c.524G>A (p.Arg175Lys) | Pathogenic | - |
| AT-49 | P56 | EA2 | *CACNA1A* | Frameshift | Het | c.1084delG (p.Glu362SerfsTer16) | Pathogenic | - |
| AT-50 | P57 | EA2 | *CACNA1A* | Frameshift | Het | c.5588_5589delTC (p.Leu1863ArgfsTer9) | Pathogenic | - |
| AT-50 | P58 | EA2 | *CACNA1A* | Frameshift | Het | c.5588_5589delTC (p.Leu1863ArgfsTer9) | Pathogenic | - |
| AT-50 | P59 | EA2 | *CACNA1A* | Frameshift | Het | c.5588_5589delTC (p.Leu1863ArgfsTer9) | Pathogenic | - |
| AT-51 | P60 | EA2 | *CACNA1A* | Missense | Het | c.5267G>A (p.Arg1756Gln) | Likely Pathogenic | - |
| AT-52 | P61 | EA2 | *CACNA1A* | Missense | Het | c.3052G>A (p.Glu1018Lys) | Possibly causative | 24108129, 30167989 |
| AT-53 | P62 | EA5 | *CACNB4* | Missense | Het | c.5C>T (p.Ser2Phe) | Possibly causative | - |
| AT-54 | P63 | EA6 | *SLC1A3* | Missense | Het | c.1044T>A (p.Phe348Leu) | Likely Pathogenic | - |
| AT-55 | P64 | - | *ARHGEF10* | Missense | Het | c.3499C>T (p.Leu1167Phe) | Likely Pathogenic | - |
| AT-56 | P65 | - | *TWNK* | Missense | Het | c.1052A>G (p.Asn351Ser) | Likely Pathogenic | - |
| AT-57 | P66 | - | *OPA1* | Missense | Comp. Het | c.1257A>G (p.Ile419Met) | Possibly causative | - |
| | | - | | Missense | | c.1922A>T (p.Glu641Val) | Possibly causative | - |
| AT-58 | P67 | - | *MFN2* | Frameshift | Het | c.2258dupT (p.Gln754AlafsTer9) | Pathogenic | 28215760, 16762064 |
| AT-59 | P68 | - | *LRSAM1* | Missense | Het | c.830G>C (p.Gly277Ala) | Likely Pathogenic | - |
| AT-60 | P69 | - | *POLG* | Missense | Homo | c.1795A>C (p.Thr599Pro) | Likely Pathogenic | - |
| AT-61 | P70 | - | *KIF1A* | Missense | Het | c.914C>T (p.Pro305Leu) | Pathogenic | - |
| AT-62 | P71 | - | *KIF1A* | Missense | Het | c.821C>G (p.Ser274Trp) | Pathogenic | - |
| AT-63 | P72 | - | *SLC33A1* | Missense | Het | c.370C>T (p.Leu124Phe) | Possibly causative | - |

| Ped. | Patient | Disease | Gene | Type of mutation | Genotype | Mutation | ACMG classification | Pubmed Ref. |
|---|---|---|---|---|---|---|---|---|
| AT-64 | P73 | - | *WASHC5* | Missense | Het | c.2797G>A (p.Ala933Thr) | Possibly causative | - |
| | | - | *SPG7* | Missense | Het | c.1529C>T (p.Ala510Val) | Possibly causative | 26626314, 25497598 |
| AT-65 | P74 | - | *SOD1* | Missense | Het | C.301G>A (p.Glu101Lys) | Likely Pathogenic | 15258228, 8875253, 22292843 |
| AT-66 | P75 | - | *TAF15* | Missense | Het | c.1280A>G (p.Tyr427Cys) | Possibly causative | 26601740 |
| AT-67 | P76 | - | *CIZ1* | Deletion | Het | c.26_49del (p.Gln9_Gln16del) | Possibly causative | - |
| AT-68 | P77 | - | *GBA* | Missense | Het | c.902G>A (p.Arg301His) | Possibly causative | - |
| AT-69 | P78 | - | *CSF1R* | Missense | Het | c.1693G>A (p.Asp565Asn) | Possibly causative | - |
| AT-70 | P79 | - | *ZMYND11* | Missense | Het | c.503G>A (p.Arg168His) | Possibly causative | - |
| AT-71 | P80 | - | *L1CAM* | Missense | Het | c.832C>T (p.Arg278Cys) | Likely Pathogenic | - |
| AT-72 | P81 | - | *ATP1A3* | Missense | Het | c.2341T>C (p.Tyr781His) | Likely Pathogenic | 25996915 |
| AT-73 | P82 | - | *DNMT1* | Missense | Het | c.1825G>A (p.Gly609Arg) | Likely Pathogenic | - |
| AT-74 | P83 | - | *GRID2* | Missense | Het | c.1577T>A (p.Ile526Asn) | Possibly causative | |

**Table 3. Relevant variants identified in 83 affected patients from our ataxia cohort.**

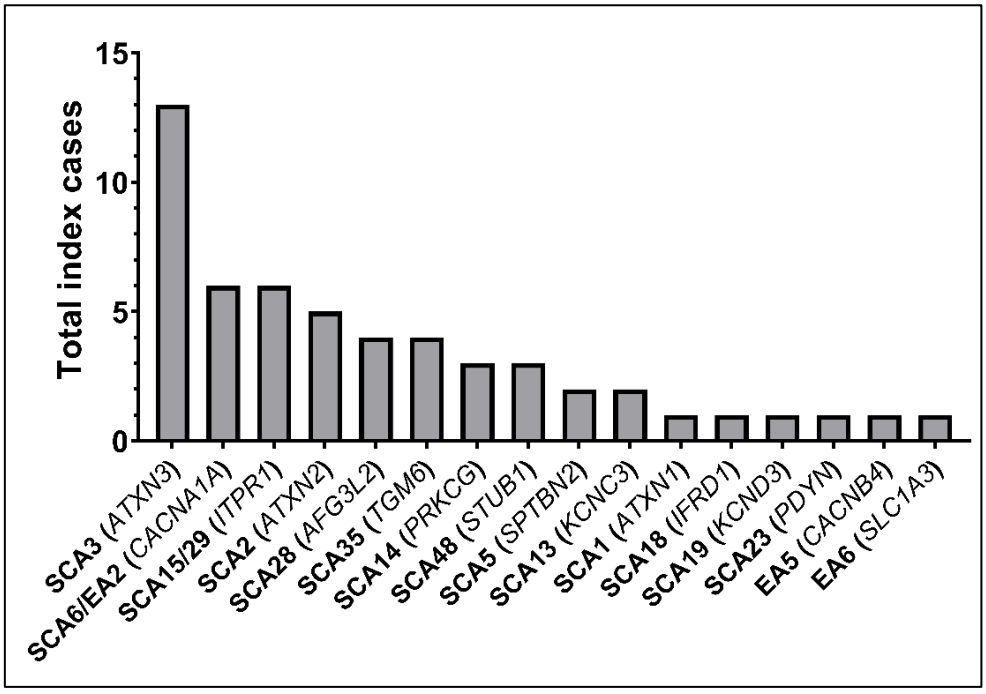


**Figure 6. Distribution of DNA variants in dominant ataxia genes identified in 54 index cases.**

### 1.2. Clinical and genetic heterogeneities in dominant ataxias

A total of 22 additional variants were identified in genes not traditionally associated with SCA phenotypes in 20 index cases presenting with ataxia or cerebellar atrophy as a primary clinical sign. Because of the overlapping phenotypes in many neurological diseases probably due to related underlying molecular mechanisms, the number of variants identified in other genes not previously

associated with SCA phenotypes in ataxia patients has been exponentially increased since the implementation of NGS in diagnostic routine (446). Those 22 variants were herein identified in 20 genes previously associated with neuropathy (seven variants in six patients), spastic paraplegia (four variants in three patients), mental retardation (two variants in two patients), and with amyotrophic lateral sclerosis (one patient), dystonia (one patient), leukoencephalopathy (one patient) and Parkinson's disease (one patient). Other three patients presented variants in genes previously associated with ataxia syndromes not including SCAs or EAs (**Figure 7**).

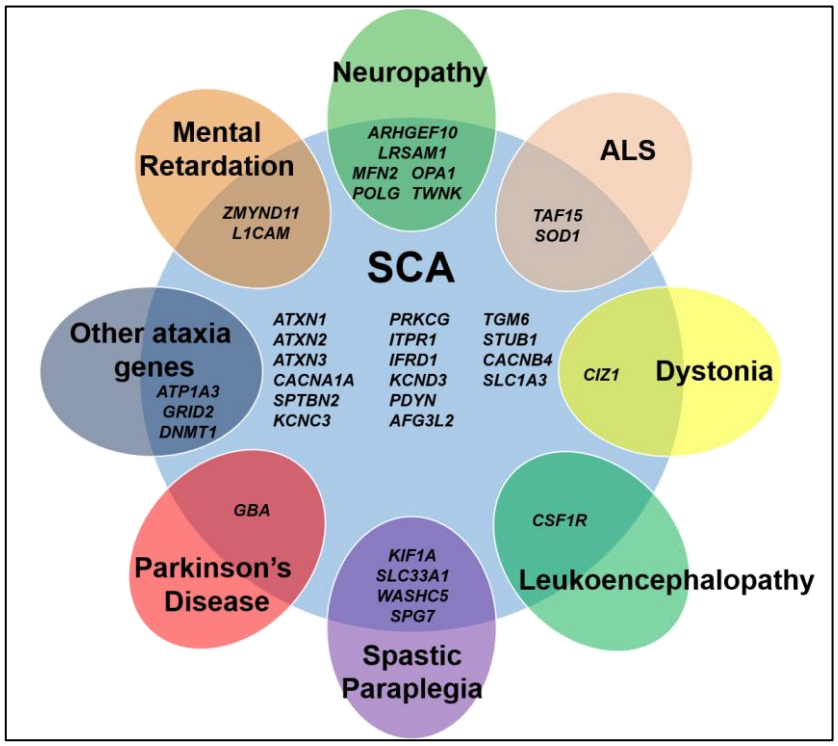


**Figure 7. Clinical and genetic heterogeneities in dominant ataxias.** Thirty-seven variants in 16 genes previously associated with dominant ataxia were identified. Twenty-two variants in 20 genes previously associated with neuropathy, spastic paraplegia, amyotrophic lateral sclerosis, dystonia, leukoencephalopathy, Parkinson's disease, mental retardation and other genes related to ataxic phenotypes were identified.

### 1.3. Variant classification

Fifty-nine different variants including 43 missense, 7 frameshift, 4 repeat expansions, 2 nonsense, 2 splicing and one deletion, were identified in 74 positive index cases (**Figure 8A**). As clinical presentations are rarely specific in dominant forms of cerebellar ataxia, classification of variant pathogenicity was based on stringent genetic criteria only as previously reported by Coutelier and collaborators (392) adapted from the ACMG guidelines (393). Following the adapted criteria, the pathogenic in silico prediction, population frequencies or variant segregation, 22 variants were classified as pathogenic, 20 variants were classified as likely pathogenic and 17 as possibly causative regarding their uncertain significance. Possibly causative variants were classified as such, mainly because of the identified variants localises in a gene not previously associated with any particular SCA subtype or because of relatively high variant frequency in population studies (albeit never higher than 1%) (**Figure 8B**). From the total of 59 different variants identified, 16 of them were described

in previously studies, while 43 novel variants are identified and described in the present study (**Figure 8C**).

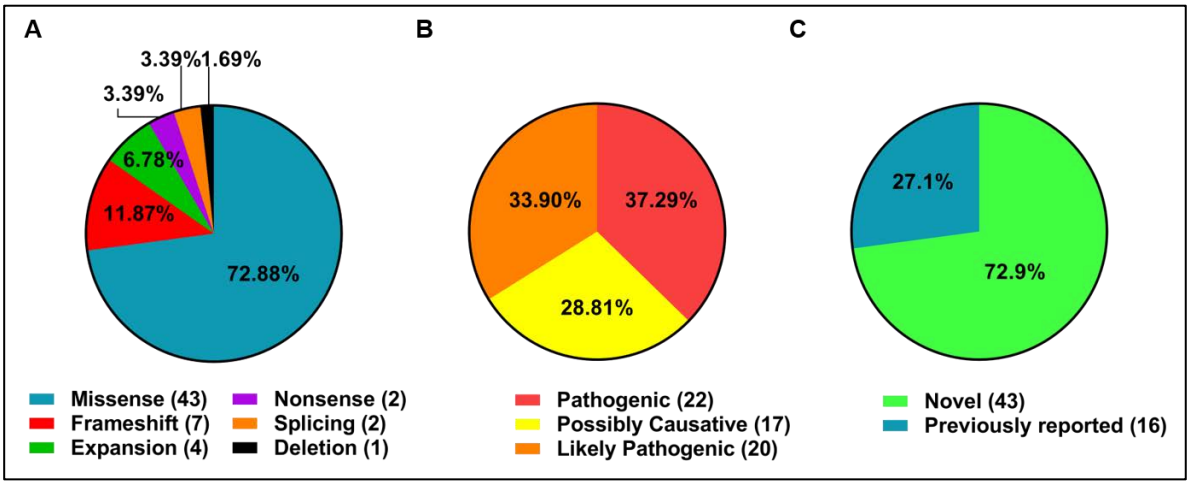


**Figure 8. Classification of identified variants.** A total of 59 different variants were identified in 36 genes. (**A**) 43 were missense variants (72.88%) seven frameshift (11.87%), four different types of repeat expansions (6.78%), two nonsense (3.39%), two splicing variants (3.39%) and one deletion (1.69%). (**B**) Variant assessment classified 22 as pathogenic (37.29%), 20 as likely pathogenic (33.90%) and 17 as possibly causative (28.81%). (**C**) Sixteen of those variants were previously described (27.1%) while 43 were novel variants (72.9%).

### SCA repeat expansions (SCA1, SCA2, SCA3 and SCA6)

From the total positive cases, patient P1 presented an expansion in *ATXN1* gene (SCA1) with 49 CAG repeats and seven patients (P2-P8) from five independent families presented CAG expansions ranging from 36 to 40 repeats in *ATNX2* gene (SCA2). Expansions ranging from 62 to 72 CAG repeats in *ATXN3* gene (SCA3) were identified in 13 index cases (P9-P21). Furthermore, repeat expansions in *CACNA1A* were identified in two index cases (P24 and P25) with 21 and 22 CAG repeats respectively and presenting clinical signs compatible with SCA6.

### SCA5 (*SPTBN2*)

Two independent unrelated cases presented heterozygous missense mutations, c.1766C>A (p.Ala589Asp) in P22 and c.6763C>T (p.Leu2255Phe) in P23, not previously described in the *SPTBN2* gene (SCA5). The pathogenicity of the c.1766C>A (p.Ala589Asp) variant was pathogenic predicted as uncertain because of inconclusive pathogenic prediction from algorithms, while c.6763C>T (p.Leu2255Phe) was predicted as probably pathogenic by all algorithms. Despite these differences in pathogenicity prediction ACMG adapted score classified both of them as likely pathogenic.

**SCA13 (*KCNC3*)**

Two index cases presented two heterozygous variants, c.1603G>A (p.Val535Met) in P26 and c.2251G>A (p.Ala751Thr) in P27, within the *KCNC3* gene (SCA13). The c.1603G>A (p.Val535Met) variant was previously described co-segregating with the disease in two Dutch affected family members, both suffering from early-onset (age 2–3 years), slowly progressive, cerebellar ataxia with mild intellectual disability (447). Furthermore, variant segregation studies were performed in patient P26 parents and concluded that the variant appeared *de novo* in the affected child. The c.2251G>A (p.Ala751Thr) variant (rs962219846) was present in three out of the 55,105 samples from the gnomAD exomes database (MAF=0.005%) and in one out of the 122,491 samples from the gnomAD genomes r3.0 database (MAF=0.0008%). Pathogenic score classified the variant as likely pathogenic regarding the prediction of three in silico algorithms and the clinical signs presented the proband. In conclusion, both patients (P26 and P27) presented with clinical signs and genetics findings compatible with SCA13.

**SCA14 (*PRKCG*)**

Three patients (P29-P31) from two independent families presented the heterozygous variant c.254G>A (p.Cys85Tyr), not previously described, in the *PRKCG* gene associated with SCA14. This variant was predicted as probably pathogenic by in silico algorithms, and it is absent in the databases which classifies the variant as likely pathogenic. Furthermore, another patient (P28) presented the heterozygous variant c.448T>G (p.Cys150Gly) in the *PRKCG* gene, absent in databases, in silico predicted as pathogenic and in double heterozygous state with the variant c.2311A>G (p.Met771Val) in the *ITPR1* gene (SCA15). This variant was also predicted as probably pathogenic by in silico algorithms and was absent in variant databases. Considering that the segregation analysis was not available, it could not be ruled out the contribution of both variants in the pathogenesis of the disease. Thus, both variants were classified as possibly causative.

**SCA15/29 (*ITPR1*)**

Variants in the *ITPR1* gene were also identified in heterozygosity in six patients. The frameshift variant c.4864delG (p.Asp1622MetfsTer29) identified in patient P32 is predicted to provoke a premature stop codon generating a protein containing 1,651 amino acids while normal *ITPR1* gene product includes 2,758 amino acids. The variant was absent in published databases. Previous studies identified the *ITPR1* deletion in a large four-generation family indicating haploinsufficiency of *ITPR1* in SCA15 (448). The missense variant c.799A>G (p.Thr267Ala) identified in patient P33 was predicted as probably pathogenic by in silico algorithms and was absent in variant databases. Furthermore, a previous study identified a base substitution c.800C<T in the same amino acid codon, but provoking a different change (p.Thr267Met). Based on this information and the adapted ACMG

classification, the variant c.799A>G (p.Thr267Ala) was classified as pathogenic. Three other missense variants c.4218C>G (p.His1406Gln) in patient P33, c.2935G>A (p.Val979Met) in patient P35 and c.4429G>A (p.Val1477Ile) in patient P36 were classified as possibly causative because of their presence in databases (rs61757110 with gnomAD exomes MAF=0.2%, ClinVar VCV000345736.4; rs776228202 with gnomAD exomes MAF=0.00016%, ClinVar VCV000804933.1; and rs200646875 with gnomAD exomes MAF=0.02%). The remaining variant c.3660C>T located at three base pairs from the exon-intron junction of the *ITPR1* gene was identified in patient P37 and was predicted to probably affect the correct splicing of exon three. This variant was also present in gnomAD exomes database (rs34635052) with a MAF=0.1% and thus classified as possibly causative.

**SCA18 (*IFRD1*)**

The heterozygous variant c.4C>G (p.Pro2Ala) in the *IFRD1* gene identified in patient P38 was initially classified as uncertain significance because of its presence in database (rs773505025 with gnomAD exomes MAF=0.0004%) and an inconclusive in silico prediction. A subsequent publication reported the identified variant associated with an isolated 62-year-old patient with palatal tremor, hypertrophic olivary degeneration, and cerebellar atrophy (449).

**SCA19/22 (*KCND3*)**

The segregation of the heterozygous variant c.1193C>T (p.Pro398Leu) in the *KCND3* gene (SCA19/SCA22) identified in patient P39 concluded that appeared *de novo* in an affected child presenting with ataxia with cognitive impairment, both clinical signs previously associated with SCA19/SCA22. Furthermore, the variant was absent in variant databases and predicted as probably pathogenic by in silico algorithms. Thus, this *de novo* variant was classified as pathogenic.

**SCA23 (*PDYN*)**

The frameshift variant c.658_659delGT (p.W220GfsX33) in the *PDYN* gene (SCA23), previously described in four independent ataxic index cases (236) was identified in heterozygosis in patient P40. Jezierska and collaborators demonstrated lower PDYN protein levels and altered PDYN protein processing in transfected cells (236).

**SCA28 (*AFG3L2*)**

Variants in the *AFG3L2* gene compatible with SCA28 were identified in eight patients from three independent families. Interestingly, four affected individuals from a large family originally from the south of Spain (P41-P44), revealed the previously reported heterozygous variant c.1996A>G (p.Met666Val) (252,392). Furthermore, Cagnoli and collaborators reported two different nucleotide

changes in the same amino acid codon generating a different amino acid change c.1997T>G (p.Met666Arg), c.1997T>C (p.Met666Thr). Interestingly this variant localises to the AFG3L2 peptidase M14 domain, where several other variants have been reported (251,450,451). Another ataxia patient (P45) presented the heterozygous variant c.31C>T (p.Arg11Trp) in the *AFG3L2* gene, with an inconclusive in silico prediction, without frequency in variant databases (rs1050447923), and classified in the ClinVar database as uncertain, classifying the variant as likely pathogenic. Patient P46 presented the heterozygous variant c.386C>G (p.Ser129Cys), and in silico predicted it as probably pathogenic and is absent in variant databases, classifying the variant as likely pathogenic. A fourth variant, c.847C>T (p.Arg283Ter), in the *AFG3L2* gene was identified in two ataxic siblings, P47 and P48. This variant generates a premature stop codon in AFG3L2 protein and it is present in databases (rs763429903; gnomAD exomes MAF=0.0012%). A different frameshift mutation, c.1958dupT (p.Thr654Asnfs*15) in *AFG3L2* exon 15, which also resulted in a premature termination, was previously reported in a late-onset ataxia patient and her daughter (452). The study also demonstrates a decreased ratio of the transcript from the mutated *AFG3L2* allele in peripheral lymphocytes of both patients. Thus, the c.847C>T (p.Arg283Ter) variant was classified as pathogenic. This high number of variants identified in *AFG3L2* in our ataxia cohort is in consonance with the relative high frequency published in previous ataxia studies (252,392).

**SCA35 (*TGM6*)**

Heterozygous variants in the *TGM6* gene associated with SCA35 were identified in four ataxia cases (P49-P52). Two of them presented two heterozygous variants, c.1523delG (p.Gly508AlafsTer4) in P49 and c.835G>T (p.Gly279Ter) in P50, which resulted each in a premature protein termination. A previously study reported a frameshift mutation c.841delG in an Hispanic patient, generating a truncated protein of only 289 amino acids while the *TGM6* normal gene product is 706 amino acids long (453). Furthermore, c.1523delG (p.Gly508AlafsTer4) and c.835G>T (p.Gly279Ter) variants were absent in databases. Another heterozygous variant c.990-1G>C was identified in patient P51, localised to the *TGM6* intron 7 and exon 8 junction without reference in variant databases and was predicted to alter the correct splicing. A previously reported splicing variant c.7+1G>T was identified in three affected family members (454) supporting evidence for haploinsufficiency underlying SCA35 pathogenesis. The fourth patient (P52) presented the heterozygous missense variant c.926G>A (p.Ser309Asn), predicted as pathogenic and referenced as rs1222406514 with a MAF=0.0007% allele frequency in the gnomAD exomes database. Thus, the variant was classified as likely pathogenic.

**SCA48 (*STUB1*)**

The recently described heterozygous variant c.823_824delCT (p.Leu275AspfsTer16) associated with SCA48 (298) in an Spanish family from Girona, Catalonia, was identified in the patient P53. Furthermore, patient P54 presented the heterozygous variant c.292T>A (p.Phe98Ile) in *STUB1* which was predicted as probably pathogenic, absent in variant databases and classified as likely pathogenic. A third heterozygous variant in the *STUB1* gene, c.524G>A (p.Arg175Lys), was identified in patient P55. This missense variant was absent in the databases and produces an amino acid change predicted as likely pathogenic. Furthermore, the nucleotide change localises to the last position of exon 3 within the intron/exon junction boundary and predicted to affect the correct splicing, suggesting STUB1 haploinsufficiency likewise the c.823_824delCT (p.Leu275AspfsTer16) previously described variant. Accordingly, the variant was classified as pathogenic.

**EA2 (*CACNA1A*)**

Two missense and two frameshift variants in the *CACNA1A* gene were identified in four index cases. The patient P56 presented with the heterozygous variant c.1084delG (p.Glu362SerfsTer16) resulting in a premature termination in transcript NM_023035.3 and absent in the variant databases. The index case P57 and two other familiar cases (P58 and P59) presented also the heterozygous frameshift variant c.5588_5589delTC (p.Leu1863ArgfsTer9) resulting in a premature termination for the transcript (NM_001127221.1) which segregated with the disease in the kindred. Several premature stop codons were previously described in the *CACNA1A* gene associated with episodic ataxia type 2 (455,456). Accordingly, both variants were classified as pathogenic. Moreover, the missense heterozygous variant c.5267G>A (p.Arg1756Gln) was identified in patient P60 and referenced as rs781588570, with MAF=0.0004% in gnomAD exomes database with uncertain significance in the ClinVar database, and with an inconclusive in silico prediction, it was classified as likely pathogenic. A fourth heterozygous variant c.3052G>A (p.Glu1018Lys) was identified in patient P61. This variant was previously reported in the literature associated with different migraine and hemiplegic phenotypes and experimental studies with transfected cells identified an underlying gain-of-function effect with electrophysiological alterations (457,458). Owing to the presence of this variant in databases (rs16024) with a relatively high frequency (MAF=0.4% in gnomAD exomes) and its inconclusive pathogenic prediction, the variant was classified as possibly causative.

**EA5 (*CACNB4*)**

The heterozygous variant c.5C>T (p.Ser2Phe) in the *CACNB4* gene previously associated with episodic ataxia type 5, was identified in patient P62. This variant was previously referenced as rs200092211 with a gnomAD exomes database MAF=0.1% with an inconclusive in silico prediction. Furthermore, ClinVar database reported this variant (VCV000193120.5) with a conflicting

interpretation of pathogenicity regarding different clinical conditions. Accordingly, the variant was classified as possibly causative.

#### EA6 (*SLC1A3*)

The patient P63 carried an heterozygous variant c.1044T>A (p.Phe348Leu) in *SLC1A3* gene previously associated with episodic ataxia type 6. This novel heterozygous variant was not previously described in databases and was predicted to be probably pathogenic by in silico algorithms. Accordingly, the variant was classified to be likely pathogenic.

### 1.4. Overlapping phenotypes

Extended NGS studies analysing other genes associated with clinical phenotypes presenting with ataxia concomitant with other neurological signs, identified 22 variants from 20 patients from the ataxia cohort. Literature review for clinical, genetic and pathological assessment of those variants pointed them as likely causative variants underlying diseases pathology for the studied cases as discussed in the following sections.

#### Polyneuropathy associated genes

Seven variants were identified in genes previously associated with clinical neuropathic diseases that could present with ataxia as a secondary sign. The heterozygous variant c.3499C>T (p.Leu1167Phe) in *ARHGEF10* was identified in patient P64 presenting with sensory ataxia polyneuropathy with cerebellar dysfunction. Despite this variant was present in databases (rs770414770) with a MAF=0.0003% in gnomAD exomes and had an inconclusive in silico prediction, the patient's sister carried the same variant presenting with similar clinical signs. Heterozygous variants in *ARHGEF10* gene have been previously associated with slowed nerve conduction velocities that could course clinically asymptomatic. Accordingly, the variant was classified as likely pathogenic.

Another heterozygous variant c.1052A>G (p.Asn351Ser) in the *TWNK* gene associated with autosomal dominant progressive external ophthalmoplegia or Perrault Syndrome which can present ataxia as a neurological sign, was identified in patient P65. The identified variant was present in databases as rs370231886 with a MAF=0.0067% in gnomAD exomes and with an inconclusive in silico prediction. Moreover, this variant was reported in ClinVar (RCV000508812.1), associated with a mitochondrial disease. Accordingly, the variant was classified as likely pathogenic.

The patient P66 presented two compound heterozygous variants c.1257A>G (p.Ile419Met) and c.1922A>T (p.Glu641Val) in the *OPA1* gene. The c.1257A>G (p.Ile419Met) missense variant, albeit not causing a phenotype per se, has been recently suggested to contribute consistently in modulating the phenotype in *OPA1* compound heterozygous subjects presenting with optic atrophy, ataxia and

polyneuropathy (459). The c.1922A>T (p.Glu641Val) variant was absent in databases and predicted as probably pathogenic by in silico algorithms, thus classifying both variants as possibly causative.

Another two variants in heterozygosis were identified in the *MFN2* and *LRSAM1* genes associated with autosomal dominant Charcot-Marie-Tooth 2A and Charcot-Marie-Tooth 2P respectively. Both disease subtypes often present with ataxia as a common clinical sign (460,461). The heterozygous c.2258dupT (p.Gln754AlafsTer9) in the *MFN2* gene identified in P67 was previously reported in an affected patient with late-onset hereditary polyneuropathy, with ataxic gait as initial clinical sign (462). The heterozygous variant c.830G>C (p.Gly277Ala) in the *LRSAM1* gene was identified in patient P68 presenting with cerebellar atrophy, dysarthria, and sensory polyneuropathy, was absent in the variant databases and predicted as probably pathogenic by in silico algorithms, was classified as likely pathogenic.

The variant c.1795A>C (p.Thr599Pro) in the *POLG* gene was identified in homozygosis in patient P69. This variant was referenced as rs1064796458 without allele frequency, with uncertain significance in ClinVar, and predicted as probably pathogenic by in silico algorithms. Homozygous and compound heterozygous variants in the *POLG* gene have been associated with adult-onset sensory ataxia with neuropathy, dysarthria, and ophthalmoparesis (SANDO; OMIM # 607459). Accordingly, the variant was classified likely pathogenic.

**Spastic paraplegia associated genes**

Hereditary spastic paraplegias (HSPs) and hereditary spinocerebellar ataxias (SCAs) have traditionally been designated in distinct clinical phenotypes according to their predominant clinical signs, but in recent years they are increasingly being recognised to have overlapping phenotypes (463). As an example, variants in the *KIF1A* gene, which have been traditionally associated with spastic paraplegia type 30 (SPG30; OMIM # 610357), have also been identified in patients presenting with gait disturbance or ataxia and cerebellar dystrophy (464,465). In the present study we identified two index cases P70 and P71 presenting both with heterozygous variants c.914C>T (p.Pro305Leu) and c.821C>G (p.Ser274Trp) in the *KIF1A* gene. Both variants were predicted to be probably pathogenic and their allele frequencies were absent in databases. Furthermore, segregation analysis of c.914C>T (p.Pro305Leu) confirmed that it appeared *de novo* in the affected offspring. Moreover, regarding the c.821C>G (p.Ser274Trp) variant, another variant in the same amino acid codon c.821C>T (p.Ser274Leu) has been described and classified as pathogenic or likely pathogenic in the ClinVar database (VCV000211298.3). Thus, both variants were classified in the present study as pathogenic.

Another patient from our ataxia cohort (P72) revealed the heterozygous variant c.370C>T (p.Leu124Phe) in the *SLC33A1* gene previously associated with autosomal dominant spastic

paraplegia type 42 (OMIM # 612539). The identified variant was referenced as rs141818342 with a MAF=0.034% allele frequency in gnomAD exomes database. Furthermore, this variant was reported in spastic paraplegia patients and classified as a variant of uncertain significance in the ClinVar database (VCV000448411.2). Accordingly, this variant was classified as a possibly causative variant in the present study.

Patient P73 presented two double heterozygous variants, c.2797G>A (p.Ala933Thr) and c.1529C>T (p.Ala510Val) in the *WASHC5* and *SPG7* genes respectively. *WASHC5* variants have been previously associated with autosomal dominant spastic paraplegia type 8 (OMIM # 603563). The identified variant in *WASHC5* was previously referenced as rs541330058 with MAF=0.002% in gnomAD exomes database and with an inconclusive in silico prediction. The c.1529C>T (p.Ala510Val) variant has been recently reported in cerebellar ataxia cases in homozygosis or compound heterozygosis with other SPG7 variants (392,466) and its possible pathological effect in heterozygosis is subject of controversy (467). Considering that the segregation analysis was not available in our kindred, it could not be ruled out the contribution of both variants in the pathogenesis of the disease. Thus, both variants were classified as variants of possibly causative in the studied case.

**ALS**

Overlapping phenotypes between ALS and ataxia have been previously associated with different genes such as *ATXN2*, *C9ORF72* or *SETX* (468–470). In the present study, the heterozygous variant C.301G>A (p.Glu101Lys) was identified in the *SOD1* gene in patient P74. The allele frequency of this variant (rs76731700) was absent in databases, and the in silico prediction was inconclusive. Moreover, the variant is classified as likely pathogenic and pathogenic in the ClinVar database (VCV000574319.1). Interestingly, the studied patient presented with initial signs of progressive ataxia which evolved to muscular weakness and peripheral neuropathy. Accordingly, the variant was classified as likely pathogenic in the present study. Another variant c.1280A>G (p.Tyr427Cys) in the *TAF15* gene previously implicated in ALS (471), was identified in patient P75. Furthermore, this variant (rs200046706), predicted as pathogenic with a MAF=0.018% in gnomAD exomes, was previously described in two Korean patients, one of them suffering from progressive motor weakness and the other from progressive dysarthria (472). Accordingly, the variant was classified as possibly causative.

**Dystonia**

A few genes have been previously reported to overlap with ataxia and dystonia phenotypes (473). In the present study, the patient P76 presented the variant c.26_49del (p.Gln9_Gln16del) in the *CIZ1* gene previously described in variant databases (rs767703623) with a MAF=0.11% in gnomAD genomes r3.0 database and reported in the ClinVar database (VCV000455982.1) in a case presenting

dystonia. The *CIZ1* gene has been previously associated with adult onset primary cervical dystonia (474). Since there was not extended clinical information available, this variant was classified as a possibly causative variant.

**Parkinson's disease**

Parkinsonism has been described in different SCA phenotypes, especially in SCA2, SCA3, SCA9, SCA12, SCA14 and SCA17, and may also be present in SCA6 and SCA8, and rarely and mildly in SCA14 (100,475). In the present study, the heterozygous variant c.902G>A (p.Arg301His) in the *GBA* gene was identified in patient P77. Heterozygous variants in the *GBA* gene have been associated with late-onset Parkinson's disease (OMIM # 168600). The identified variant with an inconclusive in silico prediction was present in databases (rs140955685) without a reported allele frequency and classified as a variant of uncertain significance in ClinVar (VCV000592663.1). Extended clinical data was not available; therefore, it was classified as a possibly causative variant.

**Leukoencephalopathy**

Ataxia has been reported as a common sign in patients suffering from leukoencephalopathy (476). In the present study, the heterozygous variant c.1693G>A (p.Asp565Asn) was identified in the *CSF1R* gene in patient P78. This variant was reported in two affected cases one of the suffering from hereditary diffuse leukoencephalopathy (477,478). Because of the absence patient's clinical data, this variant was classified as a possibly causative variant.

**Ataxia with mental retardation**

Mental retardation has been described in different SCA subtypes, mainly SCA13, SCA21 and SCA27. In the present study, the heterozygous variant c.503G>A (p.Arg168His) in the *ZMYND11* gene identified in patient P79, was predicted as probably pathogenic with a MAF=0.0003% in gnomAD exomes database (rs750701399). The *ZMYND11* gene has been previously associated with autosomal dominant mental retardation (616083) that could present with ataxia as a clinical sign (479). Since extended clinical information was not available from the studied patient, we classified the variant as a possibly causative variant.

Another heterozygous variant c.832C>T (p.Arg278Cys) in the *L1CAM* gene identified in patient P80, was predicted as probably pathogenic with a MAF=0.002% in gnomAD exomes database (rs372200840). The *L1CAM* gene has been previously associated with X-linked hydrocephalus with aqueductal stenosis (OMIM # 307000) with some patients presenting with cerebellar vermis hypoplasia (480). As the studied patient also presented with leukodystrophy, the variant was classified as a likely pathogenic variant.

**Other ataxia related genes**

There are a few other autosomal dominant syndromic diseases such as CAPOS syndrome (cerebellar ataxia, areflexia, pes cavus, optic atrophy, and sensorineural hearing loss; OMIM # 601338), ADCADN syndrome (Cerebellar ataxia, deafness, and narcolepsy, autosomal dominant; OMIM # 604121) or alternating hemiplegia of childhood type 1 (OMIM # 104290) that can present with ataxia as a main clinical sign. In the present study, patient (P81) presented the heterozygous variant c.2341T>C (p.Tyr781His) in the *ATP1A3* gene previously associated with autosomal dominant CAPOS syndrome (OMIM # 601338) characterised by cerebellar ataxia, areflexia, pes cavus, optic atrophy, and sensorineural hearing loss. The identified variant, which was absent in the databases and predicted as probably pathogenic, was previously reported in a case with alternating hemiplegia (481) which classified the variant as likely pathogenic. Another patient (P82) presented the heterozygous variant c.1825G>A (p.Gly609Arg) in the *DNMT1* gene previously associated with a myriad of neurological disorders (482) including ADCADN syndrome. The identified variant was absent in variant databases and predicted as pathogenic by in silico algorithms. The studied case clinically presented with ataxia, dystonia and cognitive decline, previously describe in *DNMT1* cases. Thus, the identified variant was classified as likely pathogenic.

Finally, patient P83 presented the heterozygous variant c.1577T>A (p.Ile526Asn) in the *GRID2* gene previously associated with autosomal recessive spinocerebellar ataxia type 18 (OMIM # 616204). The identified variant was absent in databases and was predicted as probably pathogenic by in silico algorithms. Remarkably, a recent study identified an heterozygous missense variant in the *GRID2* gene segregating with the disease in a large Algerian family (483). Therefore, it could not be ruled out the possibility that the identified variant caused the ataxic phenotype, thus classifying the variant as a possibly causative variant.

**Table 4. Summary of variants identified in this study and their relevant information.**

| Variant | Type of mutation | Gene | Genotype | dbSNP reference | gnomAD – Exomes MAF (%) | ClinVar Ref | ClinVar Significance | Pathogenicity prediction | Classification | Index cases (Total cases) | Pubmed Ref. |
|---|---|---|---|---|---|---|---|---|---|---|---|
| (CAG)49 | Expansion | *ATXN1* | Het | rs193922926 | - | VCV000008071 | Pathogenic | PP | Pathogenic | 1 | 8358429 |
| (CAG)36-40 | Expansion | *ATXN2* | Het | - | - | VCV000929858.1 | Pathogenic | PP | Pathogenic | 5 (7) | 8896555 |
| (CAG)62-72 | Expansion | *ATXN3* | Het | - | - | VCV000209995.1 | Pathogenic | PP | Pathogenic | 13 | 7874163 |
| c.1766C>A (p.Ala589Asp) | Missense | *SPTBN2* | Het | - | - | - | - | NP/PP | Likely Pathogenic | 1 | - |
| c.6763C>T (p.Leu2255Phe) | Missense | *SPTBN2* | Het | - | - | - | - | PP | Likely Pathogenic | 1 | - |
| (CAG)21-22 | Expansion | *CACNA1A* | Het | rs16054 | | VCV000562099.2 | Pathogenic | PP | Pathogenic | 2 | 8988170 |
| c.1603G>A (p.Val535Met) | Missense | *KCNC3* | Het | - | - | - | - | PP | Pathogenic | 1 | 25756792 |
| c.2251G>A (p.Ala751Thr) | Missense | *KCNC3* | Het | rs962219846 | 0.005% | - | - | NP/PP | Likely Pathogenic | 1 | - |
| c.448T>G (p.Cys150Gly) | Missense | *PRKCG* | Het | - | - | - | - | PP | Likely Pathogenic | 1 | - |
| c.254G>A (p.Cys85Tyr) | Missense | *PRKCG* | Het | - | - | - | - | PP | Likely Pathogenic | 2 (3) | - |
| c.2311A>G (p.Met771Val) | Missense | *ITPR1* | Het | - | - | - | - | PP | Likely Pathogenic | 1 | - |
| c.4864delG (p.Asp1622MetfsTer 29) | Frameshift | *ITPR1* | Het | - | - | - | - | PP | Pathogenic | 1 | - |
| c.799A>G (p.Thr267Ala) | Missense | *ITPR1* | Het | - | - | - | - | PP | Pathogenic | 1 | - |
| c.4218C>G (p.His1406Gln) | Missense | *ITPR1* | Het | rs61757110 | 0.60% | VCV000345736.4 | Likely Benign | NP/PP | Possibly causative | 1 | - |
| c.2935G>A (p.Val979Met) | Missense | *ITPR1* | Het | rs776228202 | 0.0016% | VCV000804933.1 | Uncertain | NP/PP | Possibly causative | 1 | - |
| c.4429G>A (p.Val1477Ile) | Missense | *ITPR1* | Het | rs200646875 | 0.02% | - | - | NP/PP | Possibly causative | 1 | - |

| Variant | Type of mutation | Gene | Genotype | dbSNP reference | gnomAD – Exomes MAF (%) | ClinVar Ref | ClinVar Significance | Pathogenicity prediction | Classification | Index cases (Total cases) | Pubmed Ref. |
|---|---|---|---|---|---|---|---|---|---|---|---|
| c.3660C>T* | Splicing | *ITPR1* | Het | rs34635052 | 0.20% | VCV000345732.4 | Likely Benign | PP | Possibly causative | 1 | - |
| c.4C>G (p.Pro2Ala) | Missense | *IFRD1* | Het | rs773505025 | 0.004% | - | - | PP | Pathogenic | 1 | 28601596 |
| c.1193C>T (p.Pro398Leu) | Missense | *KCND3* | Het | - | - | - | - | PP | Pathogenic | 1 | - |
| c.658_659delGT (p.W220GfsX33) | Frameshift | *PDYN* | Het | - | - | - | - | PP | Pathogenic | 1 | 23471613 |
| c.1996A>G (p.Met666Val) | Missense | *AFG3L2* | Het | rs151344514 | 0.0008% | VCV000030423.5 | Pathogenic/ Uncertain | PP | Pathogenic | 1 (4) | 21595125, 20725928 |
| c.31C>T (p.Arg11Trp) | Missense | *AFG3L2* | Het | rs1050447923 | - | VCV000805328.1 | Uncertain | NP/PP | Likely Pathogenic | 1 | - |
| c.386C>G (p.Ser129Cys) | Missense | *AFG3L2* | Het | - | - | - | - | PP | Likely Pathogenic | 1 | - |
| c.847C>T (p.Arg283Ter) | Nonsense | *AFG3L2* | Het | rs763429903 | - | - | - | PP | Pathogenic | 1 (2) | - |
| c.1523delG (p.Gly508AlafsTer4) | Frameshift | *TGM6* | Het | - | - | - | - | PP | Pathogenic | 1 | - |
| c.835G>T (p.Gly279Ter) | Nonsense | *TGM6* | Het | - | - | - | - | PP | Pathogenic | 1 | - |
| c.990-1G>C | Splicing | *TGM6* | Het | - | - | - | - | PP | Pathogenic | 1 | - |
| c.926G>A (p.Ser309Asn) | Missense | *TGM6* | Het | rs1222406514 | 0.0008% | - | - | PP | Likely Pathogenic | 1 | - |
| c.823_824delCT (p.Leu275AspfsTer16) | Frameshift | *STUB1* | Het | rs748984540 | 0.0008% | VCV000590271.1 | Pathogenic | PP | Pathogenic | 1 | 30381368 |
| c.292T>A (p.Phe98Ile) | Missense | *STUB1* | Het | - | - | - | - | PP | Likely Pathogenic | 1 | - |
| c.524G>A (p.Arg175Lys) | Missense | *STUB1* | Het | - | - | - | - | PP | Pathogenic | 1 | - |
| c.1084delG (p.Glu362SerfsTer16) | Frameshift | *CACNA1A* | Het | - | - | - | - | PP | Pathogenic | 1 | - |

| Variant | Type of mutation | Gene | Genotype | dbSNP reference | gnomAD – Exomes MAF (%) | ClinVar Ref | ClinVar Significance | Pathogenicity prediction | Classification | Index cases (Total cases) | Pubmed Ref. |
|---|---|---|---|---|---|---|---|---|---|---|---|
| c.5588_5589delTC (p.Leu1863ArgfsTer9) | Frameshift | *CACNA1A* | Het | rs1431092862 | - | - | - | PP | Pathogenic | 1 (3) | - |
| c.5267G>A (p.Arg1756Gln) | Missense | *CACNA1A* | Het | rs781588570 | 0.0004% | VCV000804609.1 | Uncertain | NP/PP | Likely Pathogenic | 1 | - |
| c.3052G>A (p.Glu1018Lys) | Missense | *CACNA1A* | Het | rs16024 | - | VCV000194928.6 | Likely Benign/ Uncertain | NP/PP | Possibly causative | 1 | 24108129, 30167989 |
| c.5C>T (p.Ser2Phe) | Missense | *CACNB4* | Het | rs200092211 | 0.14% | VCV000193120.5 | Likely Benign/Uncertain | NP/PP | Possibly causative | 1 | - |
| c.1044T>A (p.Phe348Leu) | Missense | *SLC1A3* | Het | rs773243452 | - | - | - | NP/PP | Likely Pathogenic | 1 | - |
| c.3499C>T (p.Leu1167Phe) | Missense | *ARHGEF10* | Het | rs770414770 | - | - | - | NP/PP | Likely Pathogenic | 1 | - |
| c.1052A>G (p.Asn351Ser) | Missense | *TWNK* | Het | rs370231886 | 0.0068% | RCV000508812.1 | Pathogenic | NP/PP | Likely Pathogenic | 1 | - |
| c.1257A>G (p.Ile419Met) | Missense | *OPA1* | Comp. Het | rs143319805 | 0.06% | VCV000050866.8 | Uncertain | PP | Possibly causative | 1 | 25012220 |
| c.1922A>T (p.Glu641Val) | Missense | *OPA1* | Comp. Het | - | - | - | - | PP | Possibly causative | 1 | - |
| c.2258dupT (p.Gln754AlafsTer9) | Frameshift | *MFN2* | Het | rs773371488 | - | VCV000637433.4 | Uncertain | PP | Pathogenic | 1 | 28215760, 16762064 |
| c.830G>C (p.Gly277Ala) | Missense | *LRSAM1* | Het | - | - | - | - | PP | Likely Pathogenic | 1 | - |
| c.1795A>C (p.Thr599Pro) | Missense | *POLG* | Homo | rs1064796458 | - | VCV000423488.3 | Uncertain | PP | Likely Pathogenic | 1 | - |
| c.914C>T (p.Pro305Leu) | Missense | *KIF1A* | Het | rs1131690804 | - | VCV000428604.4 | Pathogenic | PP | Pathogenic | 1 | - |
| c.821C>G (p.Ser274Trp) | Missense | *KIF1A* | Het | - | - | - | - | PP | Pathogenic | 1 | - |
| c.370C>T (p.Leu124Phe) | Missense | *SLC33A1* | Het | rs141818342 | 0.03% | VCV000448411.3 | Uncertain | NP/PP | Possibly causative | 1 | - |
| c.2797G>A (p.Ala933Thr) | Missense | *WASHC5* | Het | rs541330058 | 0.002% | - | - | NP/PP | Possibly causative | 1 | - |

| Variant | Type of mutation | Gene | Genotype | dbSNP reference | gnomAD – Exomes MAF (%) | ClinVar Ref | ClinVar Significance | Pathogenicity prediction | Classification | Index cases (Total cases) | Pubmed Ref. |
|---|---|---|---|---|---|---|---|---|---|---|---|
| c.1529C>T (p.Ala510Val) | Missense | *SPG7* | Het | rs61755320 | 0.22% | VCV000042016.12 | Pathogenic | PP | Possibly causative | 1 | 26626314, 25497598 |
| C.301G>A (p.Glu101Lys) | Missense | *SOD1* | Het | rs76731700 | - | VCV000574319.1 | Pathogenic | PP | Likely Pathogenic | 1 | 15258228, 8875253, 22292843 |
| c.1280A>G (p.Tyr427Cys) | Missense | *TAF15* | Het | rs200046706 | 0.018% | - | - | PP | Possibly causative | 1 | 26601740 |
| c.26_49del (p.Gln9_Gln16del) | Deletion | *CIZ1* | Het | - | - | - | - | PP | Possibly causative | 1 | - |
| c.902G>A (p.Arg301His) | Missense | *GBA* | Het | rs140955685 | 0.034% | VCV000592663.1 | Uncertain | PP | Possibly causative | 1 | - |
| c.1693G>A (p.Asp565Asn) | Missense | *CSF1R* | Het | - | - | - | - | PP | Possibly causative | 1 | 29544907 |
| c.503G>A (p.Arg168His) | Missense | *ZMYND11* | Het | rs750701399 | - | - | - | PP | Possibly causative | 1 | - |
| c.832C>T (p.Arg278Cys) | Missense | *L1CAM* | Het | rs372200840 | - | - | - | PP | Likely Pathogenic | 1 | - |
| c.2341T>C (p.Tyr781His) | Missense | *ATP1A3* | Het | - | - | - | - | PP | Likely Pathogenic | 1 | 25996915 |
| c.1825G>A (p.Gly609Arg) | Missense | *DNMT1* | Het | - | - | - | - | - | Likely Pathogenic | 1 | - |
| c.1577T>A (p.Ile526Asn) | Missense | *GRID2* | Het | - | - | - | - | - | Possibly causative | 1 | - |

**Table 4. List of DNA variants identified in this study from the molecular genetic analysis of 308 index patients with suspected dominant ataxia.** Pathogenicity predictions were assessed by Annovar annotation with SIFT, PolyPhen-2, Condel, FATHMM, MutationAssessor, MutationTaster, Provean, and CADD.

# Chapter II: Identification of an unstable ATTTC repeat mutation within the Disabled 1 gene (*DAB1*) causing cerebellar Purkinje cell alterations, *DAB1* RNA switch, and Reelin signalling dysregulation in Spinocerebellar ataxia type 37.

## 2.1. Identification of a new spinocerebellar ataxia subtype (SCA37) and molecular characterisation of the SCA37 critical region

During the course of this thesis we identified and described a novel spinocerebellar ataxia type subtype, SCA37, in a large ataxia pedigree (AT-901) originating from the province of Huelva in the Andalusia region in the South of Spain (281). Affected patients presented with falls, dysarthria or clumsiness evolving to a pure cerebellar syndrome distinctively characterised by early-altered saccadic, pursuit and optokinetic vertical eye movements. By using whole-genome linkage studies, we localised the causative genetic deficit in this family to an 11-Mb genomic region on 1p32, which includes the Disabled-1 (*DAB1*) gene encoding for the reelin adapter protein. Whole exome analysis did not lead to the identification of the causative mutation, which suggested its localisation in a non-coding genomic region. By using a combination of whole-genome sequencing and genotyping studies with two SNPs identified within the SCA37 critical region, rs79992829 and rs146472695, found in linkage disequilibrium, the candidate mutation was narrowed by two recombination events to a 1.742 Mb interval spanning the 5' non-coding regulatory region of the human DAB1 gene (**Figure 9**). These SNPs allowed for the identification of three additional families (AT-9012, AT-59 and AT-90) with a similar phenotype from our cohort of ataxia patients of unknown genetic cause. The four kindreds were clinically and genetically extensively investigated. Likewise as recently shown in four Portuguese ataxia families (484), we found that an unstable ATTTC pentanucleotide repeat mutation located in the SCA37 1p32 region within intron 11 of the gene encoding the disabled adapter protein DAB1 segregated with the disease in these four families presenting with the SCA37 phenotype (**Table 5**; **Figure 10** and **Figure 11**). Thus, our study associated the ATTTC expanded insertion within the *DAB1* gene with SCA37. The ATTTC repeat

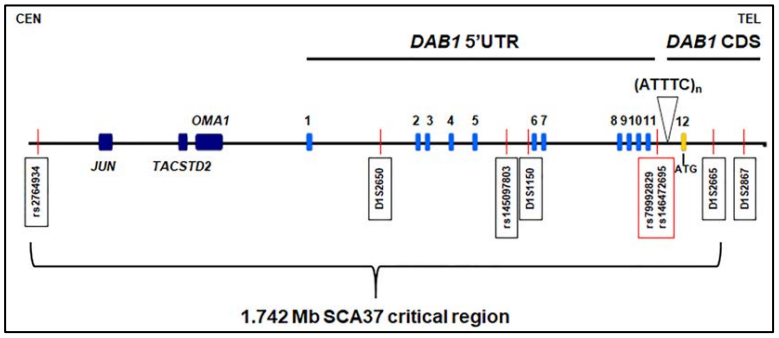


**Figure 9. Genomic structure of the SCA37 critical region.** The genomic region containing the SCA37 mutation spans 1.742 Mb genomic region on chromosome 1p32, flanked by rs2764934 and D1S2665 markers, includes the 5' UTR non-coding regulatory region of the human *DAB1* gene. Vertical red bars represent genetic markers, dark blue boxes represent other genes in the region, light blue boxes represent *DAB1* non-coding exons and yellow box represents *DAB1* coding exon 12 containing the ATG translation start site. Polymorphic markers rs79992829 and rs146472695 (highlighted in the red box) were found in linkage disequilibrium with the *SCA37* mutation and used to identify three additional Spanish SCA37 families (AT-9012, AT-59 and AT-90). Extracted from (485).

insertion lies within the intronic ATTTT repeat Alu element in the intron 11 of the *DAB1* 5'-UTR non-coding region, preceding the coding exon 12 containing the ATG translation initiation codon.

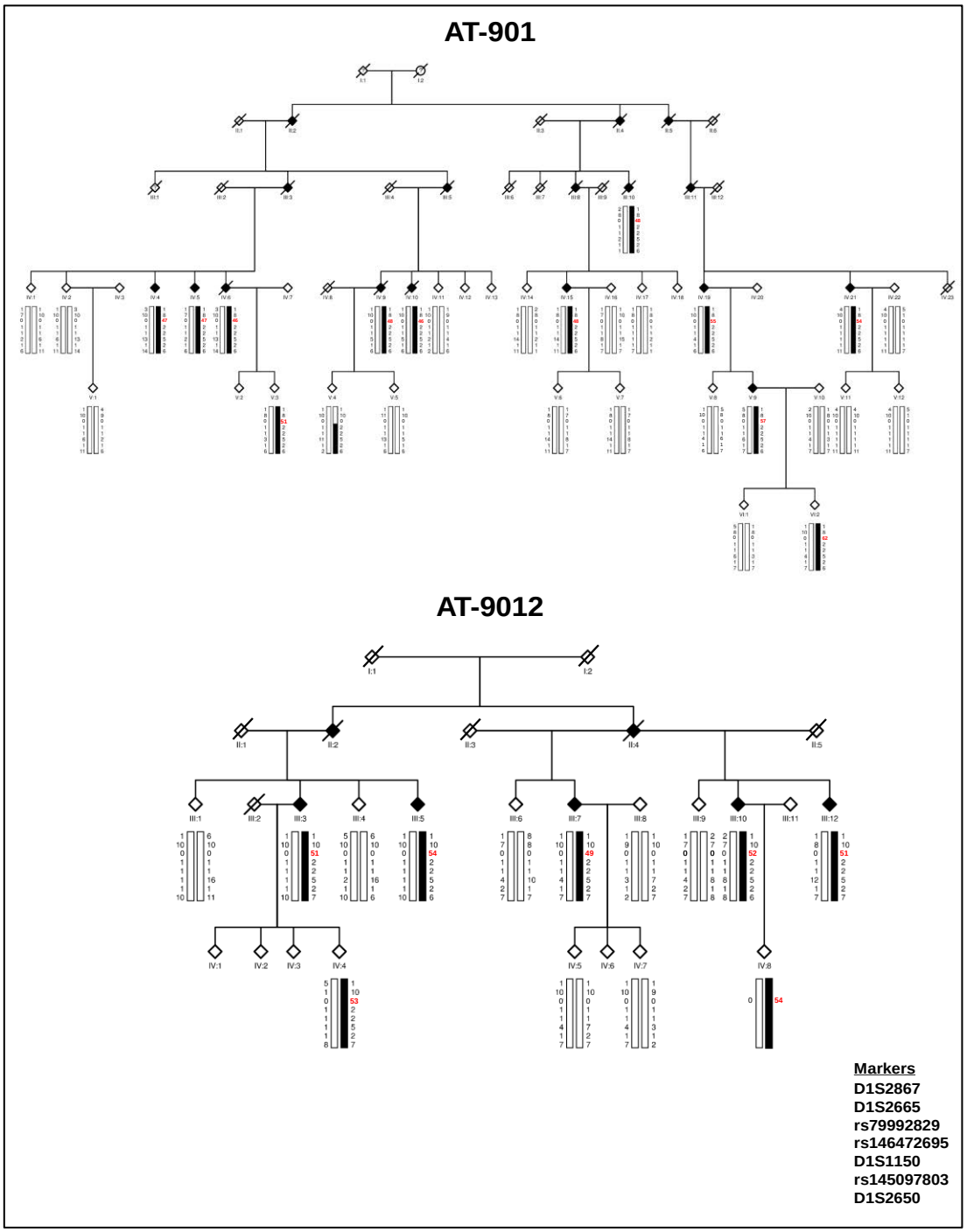


**Figure 10. Segregation of the 1p32 haplotype and the ATTTC repeat expanded mutation within the *DAB1* gene in two Spanish SCA37 families.** The expanded ATTTC pentanucleotide repeat (in red) located within the non-coding intron 11 of the *DAB1* gene encoding for the disabled adapter protein 1 segregated with the disease in all affected patients in two Spanish families presenting with the SCA37 phenotype. The haplotypes of seven polymorphic markers (D1S2867, D1S2665, rs79992829, rs146472695, D1S1150, rs145097803 and D1S2650) within the SCA37 critical region on 1p32 are indicated. Extracted from (485).

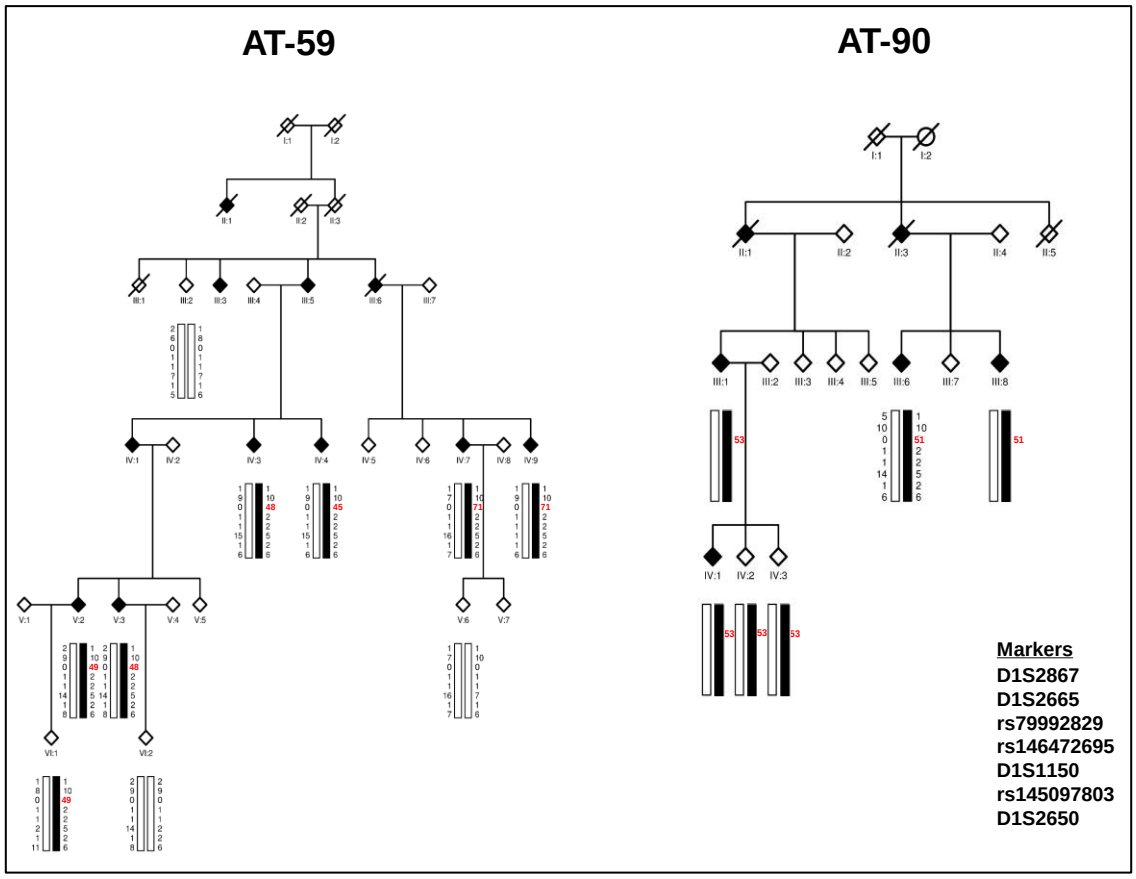


**Figure 11. Segregation of the 1p32 haplotype and the ATTTC repeat expanded mutation within the *DAB1* gene in two additional Spanish SCA37 families.** The expanded ATTTC pentanucleotide repeat (in red) located within the non-coding intron 11 of the *DAB1* gene encoding the disabled adapter protein 1 segregated with the disease in all affected patients in two additional Spanish families presenting a clinical phenotype compatible with SCA37. A total of twenty-five affected and seven at-risk individuals from the four families presented with the ATTTC expanded mutation within the *DAB1* gene. The haplotypes of seven polymorphic markers (D1S2867, D1S2665, rs79992829, rs146472695, D1S1150, rs145097803 and D1S2650) within the *SCA37* critical genomic region on 1p32 are indicated. Extracted from (485).

## 2.2. Clinical and genetic correlation in SCA37

All seven SCA37 families included in this study shared a common geographical origin in the south of Spain with the same distinctive genetic haplotype within the critical region on 1p32 suggesting a mutation founder effect (**Figure 12**; data not shown). The large AT-901 family had been previously described (281). A total of twenty-five SCA37 patients from four families were clinically diagnosed by a neurologist and a detailed clinical exam was performed in 23 of them. Ages at onset ranged from 25 to 64 years old (mean age 43.3±9.9). Initial clinical presentation included dysarthria, falls,

clumsiness or a combination of them, evolving to a generally slow progressive and pure cerebellar syndrome with scanning speech, mild trunk ataxia and severe dysmetria mostly in legs (**Table 5**). Eye movements at onset of the disease could be studied in three patients (IV:4 and IV:5 from AT-901; III:6 from AT-90) and the examination disclosed dysmetric vertical ocular saccades and irregular vertical ocular pursuit, whereas horizontal eye movements appeared normal. Those findings were confirmed by electro-oculographic studies in IV:4 and IV:5 from AT-901, who showed abnormal vertical saccades accuracy, diminished velocity and gain in vertical smooth pursuit, and slow velocity in vertical optokinetic nystagmus. Similar albeit milder abnormalities in the horizontal axis were identified during follow-up. Remarkably, saccade velocity remained normal along the course of the disease. All patients with longer standing disease, 4 to 42 years from onset, showed dysmetric saccades and irregular pursuit in both vertical and horizontal axes. Dysphagia, hand postural and action tremor, oscillopsia, nystagmus, and saccadic eye intrusions variably appeared with disease progression (**Table 5**). Patients became wheelchair-bound in 10 to 33 years from onset with the exception of one patient who showed an aggressive course becoming wheelchair-bound in five years from onset. None of them showed motor or sensory deficits, extensor plantar reflexes, fasciculations, epileptic seizures, or cognitive impairment.

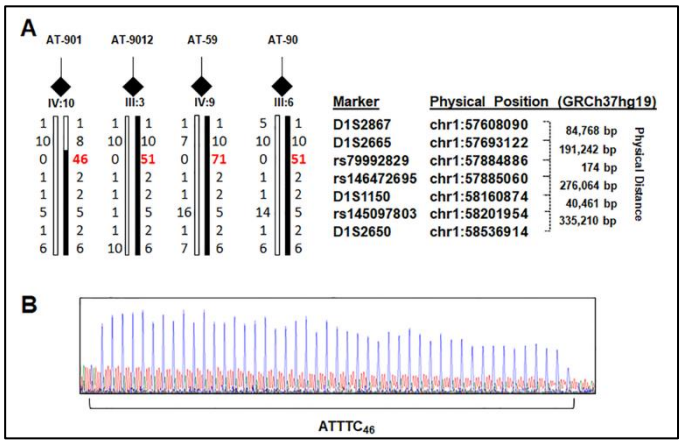


**Figure 12. The intronic ATTTC pentanucleotide repeat mutation within the DAB1 gene in four Spanish SCA37 families.** (**A**) A common haplotype with polymorphic markers D1S2867, D1S2665, rs79992829, rs146472695, D1S1150, rs145097803 and D1S2650 spanning 927,919 bp on 1p32 is shared in four independent SCA37 index cases from the four families studied. The mutant allele size in these patients is denoted in red. (**B**) Sanger sequencing showed the $ATTTC_{46}$ repeat expanded insertion in SCA37 patient 901-IV:10**.** Extracted from (485).

| Pedigree | ID | Gender | ATTTC repeats | Age of Onset (yo) | Disease duration | Clinical Sign at onset | Dysphagia | Hand postural, action tremor | Nystagmus | Saccadic eye intrusions | Oscillopsia |
|---|---|---|---|---|---|---|---|---|---|---|---|
| AT-901 | III:10 | Male | 48 | na | na | na | na | na | na | na | na |
| | IV:4 | Male | 47 | 64 | 15 | Clumsiness | - | - | + | - | - |
| | IV:5 | Female | 47 | 59 | 15 | Falls | + | - | - | - | - |
| | IV:6 | Male | 46 | 54 | 2†* | Combination | - | - | - | - | - |
| | IV.9 | Female | 48 | 55 | 27† | Dysarthria | - | + | + | + | - |
| | IV:10 | Female | 46 | 39 | 38† | Clumsiness | - | + | - | + | - |
| | IV:15 | Male | 48 | 50 | 23 | Combination | + | + | - | - | - |
| | IV:19 | Female | 55 | 56 | 28† | Dysarthria | + | - | - | - | - |
| | IV:21 | Female | 54 | 40 | 42 | Combination | + | + | + | + | - |
| | V:9 | Male | 57 | 42 | 18 | Dysarthria | + | - | - | - | - |
| | V:3 | Male | 51 | Asy (33) | - | - | - | - | - | - | - |
| | VI:2 | Male | 62 | Asy (21) | - | - | - | - | - | - | - |
| AT-9012 | III:3 | Female | 51 | 43 | 27 | Dysarthria | - | + | - | + | - |
| | III:5 | Male | 54 | 45 | 15 | Falls | - | - | - | - | - |
| | III:7 | Male | 49 | 50 | 23 | Falls | - | + | - | - | - |
| | III:10 | Female | 52 | 45 | 22 | Combination | - | - | - | - | - |
| | III:12 | Male | 51 | 46 | 18 | Combination | - | + | - | - | - |
| | IV:4 | Male | 53 | Asy (34) | - | - | - | - | - | - | - |
| | IV:8 | Female | 54 | Asy (39) | - | - | - | - | - | - | - |
| AT-59 | IV:3 | Female | 48 | 35 | 29 | Dysarthria | + | + | + | - | + |
| | IV:4 | Female | 45 | na | na | na | na | na | na | na | na |
| | IV:7 | Male | 71 | 44 | 10 | Dysarthria | - | - | + | - | - |
| | IV.9 | Female | 71 | 32 | 19 | Dysarthria | - | - | + | - | + |
| | V:2 | Female | 49 | 36 | 15 | Combination | - | - | + | - | + |
| | V:3 | Female | 48 | 25 | 20 | Clumsiness | + | - | + | - | + |
| | VI:1 | Female | 49 | Asy (20) | - | - | - | - | - | - | - |
| AT-90 | III:1 | Female | 53 | 38 | 21 | Combination | - | - | - | - | - |
| | III:6 | Male | 51 | 46 | 4 | Dysarthria | - | - | - | - | - |
| | III:8 | Female | 51 | 37 | 18 | Dysarthria | + | - | - | - | - |
| | IV:1 | Female | 53 | 26 | 12 | Dysarthria | - | - | - | - | - |
| | IV:2 | Male | 53 | Asy (35) | - | - | - | - | - | - | - |
| | IV:3 | Female | 53 | Asy (31) | - | - | - | - | - | - | - |

**Table 5. Clinical information and genetic correlation in 25 affected SCA37 patients and seven asymptomatic individuals from four independent Spanish kindreds.** Ages of onset presented with ranges from 25 to 64 years (yr). All 25 affected and seven at-risk asymptomatic individuals presented with the ATTTC repeat mutation (average 52.1), ranging from 46 to 71 and from 49 to 62 repeats, respectively. Initial clinical presentation in affected patients included dysarthria, falls, clumsiness or a combination of them, evolving to a generally slow progressive and pure cerebellar syndrome with scanning speech, mild trunk ataxia and severe dysmetria mostly in legs. All patients with longer standing disease, 4 to 42 years from onset, showed dysmetric saccades and irregular pursuit in both vertical and horizontal axes. Asy = asymptomatic; na = not available; + = present; - = absent. In parenthesis actual age. a, cancer was the cause of death; b, deceased. Extracted from (485).

Increase of the SARA score assessed severity of the disease and varied among patients and also in the same patient along disease progression. When SARA scores from 17 patients were normalised to the time from disease onset, a variable rate of progression from 0.38 to 2.05 points/year in SARA score was obtained (mean normalised SARA score 0.97±0.34). For those 12 patients with two or more SARA score assessments, the gradient of the SARA score line was calculated and yielded a wider range (0 to 4 points/year). This approximation assumed a linear progression of SARA score as previously shown in SCA37 (281) and other SCAs (486). Maximum SARA score obtained was 32 points (IV:21 from AT-901) at 42 years from onset and no ceiling effect of the scale was observed in our patients. Nerve conduction tests, transcranial magnetic stimulation, evoked potentials, electrocardiograms, echocardiograms and audiometric tests yielded normal results in all affected patients in agreement to the described clinical findings in SCA37 (281).

Brain MR images at onset of the disease in affected patients showed either vermis atrophy or generalised cerebellar atrophy. Vermis atrophy progressed to generalised cerebellar atrophy in two years. In those patients with long standing disease, established cerebellar atrophy with preserved pons was detected. Cerebellar volumetric assessment in five patients (III:8, IV:1, and III:1 from AT-90 family; IV:4 and IV:5 from AT-901 family) revealed a 24±6% decrease in cerebellar volume relative to the total intracranial volume (6.96±0.71%) compared to 30 age- and gender-matched controls (9.17±0.52%) randomly selected (age range: 24-75 years) from the open access IXI dataset (378). Midsagittal vermis relative diameter quantification in three patients (IV:4, IV:5, and III:6 from AT-901 family) showed a 17.8% decrease of the midsagittal vermis relative diameter ratio (60.75±1.21) compared to the mean ratio (73.93±3.73) of eight age- and gender-matched controls.

Thirty-three asymptomatic relatives from the four families were clinically investigated. Among them, four subjects (V:3 and VI:2 from AT-901 family; IV:4 and IV:8 from AT-9012 family) showed hypometric downwards vertical eye saccades in the first neurological exam at ages 33, 21, 34, and 39 yo, respectively. Subject V:3 also showed irregular vertical ocular pursuit. Neurological exam was otherwise normal. Oculographic registries from subjects V:3 and VI:2 showed hypometric vertical saccades, diminished velocity and gain in vertical smooth pursuit and decreased vertical optokinetic nystagmus velocity as described (281). No abnormalities were found in the horizontal axis. All four subjects were later found to carry the causative mutation (**Table 5**). Midsagittal vermis relative diameter) quantification of MRI in V:3 from AT-901 family and IV:8 from AT-9012 family showed a 9.9% decrease in the mean ratio compared to eight age- and gender-matched controls (67.2±3.9 vs 74.6±5.6, respectively). Subject VI:2 from family AT-901 showed normal results as expected due to his younger age. Vermis atrophy was qualitatively recognisable by MRI in V:3 from AT-901 and IV:8 from AT-9012, while the vermis was considered normal in VI:2 from AT-901 in agreement with the quantitative findings.

Three additional asymptomatic subjects were found to carry the causative mutation (VI:1 from AT-59; IV:2 and IV:3 from AT-90). Neurological exams were normal in all of them at ages 20, 35, and 31 years old, respectively. No oculographic registries or MRI could be obtained.

In summary, a total of 25 affected and seven at-risk asymptomatic individuals presented with the ATTTC repeat mutation (average 52.1), ranging from 46 to 71 and from 49 to 62 repeats, respectively (**Table 5**). The average age of disease onset was 40.4 years in females and 49 in males ($P<0.021$). Remarkably, a gender specific contribution of the ATTTC expansion size to the age of onset was identified in males ($r = -0.96$; $P<0.0001$; $n = 9$), but not in females ($r = -0.09$; $P>0.75$; $n = 14$) (**Figure 13A**). Increments ranging from 2 to 5 ATTTC pentanucleotide repeats were identified in four out of the six transmissions studied (**Figure 13B**). No allele contractions were observed. None of the 28 healthy relatives studied presented with the ATTTC mutation.

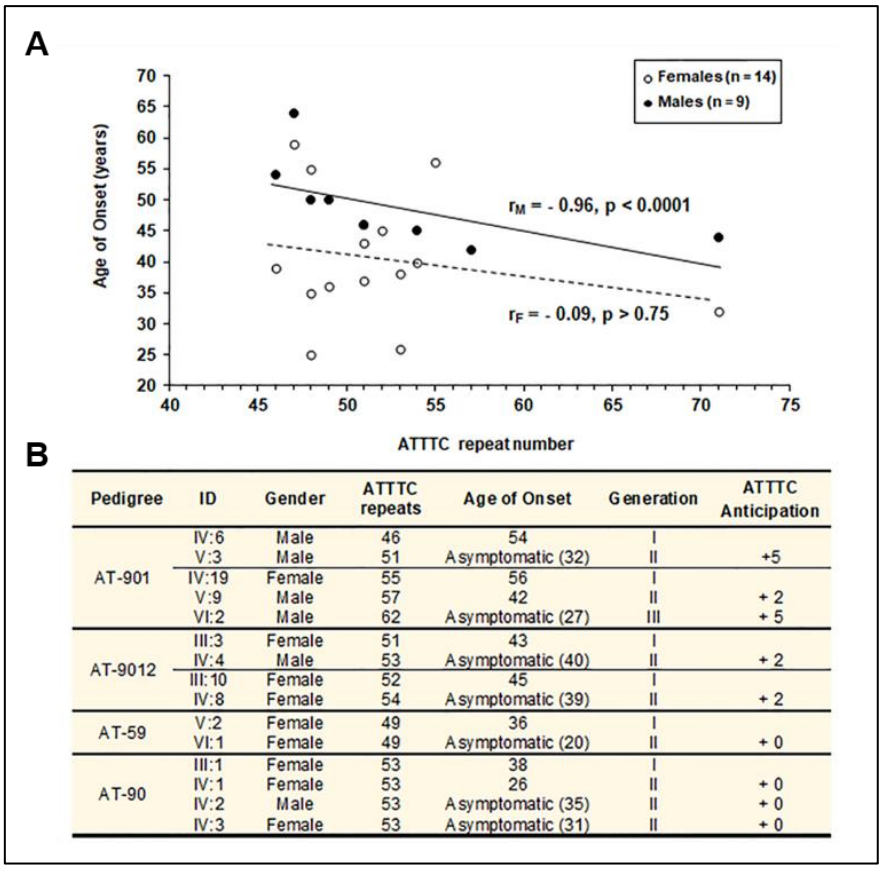


| Pedigree | ID | Gender | ATTTC repeats | Age of Onset | Generation | ATTTC Anticipation |
|---|---|---|---|---|---|---|
| AT-901 | IV:6 | Male | 46 | 54 | I | |
| | V:3 | Male | 51 | Asymptomatic (32) | II | +5 |
| | IV:19 | Female | 55 | 56 | I | |
| | V:9 | Male | 57 | 42 | II | + 2 |
| | VI:2 | Male | 62 | Asymptomatic (27) | III | + 5 |
| AT-9012 | III:3 | Female | 51 | 43 | I | |
| | IV:4 | Male | 53 | Asymptomatic (40) | II | + 2 |
| | III:10 | Female | 52 | 45 | I | |
| | IV:8 | Female | 54 | Asymptomatic (39) | II | + 2 |
| AT-59 | V:2 | Female | 49 | 36 | I | |
| | VI:1 | Female | 49 | Asymptomatic (20) | II | + 0 |
| AT-90 | III:1 | Female | 53 | 38 | I | |
| | IV:1 | Female | 53 | 26 | II | + 0 |
| | IV:2 | Male | 53 | Asymptomatic (35) | II | + 0 |
| | IV:3 | Female | 53 | Asymptomatic (31) | II | + 0 |

**Figure 13. Gender-specific contribution of the ATTTC expansion size to the age of onset and increased repeat expansion size over generations in four SCA37 Spanish kindreds.** (**A**) A gender-specific contribution of the ATTTC repeat mutation to the age of onset in SCA37 was demonstrated. A significant inverse correlation between the ATTTC repeat insertion size and the age of onset was identified in males (r=-0.96, *P*<0.0001; n=9; continuous line) but not in females (r=-0.09, *P*>0.75; n=14; dotted line). Moreover, affected females presented a significant earlier age of onset (average ATTTC repeats=51.9, average age of onset = 40.4 years) than males (average ATTTC repeats = 52.7, average age of onset = 49 years) (n=23; *P*<0.021). (**B**) An increase in the size of the ATTTC repeat expansion, but no significant inverse correlation with the age of onset in the following generation was observed in SCA37. Extracted from (485).

### 2.3. Identification of additional SCA37 cases

Once identified the SCA37 causative mutation, genetic testing of SCA37 was routinely established in the Neurogenetics diagnostic laboratory at the IGTP, particularly for those cases from the south of Spain or with a familiar history originally from Andalusian region. This enabled us to identify ten new SCA37 cases, four asymptomatic carriers, and six affected individuals presenting with clinical symptoms in agreement with our previously reported SCA37 clinical findings. Four of those individuals were relatives from the AT-90 family and three of them from the AT-901, AT-9012 and AT-59 respectively. The remaining additional three SCA37 index cases identified (**Table 6**) increased the total number of SCA37 Spanish families to seven, all of them sharing a common geographical origin (**Figure 14**).

**Table 6. Clinical information and genetic correlation in three additional unrelated SCA37 cases from three independent Spanish kindreds.**

| Pedigree | ID | Gender | ATTTC repeats | Age of Onset (yo) | Disease duration | Clinical Sign at onset | Dysphagia | Hand postural, action tremor | Nystagmus | Saccadic eye intrusions | Oscillopsia |
|---|---|---|---|---|---|---|---|---|---|---|---|
| AT-3705 | I:1 | Male | 53 | 40 | na | na | na | na | na | na | na |
| AT-3706 | I:1 | Female | 54 | 42 | 11 | Clumsiness | - | - | + | + | - |
| AT-3707 | I:1 | Female | 74 | 37 | 10 | Clumsiness and oscillopsia | - | - | + | + | + |

Thus, the seven SCA37 Spanish families identified to date are originally from Villablanca (Huelva) (families AT-901 and AT-9012), Punta Umbria (Huelva) (family AT-59), Isla Cristina (Huelva) (family AT-90), Ayamonte (Huelva) (families AT-3705 and AT-3706) and from Sevilla (family AT-3707) (**Figure 14**). The greatest distance between those locations is around 140 km from Sevilla to Ayamonte, this latest one located on the border between Spain and the south of Portugal, where the reported SCA37 Portuguese families were originally from.

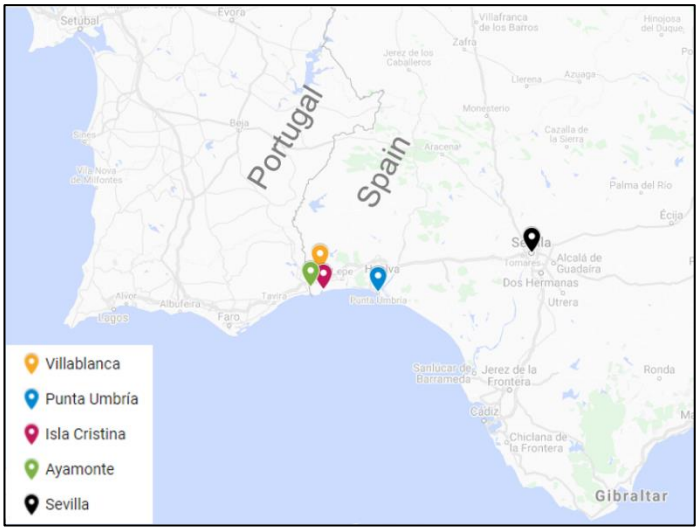


**Figure 14. Geographical distribution of seven SCA37 Spanish families. Graph generated with Google Maps** (664)**.**

## 2.4. Neuropathology of SCA37

In the present study we were able to investigate two complete brains from two SCA37 patients (IV:9 and IV:10) from the large SCA37 AT-901 Spanish family previously reported (281). Both patients had inherited the risk genetic haplotype for SCA37 and later revealed the ATTTC repeat mutation containing each 48 and 46 repeats within the *DAB1* gene. Under macroscopic inspection, the cerebral hemispheres and brainstems of the brains from both patients were unremarkable except for moderate enlargement of the ventricular system in coronal cerebral sections in patient IV:9. The cerebellum appeared atrophic with prominent fissures and folia (**Figure 15A** and **B**). The cerebellar white matter appeared reduced and dense in both patients. Light microscopy examination of the cerebral cortex showed, in general, a preserved cytoarchitectural pattern, discrete and diffuse gliosis in the primary motor cortex and no evidence of neuronal loss (data not shown). Juxtaglomerular vessels showed moderate hyaline sclerosis. Immunostaining for beta-amyloid and tau proteins in CERAD areas

revealed a moderate frequency of neuritic plaques with only few neurofibrillary tangles in both patients according to their age. Despite these findings, cytoarchitectural and neuronal populations were well preserved in these areas. Cortical microinfarctions were detected in dorsolateral frontal and temporal inferior cortices in patient IV:10 related to known vascular risk factors. No alpha-synuclein immunostaining was identified in patient IV:10 while a moderate amount of Lewy bodies and neurites were found in amygdala and entorhinal and cingulate cortices in patient IV:9. No TDP-43 inclusions were detected. The subcortical regions such as the caudate and lentiform nuclei, nucleus basalis of Meynert, posterior hypothalamus, mammillary bodies, thalamus and subthalamic nuclei were preserved, and the unique abnormality found was mild small vessel pathology in patient IV:10. The hemispheric white matter of the frontal and occipital periventricular areas was unremarkable unaltered. The brainstem appeared normal except for the moderate (patient IV:10) to intense (patient IV:9) neuronal loss and gliosis identified confined to the inferior olive (**Figure 15C**). No pathological alpha-synuclein immunostaining was found in this region in patient IV:10. Conversely, a few Lewy bodies and neurites were detected in the motor nucleus of the X cranial nerve in patient IV:9 without cell loss. The cerebellar cortex showed an extensive and generalised Purkinje cell loss (**Figure 15D**) with the remaining

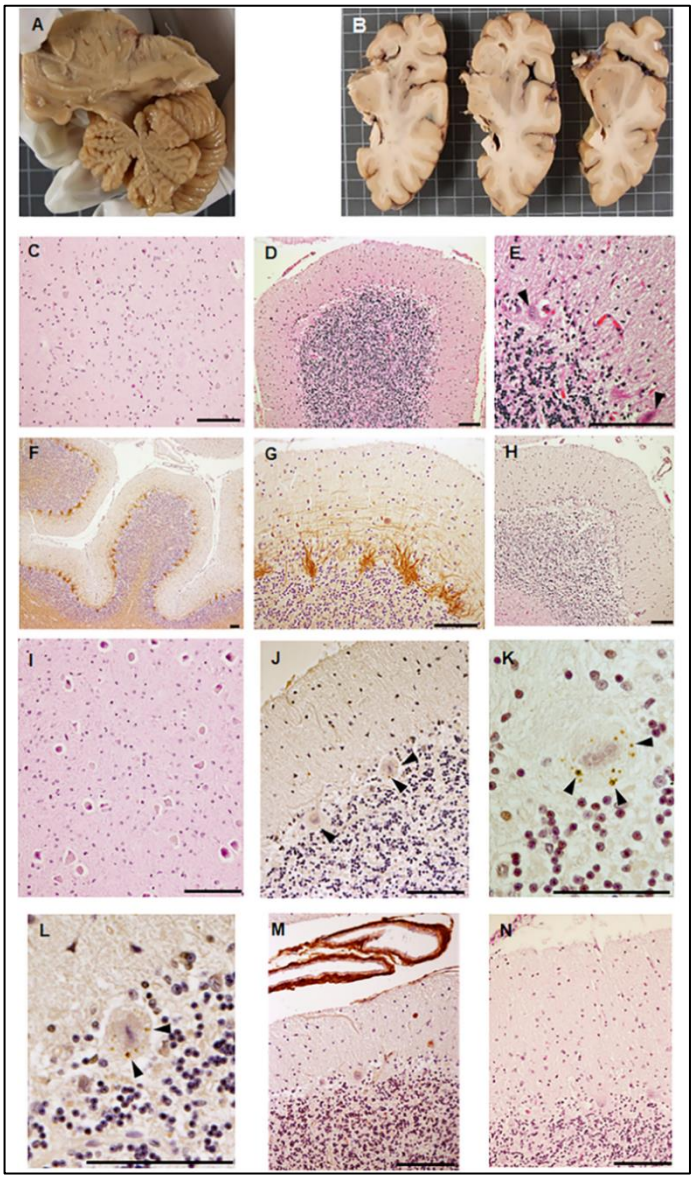


**Figure 15. Neuropathological alterations in SCA37. Pathological lesions in cerebellar sections derived from two SCA37 cases: IV:9 and IV:10 from AT-901 pedigree**. (**A** and **B**) Macroscopic imaging of cerebellum sections showed decreased volume with increased cerebellar grooves. (**C**) Neuronal loss and gliosis were identified confined to the inferior olive. (**D**) Conserved cerebellar foliage, extensive loss of Purkinje cells, and Bergmann's gliosis in the Purkinje cell layer shown by H&E staining. No changes in the granular layer were identified. (**E**) Nuclear lobulation was found in two Purkinje cells. (**F** and **G**) Immunostaining of phosphorylated neurofilaments showed abundant empty baskets in the Purkinje cell layer. (**H**) H&E staining showed extensive neuronal loss in lobule VII of the vermis and (**I**) intense gliosis in the dentate nucleus. (**J-L**) Ubiquitin immunostaining revealed distinctive perisomatic granules in Purkinje cell bodies (arrows) and (**M**) leptomeningeal vessels. (**N**) H&E staining showed specific severe gliosis in the flocculus. Magnification: 100 µm. Extracted from (485).

exhibiting severe nuclear changes such as lobulation, irregular shape, and hyperchromatism together with Bergman and astrocyte gliosis (**Figure 15E**). Phosphoneurofilament immunoreactivity revealed many empty baskets with stained perikarya (**Figure 15F** and **G**). All these changes were diffuse and intense along the whole cerebellar cortex with a relative sparing of the cerebellar amygdala in patient IV:10. Patient IV:9 showed more extensive neuronal loss in lobule VII of the vermis (**Figure 15H**). The cerebellar white matter appeared normal and the deep nuclei offered a homogeneous aspect with preserved neuronal populations and marked gliosis (**Figure 15I**). Ubiquitin staining revealed the presence of multiple punctate inclusions located in the peripheral cytoplasm suggestive of perisomatic granules in both patients which later revealed immunostaining for DAB1 protein (**Figure 15J-L**, arrows) and leptomeningeal vessels (**Figure 15M**). No intranuclear inclusions were observed. The granular layer was relatively spared and basket and Golgi cells were well preserved. Occasional axonal spheroids were seen in patient IV:10 (**Figure 18E** and **F**). The molecular layer showed mild diffuse gliosis and few hypertrophic fibers in patient IV:9 while gliosis was specifically severe in the flocculus in patient IV:10 (**Figure 15N**). The cervical spinal cord was unremarkable. Immunostaining with anti-Calbindin-D28K revealed a significant reduction of the molecular layer thickness and Purkinje cells density more predominantly in the vermis (**Figures 16B**, **C**, **E** and **F**) than in cerebellar hemispheres (**Figures 16G-K**) in both patients (**Figure 16** and **Figure 17**). Remarkably, a subpopulation of PCs showed tangential orientation (24% in IV:9 and 20.5% in IV:10; **Figure 16J-L**; **Figure 18C**) with aberrant arborisation (**Figure 18D**),

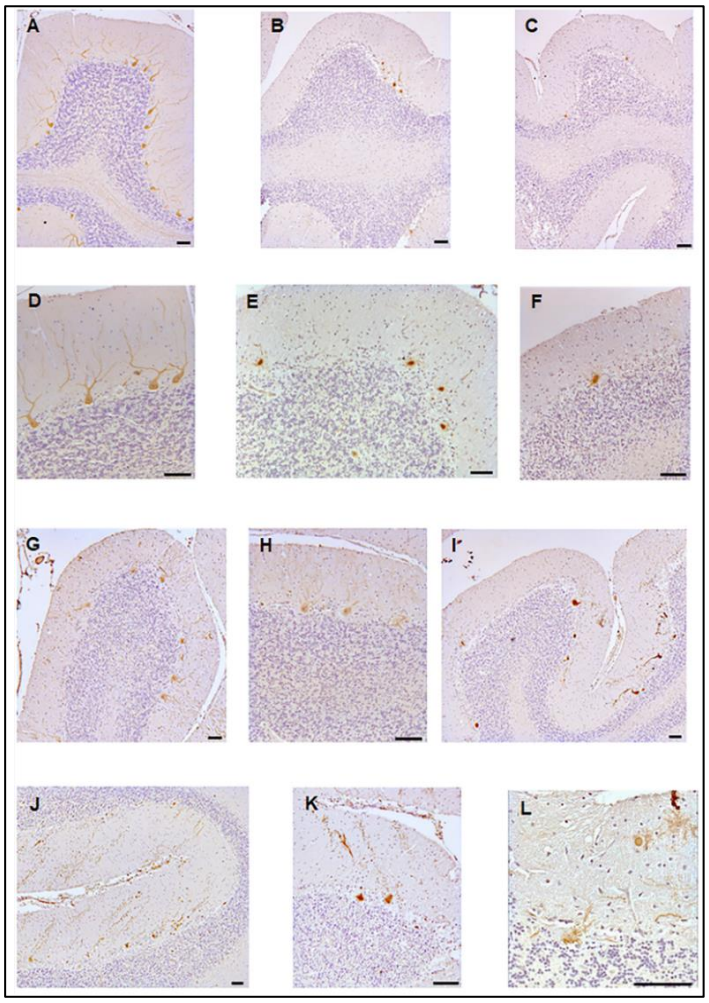


**Figure 16. Purkinje cell loss and altered dendrite arborisation in post-mortem SCA37 cerebellum.** Degeneration of Purkinje cells was more evident in the cerebellar vermis (**B** and **E**, from patient IV:9; **C** and **F**, from patient IV:10) compared to the hemispheres (**G** and **H**, from IV:9; **I** and **J** from IV:10) in the SCA37 cerebellum compared to a gender- and age-matched control (**A** and **D**). Cerebellar hemispheres showed tangential dendrite arborisation in a subpopulation of Purkinje cells in SCA37 (**J-L**). Magnification: 100 µm. Extracted from (485).

and ectopic mispositioning within the granular layer (6% in IV:9 and 6.5% in IV:10) or the molecular layer (6.5% in IV:9 and 7% in IV:10) (**Figure 18E** and **F**). GFAP immunostaining showed diffuse cerebellar cortical disorganisation in both SCA37 patients (**Figure 18H-K**). Calbindin-D28K immunostaining of the cerebellar cortex was decreased in line with PC loss in both SCA37 patients (**Figure 20**A and **B**). GFAP protein was shown up-regulated by immunoblotting in agreement with reactive astrogliosis (**Supplementary Figure 1**).

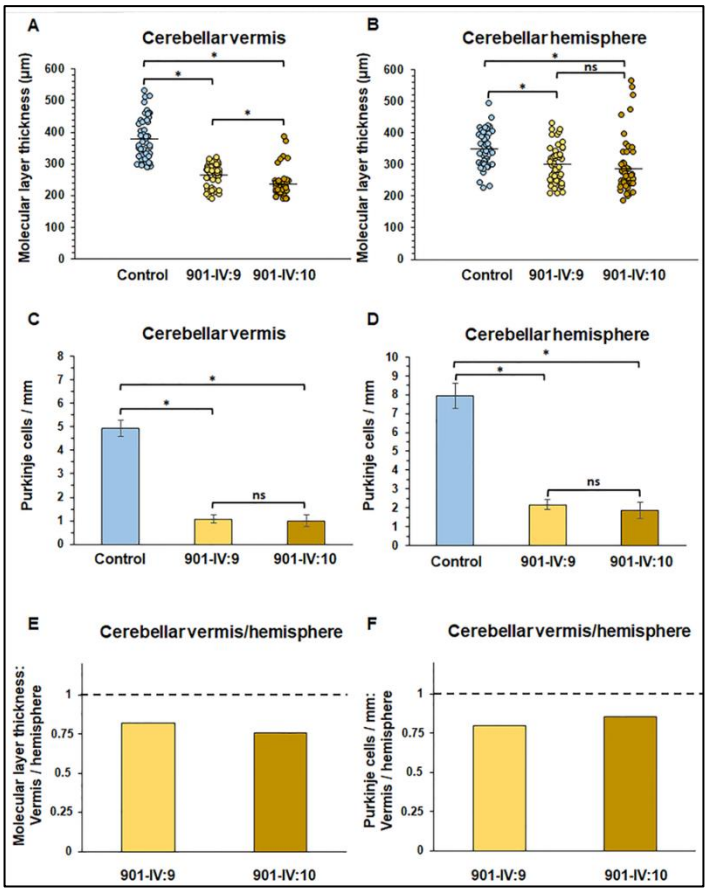


**Figure 17. Decreased molecular layer thickness and Purkinje cell loss in the SCA37 cerebellum.** Decreased thickness of the molecular layer (**A** and **B**) and Purkinje cell density (**C** and **D**) in the cerebellum from two SCA37 patients (IV:9 and IV:10 from AT-901 family) revealed a higher affectation of the vermis as compared to the hemisphere in the SCA37 cerebellum (**E** and **F**) of both patients. N = 51 examined areas. **P*<0.001; n.s., non-significant. Vertical bars denote SEM. Extracted from (485).

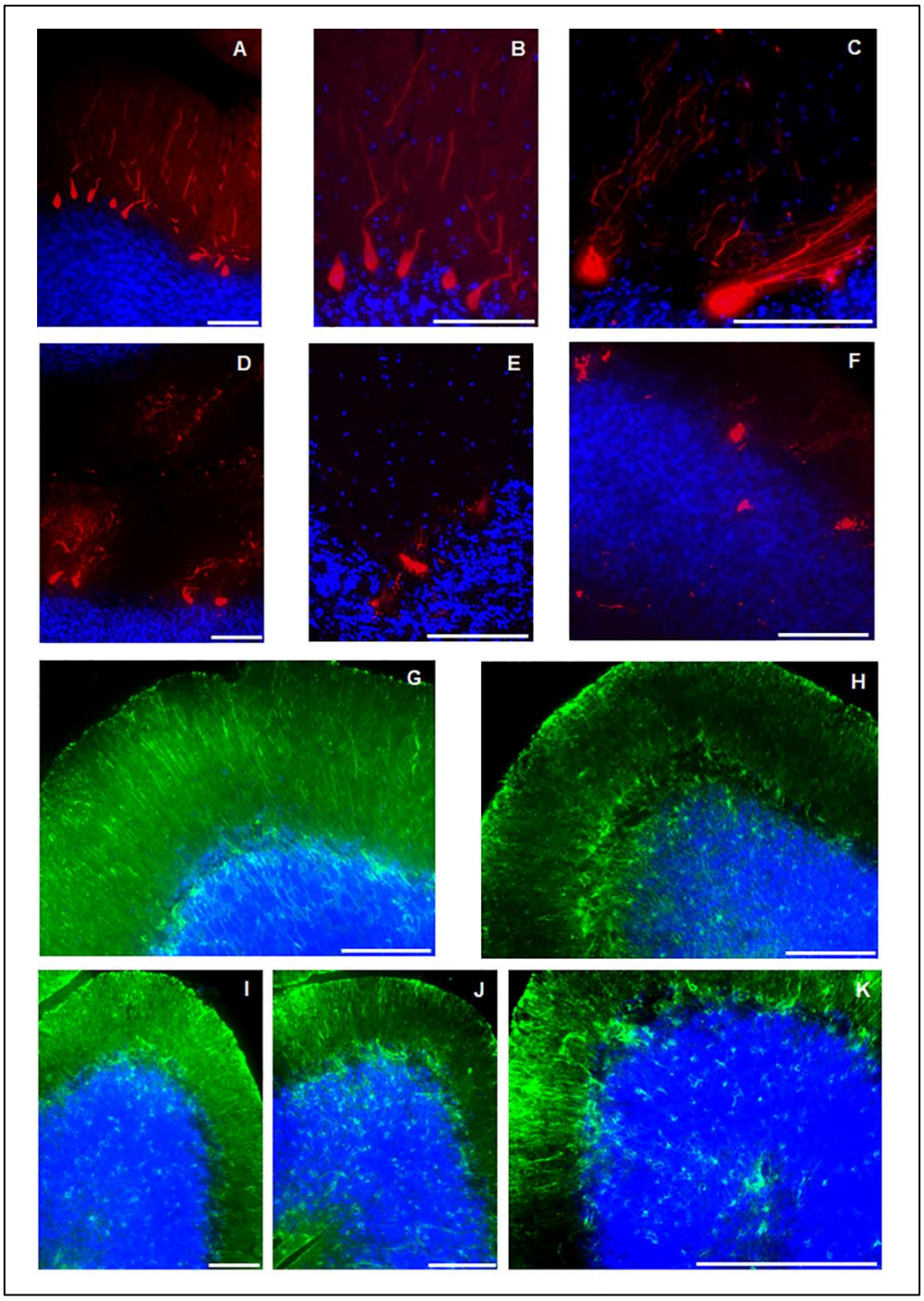


**Figure 18. Diffuse cerebellar disorganisation with tangential orientation and aberrant arborisation of Purkinje cell dendrites in SCA37.** Immunofluorescence Calbindin-D28K staining of the SCA37 cerebellar hemisphere (patients IV:9 and IV:10 from the AT-901 family) revealed tangential orientation of Purkinje cell dendrites with aberrant arborisation (**D** and **E**). Purkinje cells were misplaced in the SCA37 cerebellar cortex with occasional axonal spheroids (**E** and **F**) as compared to the age-matched control (**A** and **B**). GFAP immunostaining revealed immunoreactive astrogliosis and diffuse cerebellar cortical disorganisation in SCA37 cerebellum (**H**-**K**) in both patients compared to a gender- and age-matched control (**G**). Extracted from (485).

## 2.5. Dysregulated DAB1 expression and altered Reelin-DAB1 signalling in the SCA37 cerebellum

Immunostaining with anti-DAB1 revealed specific overexpression in SCA37 cerebellum compared to age-matched control (**Figures 19** and **Figure 20**). In control cerebellum, DAB1 was present in Purkinje cell soma and dendrites (**Figure 19A** and **B**), whereas in the SCA37 cerebellum it appeared overexpressed and exhibited perisomatic and perinuclear punctate staining in the remaining Purkinje cells (**Figure 19C-E**). A few ectopic PCs showed intense DAB1 staining in the cerebellar molecular layer (**Figure 19F**).

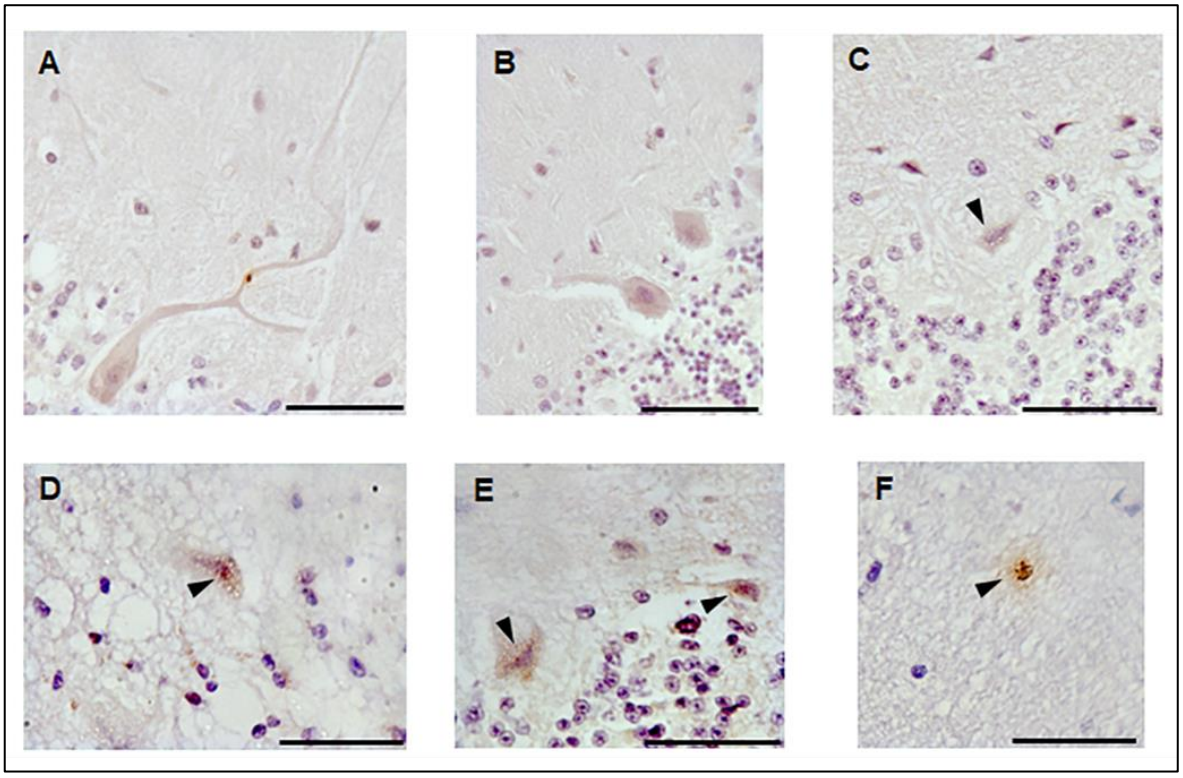


**Figure 19. Aberrant DAB1 immunostaining in the SCA37 cerebellum.** DAB1 immunostaining was increased in the SCA37 cerebellum (patients IV:9 and IV:10 from AT-901 family) compared to age-matched control. While in control cerebellum DAB1 was present in Purkinje cell soma and dendrites (**A** and **B**), in the SCA37 cerebellum (IV:9 and IV:10) it exhibited perisomatic and perinuclear punctate staining (**C**-**F**; arrows). Scale bars denote 100 μm. Extracted from (485).

The expression of DAB1 protein was found increased in both SCA37 patients. Overexpression of DAB1 80- and 63-kDa isoforms was identified in the SCA37 cerebellar vermis and hemisphere **(Figure 20A** and **B**). Furthermore, dysregulated expression of reelin proteins along with increased levels of PI3K-p85 and phosphorylation of AKT were identified in the SCA37 cerebella indicating up-regulation of Reelin-DAB1 signalling (**Figure 20A** and **B**). Remarkably, both SCA37 cerebella revealed significant up-regulation of the uncleaved 410-kDa form of Reelin, which is an isoform known to induce DAB1 phosphorylation, with the subsequent interaction with PI3K and AKT phosphorylation and activation (487).

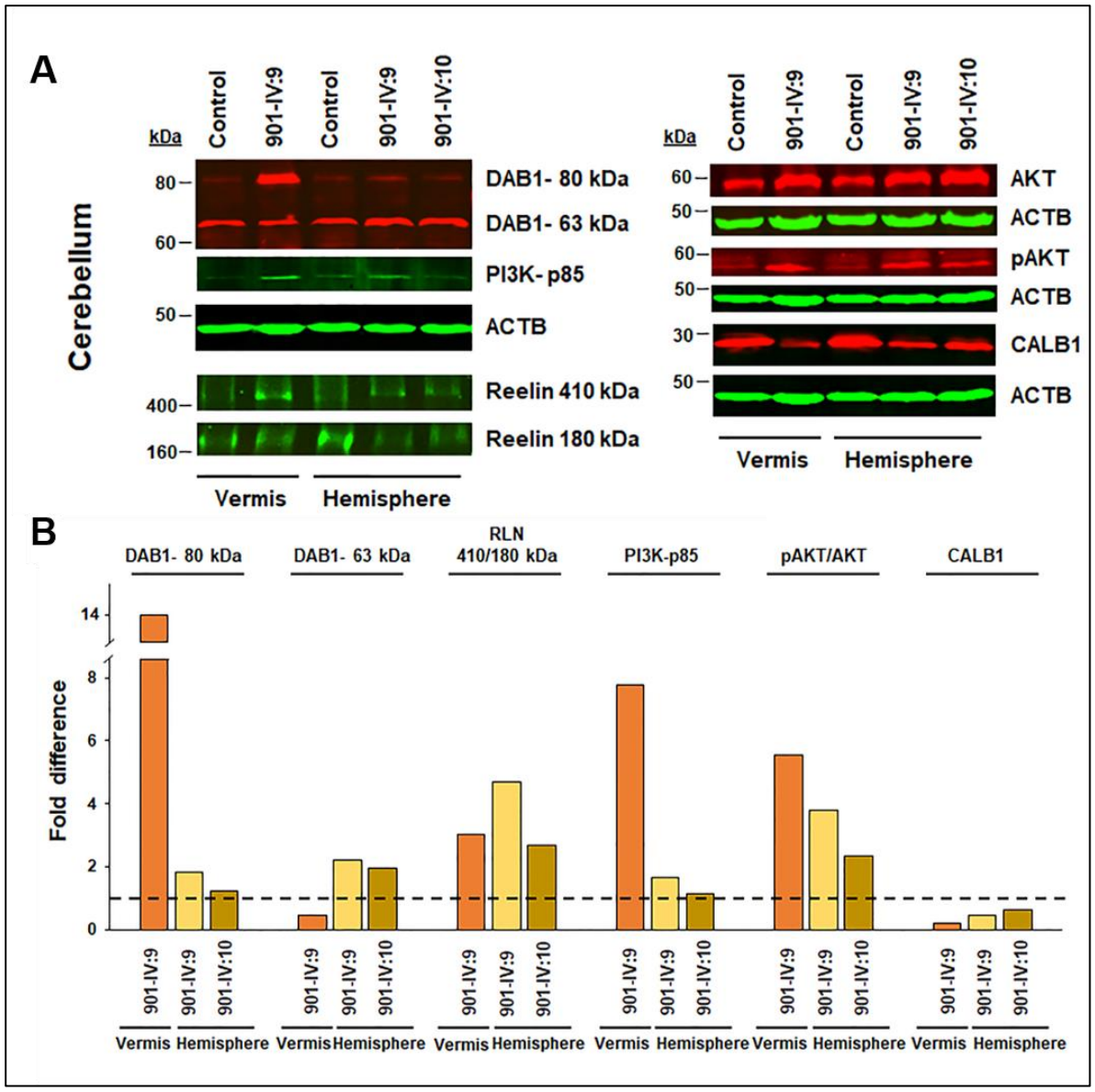


**Figure 20. DAB1 and Reelin-DAB1 signalling up-regulation in the SCA37 cerebellum**. The 80- and 63-kDa DAB1, 410-kDa reelin, PI3K-p85, and phospho-AKT proteins were found up-regulated in the SCA37 cerebellum, whereas Calbindin-D28K protein levels were found decreased in the SCA37 cerebellum due to severe Purkinje cell loss. The average levels of each protein are shown as a ratio normalised to beta-actin. All values shown for patients 901-IV:9 and 901-IV:10 are relative to the obtained control value set to 1 (dotted line**).** Extracted from (485).

To investigate whether transcriptional dysregulation in the *DAB1* gene contributed to the detected increase in DAB1 protein expression observed in SCA37 we characterised the cerebellar *DAB1* transcripts from SCA37 patients. Nine alternative non-coding *DAB1* transcripts, five of them not previously described (488), originating from alternative combinations of ten 5' UTR non-coding exons within the human *DAB1* gene were identified dysregulated in human SCA37 post-mortem cerebellum (**Figure 21**). ENCODE RNAseq analysis confirmed expression of these ten 5' UTR non-coding exons in normal human adult Purkinje cells (**Figure 22**).

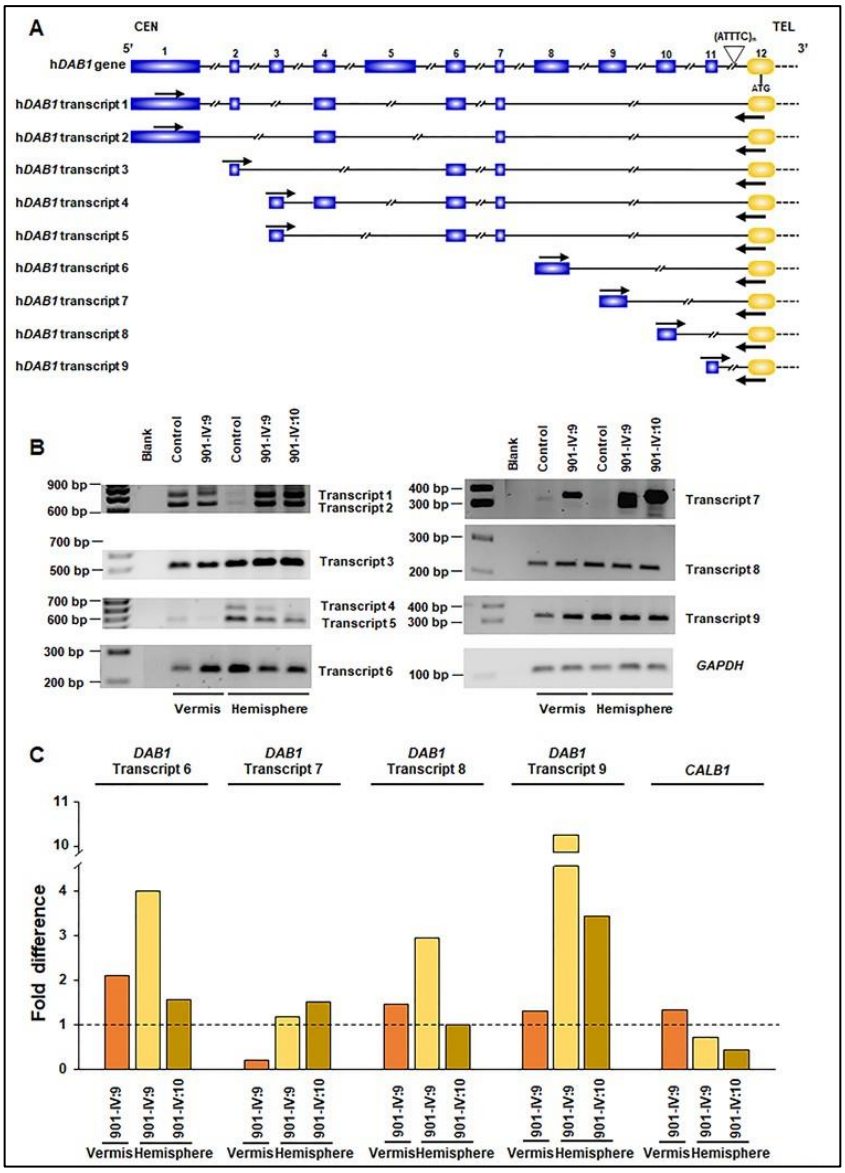


**Figure 21. Analysis of the 5' UTR non-coding DAB1 alternative transcripts in the SCA37 cerebellum.** The structure of the non-coding 5' UTR exons within the human *DAB1* gene and the resulting transcripts identified in post-mortem cerebellum from two human SCA37 patients (IV:9 and IV:10 from AT-901 family) and a gender- and age-matched control cerebellum are shown in **A**. Nine differentially spliced transcripts of the 5' UTR non-coding human *DAB1* gene were identified in human post-mortem cerebellum, with overexpression in the cerebellar vermis and hemispheres of SCA37 as compared to control (**B**). PCR amplicons are shown saturated and do not represent absolute levels. (**C**) *DAB1* cDNA levels normalised to *GAPDH* expression in Real Time qRT-PCR experiments demonstrated higher expression of DAB1 in the SCA37 cerebellum compared to control. Normalised SCA37 cDNA values shown are relative to the obtained control value set to 1 (dotted line). Arrows indicate the position of the primers used. Extracted from (485).

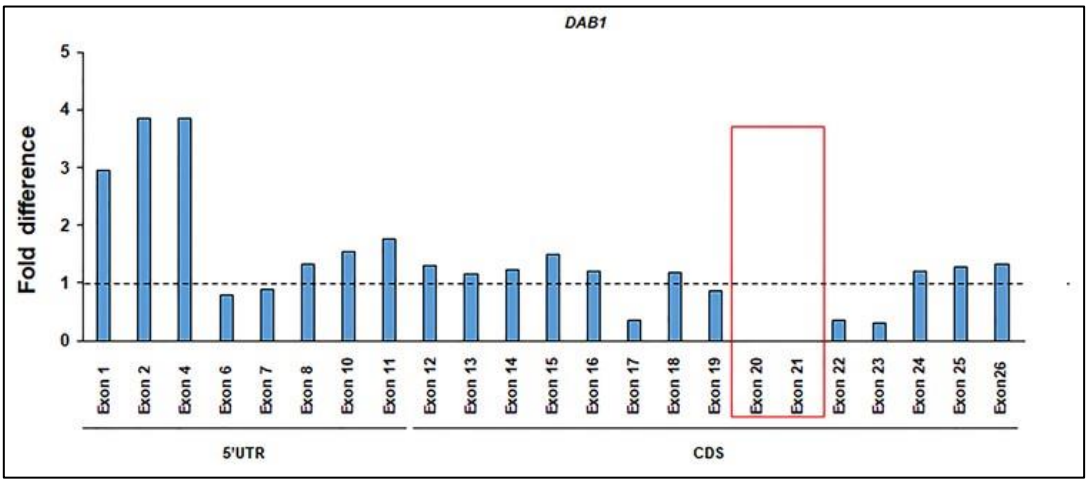


**Figure 22. Relative expression levels of DAB1 non-coding (1 to 11) and coding (12 to 26) exons in control human Purkinje cells.** ENCODE *DAB1* RNA sequences reads were compared on BAM files obtained from cerebellar Purkinje cells from a 6-year-old male child (dotted line) and a 20-year-old adult male. *GAPDH* sequences reads were used to normalise inter-sample differential expression. Ten (1-4 and 6-11) out of eleven 5' UTR exons were found expressed in adult male Purkinje cells in line with the identified exon expression in SCA37 and control cerebella shown in Figure 10. No RNA-sequence reads were identified for exons 20 and 21 (highlighted box) in each control sample. RNA-sequence reads of exons 3 and 9 were only identified in Purkinje cells of the 20-year-old adult male. Extracted from (485).

Remarkably, four different partial alternative coding transcripts originating from the human *DAB1* gene were also identified in the post-mortem human cerebellum, two of them (*DAB1-1* and *DAB1-3*) found overexpressed in SCA37, but not in control (**Figure 23A-C**).

*DAB1-1* generates the longest DAB1 protein isoform (80 kDa; **Figure 20A**), which contains most of the DAB1 phosphorylation sites involved in PI3K interaction and Reelin signalling. The expressed *DAB1-2* transcript generates the shortest 63 kDa DAB1 isoform (**Figure 20A; Supplementary Figure 2**). The remaining transcript *DAB1-4* containing the non-coding exon 11, adjacent to the ATTTC intronic mutation, and coding exons 20 and 21 were uniquely present in SCA37 but absent in control cerebellum (**Figure 23B**). Interestingly, in silico predictive algorithms identified enrichment of the YCAY NOVA motif within the human DAB1 coding exons 20 and 21 (**Figure 24**). Overexpression of these two evolutionary conserved alternative coding exons from the mouse Dab1 gene have been related to migration deficits of Purkinje cells (489). No RNA-sequence reads were identified for exons 20 and 21 in ENCODE normal PC RNA data (**Figure 22**), revealing the absence of *DAB1* transcripts containing these two coding exons in normal human cerebellum. These data indicate that RNA switch and selective expression of *DAB1* exons 20 and 21 may underlie the cerebellar pathology observed in the SCA37 cerebellar cortex.

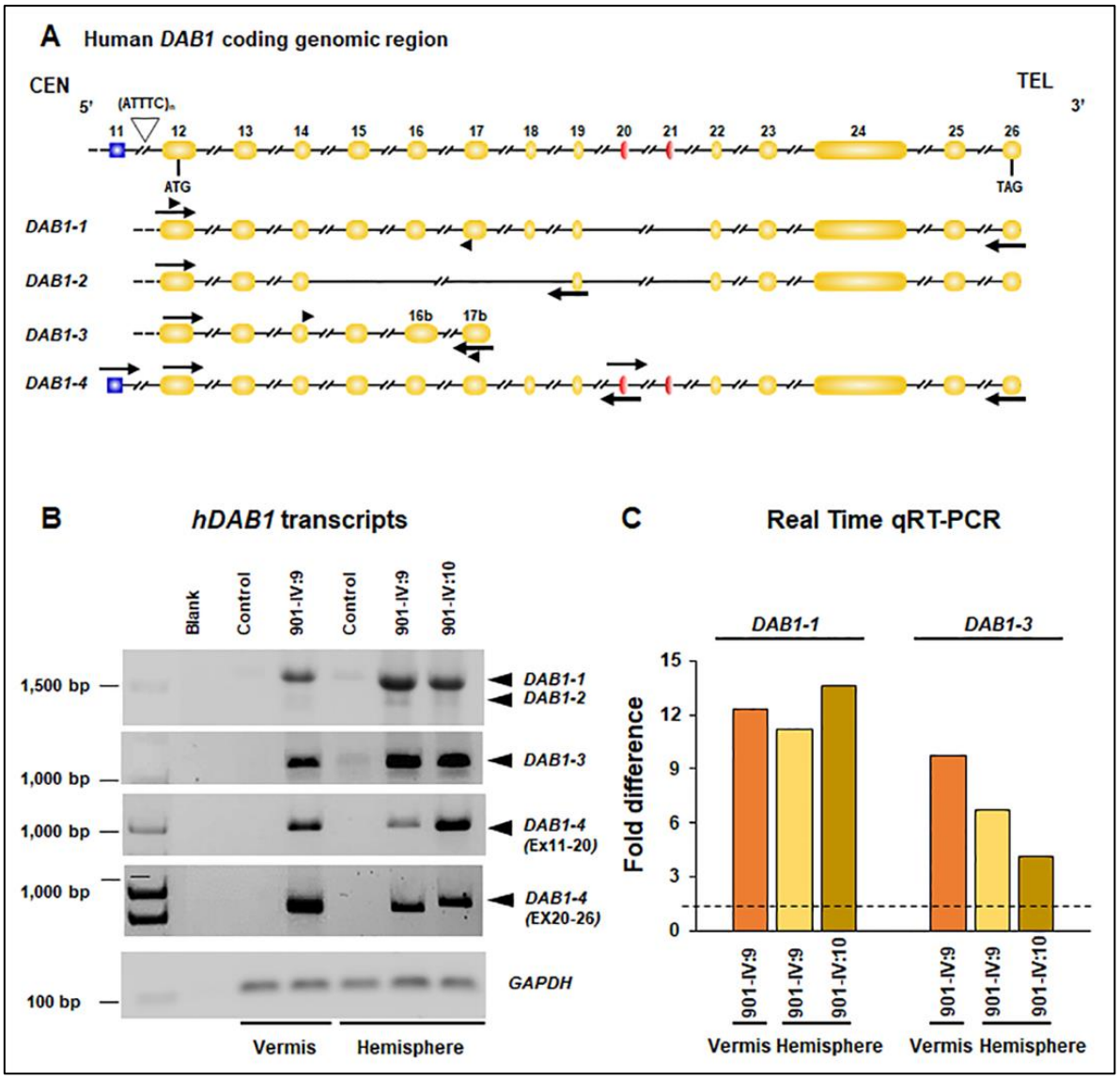


**Figure 23. *DAB1* overexpression and RNA switch in the SCA37 cerebellum**. Genomic structure of the coding exons within the human *DAB1* gene and the resulting transcripts identified in post-mortem cerebella from two human SCA37 patients (IV:9 and IV:10 from the AT-901 family) and a control are shown in (**A**). Three alternative *DAB1* transcripts (*DAB1-1*, *DAB1-3* and *DAB1-4*) were identified overexpressed in SCA37, but not in age-matched control (**B**). *DAB1-2* alternative isoform is shown in Figure 13. Coding exons 16b and 17b are identified in the alternatively spliced DAB1-3 transcript in SCA37. *DAB1-4* transcript containing non-coding exon 11, adjacent to the ATTTC intronic mutation, and coding exons 20 and 21 were uniquely present in SCA37 but absent in control cerebellum (**B**). Real Time qRT-PCR normalised *DAB1* cDNA values for transcripts *DAB1-1* and *DAB1-3* in C are shown relative to the obtained control value, which was set to 1 (dotted line). Arrows and arrowheads in A indicate positions of primers used. PCR amplicons on the agarose gels were generated by high-cycle PCR conditions to qualitative assess the product size and unique sequences, and they do not represent absolute cDNA levels. *DAB-1* and *DAB1-3* isoforms were quantified by Real Time qRT-PCR using primers (arrowheads in A) from unique non-shared sequences determined by exon mapping and sequencing (**C**). PCR primers used are listed in **Supplementary Table 3**. Extracted from (485).

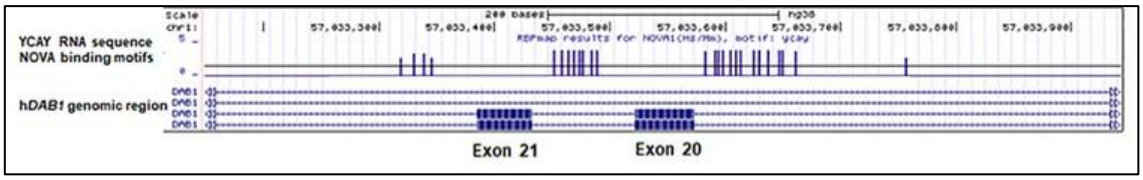


**Figure 24. Identification of YCAY NOVA motifs surrounding human *DAB1* exons 20 and 21.** Recognition of the YCAY motif by NOVA2 splicing factor would generate *DAB1* RNA switch by splicing out exons 20 and 21 which were previously implicated in Purkinje cell migration deficits. Extracted from (485).

Finally, to interrogate how the SCA37 mutation dysregulated *DAB1* expression, we analysed the SCA37 mutation by in silico algorithms and found that the ATTTC repeat mutation within intron 11 of the *DAB1* gene creates putative new XBP1 transcription factor binding motifs (**Figure 25**).

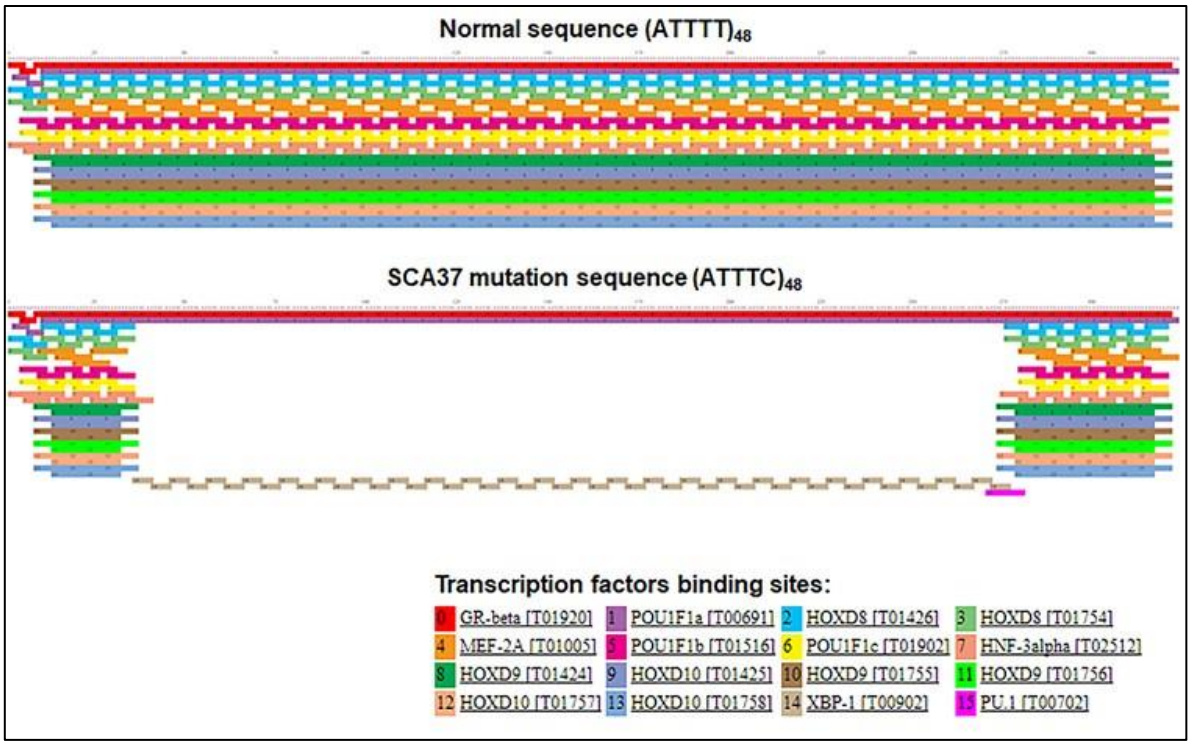


**Figure 25. Putative effects of the SCA37 expanded $(ATTTC)_{48}$ inserted mutation on transcription factor binding.** The $(ATTTC)_{48}$ expanded mutation repeat in SCA37 would disrupt 48 binding sites of six transcription factors including POU1F1a, HOXD8, MEF2A, FOXA1, HOXD9 and HOXD10. In contrast, the expanded repeat mutation in SCA37 chromosomes would create 48 new binding sites for XBP1 transcription factor, with an equiprobability of finding 0.92 sites by chance in a sequence of 1,000 nucleotides. Extracted from (485).

# Chapter III: Identification of a novel dominantly inherited spinocerebellar ataxia subtype caused by *SAMD9L* mutation triggering mitochondrial and lysosomal dysregulation and neurological deficits in a zebrafish disease model.

### 3.1. Identification and clinical characterisation of novel SCA subtype: M-SCA

A total of nine affected patients from a family originally from Menorca, Balearic Islands, were clinically diagnosed by a neurologist and a detailed clinical exam was performed in seven of them (**Figure 26**). Vertical and horizontal nystagmus (GEN) was presented as the first clinical sign with an age of onset ranging from twelve to sixty years old, biased by first time examination. Hyperreflexia was also present at initial clinical examinations. Ataxia onset ranged from thirty to sixty years old (**Table 7**). Initial nystagmus progressed with diplopia and oscillopsia in four patients (III:7, IV:6, IV:8 and IV:14; **Table 7**). Patient IV:14 also referred recurrent vertigo. Younger patients (V:1 and V:3) presented vertical and horizontal nystagmus (GEN) and hyperreflexia without ataxic signs. Patient V:1 was neurologically evaluated for the first time at the age of 12 years and disclosed horizontal and vertical nystagmus (GEN), hyperreflexia with bilateral Babinski's sign, clonus and *pes*

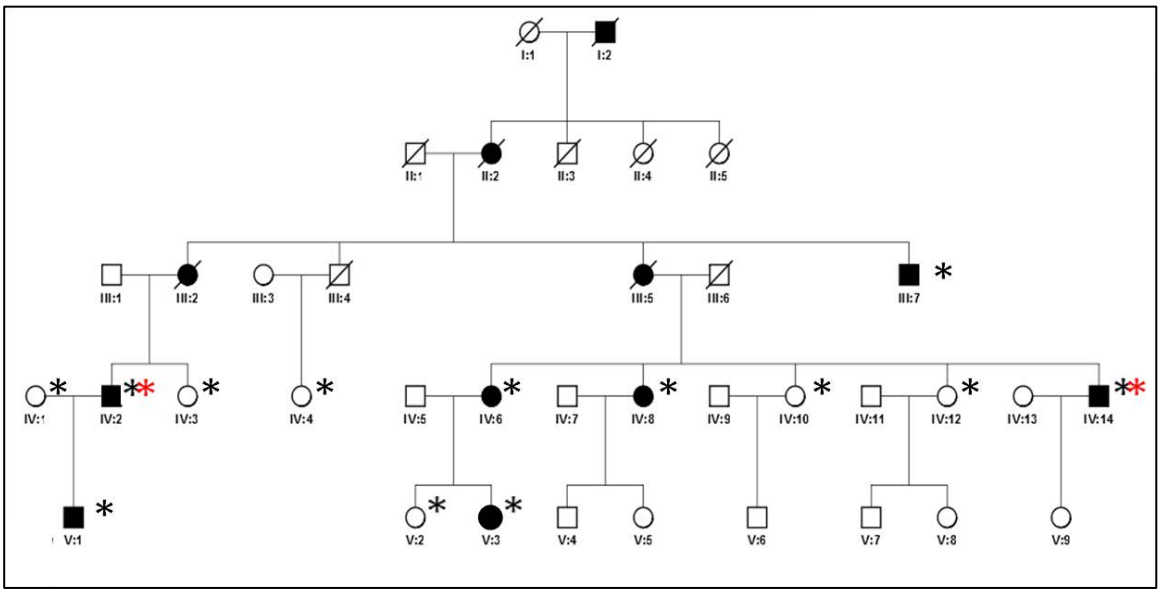


**Figure 26. Pedigree of a Spanish five-generation family from the Balearic island of Menorca with eleven affected individuals.** (*) Individuals included in linkage studies; (*) individuals studied by WES.

*cavus*. Due to family history of falls and unsteady gait, clinical examination was complemented with computed tomography which showed cerebellar atrophy (**Figure 27A**), mega cisterna magna as well as discrete ventricular dilatation and suggested initial signs of brain demyelination (**Figure 27B**). Index patient's father (IV:2) presented with gait instability since the age of 50. Clinical examination after 15 years of disease progression revealed horizontal and vertical nystagmus (GEN), dysmetria, dysdiadochokinesia, severe dysarthria and lower limbs hyperreflexia with bilateral extensor plantar response. Magnetic resonance imaging at 65 years old showed global and symmetric dilation of ventricular system, lateral sulcus and cortical grooves with an accused diffuse vermal and hemispheric cerebellar atrophy (**Figure 27C**). Cerebral parenchyma showed diffuse demyelination involving periventricular and centrum semiovale white matter suggesting hypoxic leukoencephalopathy (**Figure 27D**).

| ID | Gender | Age | Age at first clinical sign | Age at ataxia onset | First clinical sign | Disease duration | Nystagmus | Deep tendon reflexes | Babinski sign | Dysmet. | Dysart. | Severity | Oscil. | Diplop. | Other |
|---|---|---|---|---|---|---|---|---|---|---|---|---|---|---|---|
| **III:2** | F | 80[a] | 60 | 60 | Unsteady gait | 20 | V+H | Hyperreflexia | - | +++ | +++ | +++ | - | - | Wheelchair at 75 |
| **III:5** | F | 65[a] | 58 | 58 | Unsteady gait | 7 | V+H | Hyperreflexia | - | ++ | ++ | ++ | - | - | - |
| **III:7** | M | 81 | 45 | 47 | Unsteady gait | 34 | V + H | Hyperreflexia | - | +++ | +++ | +++ | + | + | Wheelchair at 78 |
| **IV:2** | M | 68 | 48 | 50 | Unsteady gait | 18 | V + H | Hyperreflexia | - | ++ | +++ | +++ | - | - | - |
| **IV:6** | F | 66 | 58 | 60 | Unsteady gait | 8 | V + H | Hyperreflexia | - | + | + | ++ | - | + | - |
| **IV:8** | F | 64 | 50 | 60 | Nystagmus | 4 | V + H | Hyperreflexia | + | + | - | + | - | + | Vertigo; Strabismus |
| **IV:14** | M | 50 | 15 | 30 | Nystagmus | 20 | V + H | Hyperreflexia | - | + | - | + | + | + | Vertigo |
| **V:1** | M | 40 | 12 | - | Nystagmus & *pes cavus* | - | V + H | Hyperreflexia | + | - | - | - | - | - | *Pes cavus*; Ankle Clonus |
| **V:3** | F | 38 | 37 | - | Nystagmus | - | V + H | Hyperreflexia | - | - | - | - | - | - | Strabismus |

**Table 7. Clinical signs in nine affected patients from the Spanish M-SCA kindred.** Ages at onset of initial clinical signs range from 12 to 60 years, biased by first time examination. The age of ataxia onset ranges from 30 to 60. Initial clinical presentation included gaze-evoked nystagmus (GEN) and hyperreflexia evolving to a generally slow progressive cerebellar syndrome with unsteady gait, dysmetria and dysarthria of variable severity. Dysmet., dysmetria; Dysart., dysarthria; Oscil., oscillopsia; Diplop., diplopia; na = not available; - = absent; + = mild or present; ++ =moderate; +++ = severe. a Deceased.

Magnetic resonance imaging of the brain showed cerebellar atrophy in three additional affected patients (IV:6, IV:8 and IV:14) with brain demyelination. Volumetric assessment for the five patients revealed a 28.96% decrease in cerebellar volume relative to the total intracranial volume (6.55% ± 0.55%) accompanied with a 36.86% decrease in cerebellar grey matter relative to the total brain grey matter (4.32% ± 0.47). These values were compared to 30 age- and gender-matched controls with cerebellar relative volume (9.22% ± 0.22%; $F_{(1,8)}$=99.506; $P$<0.0001) and cerebellar relative grey matter (6.84% ± 0.17; $F_{(1,8)}$=122.136; $P$<0.0001).

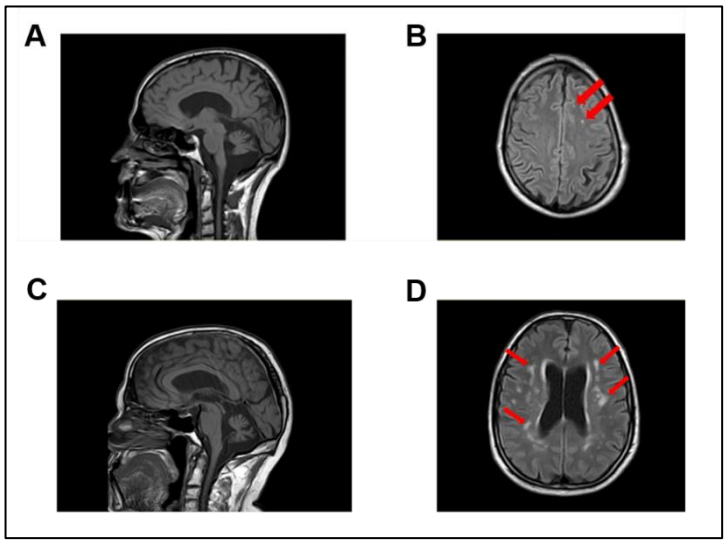


**Figure 27. Sagittal and transverse magnetic resonance imaging scans revealed cerebellar atrophy and cerebral diffuse demyelination**. Sagittal and transverse T1-weighted magnetic resonance imaging scans of patient V:1 brain revealed cerebellar atrophy (**A**) and initial signs of brain demyelination lesions (**B**) noted by red arrows. Imaging of the brain of patient's IV:1 father (IV:2) also showed cerebellar vermis atrophy (**C**) and marked cerebral diffuse demyelination (**D**) noted by red arrows.

Furthermore, all affected patients presented different grades of diffuse demyelination of the cerebral white matter. Five patients (III:7, IV:2, IV:6, IV:8 and IV:14) presented moderate axonal sensory polyneuropathy predominantly in the lower limbs (**Figure 29D** and **E**). EMG studies were normal in all seven patients evaluated. Tibial nerve SSEPs showed an abnormal latency of P37 response in patients diagnosed with sensory axonal polyneuropathy (**Figure 29F**). In two patients, SSR were

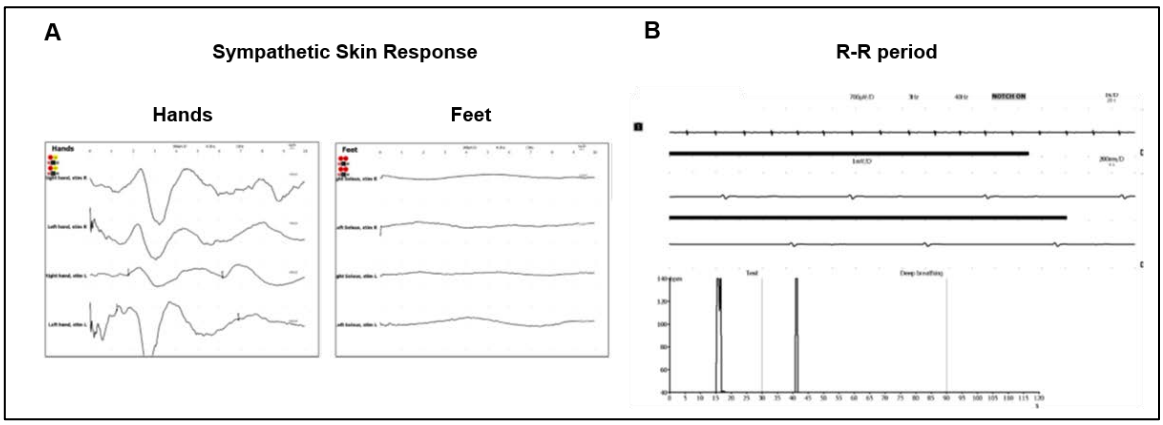


**Figure 28. Abnormal sympathetic skin response SSR and R-R period**. (**A**) Abnormal sympathetic skin response (SSR) in lower limbs displayed abnormality in two patients (IV:2 and IV:6). (**B**) Patient IV:2 showed altered R-R interval.

abnormal in lower limbs (**Figure 28A**) and one patient (IV:2) also showed an abnormal R-R period (**Figure 28B**).

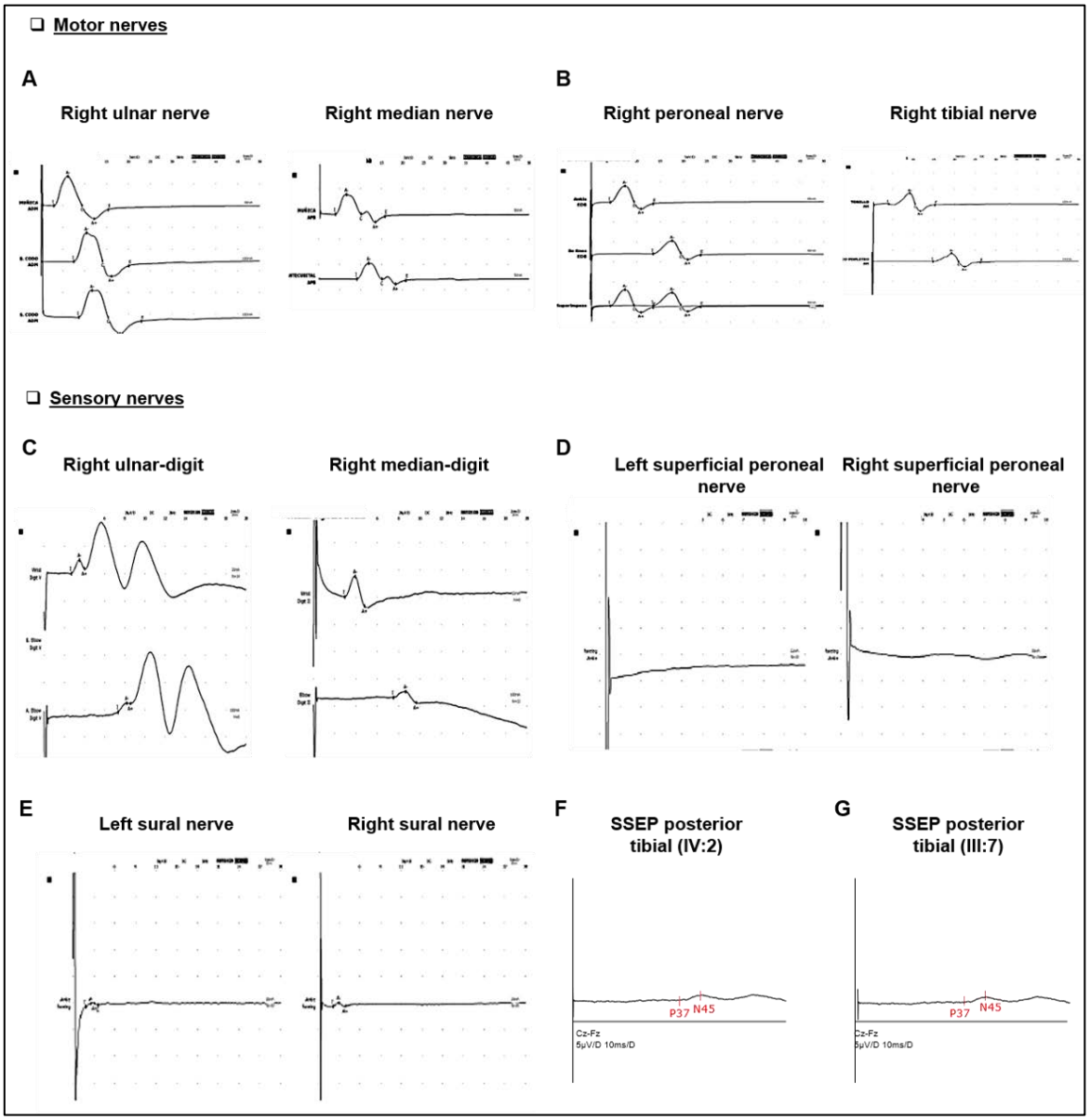


**Figure 29. Moderate axonal sensory polyneuropathy predominantly in the lower limbs of two affected patients from the M-SCA family.** (**A** and **B**) Motor nerve conductions were normal in upper and lower limbs in all patients assessed. (**D** and **E**) Sensory nerves reduced amplitude was present in lower limbs while amplitudes in upper limbs displayed normality (**C**). (**F**) Tibial nerve SSEPs showed an abnormal latency of P37 response in patients diagnosed of sensory axonal polyneuropathy. Neurophysiological data from patient IV:2 except **G** (III:7).

Interestingly, younger patient (V:1) presenting with nystagmus, hyperreflexia and cerebellar atrophy but without apparent ataxia, recorded normal electrophysiological values at 36 years of age. The progression of the disease is slow, although variable, and the SARA scores in this family followed an exponential trend ($r(4)=0.83$, $P=0.041$; **Figure 30**). For the initial stages of the disorder, this scale

was not useful for measuring disease progression because the cerebellar syndrome was not fully developed and because SARA is not considered to be a diagnostic tool; it was originally designed to measure worsening ataxia. The disease progressed with dysmetria and dysarthria and severity varied among patients. Relevantly, patients III:2 and III:7 became wheelchair-bound after fifteen and thirty years from ataxia onset. None of the patients showed fasciculations, epileptic seizures, cognitive impairment or haematological alterations (**Supplementary Figure 3**). In conclusion, for this specific SCA phenotype, we found vertical and horizontal nystagmus (GEN) and hyperreflexia as a characteristically initial signs before ataxia completely developed.

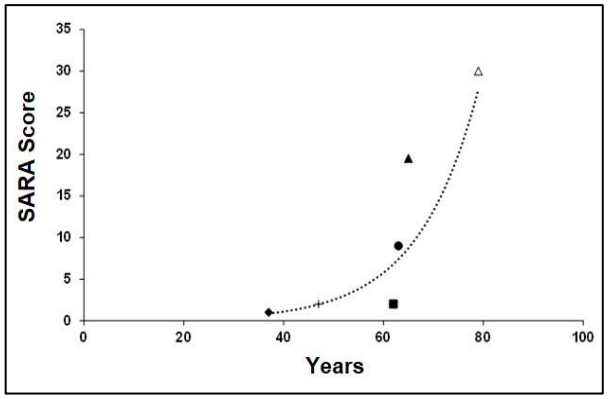


**Figure 30. SARA scores of six affected patients from the M-SCA family**. SARA of six affected patients shows variable severity and progression of the disease following an exponential pattern (r(4)=0.83, *P*=0.041).

### 3.2. Identification of the c.1877C>T (p.Ser626Leu) variant within *SAMD9L* as the causative mutation for this dominantly inherited spinocerebellar ataxia subtype

The initial genome-wide linkage analysis of five healthy and six affected relatives of the M-SCA kindred using the Illumina Infinium HumanOmni5 Chip including more than 4,000,000 markers, revealed suggestive genetic linkage to 7q21 with the highest LOD score (Zmax=3.01; *P*<0.0001) defining a 19.1 Mb candidate region flanked by the polymorphic markers rs12705836 and rs16869440 (**Figure 31A**). Simultaneously, whole-exome sequencing of patients IV:2 and IV:14 identified 445 shared heterozygous variants consistent with autosomal dominant inheritance. After filtering variants by their position within the gene, population frequency, and their predicted pathogenicity, a missense variant c.1877C>T (p.Ser626Leu) within the *SAMD9L* gene, located on 7q21, was selected as the candidate variant. The candidate variant

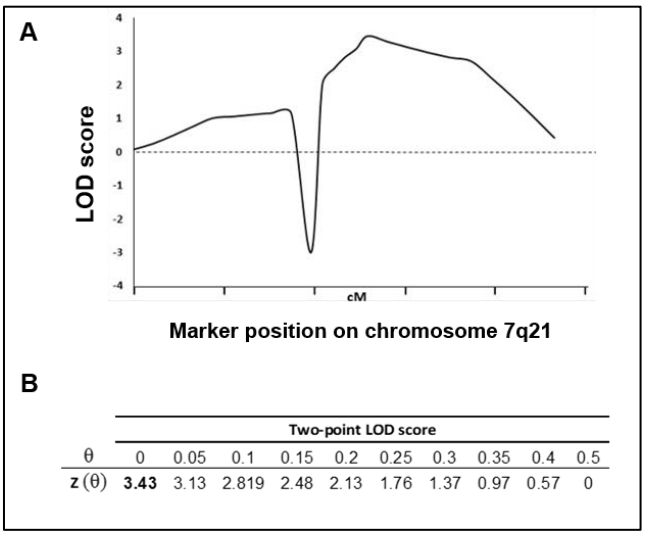


**Figure 31. Genome wide linkage analysis and two-point lod score identify the 7q21 candidate region where the *SAMD9L* gene physically maps. (A)** Logarithm of odds (LOD) score plots for chromosome 7q21. (**B**) The maximum logarithm of odds score was obtained with the c.1877C>T (p.Ser626Leu) variation within *SAMD9L* gene on chromosome 7q21 (Zmax=3.43, θ=0.00; *P*<3.53x10$^{-5}$).

segregated with the disease and was absent in six healthy individuals from the family and in eighty healthy individuals from Menorca's control population. Further linkage analysis with two additional family members revealed a significant 2-point logarithm of odds score between the locus trait and the identified variant (Zmax=3.43; θ= 0.00; $P<3.53x10^{-5}$) (**Figure 31B**). A multi-point LOD score analysis with three SNPs (rs17393952, rs4455763 and rs10263800) in the 7q21 candidate region and the candidate variant with the locus trait at 0 cM, resulted in a maximum significant multipoint LOD

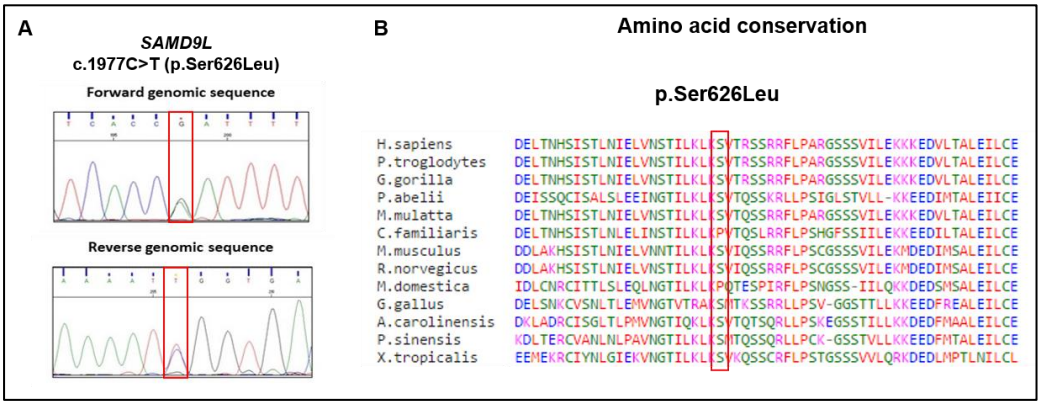


**Figure 32. The c.1877C>T (p.Ser626Leu) mutation within the *SAMD9L* gene is highly conserved, segregates with the disease, is predicted as deleterious by in silico algorithms.** (**A**) The c.1877C>T (p.Ser626Leu) *SAMD9L* variant is predicted as deleterious by six in silico algorithms. (**B**) The mutated amino acid was found highly conserved.

score Zmax of 3.46 ($P<3.28$ x$10^{-5}$). The c.1877C>T (p.Ser626Leu) variant within *SAMD9L* gene involves a serine to leucine amino acid change, and was predicted to be deleterious by SIFT, FATHMM, Mutation Assessor, Mutation Taster and Provean algorithms. It was found highly conserved through evolution (**Figure 32B**) and reported in the ClinVar database as a variant of uncertain significance identified in only one case (ClinVar: VCV000432926.2).

### 3.3. SAMD9L protein structure, domain and protein-protein interaction (PPI)

To address hSAMD9L protein structure and domains, we analysed the hSAMD9L protein sequence with HHpred protein sequence profile predictor and identified protein regions significantly similar to SAM (Ser6-85His), AAA+ ATP-ase/Hydrolase (711Lys-910Lys) and Apaf-1 ADP bound (716Glu-1018Glu) domains (**Figure 33 A** and **B**; **Supplementary Table 6**).

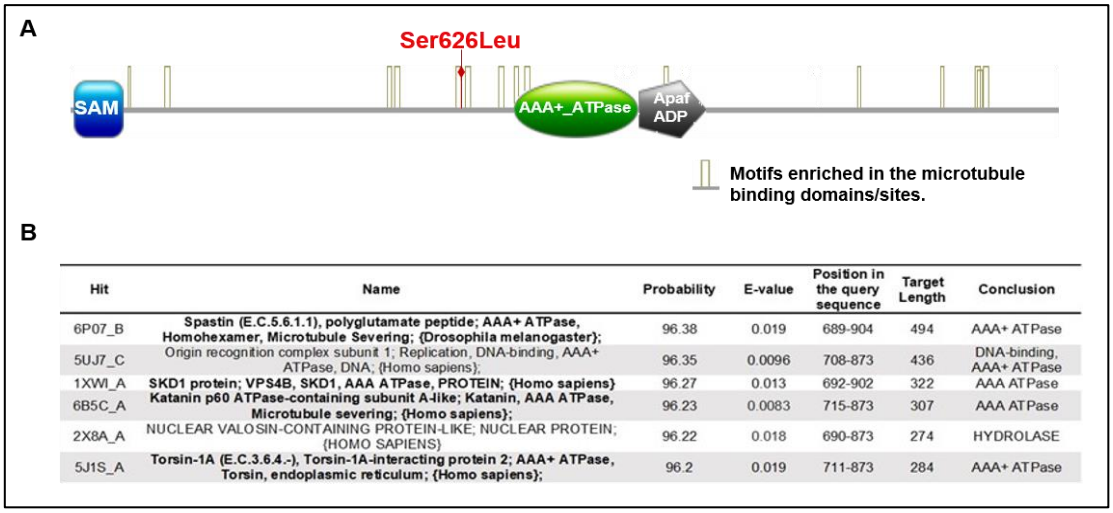


| Hit | Name | Probability | E-value | Position in the query sequence | Target Length | Conclusion |
|---|---|---|---|---|---|---|
| 6P07_B | **Spastin (E.C.5.6.1.1), polyglutamate peptide; AAA+ ATPase, Homohexamer, Microtubule Severing; {Drosophila melanogaster};** | 96.38 | 0.019 | 689-904 | 494 | AAA+ ATPase |
| 5UJ7_C | Origin recognition complex subunit 1; Replication, DNA-binding, AAA+ ATPase, DNA; {Homo sapiens}; | 96.35 | 0.0096 | 708-873 | 436 | DNA-binding, AAA+ ATPase |
| 1XWI_A | **SKD1 protein; VPS4B, SKD1, AAA ATPase, PROTEIN; {Homo sapiens}** | 96.27 | 0.013 | 692-902 | 322 | AAA ATPase |
| 6B5C_A | **Katanin p60 ATPase-containing subunit A-like; Katanin, AAA ATPase, Microtubule severing; {Homo sapiens};** | 96.23 | 0.0083 | 715-873 | 307 | AAA ATPase |
| 2X8A_A | NUCLEAR VALOSIN-CONTAINING PROTEIN-LIKE; NUCLEAR PROTEIN; {HOMO SAPIENS} | 96.22 | 0.018 | 690-873 | 274 | HYDROLASE |
| 5J1S_A | **Torsin-1A (E.C.3.6.4.-), Torsin-1A-interacting protein 2; AAA+ ATPase, Torsin, endoplasmic reticulum; {Homo sapiens};** | 96.2 | 0.019 | 711-873 | 284 | AAA+ ATPase |

**Figure 33. SAMD9L protein structure and domains.** (**A**) HHpred protein sequence profile predictor identified protein motifs significantly similar to SAM, AAA+ ATP-ase/Hydrolase, and Apaf-1 ADP bound domains. SAMD9L contains motifs enriched in microtubule binding proteins. The p.Ser626Leu localises within a microtubule predicted motif. (**B**) SAMD9L contains an ATPase/Hydrolase structural predicted domain significantly similar with SPAST, SKD1 and katanin proteins involved in microtubule severing, mitochondrial transport, and endosomal-lysosomal trafficking.

Furthermore, the analysis revealed the significant similarity with SPAST, SKD1/VPS4B, katanin and torsin-1A AAA ATPase specific protein domains, involved in microtubule and lysosomal trafficking (**Figure 33B**). Microtubule-associated protein analyser classified hSAMD9L protein as a MAP under a 90% of specificity threshold and identified a significantly enriched motif in MAPs proteins, S....LKS between amino acids 619-626 (STILKLKS) were the identified mutation c.1877C>T entails the p.Ser626Leu amino acid change (**Figure 34A; Supplementary Table 7**). The S....LKS motif is the fifth most significantly enriched motif in microtubule binding domains. Supporting this prediction, the MAPanalyzer also classified spastin, SKD1/VPS4B and katanin, as microtubule interacting proteins, (MAPs) as expected. In agreement, torsin-1A, LAMP1 and ATP5H, proteins not involved in microtubule association were correctly not

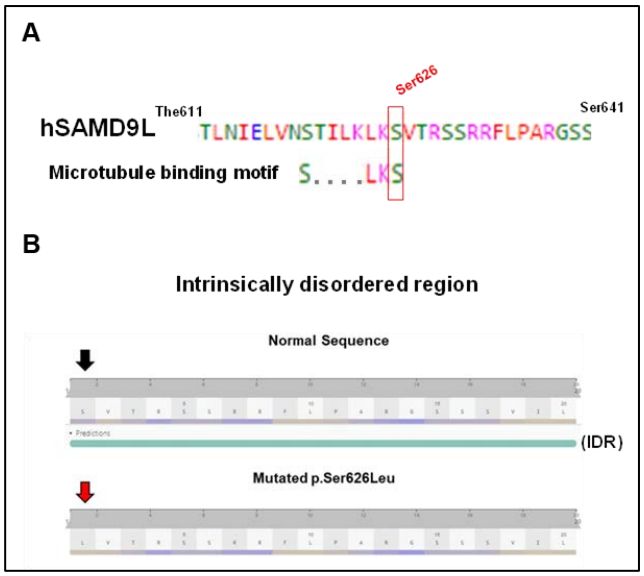


**Figure 34. The p.Ser626 amino acid change in SAMD9L protein localises to a predicted microtubule binding motif and intrinsically disordered region.** (**A**) The mutation is included within the STILKLKS motif which is a signature of microtubule binding domains. (**B**) The amino acid change abolishes the predicted intrinsic disorder region (IDR).

predicted as MAPs. Relevantly, the hSAMD9L paralog protein hSAMD9 contains the GTILKLKS amino acid sequence in the homolog protein region, missing the microtubule enriched motif S....LKS present in hSAMD9L. Comprehensive protein analysis with structural predictors identified an intrinsic disorder (ID) region around the SAMD9L amino acid residue Ser626 (**Figure 34B**). The SAMD9L amino acid change p.Ser626Leu alters the ID region predicted by PredictProtein (PROFBval and Ucon) and DisEMBL (Hot loops) algorithms, and it abolishes the identified ID region according to the prediction by InterPro (MobiDB-lite) (**Supplementary Table 8**). Furthermore, PredictProtein (PROFAcc) identified the 624-629 protein region of SAMD9L as a solvent-exposed region site. Solvent exposed regions have been implicated in mediating protein-protein interactions (PPI) (490). Interestingly, the algorithms NetPhos 3.1 and NetworKIN predicted the residue Ser626 within SAMD9L to be potentially phosphorylated by protein kinase C PKC (**Figure 35**). Mutations in PKC underlie spinocerebellar ataxia type 14 (196). Furthermore, we used the STRING program to study the interactions among SAMD9L and KATNA1, SPAST, VPS4B proteins identified by the HHpred protein sequence profile predictor algorithm (**Figure 33B**), and among the previously reported Samd9l-interacting proteins in mice Eea1 and Rab5 (491) in the context of the whole human genome (**Figure 36**). The SAMD9L and SPAST network interaction was identified via IFI44I, also known as microtubule-associated protein 44, and ATL1 proteins. The PPI enrichment analysis showed significantly more interactions among these proteins than expected ($P<2.52x10^{-7}$). Co-expression and interaction analyses linked both IFI44I and EEA1 with SAMD9L, and revealed association of the SAMD9L protein network with microtubule-associated proteins and endosomal/lysosomal pathways. Interestingly, mutations in the *ATL1*, *SPAST*, *RAB7A* or *KATNB1* genes have been previously associated with diseases presenting with hyperreflexia, sensory axonal neuropathy or sensory impairment among other signs, which overlap with clinical signs identified in this new ataxia subtype (**Supplementary Table 9**).

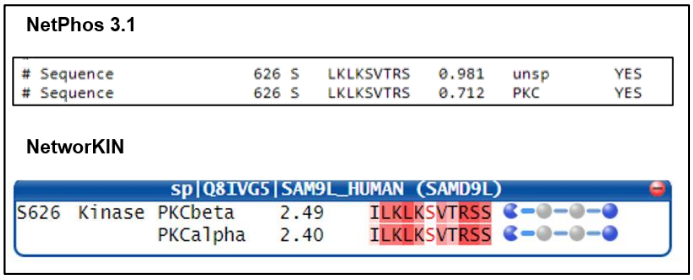


**Figure 35. Phosphorylation prediction of SAMD9L Ser626.** NetPhos 3.1 and NetworKIN predicted SAMD9L Ser626 to be potentially phosphorylated by PKC.

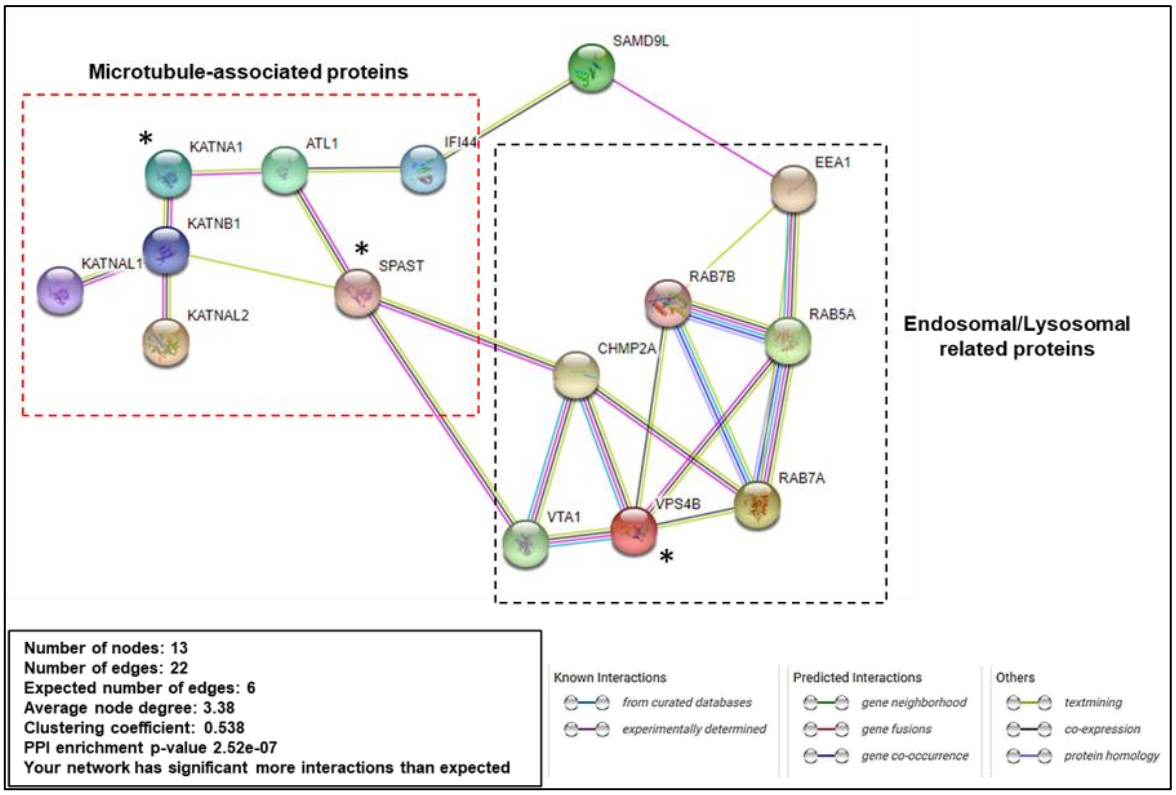


**Figure 36. STRING protein-protein (PPI) interaction network analysis of SAMD9L with structurally homologous predicted proteins identified by the HHpred protein sequence profile predictor algorithm.** STRING was analysed by implementing the KATNA1, SPAST, VPS4B proteins identified by the HHpred protein sequence profile predictor algorithm (**Figure 33B**) and with the previously reported Samd9l-interacting proteins in mice Eea1 and Rab5. The SAMD9L and SPAST network interaction was identified via IFI44I (also known as microtubule-associated protein 44) and ATL1 proteins. The PPI interaction enrichment analysis shows significantly more interactions in the indicated proteins than expected ($P<2.52x10^{-7}$)**.** Co-expression and interaction analyses link both IFI44I and EEA1 with SAMD9L. This analysis also revealed a novel association of SAMD9L with mitochondrial function. (*) Predicted proteins with structural homology with SAMD9L. Background: whole human genome**.**

### 3.4. Expression and subcellular localisation of human SAMD9L

Immunostaining with anti-SAMD9L antibody in control cerebellar sections revealed a punctate staining mainly in Purkinje cell soma and multipolar neurons of the human cerebellar dentate nucleus (**Figure 37**), suggesting a mitochondrial or vesicular staining. Some basket cells also appeared slightly stained. SAMD9L staining was also examined in fibroblast cells from age-matched control and affected patient, revealing clear mitochondrial staining and colocalising to the mitochondrial marker mitrotracker (**Figure 38A** and **B**). ENCODE RNAseq analysis confirmed relative expression of *SAMD9L* in adult Purkinje cells and almost no expression in cerebellar granule and pyramidal cells (**Figure 39**). RNA tissue expression also showed higher levels of *SAMD9L* in child cerebellum and

in embryonic cerebellum and spinal cord, in consonance with high mitochondrial activity stages and tissues involved in the pathogenesis of this new ataxia subtype.

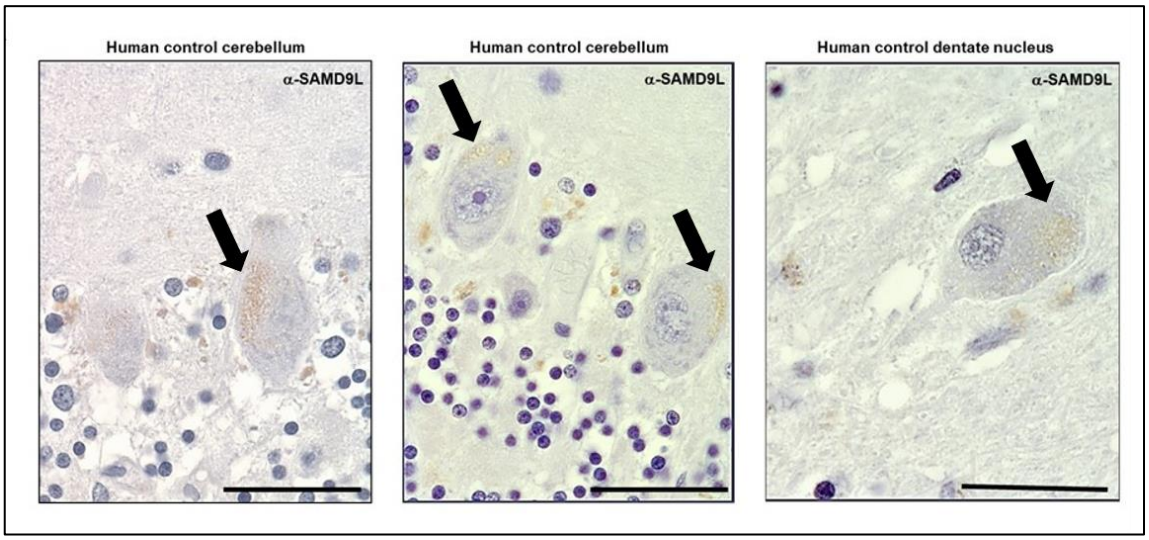


**Figure 37. SAMD9L localises to Purkinje cells and multipolar neurons in the human cerebellar cortex and dentate nucleus respectively.** Immunostaining with anti-SAMD9L antibody in control cerebellar sections revealed a punctate staining mainly in Purkinje cell soma and in multipolar neurons of the human dentate nucleus, indicative of mitochondrial or vesicular staining. Some basket cells also appear slightly stained. Magnification bars: 50 µm. Black arrows point to SAMD9L staining in Purkinje and multipolar neurons.

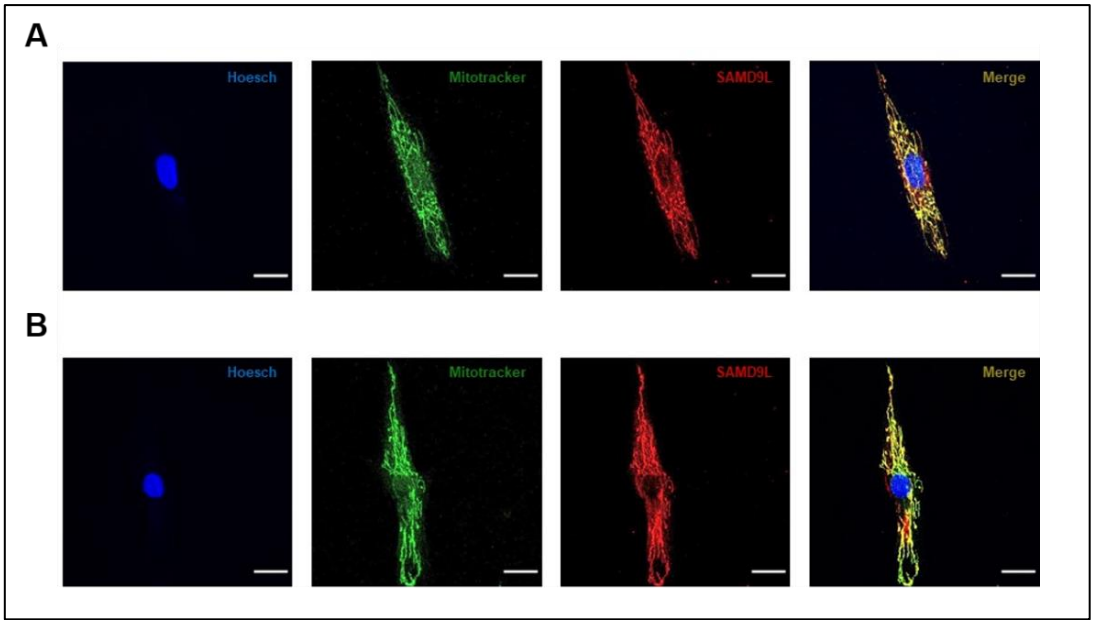


**Figure 38. SAMD9L colocalised to mitochondria in human cell fibroblasts.** Immunofluorescence staining of fibroblasts from human control (**A**) and M-SCA affected patient (**B**) showed colocalisation of SAMD9L to mitoTracker Red CMXRos demonstrating mitochondrial colocalisation. Magnification bars: 20 µm.

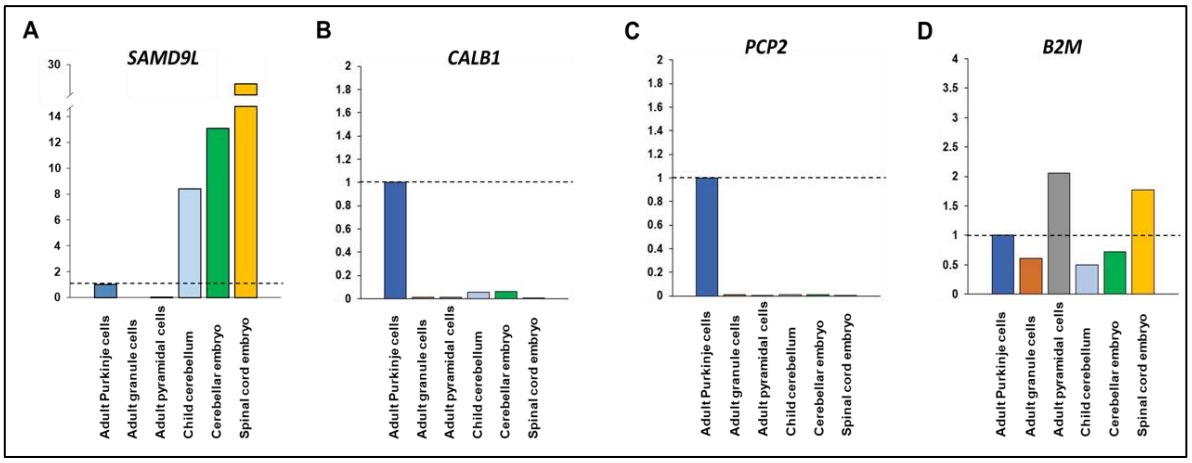


**Figure 39. Relative expression levels of *SAMD9L* mRNA in human control Purkinje, granule and pyramidal cells, cerebellum and spinal cord human tissues.** ENCODE *SAMD9L*, *CALB1*, *PCP2* and *B2M* mRNA sequences reads were compared on BAM files obtained from adult cerebellar Purkinje cells (dotted line), adult granular and pyramidal cells, 6-years-old child cerebellum, and cerebellar and spinal cord human embryos. *GAPDH* sequences reads were used to normalise intrasample differential expression. (**A**) *SAMD9L* was found only relatively expressed in adult male Purkinje cells and almost no expression was identified in cerebellar granular and pyramidal cells. mRNA tissue expression shows higher levels of *SAMD9L* in child cerebellum and cerebellar and spinal cord embryos in consonance with high mitochondrial activity and tissues involved in the pathogenesis of this new ataxia subtype. (**B** and **C**) Expression of *CALB1* and *PCP2*, two specific Purkinje cell markers, were mainly identified in adult Purkinje cells. (**D**) Expression of *B2M* gene, predominantly expressed in motor neurons, was accordingly higher in adult pyramidal cells and spinal cord embryo.

### 3.5. Mitochondrial dysregulation and altered endosome/lysosome trafficking in patients' fibroblasts

Immunoblotting of lysed and cellular fractioned fibroblasts confirmed SAMD9L mitochondrial localisation and showed decreased protein levels in the mitochondrial fraction of fibroblasts from affected individuals (**Figure 40A**). To corroborate this findings, total fractions of lysed fibroblasts were immunoblotted and reduced levels of SAMD9L in fibroblasts from affected patients was found (**Figure 40B**) without alteration in *SAMD9L* cDNA levels (**Figure 40C**).

Furthermore, potential alterations of fibroblasts' mtDNAs were analysed for mitochondrial DNA depletions and found increased copy number levels of the D-LOOP mitochondrial genomic region compared to the MT-CO3 region, suggesting an increased activity of mitochondrial replication (**Figure 40D**). Furthermore, in affected fibroblast cell lines, the ATP concentration was found increased compared to those from age-matched control fibroblasts (**Figure 40E**). Despite these mitochondrial alterations, pathogenic variants were not present in the mtDNA genome of patients' fibroblasts, and they presented similar frequency of non-pathogenic variants in the mtDNA genome compared to fibroblasts' controls. Thus, M-SCA fibroblasts showed similar levels of genomic

mtDNA damage compared to controls, discarding mtDNA damage associated with oxidative stress (**Supplementary Figure 4**) (492).

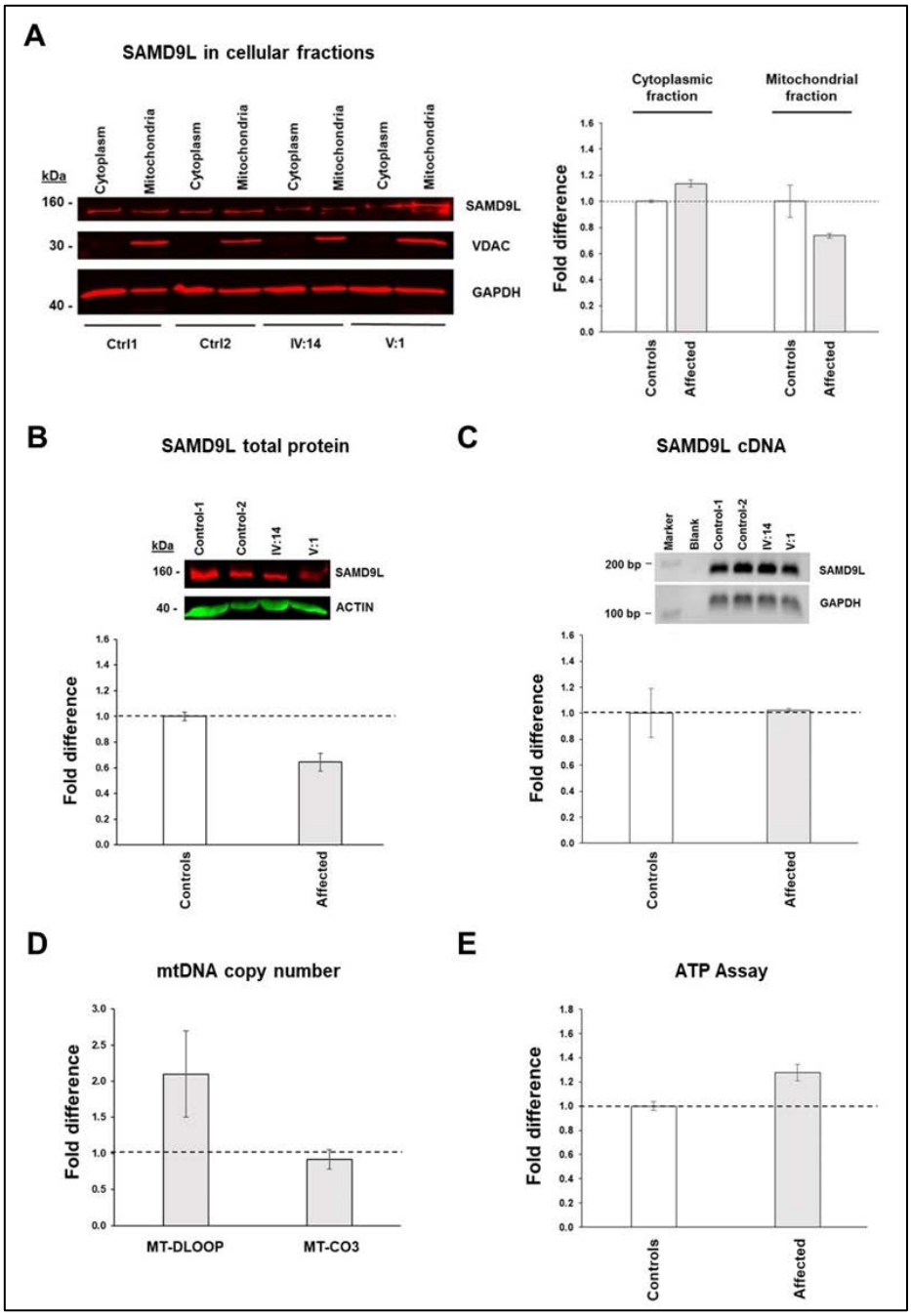


**Figure 40. Reduced SAMD9L protein levels and mitochondrial alterations in patients' fibroblasts.** (**A**) Immunoblotting of lysed and cellular fractioned fibroblasts confirmed SAMD9L mitochondrial localisation and decreased SAMD9L protein levels in the mitochondrial and total fractions (**B**) from patients' fibroblasts without alteration of *SAMD9L* cDNA levels (**C**). (**D**) Increased copy number levels of the mtDNA D-LOOP mitochondrial genomic region suggests an increased activity of mitochondrial DNA replication. (**E**) Increased ATP concentration was found in affected fibroblasts compared to age-matched controls. Controls values were set to 1 (dotted line).

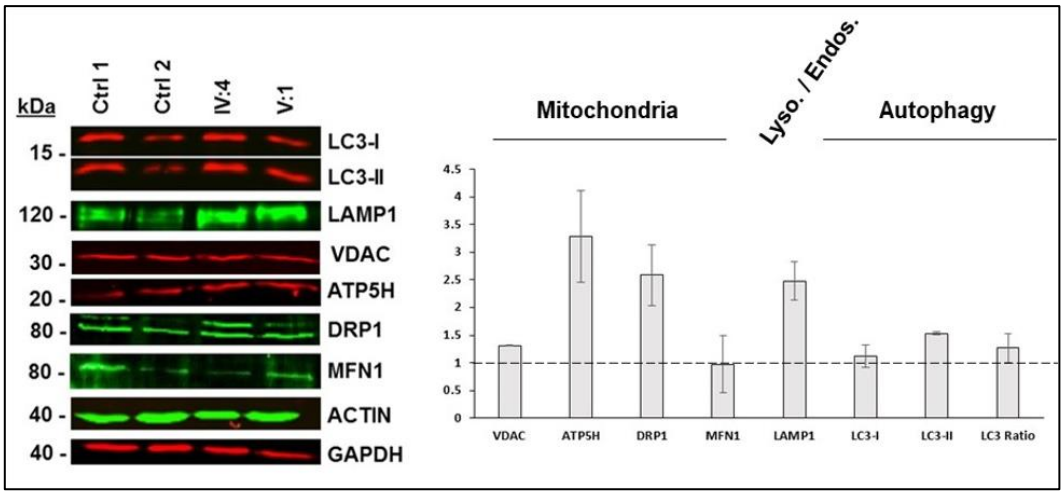


**Figure 41. Mitochondrial and endosome/lysosome dysregulation in patients' fibroblasts.** The ATP5H, DRP1 and LAMP1 proteins levels were found increased in patients' fibroblasts while no differences in VDAC, MFN1 and LC3 proteins were detected. Proteins levels were normalised to actin B (ACTIN) and GAPDH. Controls values were set to 1 (dotted line).

To further investigate mitochondrial dysregulation, we immunoblotted with anti-ATP5H mitochondrial marker and found that it was increased in patients' fibroblasts despite normal levels of VDAC protein (**Figure 41**). Because ATP5H plays a crucial role in regulating apoptosis, this evidence further supports up-regulation of ATP synthase. Additionally, DRP1 protein levels also appeared overexpressed. Interestingly, DRP1 is a dynamin-like GTPase involved in mitochondrial division which has also been associated with lysosomes in brain (493) and implicated in Purkinje cells mitochondrial transport (494). Related to lysosomes, LAMP1, a lysosomal-associated membrane protein 1 involved in endosome trafficking, also appeared overexpressed in patients' fibroblasts samples (**Figure 41**). In contrast, no differences were observed in the mitochondrial fusion marker MFN1 and in the LC3 autophagy marker. Therefore, overall these data demonstrate SAMD9L mitochondrial localisation, suggest an increase of mitochondrial DNA replication and bioenergetics, and point to dysregulation of the endosomal-lysosomal pathway in this novel SCA subtype.

To investigate cellular structural changes, high resolution images from fibroblasts obtained from patient V:1 and an age-matched control were examined by transmission electron microscopy and showed significant higher number of lysosomes in affected fibroblasts ($F_{(1,18)=}6.135$, $P$=0.023; **Figure 42D** and **G**). No mitochondrial number or mitochondrial structural alterations were identified. Therefore, these data confirm an increased number of lysosomes and discards alterations in morphology and mitochondrial number in M-SCA patient's fibroblasts.

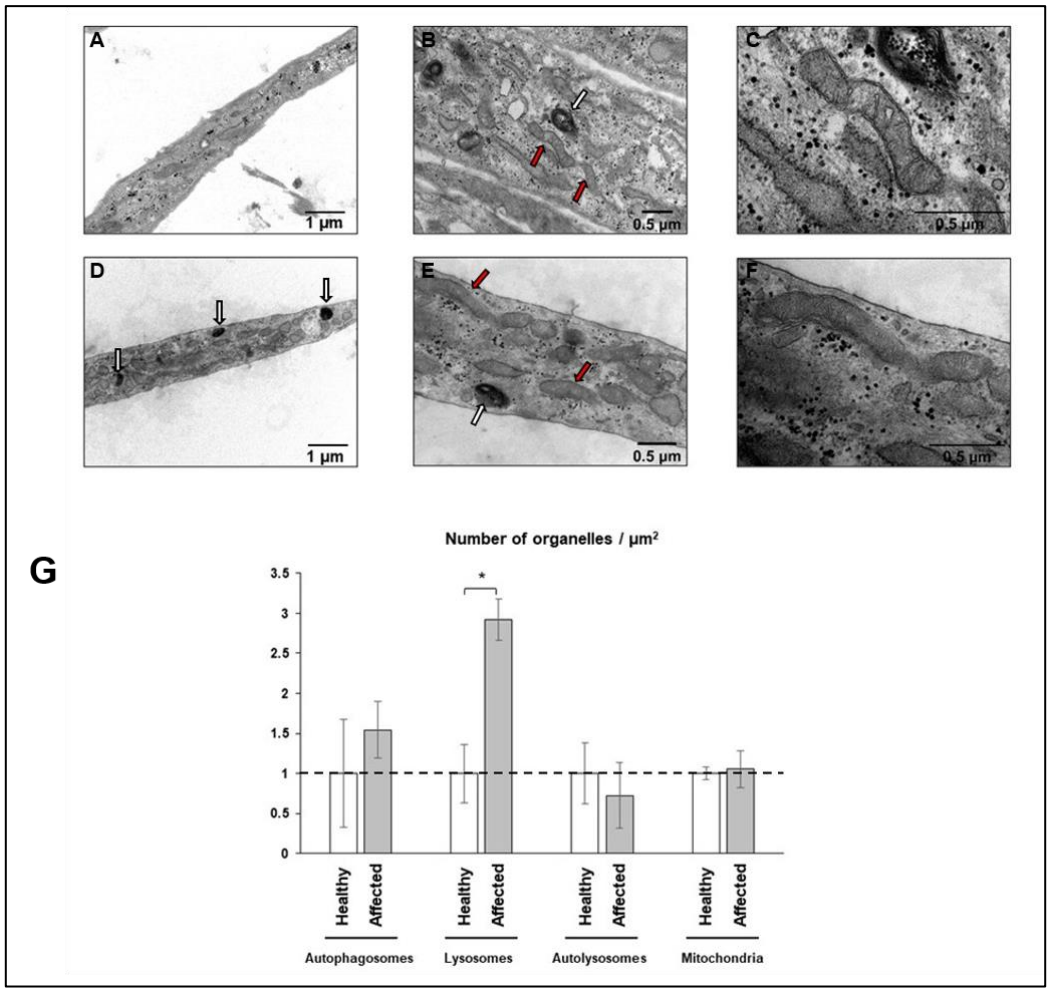


**Figure 42. Increased number of lysosomes in M-SCA patients' fibroblasts.** Transmission electron microscopy (TEM) showed significantly increased lysosome number on patients' fibroblasts (**D**) compared to controls (**A**) ($F_{(1,18)}$=6.135, *P*=0.023), while mitochondrial morphology remained normal (**B-C** and **E-F**). Red arrows point to mitochondria. White arrows point to lysosomes. Asterisk denotes significance at *P*<0.05.

### 3.6. The c.1877C>T (p.Ser626Leu) mutation in *SAMD9L* impairs locomotion and neurosensorial phenotypes in zebrafish embryos

Genomic regions of the candidate human *SAMD9L* ortholog gene sequences were identified in zebrafish by using meta-analysis data from previously generated transgenic zebrafish models (https://zmp.buschlab.org/) and compared to zebrafish cerebellar RNA-seq data from the SRA database (access: SRX4184229; **Supplementary Figure 5**). Four candidate homolog regions were annotated from the zebrafish database, but only two of those genome regions aligned to RNA-sequences from the cerebellum zebrafish. The predicted translated protein from these two zebrafish genomic regions revealed low protein identity (<30%) with that of human SAMD9L and did not show conservation for the Ser626 amino acid. For this reason, transient expression of the human wild-type and mutated *SAMD9L* mRNAs were generated in zebrafish instead of knocking out or down the endogenous zebrafish ortholog candidates.

Zebrafish embryos were injected at one-cell stage with mRNA encoding human wild-type or mutant *SAMD9L* to investigate the effects of transient gene expression on viability, motor activity and neurological behaviours. Accumulated survival at 24 and 96 hpf were not significantly impaired with any mRNA concentration tested (**Figure 43B**). Moreover, teratogenic rate did not show any concentration dependency (**Figure 43C**). Mean distance was significantly reduced in five days post fertilization fish exposed to SAMD9L-S626L compared to the wild-type SAMD9L group ($F_{(1,48)}$=4.745, $P$=0.034; **Figure 43D**). Furthermore, fish overexpressing wild-type SAMD9L showed a significantly increase in mean distance moved compared to control injected group ($F_{(1,52)}$=6.583, $P$=0.013; **Figure 43D**). No significant altered motor phenotype was observed in any other tracked fish group. Additionally, the number of head turns during the five light-dark cycles was significantly increased in WT-SAMD9L compared to the control group (Mann-Whitney U=216, $P$=0.010; **Figure 43E**), and significantly decreased in injected S626L-SAMD9L zebrafish embryos compared to the WT-SAMD9L (Mann-Whitney U=192.5, $P$=0.022; **Figure 43E**) demonstrating vestibular and sensory impairment.

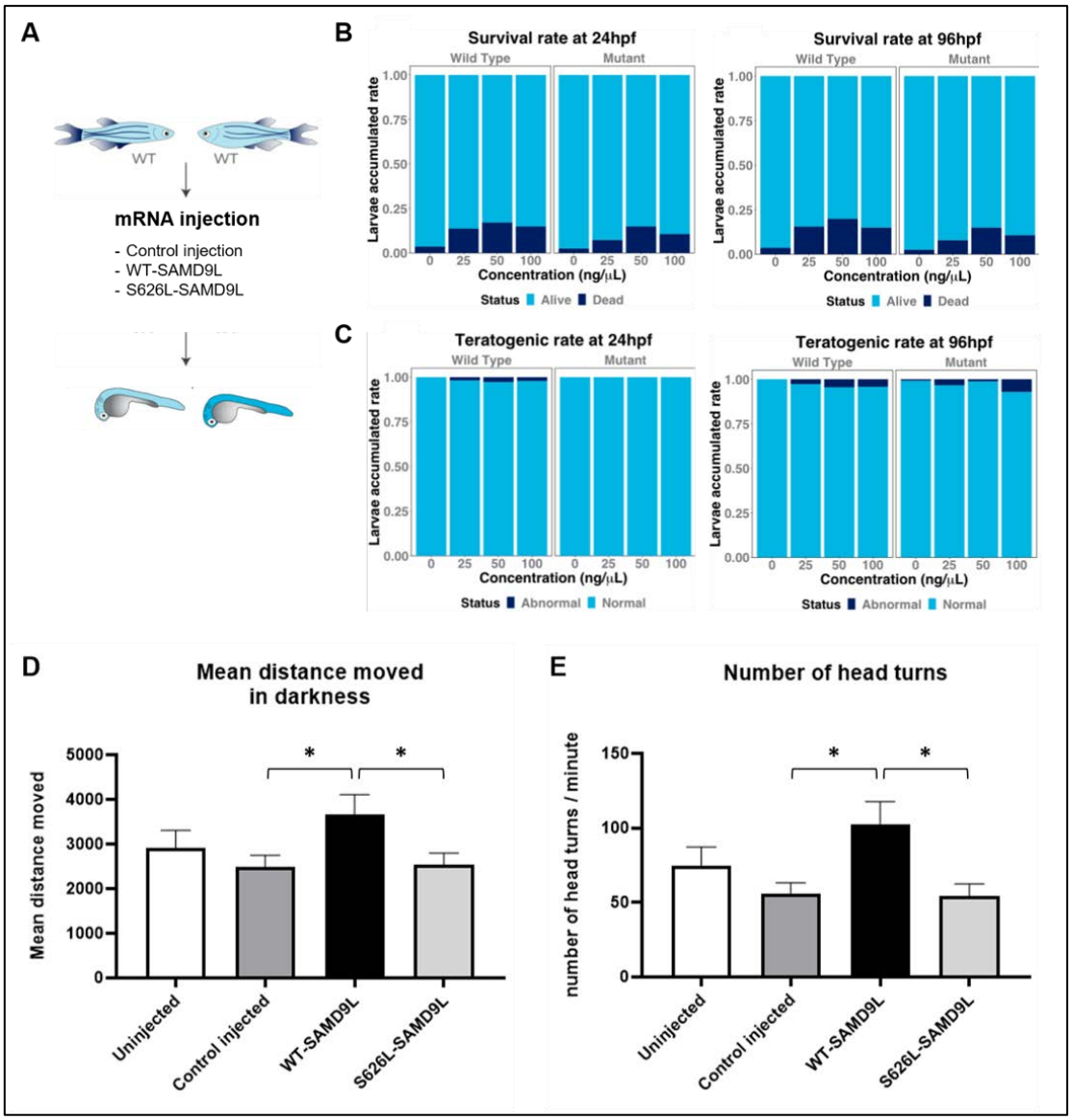


**Figure 43. Overexpression of mutant Ser626Leu SAMD9L triggers locomotive and neurosensory impairment in Zebrafish embryos.** Protocol summary (**A**), accumulated survival rate **(B)** and accumulated teratogenic rate **(C)** did not show any concentration dependency. **(D)** Mean distance travelled (mm) during five dark periods was significantly increased in the WT-SAMD9L zebrafish embryos compared to the control group ($F_{(1,52)}$=6.583, *P*=0.013), and significantly decreased in S626L-SAMD9L zebrafish embryos compared to the WT-SAMD9L group ($F_{(1,48)}$=4.745, *P*=0.034). **(E)** The number of head turns during five light-dark cycles was significantly increased in WT-SAMD9L compared to the control group (Mann-Whitney U=216, *P*=0.010), and significantly decreased in S626L-SAMD9L zebrafish embryos compared to the WT-SAMD9L (Mann-Whitney U=192.5, *P*=0.022), indicative of vestibular and sensory impairment in mutant animals.

# DISCUSSION

The present study provides relevant novel insights into the clinical, genetic and physiopathological bases of autosomal dominant spinocerebellar ataxias. Provided evidence reveals the high clinical and genetic heterogeneities of dominant cerebellar ataxias, the relative gene mutation frequency in a subcohort of Spanish ataxia patients and their overlapping genes and clinical signs and symptoms with other neurodegenerative diseases. As a result of this thesis two novel SCA subtypes were identified and characterised. We identify and demonstrate that the ATTTC pentanucleotide repeat mutation within the non-coding regulatory region of the gene encoding for the reelin adapter protein DAB1 as the genetic cause underlying spinocerebellar ataxia type 37. We describe the clinical-genetic correlations in four Spanish SCA37 families and describe the first neuropathological findings in two SCA37 brains. In addition, we identify a novel SCA subtype by demonstrating the c.1877C>T (p.Ser626Leu) mutation within the *SAMD9L* gene as the causal molecular genetic defect in a Balearic five-generation family. We thoroughly describe the clinical features of this new spinocerebellar ataxia subtype. Finally, we characterize the subcellular defects underlying the molecular pathology in these two new spinocerebellar ataxia subtypes.

***Clinical and genetic correlations evidence high heterogeneity and overlapping phenotypes of ataxia syndromes.***

In the present study we used a combination of traditional PCR techniques, amplicon-based panel next-generation sequencing and a novel R-based analysis algorithm in a cohort of 308 Spanish patients with ataxia to estimate the mutation frequency in genes previously associated with dominantly inherited cerebellar ataxias and other genes related with other neurological diseases.

The causative variants were identified in a total of 74 index cases (24%) out of 308 index cases included in the study, with 20 of them carrying variants in other genes not previously associated with dominant ataxia. Previous several studies reported a higher diagnostic yield using NGS technologies in undiagnosed ataxias cases, but they included all types of inheritances and some studies were performed in a very small cohort of patients thus, biasing diagnostic yield for dominant inherited forms. Indeed, diagnostic rate in 12 previous studies, focusing only on dominant ataxias, ranged between 8% and 36% (295,392,495–504), with the higher rate (36%) obtained in a study using whole exome sequencing in a small cohort of 11 cases suggestive of dominant inheritance (501). The most extensive and similar study on dominantly inherited ataxias was performed by Coutelier and collaborators in Paris (392) yielding a diagnostic in 59 patients out of 412 cases (14.3%). A very recent study identified probably pathogenic or likely pathogenic variants in 14 different genes in 22.2% of undiagnosed ataxia patients (505). Thus, the diagnostic rate obtained in the present study is in accordance with previous reported frequencies for dominant ataxias. In order to increase diagnosis yield, novel ataxia genes need to be identified and alternative recently developed technologies such as Pacific Biosciences (PacBio) and Oxford Nanopore Technologies (ONT) both for enabling long

read sequencing (506) should be implemented to facilitate the identification of other types of genetic variants such as structural and copy number variants (CNVs), regulatory variants or repeat expansions, that nowadays escape from NGS detection.

Polyglutamine expansions counts for the 6.81% of the total ataxia index cases, being SCA3 (*ATXN3*) repeat expansion the most prevalent mutation, followed by SCA2 (*ATXN2*) and SCA6 (*CACNA1A*) polyglutamine expansions, in consonance with previously published studies in our population (25). Two expanded repeats were identified in the *CACNA1A* gene in two patients presenting with SCA6. In addition, four other index cases presented two novel frameshift mutations and two missense mutations respectively. One of the frameshift mutations (c.5588_5589delTC; p.Leu1863ArgfsTer9) segregated with the disease in three affected family members. Those three affected individuals and the patient carrying the c.1084delG (p.Glu362SerfsTer16) frameshift mutation presented with ataxia episodes, while patients with missense mutations c.5267G>A (p.Arg1756Gln) and c.3052G>A (p.Glu1018Lys) presented with progressive ataxia in consonance with previously described genotype-phenotype correlations (126). Episodic ataxia type 2 (EA2) is caused mainly by mutations generating protein truncation or abnormal splicing, and rarely by missense mutations in CACNA1A protein α-1A subunit, which are mainly associated with progressive autosomal dominant cerebellar ataxia (311,507). Therefore, mutations within the *CACNA1A* gene are a frequent cause of progressive or episodic dominant ataxia in consonance with a recent ataxia panel study of the European ataxia population (392).

Variants in the *ITPR1* gene have been described to cause cerebellar diseases including slow progressive spinocerebellar ataxia type 15 (SCA15) of adult onset, congenital non-progressive spinocerebellar ataxia with mild cognitive impairment (SCA29) and with Gillespie's Syndrome characterised by bilateral iris hypoplasia, congenital muscle hypotonia, non-progressive cerebellar ataxia, and variable intellectual disability (508). Heterozygous deletions of the *ITPR1* gene are known to cause SCA15 while missense mutations have been mainly associated with SCA29 which presents with an earlier ataxia onset (509). In the present study, four novel missense, one novel frameshift, and one novel variant in an exon-intron splicing region were identified in the *ITPR1* gene. Although extensive clinical information was not available for these cases, the genotype information suggests that the frameshift and splicing mutation could contribute to a more late-onset form of ataxia because of protein loss-of-function mutations, whereas the missense mutations could account for a typical SCA29 clinical phenotype, despite the fact that recent studies described missense mutations associated with SCA15 (210,510). Interestingly, the missense variant c.799A>G (p.Thr267Ala) identified, localises at the same amino acid codon as a previously reported variant associated in SCA29 (509) but with a different amino acid change (p.Thr267Met). Furthermore, the remaining identified missense mutations were localised to the coupling/regulatory domain of the ITPR1 protein where mutations are predicted to alter calcium channel function (255).

Four different variants were identified in the *TGM6* gene associated with SCA35. A recent study suggested a significant inflation in *TGM6* associated variants regarding the cumulative frequency of *TGM6* reported pathogenic variants and population frequencies (274). Three *TGM6* variants identified in this study were predicted to generate a truncated protein product and were not previously reported in the literature neither in the previously mentioned *TGM6* study.

Heterozygous mutations in the *AFG3L2* gene cause spinocerebellar ataxia 28 (SCA28) while homozygous mutations in the same gene cause recessive spastic ataxia 5 (SPAX5). SCA28 pathogenic mutations are consist mainly of heterozygous missense variants within the protein proteolytic domain encoded by *AFG3L2* exons 15 and 16 (252). Other identified variants included one missense in the fourth exon, one missense in exon 10, two truncating frameshift in exon 15, and a deletion spanning exons 14–16 (31,452). In the present study four index cases presented four different variants, three of them not previously described. The previously reported variant c.1996A>G (p.Met666Val) located in the most frequent mutated amino acid (252), was identified in an index patient and segregated with the disease in three additional related individuals. Interestingly, in the present study two of the novel identified missense variants c.31C>T (p.Arg11Trp) and c.386C>G (p.Ser129Cys), were located at the mitochondrial targeting signal close to a transmembrane domain (252). Considering that the *AFG3L2* gene encodes a protein localised to mitochondria and involved in protein synthesis and Purkinje cell survival (511), novel identified variants could alter its normal function regarding their localisation and cerebellar function. Furthermore, a novel nonsense mutation c.847C>T (p.Arg283Ter) located in another predicted transmembrane domain, was identified in an affected individual with early onset ataxia and was also present in an affected sibling with similar clinical symptoms.

SCA14 is mainly associated to missense mutations in the *PRKCG* gene but a nonsense mutation has been recently reported (197). In the present study, a recurrent missense mutation c.254G>A (p.Cys85Tyr) was identified in two independent index cases. Furthermore, this variant segregate in one affected sibling and, interestingly, it locates in a cysteine-rich C1 domain (C1A), where several variants have been described showing a critical role in PKC inhibitory activity (512). Additionally, a patient carried two digenic mutations: a heterozygous missense variant c.448T>G (p.Cys150Gly) in a cysteine-rich C1 protein domain C1B of *PKC,* and a heterozygous c.2311A>G (p.Met771Val) variant within the *ITPR1* gene, this predicted to have a lower pathogenic impact. Interestingly, digenic mutations have been previously identified in a few ataxia patients (496,513–515), further supporting the contribution of the identified digenic variants in the pathogenesis of the ataxia phenotype in our patient.

The original association between SCA48 clinical symptoms and the *STUB1* gene was described in a Catalan family by Genis and collaborators (298). In the present study we identified the frameshift

mutation c.823_824delCT (p.Leu275AspfsTer16) reported originally in the initial study in a patient from the same geographical region. Furthermore, two additional index cases presented heterozygous missense mutations not previously reported. A recent European study identified 7% positive SCA48 cases in a cohort of European ataxia cases, highlighting the high prevalence of this SCA subtype (27). A significantly later onset and a less severe disease have been reported in *STUB1* heterozygous carriers compared to compound heterozygous or homozygous *STUB1* variant carriers, associated with recessive spinocerebellar ataxia type 16 (SCAR16), suggesting haploinsufficiency as the underlying mechanism (27). Interestingly, our patient, carrying the frameshift mutation c.823_824delCT (p.Leu275AspfsTer16) previously described, presented with ataxia and cognitive impairment as previously reported in 54% of SCA48 cases (27).

In addition, one patient presented with the missense heterozygous variant c.5C>T (p.Ser2Phe) in the *CACNB4* gene and another the c.1044T>A (p.Phe348Leu) in the *SLC1A3* gene. Interestingly both patients presented with progressive ataxia instead of the episodic attacks previously described in EA5 and EA6 ataxia forms (311).

Extensive clinical overlap exists among a wide range of movement disorders. The routine implementation of NGS increasing the genetic diagnostic yield, revealed a large clinical and genetic overlap among different ataxia subtypes, and among ataxias and other neurodegenerative diseases like hereditary spastic paraplegia (516), dystonia (517), Charcot-Marie-Tooth disease (518), ALS (468), parkinsonism (100) or mental retardation (519), evidencing the high clinical heterogeneity of inherited ataxias.

Ataxic neuropathies are a heterogenous group of neurological disorders presenting affected peripheral nervous system and characterised by sensory ataxia as a clinical symptom (520). A missense mutation in the *ARHGEF10* gene was previously associated with an autosomal dominant neuropathy form characterised by the presence of thin myelinated fibers in a Belgian family (521,522). In the present study, an index case and his sister presented hereditary ataxic sensitive polyneuropathy with cerebellar affectation. Likewise, the coexistence of polyneuropathy and cerebellar degeneration has been extensively associated with other dominant ataxias as in SCA2, SCA3, SCA18 or SCA43 (137).

*LRSAM1* gene mutations are a cause of axonal CMT2P presenting with both autosomal dominant and recessive forms (523). An index patient in the present study presented a clinical picture of dysarthria, spastic gait, sensory neuropathy with cerebellar atrophy. Recently, four families were identified presenting with an autosomal inheritance form of Charcot-Marie-Tooth disease characterised by marked sensory ataxia that presented mutations in *LRSAM1* gene (461), supporting its association with ataxic symptoms.

In addition, a heterozygous mutation in the *MFN2* gene identified in a patient presenting with a clinical picture of sensory neuronopathy, progressive ataxia and ophthalmoplegia was previously described in a sporadic case with hereditary neuropathy, debuting with ataxic gait (462). *MFN2* was previously associated with CMT2A2A, CMT2A2B and hereditary motor and sensory neuropathy type VIA (OMIM * 608507). Moreover, mutations in the *MFN2* gene have been associated with mitochondrial pathologies presenting with optic atrophy (524) evidence that may explain the patient's ophthalmoplegia.

Variants in the *OPA1, POLG* and *TWNK* genes were also identified in this study. These genes have been associated with more complex phenotypes of mitochondria related symptoms including ataxia, optic atrophy and spasticity (525–527).

Clinical and genetic heterogeneities are also characteristic of ALS disease presenting genotype/phenotype overlapping with others diseases such as Parkinsonism syndromes, frontotemporal dementias or ataxias (528). The identified heterozygous variant c.1280A>G (p.Tyr427Cys) in the *TAF15* gene implicated in the pathogenesis of ALS, was previously found in two unrelated cases, one presenting with progressive motor weakness and the other progressive dysarthria (472). The *SOD1* gene has traditionally been associated with ALS of autosomal dominant inheritance. The variant identified in this study was previously found in several individuals with ALS (529–531) and in a family with autosomal dominant inheritance of the disease (532). Interestingly, our case presented ataxia with peripheral polyneuropathy attributed to diabetes mellitus. Thereafter, the disease progressed with respiratory failure. Neurological examinations determined that the clinical picture was more similar to an ALS form. Additionally, a recent study described a novel syndrome with deficiency in SOD1 distinctive from amyotrophic lateral sclerosis presented with progressive ataxia (533), evidencing the clinical overlap between motor neuron disease and ataxia syndromes associated with SOD1 deficits.

In fact, there is a relevant spectrum of genes causing numerous disorders manifesting ataxia and dystonia symptoms. Interestingly, there is also a pathophysiological link between both phenotypes, and the role of cerebellum in the pathology of dystonia has been extensively reported (473). The heterozygous in-frame deletion in a patient presenting with ataxia as a primary sign, was previously reported in the databases (ClinVar. RCV000536794.1) in affected patients with dystonia as primary sign. Thus, regarding the overlapping phenotype-genotype correlation between ataxia and dystonia, we have to take into consideration this variant as the causative mutation.

The adult cerebellum is vulnerable to be implicated in several hereditary leukodystrophies such as those with adult onset presenting with ataxia and cerebellar lesions (534). One patient in the present study revealed the possibly causative heterozygous variant c.1693G>A (p.Asp565Asn) in exon 12 of the *CSF1R* gene. This variant was previously associated with autosomal dominant late-onset

leukodystrophy (535). Patients with mutations in *CSF1R* manifest gait disturbance as a cardinal symptom, including ataxia, reinforcing the role of the identified mutation in the pathogenesis of the disease (536).

Various genes traditionally associated with either ataxia or spastic paraplegia have been shown to cause a wide range of overlapping symptoms between both conditions (463). Actually, spasticity and pyramidal features are a hallmark of a group of hereditary ataxias, mainly associated with recessive mode of inheritance such as ARSACS (*SACS*), SPAX2 (*KIF1C*) or SPAX3 (*MARS2*) (537). Moreover, some dominant ataxias are also inherited in a recessive manner such as those variants in *GRID2, AFG3L2* and *SPTBN2* genes, and those clinical cases could also present spastic paraplegia as a clinical sign (463). Conversely, patients with the HSP subtypes SPG4, SPG6, SPG31 and SPG37 may also present with cerebellar atrophy (538). Another example is the identification of *SPG7* mutations as a common cause of undiagnosed ataxia (539). The ataxia-spasticity disease spectrum is further supported by ataxic and hereditary spastic paraplegias forms that share not only overlapping phenotypes and underlying causative genes, but also common cellular pathways and disease mechanisms revealing common pathophysiological processes. Consistently, their mechanistic overlap may underlie their clinical overlap (463).

Therefore, considering the phenotypic overlap between cerebellar ataxias and hereditary spastic paraplegias, a combined analysis by NGS of genes implicated in both groups of disorders is justified. As an example, heterozygous *KIF1A* variants typically associated with spasticity also underlie a wide spectrum of neurodevelopmental and neurodegenerative disorders including patients presenting with early onset or congenital ataxic phenotype (519). Furthermore, de novo *KIF1A* mutations were identified in patients with intellectual disability, spasticity and cerebellar atrophy and/or optic nerve atrophy (465). In agreement with these reported findings, both patients identified in the present study carried an infantile onset ataxia with moderate mental retardation, with spastic-ataxic gait carried a *de novo* mutation c.914C>T (p.Pro305Leu) in the *KIF1A* gene confirmed by segregation studies.

The *SPG7* gene was initially associated with autosomal recessive spastic paraplegia (540) and optic neuropathy with cerebellar ataxia occurring in 39% of patients with a clear dominant pattern in one family (541). Furthermore, biallelic mutations in *SPG7* have been recognized as a major cause of undiagnosed ataxia (392,539). Likewise, *WASHC5* heterozygous variants have been previously associated with autosomal dominant spastic paraplegia type 8 (OMIM # 603563) with some patients presenting with upper limb ataxia (542). One of our cases presenting with ataxia as mainly clinical sign, harboured two double heterozygous variants c.2797G>A (p.Ala933Thr) and c.1529C>T (p.Ala510Val) in *WASHC5* and *SPG7* genes respectively. The c.1529C>T (p.Ala510Val) *SPG7* heterozygous variant has been recently reported in cerebellar ataxia cases in homozygous or compound heterozygosis with other *SPG7* variants (380,452) and its pathogenicity has been clearly

determined, albeit its pathological effect in heterozygosis has been suggested and discussed (453). Thus, in this case we cannot rule out that the p.Ala510Val heterozygous mutation together with the *WASHC5* mutation triggers a synergistic action from both variants as previously suggested in other dominant ataxia genes (27,392).

A c.370C>T (p.Leu124Phe) heterozygous mutation has been also identified in the *SLC33A1* gene previously associated with SPG42 of autosomal dominant inheritance (543).This variant has been previously described in the database in cases with spastic paraplegia (ClinVar RCV000633017.2; RCV000516545.1). Thus, due to the mentioned phenotype-genotype overlap between ataxias and paraplegias, it is a clear candidate causative variant.

In the present study we also identified a patient presenting with progressive dysarthria, nasal voice, and telekinetic tremor in both upper limbs presenting with a missense heterozygous variant in the *GBA* gene. The *GBA* gene has been previously associated with Gaucher's disease with recessive inheritance and with dominantly inherited late onset Parkinson's disease. Interestingly, Gaucher's patients with recessive variants in the *GBA* gene could also present with ataxia as a main clinical symptom (544) and heterozygous carriers could also present with multiple system atrophy (MSA), which is an adult- onset disease, characterised by parkinsonism and cerebellar ataxia (544). This evidence together with the tremor presented in the clinical phenotype of the studied patient suggest that the variant is a candidate mutation causative of the disease.

The implications of mutations initially associated with recessive cerebellar ataxias in some dominant ataxia forms have been widely discussed in previous studies (500,545). As an example, homozygous *GRID2* deletions or compound heterozygous deletions involves tonic up-gaze and delayed cognitive development, encephalopathy or oculomotor apraxia (546). A heterozygous deletion spanning the first exon of *GRID2* was also described in a complicated form of spastic paraplegia with frontotemporal dementia (483). In the same study, authors reported a missense mutation c.1966C>G p.Leu656Val in the *GRID2* gene in a heterozygosis in adults, and in homozygosis in one child with congenital ataxia, compatible with a semidominant transmission. Thus, the identified heterozygous variant c.1577T>A (p.Ile526Asn) within the *GRID2* gene in patient P83, not previously reported, is a solid candidate variant to be associated with the ataxia phenotype.

The *ATP1A3* gene has been previously associated with adult rapid-onset ataxia (547). In the present study we identified a patient presenting the variant c.2341T>C (p.Tyr781His) with a similar phenotype to a sporadic case previously described affected of alternate hemiplegia of infancy (481).

Furthermore, we identified the heterozygous variant c.1825G>A (p.Gly609Arg) in the *DNMT1* gene in a patient presenting with tremor, ataxia, dystonia and cognitive decline. Mutations in *DNMT1* cause autosomal dominant cerebellar ataxia, deafness and narcolepsy (548) as well as pure cerebellar ataxia (549). DNMT1-complex disorder in a case presenting with childhood ataxia, treatment-refractory

seizures, and rapid cognitive decline in his fifties has been recently described (550). All these data together suggest the identified variant as a candidate to explain the patient's phenotype.

Mental retardation is a specific clinical feature in SCA13 (551). In the present study we identified one heterozygous variant in the *ZMYND11* gene in a patient presenting with ataxia and one heterozygous variant in the *L1CAM* gene in a patient presenting with ataxia and leukodystrophy. The *L1CAM* gene has previously associated with L1 syndrome, which is characterised by hydrocephalus, mental retardation, aphasia, adducted thumbs and motor dysfunctions, such as ataxia, paraplegia and shuffling gate (552). Interestingly, our case with the c.832C>T (p.Arg278Cys) variant in the *L1CAM* gene presented ataxia with leukoencephalopathy symptoms that could fit with L1 syndrome. Previous studies associated mutations in the *ZMYND11* gene with motor delay presenting ataxia in an autosomal dominant case (479). Therefore, the overlapping clinical symptoms suggested the identified variant as a candidate causative mutation.

In conclusion, we studied a subcohort of 308 index cases presenting with dominantly inherited cerebellar ataxia. By combining repeat expansion detection with NGS and a novel R-based algorithm analysis, we identified the causative variants in 24% of all ataxia cases. This agrees with the prevalence reported in the literature regarding dominant ataxias. We also confirmed the primary causative implication of other genes not traditionally associated with dominant ataxias, presenting clinical and genetic overlap such as *ARHGEF10, TWNK, OPA1, MFN2, LRSAM1, POLG, KIF1A, SLC33A1, WASHC5, SPG7, SOD1, TAF15, CIZ1, GBA, CSF1R, ZMYND11, L1CAM, ATP1A3, DNMT1* and *GRID2* genes.

***An unstable ATTTC repeat mutation within the Disabled 1 gene causes cerebellar Purkinje cell alterations, DAB1 RNA switch, and Reelin signalling dysregulation in the spinocerebellar ataxia type 37.***

Since the identification of pathogenic repeat expansions as the underlying cause of a few neurological diseases in the 1990s, including the dominant ataxias such as SCAs 1, 2, 3, 6, 7, 10, 12, 17 and DRPLA. The list of neurodegenerative and neuromuscular disorders characterised by unstable repeat expansions has grown to over 40 (553). The disease-causing mechanisms for expanded repeat mutations include protein gain-of-function, protein loss-of-function, toxic RNA gain-of-function, non-ATG-initiated translation (RAN) peptides, and transcriptional dysregulation (554). Non-coding expanded repeat sequences have been implicated in transcriptional dysregulation by altering transcription factor binding (555), and epigenetic alterations (556). RNA mediated-toxicity has emerged as a recurrent toxic-gain-of-function mechanism in the pathogenesis of several other SCAs and neurodegenerative diseases and has been associated with SCA8 (557), SCA10, SCA31 (558), ALS and frontotemporal dementia (559), Huntington’s disease (560), myotonic dystrophy types 1 and 2 (561), fragile X-associated tremor ataxia syndrome (562), Charcot-Marie-Tooth disease type

2D (563), dominant intermediate Charcot-Marie-Tooth disease (564), oculopharyngeal muscular dystrophy (565) and spinal muscular atrophy (566). Short-tandem repeats of various nucleotide motifs are frequently found in transcripts. These sequences might configure into alternative or pathological RNA structures depending on the motif type and number of reiterations playing an important role in RNA processing regulation (567). A myriad of pathogenic mechanisms has been assigned to toxic RNA repeats including aberrant alternative splicing, the inhibition of nuclear transport and export, induction of the innate immune response, alteration of microRNA biogenesis, and abnormal activation of RNA interference. For instance, the non-coding intronic expanded hexanucleotide GGGGCC repeat associated with ALS/FTD is able to alter *C9orf72* RNA processing, in terms of transcription, splicing, and localisation (568).

Herein, we provide evidence that an unstable intronic ATTTC repeat mutation dysregulates *DAB1* expression and induces RNA switch, with a consequent up-regulation of Reelin-DAB1 signalling in the SCA37 cerebellum (485). Furthermore, the identification of seven SCA37 Spanish families originally from the south-west of Spain sharing a common haplotype, together with the seven families identified originally from the south of Portugal (484), strongly suggest a founder effect of the SCA37 mutation. Remarkably, a gender-specific contribution of the ATTTC repeat mutation to the age of onset was observed in males, but not in female patients. In this regard, sexually dimorphic expression of Reelin in the cerebellum was observed in reeler mouse models and a few human neurodegenerative disorders, highlighting the role of sex hormones in the modulation of the Reelin-signalling response (569–572).

A remarkable hallmark feature in the studied SCA37 ataxia patients is the presence of early vertical eye movement alterations, which often precede the ataxia symptoms. Impaired horizontal eye movements are regarded as a well-known clinical sign in several SCAs subtypes including SCA1 (55), SCA2 (573–575), SCA3 (576), SCA4 (261), SCA5 (120), SCA6 (577), SCA7 (139), SCA8 (578), SCA17 (216). These abnormalities may appear even in pre-symptomatic stages, such as in SCA1 (62,69), SCA2 (579), SCA3 (580), SCA6 (577), SCA7 (139), SCA17 (216) and have been considered an endophenotype in few subtypes including SCA1 (581), SCA2 (574), SCA7 (139). However, vertical eye movement abnormalities have rarely been reported, to the best of our knowledge only in SCA6 (577), SCA26 (241), and SCA30 (207), and by the time they appear, clear horizontal axis abnormalities are also found.

The main eye movement findings in our SCA37 patients consisted of abnormal saccade accuracy, especially downwards, with slow optokinetic nystagmus and pursuit, all of them initially found in the vertical axis (281). The observed normal saccade velocity suggests relative sparing of the pons (582), already suspected by the neuroimaging findings in the AT-901 SCA37 family, and later confirmed by our neuropathological investigations. Saccade accuracy is controlled by cerebellar lobules VI and VII of the posterior vermis and their projections through the caudal pole of the fastigial nucleus to the

brain stem saccade-generating system in primates (583). In humans, transcranial magnetic stimulation, functional magnetic resonance imaging, mapping lesions based on magnetic resonance imaging in patients with cerebellar infarctions (584) as well as clinical data from degenerative ataxic disorders (581), confirm the participation of the posterior vermis in the definition of saccades properties, such as accuracy, latency, trajectory, and dynamics. Additionally, the superior colliculus is involved in the generation of saccades by several routes (583). Optokinetic nystagmus and smooth pursuit are mediated, but not exclusively, by the flocculus in primates (584). Among several projections, the climbing fibers input to the flocculus has been well systematised in rabbits and again is mediated by the inferior olive (583). As for pursuit, two parallel cortical-cerebellar-olive loops have been proposed, both include inferior olive structures (583). Consistently, patient IV:10 showed marked neuronal loss in lobule VII and severe gliosis in the flocculus. Remarkably, both siblings revealed prominent neuronal loss and gliosis in the inferior olive. We propose that these anatomical structures and physiological PC behaviour may be involved in the specific clinical disease pattern seen in our patients.

Considerable overlap in the neurodegenerative pattern has been shown in post-mortem neuropathology for the polyglutamine (polyQ) ataxias, in which intranuclear (SCA1, SCA3, SCA7, SCA17, DRPLA) or intracytoplasmic (SCA2, SCA6) ubiquitin-immunostained polyQ inclusions are a common feature (29,98). In SCA12, ubiquitinated nuclear inclusions resembling Marinesco bodies are identified in the cerebellum, striatum, and motor cortex (182). For the remaining non-polyglutamine SCAs, post-mortem neuropathology data is limited to SCA4 (118), SCA10 (165), SCA11 (168), SCA14 (198), SCA19/22 (585), SCA23 (586), SCA28 (253), SCA31 (266,587), SCA36 (588), and SCA48 (589). Remarkably, a typical feature of SCA31 is the presence of an halo-like amorphous material surrounding cerebellar Purkinje cells, which contain small ubiquitin-positive granules consisting of synaptophysin-positive vesicles and a fragmented Golgi apparatus (266). None of these subcellular hallmarks were observed in the SCA37 cerebellum of our patients.

Our data revealed remarkable dysregulation of *DAB1* expression in the SCA37 cerebellum, and because normal *DAB1* expression in the cerebellum is mostly restricted to Purkinje cells, our neuropathological findings are consistent with a main Purkinje cell pathology causative of a pure cerebellar disease. Mouse Dab1 is an adaptor molecule mediating signalling from reelin receptors, which upon binding underpin migration and lamination of neurons in the developing cortex, hippocampus and cerebellum (590,591). In the post-natal cerebellum, reelin signalling triggers the dispersal and positioning of Purkinje cells into their final position in the adult PC monolayer and disposes their dendritic deployment by binding with the PC receptors, very low-density lipoprotein receptor (VLDLR) and apolipoprotein E receptor 2 (APOER2). Upon reelin binding, DAB1 is tyrosine-phosphorylated by SRC tyrosine kinases FYN and SRC thus activating PI3K/AKT, ERK and CRK/CRKL signalling pathways before it is degraded by the ubiquitin-proteasome pathway.

Remarkably, the cerebella in mutant reeler, scrambler and yotari mice, all having loss-of-function mutations in *Reelin* or *Dab1* genes, are anatomically very similar, with lack of foliation and Purkinje cells failing to migrate and largely remaining in several ectopic clusters deep in the cerebellar cortex, while the granule cells appear to migrate normally (592,593). In this regard, our data support that a gain-of-function mutation by upregulation of DAB1 alternate isoforms underlies SCA37 with mislocalisation of Purkinje neurons in the cerebellar cortex reflecting improper positioning and selective migration deficits. DAB1 has been shown to regulate the intracellular trafficking of reelin receptors and intracellular reelin levels after the reelin/receptor complex internalisation (594). The identification of significantly increased uncleaved 410-kDa Reelin protein, which was previously shown to induce DAB1 phosphorylation (487), may be responsible for the cerebellar over-activation of Reelin-DAB1 signalling in SCA37. This in turn would dysregulate Reelin-DAB1 function in the regulation of neuronal migration through the upregulation of PI3K and AKT (595). To address how the *SCA37* mutation dysregulated *DAB1* expression, we used in silico algorithms, which showed that the ATTTC mutation within intron 11 of the *DAB1* gene creates new putative XBP1 transcription factor binding motifs. XBP1 is a transcription factor known to be up-regulated in embryos, down-regulated during adulthood, and activated during aging by the UPR response to ER stress (596), and has been implicated in Purkinje cell degeneration in Spinocerebellar ataxia type 17 (597). Remarkably, DAB1-related pathology studies in *Nova2* null mice identified overexpression of a *Dab1*-isoform containing two evolutionary conserved exons homologues to human exons 20 an 21 in the *DAB1* gene (489). Both exons were responsible for the Purkinje cells migration defects identified in *Nova2* null mice. Therefore, the study demonstrated the role of the RNA-binding protein NOVA2 in regulating *Dab1* RNA switch by alternative splicing to mediate neuronal responsiveness to reelin signalling. Our data showing overexpression of *DAB1-4* transcript containing exons 20 and 21 in the SCA37 cerebellum compared to un-detectable levels in gender- and age-matched control, supports a role for *DAB1* RNA switch slipping away from these 2 coding exons as seen by NOVA2 inhibition. This is supported by in silico predictive algorithms that identified enrichment of the YCAY NOVA motif within the human *DAB1* exons 20 and 21, and the fact that no RNA-sequence reads were identified for exons 20 and 21 in the ENCODE database for normal PC RNA data.

Therefore, binding of active XBP1, up-regulated in the embryo or by the unfolded protein response (UPR) during aging, to the ATTTC repeats mutation in SCA37 may up-regulate *DAB1* expression of specific transcripts containing exons 20 and 21, slipped away from NOVA2 inhibition. We propose that this molecular mechanism possibly underlies the neuronal migration deficits and progressive neurodegeneration of Purkinje cells in the SCA37 cerebellum.

In conclusion, in this study we demonstrated that an intronic ATTTC unstable repeat mutation within the non-coding regulatory region of the *DAB1* gene is the genetic defect causing spinocerebellar ataxia type 37. We reported the first neuropathological post-mortem findings of SCA37, which are

confined to the cerebellum in agreement with a pure cerebellar syndrome. Importantly, our data showed DAB1 overexpression and RNA switch, accompanied by dysregulation of the Reelin-DAB1 and PI3K/AKT signalling pathway as the main mechanism underlying cerebellar neurodegeneration in SCA37.

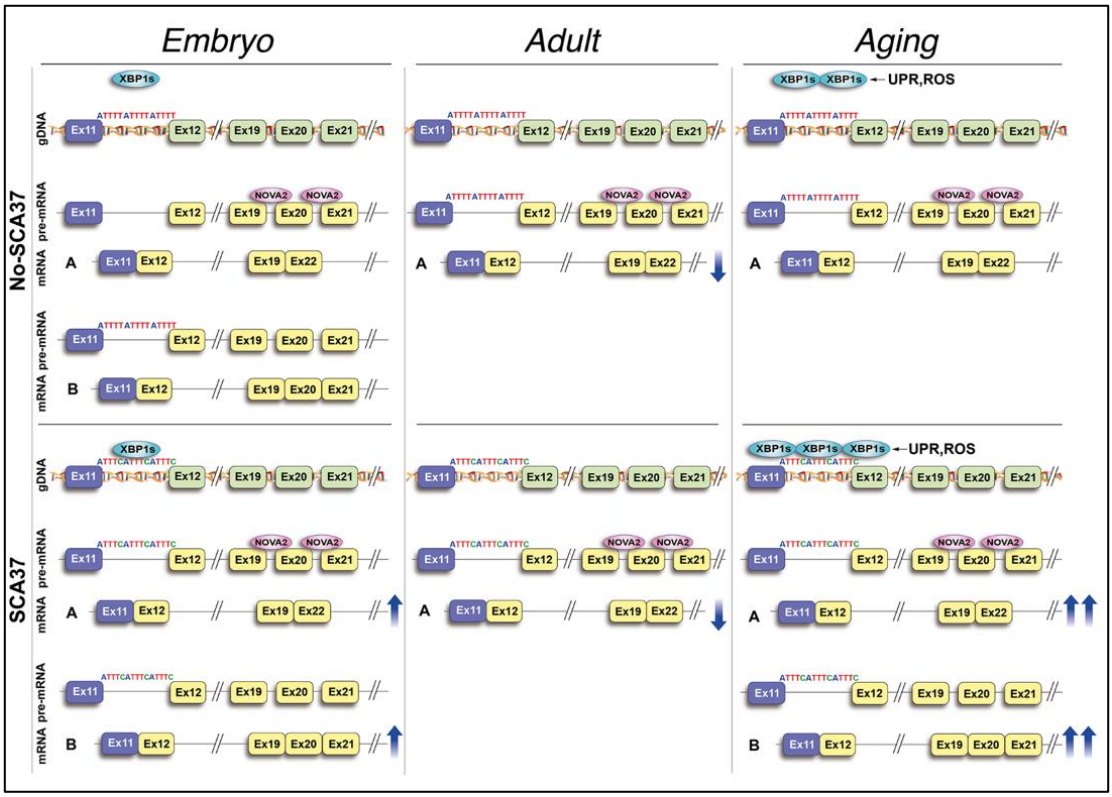


**Figure 44. A proposed model of the mechanism underlying cerebellar DAB1 dysregulation and RNA switch in SCA37.** Active XBP1 transcription factor is known to be up-regulated in the embryo by the unfolded protein response (UPR) to participate in the normal development of the nervous system and neuronal differentiation. In the mouse, Nova2 splices out *Dab1* coding exons 20 and 21 and dysregulation of this splicing event over-represents Dab1-containing exons 20 and 21 transcripts which are associated with neuronal migration defects. Consequently, binding of active XBP1 to the ATTTC repeat mutation in SCA37, but not to the ATTTT in normal chromosomes, up-regulates expression of *DAB1* mRNA transcripts containing exons 20 and 21, slipped away from NOVA2 inhibition, which would cause neuronal migration deficits in the SCA37 cerebellum. Absent UPR in the post-natal cerebellum and thus of XBP1 protein would limit *DAB1* post-natal expression in SCA37. However, aggregation of misfolded proteins by ER stress with aging would activate UPR and thus XBP1 expression and ATTTC-binding, and therefore increasing the number of *DAB1* transcripts leading to cerebellar DAB1 overexpression and RNA switch in the SCA37 cerebellum. Overexpressed ubiquitinated DAB1-containing exons 20 and 21 protein would aggregate in perisomatic inclusions in Purkinje cell bodies due to proteasome overload. Extracted from (485).

***Novel dominantly inherited spinocerebellar ataxia subtype caused by SAMD9L mutation triggering mitochondrial and lysosomal dysregulation and neurological deficits in a zebrafish disease model.***

In the present study, we demonstrate that the c.1877C>T (p.Ser626Leu) mutation within the fifth exon of the gene encoding for the sterile alpha motif domain containing 9 like protein *SAMD9L* as the genetic cause underlying a new spinocerebellar ataxia subtype in a Spanish five-generation family from the Balearic island of Menorca (manuscript under preparation).

We describe the clinical features in seven affected individuals variably presenting with ataxia, nystagmus, dysarthria, polyneuropathy and pyramidal signs and the functional studies in patients' fibroblasts demonstrating for the first time the mitochondrial localisation of human SAMD9L protein and the mitochondrial and lysosomal defects underlying the molecular pathology in this new ataxia subtype.

The phenotype of this new spinocerebellar ataxia subtype is characterised by the presence of vertical and horizontal gaze evoked nystagmus and hyperreflexia, which precede the sensory polyneuropathy and ataxia symptoms. Gaze-evoked nystagmus (GEN) in all directions indicates a cerebellar dysfunction and can have multiple causes in cerebellar ataxias; purely vertical GEN is due to a midbrain lesion, while purely horizontal GEN is due to a pontomedullary lesion (598). GEN is a common feature sign in several SCAs subtype and has been identified in SCA1 (72), SCA3/MJD (599), SCA5 (120), SCA6 (600), SCA10 (601), SCA11 (168), SCA13 (189), SCA14 (188), SCA15/16 (204), SCA18 (222), SCA19/22 (225), SCA20 (232), rarely in SCA23 (236), SCA25 (240), SCA27 (243), SCA28 (250), SCA31 (261), frequently in SCA36 (in 30% of the cases) (277), SCA38 (282) and SCA42 (only horizontal) (290). However, nystagmus has rarely been described as an early ocular alteration, to the best of our knowledge only in SCA3/MJD (580) and SCA6 (577).

Hyperreflexia refers to hyperactive or repeating (clonic) reflexes. These neurological signs are usually indicative of an interruption of corticospinal and other descending pathways that influence the reflex arc due to a suprasegmental lesion, that is, a lesion above the level of the spinal reflex (602). Hyperreflexia has also been described as a prominent sign in several SCAs subtypes including SCA1 (603), SCA2 (16%), SCA3 (604), SCA6 (50%) (600), SCA7 (605), SCA8 (606), SCA10 (7,5%) (604), SCA11 (170), SCA12 (177), SCA13 (occasionally) (607), SCA14 (608), SCA15/16 (609), SCA17 (610), SCA19/22 (in 3 patients) (227), rarely in SCA23 (in 4/13 patients) (237), SCA28 (250), SCA30 (258), sometimes in SCA34 (269), SCA35 (272), SCA36 (276), SCA40 (286) and SCA42 (290).

Abnormalities in sensory nerve conduction have been previously described in different types of SCA. In SCA1, there has been reported reduced or absent sensory nerve action potential (SNAP) amplitude with or without reduced NCVs; in SCA2, reduced or absent SNAP amplitude with reduced NCVs; in

SCA4 and SCA25, absent SNAPs; and in SCA3, SCA8, SCA12 and SCA17, reduced SNAP amplitudes (50). Sympathetic skin responses dysfunction has been previously reported only in SCA2 (611) and SCA3 (612). Thus, SSR alterations correlate closely with disease functional stage as it seems that occurs in M-SCA patients where only older patients presented with altered sympathetic skin responses. Relevantly, none of them presented comorbidities that could interfere in the result of autonomic nervous system tests as diabetes mellitus. Interestingly, González-Salazar and collaborators recently reported that SPG4 patients with mutations in *SPAST* gene present also sudomotor dysfunction (613). SPG4 could also present with hyperreflexia and pyramidal signs, with some patients also manifesting cerebellar ataxia (614). Spastin protein has been associated with microtubules and lysosomal trafficking (615), and it contains an AAA-ATPase domain predicted to be significant similar with SAMD9L protein region as demonstrated in this study.

Accordingly, SCA1, SCA3, SCA6, SCA11, SCA14, SCA15/16 and SCA28 should all be considered in the differential clinical diagnosis, but if the MRI data reveals early brain demyelinating lesions this novel spinocerebellar ataxia subtype with *SAMD9L* mutations should be first evaluated. Besides brain demyelinating lesions, GEN and hyperrefelxia appeared early at the presymtomatic stages preceding ataxia symptoms in the novel SCA subtype.

Herein, we provide evidence that the missense mutation c.1877C>T (p.Ser626Leu) within the fifth exon of the *SAMD9L* gene decreased SAMD9L protein levels along with increased ATP5H, DRP1 and LAMP1 proteins evidencing mitochondrial and lysosomal/endosomal deficits in patients' fibroblasts. Furthermore, we describe for the first time the mitochondrial localisation of human SAMD9L.

It is important to note a myriad of intra- and inter-familiar pleiotropic effects associated with mutations within the *SAMD9L* gene or its paralogue *SAMD9*, both genes localising side-by-side on chromosome 7q21 (616). Germline frameshift *SAMD9L* mutations were described in children presenting with inflammation of subcutaneous fat (617), and missense gain-of-function mutations in *SAMD9L* in ataxia-pancytopenia syndrome (ATXPC), characterised by a progressive neurological phenotype, pancytopenia and hypocellular bone marrow (618,619). Based on the evidence that Samd9l-deficient mice develop myeloid disease resembling that of human myelodysplastic syndrome (MDS) caused by monosomy 7, it was proposed a functional role of *SAMD9L* as a tumour suppressor gene (491,620). On the other hand, heterozygous missense mutations within *SAMD9* have been associated with MIRAGE syndrome, a severe early-onset condition characterised by myelodysplasia, infections, restricted growth, adrenal hypoplasia, genital phenotypes, and enteropathy (621). All these clinical conditions have a unifying phenotype of early onset myelodysplasia with monosomy 7 mainly described in paediatric cohorts with MDS and often without syndromic manifestation (622,623).

While the penetrance of *SAMD9L* mutations in haematological disease is reduced (estimated 70%) (628), their contribution to the neurological phenotypes is much lower and their pathogenicity remains unknown (622).

To date, 26 gain-of-function mutations have been identified within *SAMD9L* mostly associated with haematological malignancies such as cytopenias or MDS in the presence of uniparental monosomy of chromosome 7 or partial haploinsufficiency del(7q) (617,619,622–625). Since previously reported, germline *SAMD9L* mutations showed decreased variant allele frequency (VAF) (616). In the present study no differences between wild-type and mutant allele NGS reads of *SAMD9L* were found in DNAs obtained from blood samples from our patients of the Menorca family, thus ruling out *SAMD9L* partial or total haploinsufficiency in patients' haematological lineages. This may explain why no clinical history of haematological findings were identified in the five-generation M-SCA family.

Monosomy 7, a high-risk lesion of haematological malignancy with clonal evolution, was observed as a recurrent complication in *SAMD9L*-related MDS, and has been shown in the presence of somatic driver mutations within *SETBP1*, *ASXL1*, *RUNX1*, *PTPN11*, *KRAS*, *CBL*, *EZH2*, *ETV6*, *BRAF*, or *RAD21* genes (623). It seems plausible that for a patient to develop MDS, *SAMD9L* mutations need to occur in addition to at least one previous genetic event such as monosomy 7, partial or total del(7q) haploinsufficiency, or mutations in those driver genes. None of these three scenarios were demonstrated in our patients.

Most missense mutations within *SAMD9L* identified to date locate in the C-terminal region of the protein and were shown to inhibit cell growth (626). In contrast, the p.Ser626Leu identified in this study localises closer to the N-terminal region of SAMD9L, and transformed SHSY-5Y cells with the mutant allele did not trigger any cell cycle arrest or altered cell growth. This evidence along with the absence of partial 7q haploinsufficiency and no mutations in those driver genes, and the location of the mutation in the amino terminal region of SAMD9L protein may explain the lack of haematological malignancies in M-SCA carriers.

Hence, the genetic and genomic studies together with the pathogenic predictors and functional data resulted from this thesis, supports the c.1877C>T (p.Ser626Leu) variant within *SAMD9L* as the causative mutation of this novel ataxia subtype (pending of assignment by the Human Genome International Nomenclature Committee). SAMD9L protein levels were found decreased in patients' fibroblasts carrying the mutation. Moreover, c.1877C>T (p.Ser626Leu) mutation localises to a protein intrinsically disorder region (IDR) predicted by three different algorithms. IDRs are polypeptide segments that do not contain sufficient hydrophobic amino acids to mediate co-operative folding. Instead, they typically contain a higher proportion of polar or charged amino acids (627). Interestingly, previous studies demonstrated that mutations within IDRs regions cause diseases by creating dileucine motifs and affecting protein interaction including mutations in the *ITPR1* gene

associated with SCA15/29 (628). Remarkably, the c.1877C>T mutation triggers a serine (hydrophobic and polar) to leucine (hydrophilic and non-polar), changing amino acid properties at the 626 amino acid position. Moreover, phosphorylation predictors identified this Ser626 as a candidate target for PKC kinase, of which some isoforms have shown mitochondrial localisation (629) and some of them interacting with DRP1 (630). Remarkably, mutations in the PKC gamma gene (*PRKCG*) have been associated with SCA14.

Our data demonstrate for the first time the subcellular localisation of human SAMD9L protein to cerebellar Purkinje cells and to mitochondria in human fibroblasts. Likewise, the analysis of ENCODE RNA data from different cells types corroborates the expression of *SAMD9L* mainly in Purkinje cells, cerebellar and spinal cord tissues in consonance with the neuropathological systems affected in the pathogenesis of this new ataxia subtype. To address how the c.1877C>T (p.Ser626Leu) *SAMD9L* mutation could trigger mitochondrial dysregulation, we used in silico algorithm which showed that the 626Ser in SAMD9L protein locates in a predicted microtubule binding motif which is highly conserved along primate species and absent in the hSAMD9 protein paralog. Remarkably, homology and structural predictor identified significant similarity of SAMD9L protein region with AAA ATPase domains from spastin, VPS4B (also known as SKD1), katanin and torsin-1A, which are all associated with microtubules or involved in lysosomal trafficking. Katanin and spastin are both microtubule-severing proteins which transduce the energy from ATP hydrolysis into mechanical force. Relevantly, mutations within the *SPAST* gene have been previously associated with autosomal dominant spastic paraplegia type 4 (SPG4) (631) presenting with hyperreflexia and pyramidal signs, with some patients also manifesting cerebellar ataxia (614). Furthermore, mutant spastin has been demonstrated to disrupt lysosomal function (632) and to alter interaction with microtubules entailing to abnormal cellular distribution of mitochondria, suggesting organelle transport alteration on the microtubule cytoskeleton, including transport to distal axons (633). Even though to date no mutations in katanin subunits have been associated with neurodegenerative diseases, its experimental suppression on cultured neurons affected axonal growth and branching (634). In contrast, VPS4B protein belongs to the AAA protein family involved in lysosomal/endosomal membrane trafficking, regulating the maturation of autophagosomes to degradative autolysosomes, where the small GTP binding protein Rab7 is also implicated (635,636). Rab7 belongs to Rab GTPases proteins which are key regulators of multivesicular body maturation from early endosomes, as well as the fusion of multivesicular bodies with lysosomes being required to mediate lysosomal degradation in all cells (637,638). Interestingly another Rab GTPase, Rab5, mediates the signalling for endosome internalization entailing neurite outgrowth and dendritic branching (639) and undergo Rab5-to-Rab7 conversion (640) triggering Rab7-associated vesicles undergo retrograde transport to the cell body to modulate gene expression in the nucleus to promote

survival and maintenance (638). Furthermore, Rab5 regulates endosomes motility by stimulating their stable association with microtubules (641). Relevantly, colocalisation of Rab5 and Samd9l has been found in mouse lung fibroblasts and in mouse KL cells partially (491). Rab GTPases and associated membrane trafficking processes have been implicated in different neurodegenerative diseases as Charcot–Marie–Tooth, amyotrophic lateral sclerosis, Alzheimer's disease, Parkinson's disease and Huntington's disease (638) and a few studies described lysosome dysfunction in the pathogenesis of spinocerebellar ataxias including Machado-Joseph disease (642), SCA6 (643), SCA7 (644) and SCA21 (645). To date, only mutations in the *AFG3L2* coding for mitochondrial protein ATP-dependent metalloprotease have been directly associated with a dominantly inherited ataxia, the spinocerebellar ataxia subtype 28 (SCA28) (251), despite that mitochondrial dysfunction has been described as a common feature in SCA1, SCA2, SCA3, SCA7, SCA10 and SCA12 (36,81,646–649).

To assess the molecular implication of SAMD9L on locomotion and neurosensory functions, we generated a novel zebrafish disease model overexpressing human wild-type and mutated *SAMD9L* mRNAs. Noteworthy is the complexity of the zebrafish genome revealing four different candidate *SAMD9L* orthologs. This prevented us from the generation of a stable expression model by CRISPR-Cas genome edition. Therefore, to confirm the molecular implication of SAMD9L on locomotion activity and neurosensory pathways, and to evaluate the biological effects of the p.Ser626Leu mutation in *SAMD9L*, we expressed human wild-type and mutated *SAMD9L* mRNAs in zebrafish embryos. The mean distance travelled by embryos injected with wild-type *SAMD9L* was significantly longer compared to the control, consistent with a specific effect on locomotion activity. The significant shorter distance covered by embryos injected with the mutated mRNA compared to the wild-type group denoted a partial loss-of-function or haploinsufficiency created by the mutation. Partial loss-of-function mechanism alone or coexisting with gain of function effects by mutated allele contributes to disease pathogenesis in several dominant ataxia forms such as SCA1, which presents with a similar phenotype to that of our kindred (28,31,650,651) and has been reported in neurodegenerative zebrafish models of neurodegeneration (652–654). Furthermore, significant increased head turns were observed in wild-type SAMD9L and decreased in mutated SAMD9L groups, indicative of vestibular and/or sensory impairment, both neurological signs identified in our affected patients of the M-SCA family. Vestibular circuit development is characterised by a critical period for sensory signalling controlling head turns and sensory inputs from the vestibular organ and visual information that are processed in different parts of the brain to maintain balance (655,656). Mauthner cells (M-cells) are reticulospinal neuron cells in the teleost hindbrain involved in the inhibitory network and controls fast turning movements and form synaptic contact with trunk motor neurons (657–659). Furthermore, single and multi-cell input reaches the supra-spinal circuits for sensory perception, regulating turning strength,

considering reticular networks in brainstem as potential regulatory candidates since they incorporate ascending and descending connections to the spinal cord, modulating spinal reflexes (660). Remarkably, weak directional tunning signals were observed in the cerebellum of 5-7 dpf zebrafish embryos (661). Thus, considering that the turning response of zebrafish larvae is regulated according to their sensory receptive position (662), we could determine sensory deficits in overexpressed mutated *SAMD9L* zebrafish embryos.

In conclusion, in this study we demonstrate the c.1877C>T (p.Ser626Leu) mutation within the fifth exon of the gene encoding for the sterile alpha motif domain containing 9 like protein *SAMD9L* as the genetic defect causing a novel ataxia subtype. Based on the evidence provided, we propose SAMD9L as a protein potentially involved in mitochondrial and lysosome/endosome vesicle transport underlying the neuronal deficits and progressive neurodegeneration in this new SCA subtype (pending of assignation by the HUGO Gene nomenclature Committee).

We further describe the clinical phenotype which remarkably presents with vertical and horizontal nystagmus (GEN) and we identify vertical and horizontal nystagmus (GEN) and hyperreflexia as early clinical alterations before ataxia develops. We report for the first time the sub-cellular localisation of human SAMD9L in Purkinje and fibroblasts cells, we demonstrate mitochondria and lysosome dysregulation in patients' fibroblasts, and finally we provide evidence for SAMD9L involvement in motor and sensory functions.

# CONCLUSIONS

1. This study demonstrates the high clinical and genetic heterogeneity of dominant ataxias and reveals the extensive clinical overlap with a wide range of neurological disorders with the identification of causative genes previously not associated with primary ataxia.

   By using a comprehensive approach involving thorough clinical phenotype evaluation, expanded repeats detection and personalized next-generation sequencing, the underlying genetic cause could be identified in 26.6% of our ataxia cohort.

2. A total of 61 causative mutations were identified: 45 novel (35 missense, 1 deletion, 4 frameshift, 2 nonsense, 2 splicing mutations and 1 expanded pentanucleotide insertion), and 16 previously reported (9 missense, 3 frameshift and 4 repeat expansions).

3. A novel spinocerebellar ataxia subtype, SCA37 was identified and characterised. Furthermore, the molecular causative defect was identified and consists of an ATTTC unstable insertion within the 5'UTR non-coding region of the *DAB1* gene as the genetic cause of the SCA37 phenotype in seven ataxia families from the Andalusia region of Huelva in the South of Spain, indicative of a mutation founder effect.

4. A significant inverse correlation between the ATTTC repeat insertion size and the age of onset in SCA37 was identified in males, but not in females.

   Neuropathological hallmarks were identified for the first time in SCA37, which consist of ubiquitin and DAB1 immunostained distinctive perisomatic granules in Purkinje cell bodies of the SCA37 cerebellum.

5. DAB1 immunostaining was shown increased in the SCA37 cerebellum.

6. Reelin-DAB1 signalling (reelin, DAB1, PI3K-p85, AKT and AKT phosphorylation) involved in neuronal migration was shown dysregulated in SCA37.

7. Six novel RNA transcripts from the *DAB1* gene, with one of them containing exons 20 and 21, were found overexpressed in the SCA37 cerebellar cortex. Overexpression of these two alternative coding exons, evolutionarily conserved in the mouse *Dab1* gene, was previously implicated in migration deficits of Purkinje cells.

8. The ATTTC mutation creates a few new binding motifs for the XBP1 transcription factor associated with the unfolded protein response (UPR) in support of a gain-of-function mechanism of neurodegeneration in SCA37.

9. A novel autosomal dominant spinocerebellar ataxia (SCA) subtype was identified. It is clinically characterised by progressive late-onset ataxia with sensory polyneuropathy, preceded by

cerebellar atrophy, vertical and horizontal gaze-evoked nystagmus, and hyperreflexia. A distinctive clinical feature is the presence of cerebral demyelination.

10. Herein, we identify a c.1877C>T (p.Ser626Leu) missense mutation within the fifth exon of the *SAMD9L* gene encoding the sterile alpha motif domain containing 9 like protein as the causative genetic defect in this novel ataxia subtype.

11. The *SAMD9L* mutation is highly conserved, segregates with the disease in a five-generation Spanish kindred, is predicted as deleterious by in silico algorithms, abolishes a predicted disease-causing intrinsically disordered region (IDR) and is included in the S....LKS signature motif of microtubule binding domains.

12. SAMD9L contains an ATPase/Hydrolase structural predicted domain significantly similar with SPAST, SKD1 and katanin proteins involved in microtubule severing, mitochondrial transport, and endosomal-lysosomal trafficking.

13. SAMD9L localises to mitochondria in Purkinje cells in the human cerebellar cortex and multipolar neurons of the human dentate nucleus, while its protein levels are significantly decreased in patients' fibroblasts leading to an increase of mitochondrial DNA replication and bioenergetics together with dysregulation of the endosomal-lysosomal pathway.

14. Using Zebrafish embryos overexpressing human wild-type and mutated *SAMD9L* we demonstrate its involvement in motor and sensory functions, pointing to a loss of function or haploinsufficiency triggered by p.Ser626Leu mutation in the molecular pathogenesis of the disease.

In conclusion, this study provides relevant clinical, genetic and physiopathological insights into the spinocerebellar ataxias. Implementation of NGS and a novel R-based algorithm confirmed the elevated heterogeneity of dominant ataxias, enabled diagnosis of 26.6% ataxia cases and the identification of 45 novel DNA variants (35 missense, 1 deletion, 4 frameshift, 2 nonsense, 2 splicing mutations and 1 expanded pentanucleotide insertion). Furthermore, two novel spinocerebellar ataxias subtypes, SCA37 and M-SCA (pending of assignment), were identified and characterised, and their underlying genetic and molecular physiopathological mechanisms elucidated, deciphering new molecular and cellular potential targets for treatment.

# REFERENCES

1. Matilla-Dueñas A, Goold R, Giunti P. Molecular pathogenesis of spinocerebellar ataxias. *Brain*, 129, 1357–1370 (2006).

2. Matilla-Dueñas A, Corral-Juan M, Rodríguez-Palmero Seuma A, et al. Rare Neurodegenerative Diseases: Clinical and Genetic Update. *Adv Exp Med Biol*, 1031, 443–496 (2017).

3. Corral-Juan M, Corral J, San Nicolás H, et al. Genetics of the Autosomal Dominant Spinocerebellar Ataxias. *eLS, John Wiley & Sons, Ltd*, Chichester, UK (2011).

4. Matilla-Dueñas A. The Ever Expanding Spinocerebellar Ataxias. Editorial. *The Cerebellum*, 11, 821–827 (2012).

5. Harding AE. The clinical features and classification of the late onset autosomal dominant cerebellar ataxias. *Brain*, 105, 1–28 (1982).

6. Jacobi H, Rakowicz M, Rola R, et al. Inventory of Non-Ataxia Signs (INAS): Validation of a New Clinical Assessment Instrument. *The Cerebellum*, 12, 418–428 (2013).

7. Schmitz-Hubsch T, du Montcel ST, Baliko L, et al. Scale for the assessment and rating of ataxia: Development of a new clinical scale. *Neurology*, 66, 1717–1720 (2006).

8. Orr HT, Chung M, Banfi S, et al. Expansion of an unstable trinucleotide CAG repeat in spinocerebellar ataxia type 1. *Nat Genet*, 4, 221–226 (1993).

9. Sequeiros J, Martindale J, Seneca S. EMQN Best Practice Guidelines for molecular genetic testing of SCAs. *Eur J Hum Genet*, 18, 1173–1176 (2010).

10. Klockgether T, Mariotti C, Paulson HL. Spinocerebellar ataxia. *Nat Rev Dis Prim*, 5, 24 (2019).

11. Ruano L, Melo C, Silva MC, et al. The Global Epidemiology of Hereditary Ataxia and Spastic Paraplegia: A Systematic Review of Prevalence Studies. *Neuroepidemiology*, 42, 174–183 (2014).

12. Klockgether T. Update on degenerative ataxias. *Curr Opin Neurol*, 24, 339–345 (2011).

13. Hersheson J, Haworth A, Houlden H. The inherited ataxias: Genetic heterogeneity, mutation databases, and future directions in research and clinical diagnostics. *Hum Mutat*, 33, 1324–1332 (2012).

14. Krysa W, Sulek A, Rakowicz M, et al. High relative frequency of SCA1 in Poland reflecting a potential founder effect. *Neurol Sci*, 37, 1319–1325 (2016).

15. Storey E, du Sart D, Shaw JH, et al. Frequency of spinocerebellar ataxia types 1, 2, 3, 6, and 7 in Australian patients with spinocerebellar ataxia. *Am J Med Genet*, 95, 351–358 (2000).

16. Velázquez-Pérez L, Medrano-Montero J, Rodríguez-Labrada R, et al. Hereditary Ataxias in Cuba: A Nationwide Epidemiological and Clinical Study in 1001 Patients. *The Cerebellum*, 19, 252–264 (2020).

17. Teive HAG, Meira AT, Camargo CHF, et al. The Geographic Diversity of Spinocerebellar Ataxias (SCAs) in the Americas: A Systematic Review. *Mov Disord Clin Pract*, 6, 531–540 (2019).

18. Gheno TC, Furtado G V., Saute JAM, et al. Spinocerebellar ataxia type 10: common haplotype and

disease progression rate in Peru and Brazil. *Eur J Neurol*, 24, 892-e36 (2017).

19. Lieto M, Riso V, Galatolo D, et al. The complex phenotype of spinocerebellar ataxia type 48 in eight unrelated Italian families. *Eur J Neurol*, 27, 498–505 (2020).

20. Scott SS de O, Pedroso JL, Barsottini OGP, et al. Natural history and epidemiology of the spinocerebellar ataxias: Insights from the first description to nowadays. *J Neurol Sci*, 417, 117082 (2020).

21. de Castilhos RM, Furtado GV, Gheno TC, et al. Spinocerebellar Ataxias in Brazil—Frequencies and Modulating Effects of Related Genes. *The Cerebellum*, 13, 17–28 (2014).

22. Sullivan R, Yau WY, O'Connor E, et al. Spinocerebellar ataxia: an update. *J Neurol*, 266, 533–544 (2019).

23. Paradisi I, Ikonomu V, Arias S. Spinocerebellar ataxias in Venezuela: genetic epidemiology and their most likely ethnic descent. *J Hum Genet*, 61, 215–222 (2016).

24. Jonasson J, Juvonen V, Sistonen P, et al. Evidence for a common Spinocerebellar ataxia type 7 (SCA7) founder mutation in Scandinavia. *Eur J Hum Genet*, 8, 918–922 (2000).

25. Infante J, Combarros O, Volpini V, et al. Autosomal dominant cerebellar ataxias in Spain: Molecular and clinical correlations, prevalence estimation and survival analysis. *Acta Neurol Scand*, 111, 391–399 (2005).

26. García-Murias M, Quintáns B, Arias M, et al. 'Costa da Morte' ataxia is spinocerebellar ataxia 36: clinical and genetic characterization. *Brain*, 135, 1423–1435 (2012).

27. Roux T, Barbier M, Papin M, et al. Clinical, neuropathological, and genetic characterization of STUB1 variants in cerebellar ataxias: a frequent cause of predominant cognitive impairment. *Genet Med*, 22, 1851–1862 (2020).

28. Matilla-Dueñas A, Ashizawa T, Brice A, et al. Consensus Paper: Pathological Mechanisms Underlying Neurodegeneration in Spinocerebellar Ataxias. *The Cerebellum*, 13, 269–302 (2014).

29. Seidel K, Siswanto S, Brunt ERP, et al. Brain pathology of spinocerebellar ataxias. *Acta Neuropathol*, 124, 1–21 (2012).

30. Watson LM, Bamber E, Schnekenberg RP, et al. Dominant Mutations in GRM1 Cause Spinocerebellar Ataxia Type 44. *Am J Hum Genet*, 101, 451–458 (2017).

31. Tulli S, Del Bondio A, Baderna V, et al. Pathogenic variants in the AFG3L2 proteolytic domain cause SCA28 through haploinsufficiency and proteostatic stress-driven OMA1 activation. *J Med Genet*, 56, 499–511 (2019).

32. Matilla A, Koshy BT, Cummings CJ, et al. The cerebellar leucine-rich acidic nuclear protein interacts with ataxin-1. *Nature*, 389, 974–978 (1997).

33. Shimohata T, Nakajima T, Yamada M, et al. Expanded polyglutamine stretches interact with TAFII130, interfering with CREB-dependent transcription. *Nat Genet*, 26, 29–36 (2000).

34. Kouzarides T. Acetylation: a regulatory modification to rival phosphorylation? *EMBO J*, 19, 1176–1179 (2000).

35. Chen I-C, Lin H-Y, Lee G-C, et al. Spinocerebellar ataxia type 8 larger triplet expansion alters histone modification and induces RNA foci. *BMC Mol Biol*, 10, 9 (2009).

36. White MC, Gao R, Xu W, et al. Inactivation of hnRNP K by Expanded Intronic AUUCU Repeat Induces Apoptosis Via Translocation of PKCδ to Mitochondria in Spinocerebellar Ataxia 10. *PLoS Genet*, 6, e1000984 (2010).

37. Sato N, Amino T, Kobayashi K, et al. Spinocerebellar Ataxia Type 31 Is Associated with "Inserted" Penta-Nucleotide Repeats Containing (TGGAA)n. *Am J Hum Genet*, 85, 544–557 (2009).

38. Clark HB, Burright EN, Yunis WS, et al. Purkinje Cell Expression of a Mutant Allele of SCA1 in Transgenic Mice Leads to Disparate Effects on Motor Behaviors, Followed by a Progressive Cerebellar Dysfunction and Histological Alterations. *J Neurosci*, 17, 7385–7395 (1997).

39. Perkins EM, Clarkson YL, Sabatier N, et al. Loss of -III Spectrin Leads to Purkinje Cell Dysfunction Recapitulating the Behavior and Neuropathology of Spinocerebellar Ataxia Type 5 in Humans. *J Neurosci*, 30, 4857–4867 (2010).

40. Lin X, Antalffy B, Kang D, et al. Polyglutamine expansion down-regulates specific neuronal genes before pathologic changes in SCA1. *Nat Neurosci*, 3, 157–163 (2000).

41. Liu J, Tang T-S, Tu H, et al. Deranged Calcium Signaling and Neurodegeneration in Spinocerebellar Ataxia Type 2. *J Neurosci*, 29, 9148–9162 (2009).

42. Matilla-Dueñas A, Sánchez I, Corral-Juan M, et al. Cellular and Molecular Pathways Triggering Neurodegeneration in the Spinocerebellar Ataxias. *The Cerebellum*, 9, 148–166 (2010).

43. Wang H-L, Yeh T-H, Chou A-H, et al. Polyglutamine-expanded ataxin-7 activates mitochondrial apoptotic pathway of cerebellar neurons by upregulating Bax and downregulating Bcl-xL. *Cell Signal*, 18, 541–552 (2006).

44. Chou A-H, Yeh T-H, Kuo Y-L, et al. Polyglutamine-expanded ataxin-3 activates mitochondrial apoptotic pathway by upregulating Bax and downregulating Bcl-xL. *Neurobiol Dis*, 21, 333–345 (2006).

45. Maltecca F, Magnoni R, Cerri F, et al. Haploinsufficiency of AFG3L2, the Gene Responsible for Spinocerebellar Ataxia Type 28, Causes Mitochondria-Mediated Purkinje Cell Dark Degeneration. *J Neurosci*, 29, 9244–9254 (2009).

46. Chen H-K, Fernandez-Funez P, Acevedo SF, et al. Interaction of Akt-Phosphorylated Ataxin-1 with 14-3-3 Mediates Neurodegeneration in Spinocerebellar Ataxia Type 1. *Cell*, 113, 457–468 (2003).

47. Albrecht M, Golatta M, Wüllner U, et al. Structural and functional analysis of ataxin-2 and ataxin-3. *Eur J Biochem*, 271, 3155–3170 (2004).

48. Ikeda Y, Dick KA, Weatherspoon MR, et al. Spectrin mutations cause spinocerebellar ataxia type 5. *Nat Genet*, 38, 184–190 (2006).

49. Orr HT, Zoghbi HY. Trinucleotide Repeat Disorders. *Annu Rev Neurosci*, 30, 575–621 (2007).

50. Liang L, Chen T, Wu Y. The electrophysiology of spinocerebellar ataxias. *Neurophysiol Clin Neurophysiol*, 46, 27–34 (2016).

51. Yadav R, Pal PK, Krishna N, et al. Electrophysiological evaluation of spinocerebellar ataxias 1, 2 and 3. *J Neurol Sci*, 312, 142–145 (2012).

52. Schöls L, Rieß O, Schöls S, et al. Spinocerebellar ataxia type 1: clinical and neurophysiological characteristics in German kindreds. *Acta Neurol Scand*, 92, 478–485 (2009).

53. Abele M. Autosomal dominant cerebellar ataxia type I. Nerve conduction and evoked potential studies in families with SCA1, SCA2 and SCA3. *Brain*, 120, 2141–2148 (1997).

54. Alexandre MF, Rivaud-Péchoux S, Challe G, et al. Functional Consequences of Oculomotor Disorders in Hereditary Cerebellar Ataxias. *The Cerebellum*, 12, 396–405 (2013).

55. Klostermann W, Zühlke C, Heide W, et al. Slow saccades and other eye movement disorders in spinocerebellar atrophy type 1. *J Neurol*, 244, 105–111 (1997).

56. Kim JS, Kim JS, Youn J, et al. Ocular motor characteristics of different subtypes of spinocerebellar ataxia: Distinguishing features. *Mov Disord*, 28, 1271–1277 (2013).

57. Manto MU. Cerebellar Disorders: A Practical Approach to Diagnosis and Management. *Cambridge Univ Press*, 1–299 (2010).

58. Goel G, Pal PK, Ravishankar S, et al. Gray matter volume deficits in spinocerebellar ataxia: An optimized voxel based morphometric study. *Parkinsonism Relat Disord*, 17, 521–527 (2011).

59. Martins CR, Martinez ARM, de Rezende TJR, et al. Spinal Cord Damage in Spinocerebellar Ataxia Type 1. *The Cerebellum*, 16, 792–796 (2017).

60. Zoghbi HY, Jodice C, Sandkuijl LA, et al. The gene for autosomal dominant spinocerebellar ataxia (SCA1) maps telomeric to the HLA complex and is closely linked to the D6S89 locus in three large kindreds. *Am J Hum Genet*, 49, 23–30 (1991).

61. Zoghbi HY, Orr HT. Pathogenic Mechanisms of a Polyglutamine-mediated Neurodegenerative Disease, Spinocerebellar Ataxia Type 1. *J Biol Chem*, 284, 7425–7429 (2009).

62. Matilla T, Volpinl V, Genis D, et al. Presymptomatic analysis of spinocerebellar ataxia type 1 (SCA1) via the expansion of the SCA1 CAG-repeat in a large pedigree displaying anticipation and parental male bias. *Hum Mol Genet*, 2, 2123–2128 (1993).

63. Pearson CE, Eichler EE, Lorenzetti D, et al. Interruptions in the Triplet Repeats of SCA1 and FRAXA Reduce the Propensity and Complexity of Slipped Strand DNA (S-DNA) Formation. *Biochemistry*, 37, 2701–2708 (1998).

64. Zühlke C, Dalski A, Hellenbroich Y, et al. Spinocerebellar ataxia type 1 (SCA1): Phenotype-genotype correlation studies in intermediate alleles. *Eur J Hum Genet*, 10, 204–209 (2002).

65. Goldfarb LG, Vasconcelos O, Platonov FA, et al. Unstable triplet repeat and phenotypic variability of spinocerebellar ataxia type 1. *Ann Neurol*, 39, 500–506 (1996).

66. Buijsen RAM, Toonen LJA, Gardiner SL, et al. Genetics, Mechanisms, and Therapeutic Progress in Polyglutamine Spinocerebellar Ataxias. *Neurotherapeutics*, 16, 263–286 (2019).

67. Schöls L, Bauer P, Schmidt T, et al. Autosomal dominant cerebellar ataxias: clinical features, genetics, and pathogenesis. *Lancet Neurol*, 3, 291–304 (2004).

68. Rüb U, Bürk K, Timmann D, et al. Spinocerebellar ataxia type 1 (SCA1): new pathoanatomical and clinico-pathological insights. *Neuropathol Appl Neurobiol*, 38, 665–680 (2012).

69. Genis D, Matilla T, Volpini V, et al. Clinical, neuropathologic, and genetic studies of a large spinocerebellar ataxia type 1 (SCA1) kindred. *Neurology*, 45, 24–30 (1995).

70. Servadio A, Koshy B, Armstrong D, et al. Expression analysis of the ataxin–1 protein in tissues from normal and spinocerebellar ataxia type 1 individuals. *Nat Genet*, 10, 94–98 (1995).

71. Banfi S, Servadio A, Chung M, et al. Identification and characterization of the gene causing type 1 spinocerebellar ataxia. *Nat Genet*, 7, 513–520 (1994).

72. Matilla-Dueñas A, Goold R, Giunti P. Clinical, genetic, molecular, and pathophysiological insights into spinocerebellar ataxia type 1. *The Cerebellum*, 7, 106–114 (2008).

73. Koshy B. Spinocerebellar ataxia type-1 and spinobulbar muscular atrophy gene products interact with glyceraldehyde-3-phosphate dehydrogenase. *Hum Mol Genet*, 5, 1311–1318 (1996).

74. Lim J, Crespo-Barreto J, Jafar-Nejad P, et al. Opposing effects of polyglutamine expansion on native protein complexes contribute to SCA1. *Nature*, 452, 713–718 (2008).

75. Burright EN, Brent Clark H, Servadio A, et al. SCA1 transgenic mice: A model for neurodegeneration caused by an expanded CAG trinucleotide repeat. *Cell*, 82, 937–948 (1995).

76. Rousseaux MWC, Tschumperlin T, Lu H-C, et al. ATXN1-CIC Complex Is the Primary Driver of Cerebellar Pathology in Spinocerebellar Ataxia Type 1 through a Gain-of-Function Mechanism. *Neuron*, 97, 1235-1243.e5 (2018).

77. Matilla A, Roberson ED, Banfi S, et al. Mice Lacking Ataxin-1 Display Learning Deficits and Decreased Hippocampal Paired-Pulse Facilitation. *J Neurosci*, 18, 5508–5516 (1998).

78. Duvick L, Barnes J, Ebner B, et al. SCA1-like Disease in Mice Expressing Wild-Type Ataxin-1 with a

Serine to Aspartic Acid Replacement at Residue 776. *Neuron*, 67, 929–935 (2010).

79. Pérez Ortiz JM, Mollema N, Toker N, et al. Reduction of protein kinase A-mediated phosphorylation of ATXN1-S776 in Purkinje cells delays onset of Ataxia in a SCA1 mouse model. *Neurobiol Dis*, 116, 93–105 (2018).

80. Sánchez I, Piñol P, Corral-Juan M, et al. A novel function of Ataxin-1 in the modulation of PP2A activity is dysregulated in the spinocerebellar ataxia type 1. *Hum Mol Genet*, 22, 3425–3437 (2013).

81. Sánchez I, Balagué E, Matilla-Dueñas A. Ataxin-1 regulates the cerebellar bioenergetics proteome through the GSK3β-mTOR pathway which is altered in Spinocerebellar ataxia type 1 (SCA1). *Hum Mol Genet*, 25, 4021–4040 (2016).

82. Magaña JJ, Velázquez-Pérez L, Cisneros B. Spinocerebellar Ataxia Type 2: Clinical Presentation, Molecular Mechanisms, and Therapeutic Perspectives. *Mol Neurobiol*, 47, 90–104 (2013).

83. Velázquez-Pérez LC, Rodríguez-Labrada R, Fernandez-Ruiz J. Spinocerebellar Ataxia Type 2: Clinicogenetic Aspects, Mechanistic Insights, and Management Approaches. *Front Neurol*, 8 (2017).

84. Crum BA, Josephs KA. Varied electrophysiologic patterns in spinocerebellar ataxia type 2. *Eur J Neurol*, 13, 194–197 (2006).

85. Velázquez Pérez L, Sánchez Cruz G, Canales Ochoa N, et al. Electrophysiological features in patients and presymptomatic relatives with spinocerebellar ataxia type 2. *J Neurol Sci*, 263, 158–164 (2007).

86. Pelosi L, Iodice R, Antenora A, et al. Spinocerebellar ataxia type 2—neuronopathy or neuropathy? *Muscle Nerve*, 60, 271–278 (2019).

87. Federighi P, Cevenini G, Dotti MT, et al. Differences in saccade dynamics between spinocerebellar ataxia 2 and late-onset cerebellar ataxias. *Brain*, 134, 879–891 (2011).

88. Rodríguez-Labrada R, Velázquez-Pérez L, Auburger G, et al. Spinocerebellar ataxia type 2: Measures of saccade changes improve power for clinical trials. *Mov Disord*, 31, 570–578 (2016).

89. Moscovich M, Okun MS, Favilla C, et al. Clinical evaluation of eye movements in spinocerebellar ataxias: A prospective multicenter study. *J Neuro-Ophthalmology*, 35, 16–21 (2015).

90. Meira AT, Arruda WO, Ono SE, et al. Neuroradiological Findings in the Spinocerebellar Ataxias. *Tremor Other Hyperkinet Mov (N Y)*, 9 (2019).

91. Pulst S-M, Nechiporuk A, Nechiporuk T, et al. Moderate expansion of a normally biallelic trinucleotide repeat in spinocerebellar ataxia type 2. *Nat Genet*, 14, 269–276 (1996).

92. Cagnoli C, Stevanin G, Michielotto C, et al. Large Pathogenic Expansions in the SCA2 and SCA7 Genes Can Be Detected by Fluorescent Repeat-Primed Polymerase Chain Reaction Assay. *J Mol Diagnostics*, 8, 128–132 (2006).

93. Antenora A, Bruzzese D, Lieto M, et al. Predictors of survival in spinocerebellar ataxia type 2

population from Southern Italy. *Neurol Sci*, 39, 1857–1860 (2018).

94. Rüb U, Seidel K, Özerden I, et al. Consistent affection of the central somatosensory system in spinocerebellar ataxia type 2 and type 3 and its significance for clinical symptoms and rehabilitative therapy. *Brain Res Rev*, 53, 235–249 (2007).

95. Pang JT, Giunti P, Chamberlain S, et al. Neuronal intranuclear inclusions in SCA2: a genetic, morphological and immunohistochemical study of two cases. *Brain*, 125, 656–663 (2002).

96. Egorova PA, Bezprozvanny IB. Molecular Mechanisms and Therapeutics for Spinocerebellar Ataxia Type 2. *Neurotherapeutics*, 16, 1050–1073 (2019).

97. Coutinho P, Andrade C. Autosomal dominant system degeneration in Portuguese families of the Azores Islands: A new genetic disorder involving cerebellar, pyramidal, extrapyramidal and spinal cord motor functions. *Neurology*, 28, 703–703 (1978).

98. Rüb U, Schöls L, Paulson H, et al. Clinical features, neurogenetics and neuropathology of the polyglutamine spinocerebellar ataxias type 1, 2, 3, 6 and 7. *Prog Neurobiol*, 104, 38–66 (2013).

99. Paulson HL, Shakkottai VG, Clark HB, et al. Polyglutamine spinocerebellar ataxias — from genes to potential treatments. *Nat Rev Neurosci*, 18, 613–626 (2017).

100. Park H, Kim H-J, Jeon BS. Parkinsonism in Spinocerebellar Ataxia. *Biomed Res Int*, 2015, 1–11 (2015).

101. Diallo A, Jacobi H, Cook A, et al. Survival in patients with spinocerebellar ataxia types 1, 2, 3, and 6 (EUROSCA): a longitudinal cohort study. *Lancet Neurol*, 17, 327–334 (2018).

102. Pal P, Chandran V, Jhunjhunwala K, et al. Multimodal evoked potentials in spinocerebellar ataxia types 1, 2, and 3. *Ann Indian Acad Neurol*, 17, 321 (2014).

103. Hotson JR, Langston EB, Louis AA, et al. The search for a physiologic marker of Machado-Joseph disease. *Neurology*, 37, 112–112 (1987).

104. Kondo H, Harayama H, Shinozawa K, et al. [Auditory brainstem response and somatosensory evoked potential in Machado-Joseph disease in Japanese families]. *Rinsho Shinkeigaku*, 30, 723–7 (1990).

105. Vale J, Bugalho P, Silveira I, et al. Autosomal dominant cerebellar ataxia: frequency analysis and clinical characterization of 45 families from Portugal. *Eur J Neurol*, 17, 124–128 (2010).

106. Takiyama Y, Nishizawa M, Tanaka H, et al. The gene for Machado–Joseph disease maps to human chromosome 14q. *Nat Genet*, 4, 300–304 (1993).

107. Gispert S, Twells R, Orozco G, et al. Chromosomal assignment of the second locus for autosomal dominant cerebellar ataxia (SCA2) to chromosome 12q23–24.1. *Nat Genet*, 4, 295–299 (1993).

108. Kawaguchi Y, Okamoto T, Taniwaki M, et al. CAG expansions in a novel gene for Machado-Joseph disease at chromosome 14q32.1. *Nat Genet*, 8, 221–228 (1994).

109. Matilla T, McCall A, Subramony SH, et al. Molecular and clinical correlations in spinocerebellar ataxia

type 3 and Machado-Joseph disease. *Ann Neurol*, 38, 68–72 (1995).

110. Rub U, de Vos RAI, Brunt ER, et al. Spinocerebellar Ataxia Type 3 (SCA3): Thalamic Neurodegeneration Occurs Independently from Thalamic Ataxin-3 Immunopositive Neuronal Intranuclear Inclusions. *Brain Pathol*, 16, 218–227 (2006).

111. Durr A, Stevanin G, Cancel G, et al. Spinocerebellar ataxia 3 and machado-joseph disease: Clinical, molecular, and neuropathological features. *Ann Neurol*, 39, 490–499 (1996).

112. Ashizawa T, Öz G, Paulson HL. Spinocerebellar ataxias: prospects and challenges for therapy development. *Nat Rev Neurol*, 14, 590–605 (2018).

113. Maruyama H, Nakamura S, Matsuyama Z, et al. Molecular features of the CAG repeats and clinical manifestation of Machado--Joseph disease. *Hum Mol Genet*, 4, 807–812 (1995).

114. Gardiner SL, Boogaard MW, Trompet S, et al. Prevalence of Carriers of Intermediate and Pathological Polyglutamine Disease–Associated Alleles Among Large Population-Based Cohorts. *JAMA Neurol*, 76, 650 (2019).

115. Gaspar C, Lopes-Cendes I, Hayes S, et al. Ancestral Origins of the Machado-Joseph Disease Mutation: A Worldwide Haplotype Study. *Am J Hum Genet*, 68, 523–528 (2001).

116. Flanigan K, Gardner K, Alderson K, et al. Autosomal dominant spinocerebellar ataxia with sensory axonal neuropathy (SCA4): clinical description and genetic localization to chromosome 16q22.1. *Am J Hum Genet*, 59, 392–9 (1996).

117. Hellenbroich Y, Bubel S, Pawlack H, et al. Refinement of the spinocerebellar ataxia type 4 locus in a large German family and exclusion of CAG repeat expansions in this region. *J Neurol*, 250, 668–671 (2003).

118. Hellenbroich Y, Gierga K, Reusche E, et al. Spinocerebellar ataxia type 4 (SCA4): Initial pathoanatomical study reveals widespread cerebellar and brainstem degeneration. *J Neural Transm*, 113, 829–843 (2006).

119. Rea G, Tirupathi S, Williams J, et al. Infantile Onset of Spinocerebellar Ataxia Type 5 (SCA-5) in a 6 Month Old with Ataxic Cerebral Palsy. *The Cerebellum*, 19, 161–163 (2020).

120. Burk K, Zuhlke C, Konig IR, et al. Spinocerebellar ataxia type 5: Clinical and molecular genetic features of a German kindred. *Neurology*, 62, 327–329 (2004).

121. Stevanin G, Herman A, Brice A, et al. Clinical and MRI findings in spinocerebellar ataxia type 5. *Neurology*, 53, 1355–1355 (1999).

122. Kumar H, Mondal B, Paul P, et al. An update on Spino-cerebellar ataxias. *Ann Indian Acad Neurol*, 16, 295 (2013).

123. Ranum LPW, Schut LJ, Lundgren JK, et al. Spinocerebellar ataxia type 5 in a family descended from the grandparents of President Lincoln maps to chromosome 11. *Nat Genet*, 8, 280–284 (1994).

124. Nicita F, Nardella M, Bellacchio E, et al. Heterozygous missense variants of SPTBN2 are a frequent cause of congenital cerebellar ataxia. *Clin Genet*, 96, 169–175 (2019).

125. Dick KA, Ikeda Y, Day JW, et al. Spinocerebellar ataxia type 5. *Handb Clin Neurol*, 451–459 (2012).

126. Du X, Gomez CM. Spinocerebellar Ataxia Type 6: Molecular Mechanisms and Calcium Channel Genetics. *Advances in Experimental Medicine and Biology*, pp. 147–173 (2018).

127. Kumagai R, Kaseda Y, Kawakami H, et al. Electrophysiological studies in spinocerebellar ataxia type 6. *Neuroreport*, 11, 969–972 (2000).

128. van de Warrenburg BPC, Notermans NC, Schelhaas HJ, et al. Peripheral Nerve Involvement in Spinocerebellar Ataxias. *Arch Neurol*, 61, 257 (2004).

129. Zhang X-Y, Wang J-J, Zhu J-N. Cerebellar fastigial nucleus: from anatomic construction to physiological functions. *Cerebellum & Ataxias*, 3, 9 (2016).

130. Zhuchenko O, Bailey J, Bonnen P, et al. Autosomal dominant cerebellar ataxia (SCA6) associated with small polyglutamine expansions in the α1A-voltage-dependent calcium channel. *Nat Genet*, 15, 62–69 (1997).

131. Sequeiros J, Martins S, Silveira I. Epidemiology and population genetics of degenerative ataxias. *Handb Clin Neurol*, 227–251 (2012).

132. Matsuyama Z. Molecular features of the CAG repeats of spinocerebellar ataxia 6 (SCA6). *Hum Mol Genet*, 6, 1283–1287 (1997).

133. Gierga K, Schelhaas HJ, Brunt ER, et al. Spinocerebellar ataxia type 6 (SCA6): neurodegeneration goes beyond the known brain predilection sites. *Neuropathol Appl Neurobiol*, 35, 515–527 (2009).

134. Ishikawa K, Owada K, Ishida K, et al. Cytoplasmic and nuclear polyglutamine aggregates in SCA6 Purkinje cells. *Neurology*, 56, 1753–1756 (2001).

135. Gouw LG, Kaplan CD, Haines JH, et al. Retinal degeneration characterizes a spinocerebellar ataxia mapping to chromosome 3p. *Nat Genet*, 10, 89–93 (1995).

136. Niewiadomska-Cimicka A, Hache A, Trottier Y. Gene Deregulation and Underlying Mechanisms in Spinocerebellar Ataxias With Polyglutamine Expansion. *Front Neurosci*, 14 (2020).

137. Kubis N, Durr A, Gugenheim M, et al. Polyneuropathy in autosomal dominant cerebellar ataxias: Phenotype-genotype correlation. *Muscle Nerve*, 22, 712–717 (1999).

138. Michalik A, Martin J-J, Van Broeckhoven C. Spinocerebellar ataxia type 7 associated with pigmentary retinal dystrophy. *Eur J Hum Genet*, 12, 2–15 (2004).

139. Oh AK, Jacobson KM, Jen JC, et al. Slowing of voluntary and involuntary saccades: An early sign in spinocerebellar ataxia type 7. *Ann Neurol*, 49, 801–804 (2001).

140. Trottier Y, Lutz Y, Stevanin G, et al. Polyglutamine expansion as a pathological epitope in Huntington's

disease and four dominant cerebellar ataxias. *Nature*, 378, 403–406 (1995).

141. David G, Abbas N, Stevanin G, et al. Cloning of the SCA7 gene reveals a highly unstable CAG repeat expansion. *Nat Genet*, 17, 65–70 (1997).

142. Johansson J. Expanded CAG repeats in Swedish spinocerebellar ataxia type 7 (SCA7) patients: effect of CAG repeat length on the clinical manifestation. *Hum Mol Genet*, 7, 171–176 (1998).

143. Karam A, Trottier Y. Molecular Mechanisms and Therapeutic Strategies in Spinocerebellar Ataxia Type 7. *Adv Exp Med Biol*, 197–218 (2018).

144. Rüb U, Brunt ER, Seidel K, et al. Spinocerebellar ataxia type 7 (SCA7): widespread brain damage in an adult-onset patient with progressive visual impairments in comparison with an adult-onset patient without visual impairments. *Neuropathol Appl Neurobiol*, 34, 155–168 (2008).

145. McCullough SD, Grant PA. Histone Acetylation, Acetyltransferases, and Ataxia—Alteration of Histone Acetylation and Chromatin Dynamics is Implicated in the Pathogenesis of Polyglutamine-Expansion Disorders. *Adv Protein Chem Struct Biol*, 165–203 (2010).

146. Matilla A. Association of ataxin-7 with the proteasome subunit S4 of the 19S regulatory complex. *Hum Mol Genet*, 10, 2821–2831 (2001).

147. Hu Y, Hashimoto Y, Ishii T, et al. Sequence configuration of spinocerebellar ataxia type 8 repeat expansions in a Japanese cohort of 797 ataxia subjects. *J Neurol Sci*, 382, 87–90 (2017).

148. Gasser T, Finsterer J, Baets J, et al. EFNS guidelines on the molecular diagnosis of ataxias and spastic paraplegias. *Eur J Neurol*, 17, 179–188 (2010).

149. Ikeda Y, Shizuka M, Watanabe M, et al. Molecular and clinical analyses of spinocerebellar ataxia type 8 in Japan. *Neurology*, 54, 950–955 (2000).

150. Lilja A, Hämäläinen P, Kaitaranta E, et al. Cognitive impairment in spinocerebellar ataxia type 8. *J Neurol Sci*, 237, 31–38 (2005).

151. Koob MD, Moseley ML, Schut LJ, et al. An untranslated CTG expansion causes a novel form of spinocerebellar ataxia (SCA8). *Nat Genet*, 21, 379–384 (1999).

152. Schöls L, Bauer I, Zühlke C, et al. Do CTG expansions at the SCA8 locus cause ataxia? *Ann Neurol*, 54, 110–115 (2003).

153. Corral J, Genís D, Banchs I, et al. Giant SCA8 alleles in nine children whose mother has two moderately large ones. *Ann Neurol*, 57, 549–553 (2005).

154. Ikeda Y, Dalton JC, Moseley ML, et al. Spinocerebellar Ataxia Type 8: Molecular Genetic Comparisonsand Haplotype Analysis of 37 Families with Ataxia. *Am J Hum Genet*, 75, 3–16 (2004).

155. Moseley ML, Zu T, Ikeda Y, et al. Bidirectional expression of CUG and CAG expansion transcripts and intranuclear polyglutamine inclusions in spinocerebellar ataxia type 8. *Nat Genet*, 38, 758–769

(2006).

156. Ito H, Kawakami H, Wate R, et al. Clinicopathologic investigation of a family with expanded SCA8 CTA/CTG repeats. *Neurology*, 67, 1479–1481 (2006).

157. Ayhan F, Perez BA, Shorrock HK, et al. SCA8 RAN polySer protein preferentially accumulates in white matter regions and is regulated by eIF3F. *EMBO J*, 37 (2018).

158. Higgins JJ, Pho LT, Ide SE, et al. Evidence for a new spinocerebellar ataxia locus. *Mov Disord*, 12, 412–417 (1997).

159. Moro A, Teive HAG. Cognitive impairment in Spinocerebellar ataxia type 10. *Dement Neuropsychol*, 10, 310–314 (2016).

160. Lin X, Ashizawa T. Recent progress in spinocerebellar ataxia type-10 (SCA10). *The Cerebellum*, 4, 37–42 (2005).

161. Rasmussen A, Matsuura T, Ruano L, et al. Clinical and genetic analysis of 4 Mexican families with spinocerebellar ataxia type 10. *Ann Neurol*, 50, 234–239 (2001).

162. Zu L, Figueroa KP, Grewal R, et al. Mapping of a New Autosomal Dominant Spinocerebellar Ataxia to Chromosome 22. *Am J Hum Genet*, 64, 594–599 (1999).

163. Matsuura T, Yamagata T, Burgess DL, et al. Large expansion of the ATTCT pentanucleotide repeat in spinocerebellar ataxia type 10. *Nat Genet*, 26, 191–194 (2000).

164. Goel D, Suroliya V, Shamim U, et al. Spinocerebellar ataxia type 10 (SCA10): Mutation analysis and common haplotype based inference suggest its rarity in Indian population. *eNeurologicalSci*, 17, 100211 (2019).

165. Xia G, McFarland KN, Wang K, et al. Purkinje cell loss is the major brain pathology of spinocerebellar ataxia type 10. *J Neurol Neurosurg Psychiatry*, 84, 1409–1411 (2013).

166. Yang W-Y, Gao R, Southern M, et al. Design of a bioactive small molecule that targets r(AUUCU) repeats in spinocerebellar ataxia 10. *Nat Commun*, 7, 11647 (2016).

167. Chen Z, Puzriakova A, Houlden H. Spinocerebellar Ataxia Type 11. *GeneReviews®* (1993).

168. Johnson J, Wood N, Giunti P, et al. Clinical and genetic analysis of spinocerebellar ataxia type 11. *The Cerebellum*, 7, 159–164 (2008).

169. Giunti P, Houlden H, Gardner-Thorpe C, et al. Spinocerebellar ataxia type 11. *Handb Clin Neurol*, 521–534 (2012).

170. Worth PF, Giunti P, Gardner-Thorpe C, et al. Autosomal Dominant Cerebellar Ataxia Type III: Linkage in a Large British Family to a 7.6-cM Region on Chromosome 15q14-21.3. *Am J Hum Genet*, 65, 420–426 (1999).

171. Houlden H, Johnson J, Gardner-Thorpe C, et al. Mutations in TTBK2, encoding a kinase implicated in

tau phosphorylation, segregate with spinocerebellar ataxia type 11. *Nat Genet*, 39, 1434–1436 (2007).

172. Deng Y, Fu J, Zhong Y, et al. First finding of familial spinal cerebellar Ataxia11 in China: clinical, imaging and genetic features. *Neurol Sci*, 41, 155–160 (2020).

173. Bowie E, Norris R, Anderson K V., et al. Spinocerebellar ataxia type 11-associated alleles of Ttbk2 dominantly interfere with ciliogenesis and cilium stability. *PLOS Genet*, 14, e1007844 (2018).

174. Holmes SE, Hearn EO, Ross CA, et al. SCA12: an unusual mutation leads to an unusual spinocerebellar ataxia. *Brain Res Bull*, 56, 397–403 (2001).

175. O'Hearn E, Holmes SE, Calvert PC, et al. SCA-12: Tremor with cerebellar and cortical atrophy is associated with a CAG repeat expansion. *Neurology*, 56, 299–303 (2001).

176. Holmes SE, O'Hearn E, Margolis RL. Why is SCA12 different from other SCAs? *Cytogenet Genome Res*, 100, 189–197 (2003).

177. Holmes SE, O'Hearn EE, McInnis MG, et al. Expansion of a novel CAG trinucleotide repeat in the 5′ region of PPP2R2B is associated with SCA12. *Nat Genet*, 23, 391–392 (1999).

178. Aydin G, Dekomien G, Hoffjan S, et al. Frequency of SCA8, SCA10, SCA12, SCA36, FXTAS and C9orf72 repeat expansions in SCA patients negative for the most common SCA subtypes. *BMC Neurol*, 18, 3 (2018).

179. Cholfin JA. The SCA12 Mutation as a Rare Cause of Spinocerebellar Ataxia. *Arch Neurol*, 58, 1833 (2001).

180. Bahl S, Virdi K, Mittal U, et al. Evidence of a Common Founder for SCA12 in the Indian Population. *Ann Hum Genet*, 69, 528–534 (2005).

181. Srivastava AK, Takkar A, Garg A, et al. Clinical behaviour of spinocerebellar ataxia type 12 and intermediate length abnormal CAG repeats in PPP2R2B. *Brain*, 140, 27–36 (2017).

182. O'Hearn EE, Hwang HS, Holmes SE, et al. Neuropathology and Cellular Pathogenesis of Spinocerebellar Ataxia Type 12. *Mov Disord*, 30, 1813–1824 (2015).

183. Cohen RL, Margolis RL. Spinocerebellar ataxia type 12. *Curr Opin Neurol*, 29, 735–742 (2016).

184. Waters MF, Pulst SM. SCA13. *The Cerebellum*, 7, 165–169 (2008).

185. Hsieh J-Y, Ulrich BN, Issa FA, et al. Infant and adult SCA13 mutations differentially affect Purkinje cell excitability, maturation, and viability in vivo. *Elife*, 9 (2020).

186. Khare S, Galeano K, Zhang Y, et al. C-terminal proline deletions in KCNC3 cause delayed channel inactivation and an adult-onset progressive SCA13 with spasticity. *The Cerebellum*, 17, 692–697 (2018).

187. Khare S, Nick JA, Zhang Y, et al. A KCNC3 mutation causes a neurodevelopmental, non-progressive SCA13 subtype associated with dominant negative effects and aberrant EGFR trafficking. *PLoS One*,

12, e0173565 (2017).

188. Rosini F, Pretegiani E, Battisti C, et al. Eye movement changes in autosomal dominant spinocerebellar ataxias. *Neurol Sci*, 41, 1719–1734 (2020).

189. Herman-Bert A, Stevanin G, Netter J-C, et al. Mapping of Spinocerebellar Ataxia 13 to Chromosome 19q13.3-q13.4 in a Family with Autosomal Dominant Cerebellar Ataxia and Mental Retardation. *Am J Hum Genet*, 67, 229–235 (2000).

190. Waters MF, Fee D, Figueroa KP, et al. An autosomal dominant ataxia maps to 19q13: Allelic heterogeneity of SCA13 or novel locus? *Neurology*, 65, 1111–1113 (2005).

191. Waters MF, Minassian NA, Stevanin G, et al. Mutations in voltage-gated potassium channel KCNC3 cause degenerative and developmental central nervous system phenotypes. *Nat Genet*, 38, 447–451 (2006).

192. Chen D-H, Raskind WH, Bird TD. Spinocerebellar ataxia type 14. *Handb Clin Neurol*, 555–559 (2012).

193. Dalski A, Mitulla B, Bürk K, et al. Mutation of the highly conserved cysteine residue 131 of the SCA14 associated PRKCG gene in a family with slow progressive cerebellar ataxia. *J Neurol*, 253, 1111–1112 (2006).

194. Yamashita I, Sasaki H, Yabe I, et al. A novel locus for dominant cerebellar ataxia (SCA14) maps to a 10.2-cM interval flanked by D19S206 and D19S605 on chromosome 19q13.4-qter. *Ann Neurol*, 48, 156–163 (2000).

195. Brkanac Z, Bylenok L, Fernandez M, et al. A New Dominant Spinocerebellar Ataxia Linked to Chromosome 19q13.4-qter. *Arch Neurol*, 59, 1291 (2002).

196. Chen D-H, Brkanac Z, Christophe Verlinde LMJ, et al. Missense Mutations in the Regulatory Domain of PKCγ: A New Mechanism for Dominant Nonepisodic Cerebellar Ataxia. *Am J Hum Genet*, 72, 839–849 (2003).

197. Shirafuji T, Shimazaki H, Miyagi T, et al. Spinocerebellar ataxia type 14 caused by a nonsense mutation in the PRKCG gene. *Mol Cell Neurosci*, 98, 46–53 (2019).

198. Wong MMK, Hoekstra SD, Vowles J, et al. Neurodegeneration in SCA14 is associated with increased PKCγ kinase activity, mislocalization and aggregation. *Acta Neuropathol Commun*, 6, 99 (2018).

199. Seki T, Matsubayashi H, Amano T, et al. Phosphorylation of PKC activation loop plays an important role in receptor-mediated translocation of PKC. *Genes to Cells*, 10, 225–239 (2005).

200. Seki T, Shimahara T, Yamamoto K, et al. Mutant γPKC found in spinocerebellar ataxia type 14 induces aggregate-independent maldevelopment of dendrites in primary cultured Purkinje cells. *Neurobiol Dis*, 33, 260–273 (2009).

201. Chopra R, Wasserman AH, Pulst SM, et al. Protein kinase C activity is a protective modifier of Purkinje neuron degeneration in cerebellar ataxia. *Hum Mol Genet*, 27, 1396–1410 (2018).

202. Verbeek DS, Goedhart J, Bruinsma L, et al. PKC mutations in spinocerebellar ataxia type 14 affect C1 domain accessibility and kinase activity leading to aberrant MAPK signaling. *J Cell Sci*, 121, 2339–2349 (2008).

203. Takahashi H, Adachi N, Shirafuji T, et al. Identification and characterization of PKCγ, a kinase associated with SCA14, as an amyloidogenic protein. *Hum Mol Genet*, 24, 525–539 (2015).

204. Storey E, Gardner RJM. Spinocerebellar ataxia type 15. *Handb Clin Neurol*, 561–565 (2012).

205. Gardner M, Knight M, Hara K, et al. Spinocerebellar ataxia type 15. *The Cerebellum*, 4, 47–50 (2005).

206. Novak MJU, Sweeney MG, Li A, et al. An ITPR1 gene deletion causes spinocerebellar ataxia 15/16: A genetic, clinical and radiological description. *Mov Disord*, 25, 2176–2182 (2010).

207. Storey E, Gardner RJM, Knight MA, et al. A new autosomal dominant pure cerebellar ataxia. *Neurology*, 57, 1913–1915 (2001).

208. Knight MA, Kennerson ML, Anney RJ, et al. Spinocerebellar ataxia type 15 (SCA15) maps to 3p24.2-3pter: exclusion of the ITPR1 gene, the human orthologue of an ataxic mouse mutant. *Neurobiol Dis*, 13, 147–157 (2003).

209. van de Leemput J, Chandran J, Knight MA, et al. Deletion at ITPR1 Underlies Ataxia in Mice and Spinocerebellar Ataxia 15 in Humans. *PLoS Genet*, 3, e108 (2007).

210. Hara K, Shiga A, Nozaki H, et al. Total deletion and a missense mutation of ITPR1 in Japanese SCA15 families. *Neurology*, 71, 547–551 (2008).

211. Obayashi M, Ishikawa K, Izumi Y, et al. Prevalence of inositol 1, 4, 5-triphosphate receptor type 1 gene deletion, the mutation for spinocerebellar ataxia type 15, in Japan screened by gene dosage. *J Hum Genet*, 57, 202–206 (2012).

212. Bezprozvanny I. Role of Inositol 1,4,5-Trishosphate Receptors in Pathogenesis of Huntington's Disease and Spinocerebellar Ataxias. *Neurochem Res*, 36, 1186–1197 (2011).

213. Casey JP, Hirouchi T, Hisatsune C, et al. A novel gain-of-function mutation in the ITPR1 suppressor domain causes spinocerebellar ataxia with altered Ca2+ signal patterns. *J Neurol*, 264, 1444–1453 (2017).

214. Toyoshima Y, Takahashi H. Spinocerebellar Ataxia Type 17 (SCA17). *Adv Exp Med Biol*, 219–231 (2018).

215. Manganelli F, Perretti A, Nolano M, et al. Electrophysiologic characterization in spinocerebellar ataxia 17. *Neurology*, 66, 932–934 (2006).

216. Hubner J, Sprenger A, Klein C, et al. Eye movement abnormalities in spinocerebellar ataxia type 17 (SCA17). *Neurology*, 69, 1160–1168 (2007).

217. Zühlke C, Hellenbroich Y, Dalski A, et al. Different types of repeat expansion in the TATA-binding

protein gene are associated with a new form of inherited ataxia. *Eur J Hum Genet*, 9, 160–164 (2001).

218. Rolfs A, Koeppen AH, Bauer I, et al. Clinical features and neuropathology of autosomal dominant spinocerebellar ataxia (SCA17). *Ann Neurol*, 54, 367–375 (2003).

219. Tsoi H, Lau TC-K, Tsang S-Y, et al. CAG expansion induces nucleolar stress in polyglutamine diseases. *Proc Natl Acad Sci*, 109, 13428–13433 (2012).

220. Brkanac Z, Spencer D, Shendure J, et al. IFRD1 Is a Candidate Gene for SMNA on Chromosome 7q22-q23. *Am J Hum Genet*, 84, 692–697 (2009).

221. Lin P, Zhang D, Xu G, et al. Identification of IFRD1 variant in a Han Chinese family with autosomal dominant hereditary spastic paraplegia associated with peripheral neuropathy and ataxia. *J Hum Genet*, 63, 521–524 (2018).

222. Brkanac Z, Fernandez M, Matsushita M, et al. Autosomal dominant sensory/motor neuropathy with Ataxia (SMNA): Linkage to chromosome 7q22-q32. *Am J Med Genet*, 114, 450–457 (2002).

223. Paucar M, Bergendal Å, Gustavsson P, et al. Novel Features and Abnormal Pattern of Cerebral Glucose Metabolism in Spinocerebellar Ataxia 19. *The Cerebellum*, 17, 465–476 (2018).

224. Schelhaas HJ. SCA19 and SCA22: evidence for one locus with a worldwide distribution. *Brain*, 127, E6 (2004).

225. Chung M, Lu Y, Cheng N, et al. A novel autosomal dominant spinocerebellar ataxia (SCA22) linked to chromosome 1p21-q23. *Brain*, 126, 1293–1299 (2003).

226. Verbeek D, Schelhaas J, Ippel E, et al. Identification of a novel SCA locus ( SCA19 ) in a Dutch autosomal dominant cerebellar ataxia family on chromosome region 1p21-q21. *Hum Genet*, 111, 388–393 (2002).

227. Lee Y-C, Durr A, Majczenko K, et al. Mutations in KCND3 cause spinocerebellar ataxia type 22. *Ann Neurol*, 72, 859–869 (2012).

228. Hsiao C, Fu S, Liu Y, et al. Novel SCA19/22-associated KCND3 mutations disrupt human K V 4.3 protein biosynthesis and channel gating. *Hum Mutat*, 40, 2088–2107 (2019).

229. Knight MA, Hernandez D, Diede SJ, et al. A duplication at chromosome 11q12.2-11q12.3 is associated with spinocerebellar ataxia type 20. *Hum Mol Genet*, 17, 3847–3853 (2008).

230. Storey E, Gardner RJM. Spinocerebellar ataxia type 20. *Handb Clin Neurol*, 567–573 (2012).

231. Storey E, Knight M, Forrest S, et al. Spinocerebellar ataxia type 20. *The Cerebellum*, 4, 55–57 (2005).

232. Knight MA. Dominantly inherited ataxia and dysphonia with dentate calcification: spinocerebellar ataxia type 20. *Brain*, 127, 1172–1181 (2004).

233. Delplanque J, Devos D, Huin V, et al. TMEM240 mutations cause spinocerebellar ataxia 21 with mental retardation and severe cognitive impairment. *Brain*, 137, 2657–2663 (2014).

234. Homa M, Loyens A, Eddarkaoui S, et al. The TMEM240 Protein, Mutated in SCA21, Is Expressed in Purkinje Cells and Synaptic Terminals. *The Cerebellum*, 19, 358–369 (2020).

235. Satoh S, Kondo Y, Ohara S, et al. Intrafamilial phenotypic variation in spinocerebellar ataxia type 23. *Cerebellum & Ataxias*, 7, 7 (2020).

236. Jezierska J, Stevanin G, Watanabe H, et al. Identification and characterization of novel PDYN mutations in dominant cerebellar ataxia cases. *J Neurol*, 260, 1807–1812 (2013).

237. Verbeek DS. Mapping of the SCA23 locus involved in autosomal dominant cerebellar ataxia to chromosome region 20p13-12.3. *Brain*, 127, 2551–2557 (2004).

238. Bakalkin G, Watanabe H, Jezierska J, et al. Prodynorphin Mutations Cause the Neurodegenerative Disorder Spinocerebellar Ataxia Type 23. *Am J Hum Genet*, 87, 593–603 (2010).

239. Smeets CJLM, Jezierska J, Watanabe H, et al. Elevated mutant dynorphin A causes Purkinje cell loss and motor dysfunction in spinocerebellar ataxia type 23. *Brain*, 138, 2537–2552 (2015).

240. Stevanin G, Bouslam N, Thobois S, et al. Spinocerebellar ataxia with sensory neuropathy (SCA25) maps to chromosome 2p. *Ann Neurol*, 55, 97–104 (2004).

241. Yu G-Y, Howell MJ, Roller MJ, et al. Spinocerebellar ataxia type 26 maps to chromosome 19p13.3 adjacent to SCA6. *Ann Neurol*, 57, 349–354 (2005).

242. Hekman KE, Yu G-Y, Brown CD, et al. A conserved eEF2 coding variant in SCA26 leads to loss of translational fidelity and increased susceptibility to proteostatic insult. *Hum Mol Genet*, 21, 5472–5483 (2012).

243. van Swieten JC, Brusse E, de Graaf BM, et al. A Mutation in the Fibroblast Growth Factor 14 Gene Is Associated with Autosomal Dominant Cerebral Ataxia. *Am J Hum Genet*, 72, 191–199 (2003).

244. Paucar M, Lundin J, Alshammari T, et al. Broader phenotypic traits and widespread brain hypometabolism in spinocerebellar ataxia 27. *J Intern Med*, 288, 103–115 (2020).

245. Shakkottai VG, Xiao M, Xu L, et al. FGF14 regulates the intrinsic excitability of cerebellar Purkinje neurons. *Neurobiol Dis*, 33, 81–88 (2009).

246. Bosch MK, Carrasquillo Y, Ransdell JL, et al. Intracellular FGF14 (iFGF14) Is Required for Spontaneous and Evoked Firing in Cerebellar Purkinje Neurons and for Motor Coordination and Balance. *J Neurosci*, 35, 6752–6769 (2015).

247. Tunc S, Dulovic-Mahlow M, Baumann H, et al. Spinocerebellar Ataxia Type 28—Phenotypic and Molecular Characterization of a Family with Heterozygous and Compound-Heterozygous Mutations in AFG3L2. *The Cerebellum*, 18, 817–822 (2019).

248. Mariotti C, Brusco A, Di Bella D, et al. Spinocerebellar ataxia type 28: A novel autosomal dominant cerebellar ataxia characterized by slow progression and ophthalmoparesis. *The Cerebellum*, 7, 184–188 (2008).

249. Politi LS, Bianchi Marzoli S, Godi C, et al. MRI Evidence of Cerebellar and Extraocular Muscle Atrophy Differently Contributing to Eye Movement Abnormalities in SCA2 and SCA28 Diseases. *Investig Opthalmology Vis Sci*, 57, 2714 (2016).

250. Cagnoli C, Mariotti C, Taroni F, et al. SCA28, a novel form of autosomal dominant cerebellar ataxia on chromosome 18p11.22–q11.2. *Brain*, 129, 235–242 (2006).

251. Di Bella D, Lazzaro F, Brusco A, et al. Mutations in the mitochondrial protease gene AFG3L2 cause dominant hereditary ataxia SCA28. *Nat Genet*, 42, 313–321 (2010).

252. Cagnoli C, Stevanin G, Brussino A, et al. Missense mutations in the AFG3L2 proteolytic domain account for ~1.5% of European autosomal dominant cerebellar ataxias. *Hum Mutat*, 31, 1117–1124 (2010).

253. Smets K, Deconinck T, Baets J, et al. Partial deletion of AFG3L2 causing spinocerebellar ataxia type 28. *Neurology*, 82, 2092–2100 (2014).

254. Ando H, Hirose M, Mikoshiba K. Aberrant IP 3 receptor activities revealed by comprehensive analysis of pathological mutations causing spinocerebellar ataxia 29. *Proc Natl Acad Sci*, 115, 12259–12264 (2018).

255. Huang L, Chardon J, Carter MT, et al. Missense mutations in ITPR1 cause autosomal dominant congenital nonprogressive spinocerebellar ataxia. *Orphanet J Rare Dis*, 7, 67 (2012).

256. Dudding TE, Friend K, Schofield PW, et al. Autosomal dominant congenital non-progressive ataxia overlaps with the SCA15 locus. *Neurology*, 63, 2288–2292 (2004).

257. Synofzik M, Helbig KL, Harmuth F, et al. De novo ITPR1 variants are a recurrent cause of early-onset ataxia, acting via loss of channel function. *Eur J Hum Genet*, 26, 1623–1634 (2018).

258. Storey E, Bahlo M, Fahey M, et al. A new dominantly inherited pure cerebellar ataxia, SCA 30. *J Neurol Neurosurg Psychiatry*, 80, 408–411 (2008).

259. Hirano R, Takashima H, Okubo R, et al. Clinical and genetic characterization of 16q-linked autosomal dominant spinocerebellar ataxia in South Kyushu, Japan. *J Hum Genet*, 54, 377–381 (2009).

260. Ishikawa K, Nagai Y. Molecular Mechanisms and Future Therapeutics for Spinocerebellar Ataxia Type 31 (SCA31). *Neurotherapeutics*, 16, 1106–1114 (2019).

261. Nagaoka U, Takashima M, Ishikawa K, et al. A gene on SCA4 locus causes dominantly inherited pure cerebellar ataxia. *Neurology*, 54, 1971–1975 (2000).

262. Li M, Ishikawa K, Toru S, et al. Physical map and haplotype analysis of 16q-linked autosomal dominant cerebellar ataxia (ADCA) type III in Japan. *J Hum Genet*, 48, 0111–0118 (2003).

263. Ishikawa K, Toru S, Tsunemi T, et al. An Autosomal Dominant Cerebellar Ataxia Linked to Chromosome 16q22.1 Is Associated with a Single-Nucleotide Substitution in the 5′ Untranslated Region of the Gene Encoding a Protein with Spectrin Repeat and Rho Guanine-Nucleotide Exchange-

Factor Domains. *Am J Hum Genet*, 77, 280–296 (2005).

264. Amino T, Ishikawa K, Toru S, et al. Redefining the disease locus of 16q22.1-linked autosomal dominant cerebellar ataxia. *J Hum Genet*, 52, 643–649 (2007).

265. Pedroso JL, Abrahao A, Ishikawa K, et al. When should we test patients with familial ataxias for SCA31? A misdiagnosed condition outside Japan? *J Neurol Sci*, 355, 206–208 (2015).

266. Yoshida K, Asakawa M, Suzuki-Kouyama E, et al. Distinctive features of degenerating Purkinje cells in spinocerebellar ataxia type 31. *Neuropathology*, 34, 261–7 (2014).

267. Jiang H, Zhu H-P, Gomez CM. Abstracts of the Fourteenth International Congress of Parkinson's Disease and Movement Disorders. *Mov Disord*, 25, S181–S565 (2010).

268. Cadieux-Dion M, Turcotte-Gauthier M, Noreau A, et al. Expanding the Clinical Phenotype Associated With ELOVL4 Mutation. *JAMA Neurol*, 71, 470 (2014).

269. Ozaki K, Doi H, Mitsui J, et al. A Novel Mutation in ELOVL4 Leading to Spinocerebellar Ataxia (SCA) With the Hot Cross Bun Sign but Lacking Erythrokeratodermia. *JAMA Neurol*, 72, 797 (2015).

270. Beaudin M, Sellami L, Martel C, et al. Characterization of the phenotype with cognitive impairment and protein mislocalization in SCA34. *Neurol Genet*, 6, e403 (2020).

271. Guo Y-C, Lin J-J, Liao Y-C, et al. Spinocerebellar ataxia 35: Novel mutations in TGM6 with clinical and genetic characterization. *Neurology*, 83, 1554–1561 (2014).

272. Wang JL, Yang X, Xia K, et al. TGM6 identified as a novel causative gene of spinocerebellar ataxias using exome sequencing. *Brain*, 133, 3510–3518 (2010).

273. Chen Y, Wu D, Luo B, et al. TGM6 L517W is not a pathogenic variant for spinocerebellar ataxia type 35. *Neurol Genet*, 6, e424 (2020).

274. Fung JLF, Tsang MHY, Leung GKC, et al. A significant inflation in TGM6 genetic risk casts doubt in its causation in spinocerebellar ataxia type 35. *Parkinsonism Relat Disord*, 63, 42–45 (2019).

275. Tripathy D, Vignoli B, Ramesh N, et al. Mutations in TGM6 induce the unfolded protein response in SCA35. *Hum Mol Genet*, 26, 3749–3762 (2017).

276. Kobayashi H, Abe K, Matsuura T, et al. Expansion of Intronic GGCCTG Hexanucleotide Repeat in NOP56 Causes SCA36, a Type of Spinocerebellar Ataxia Accompanied by Motor Neuron Involvement. *Am J Hum Genet*, 89, 121–130 (2011).

277. Ikeda Y, Ohta Y, Kobayashi H, et al. Clinical features of SCA36: A novel spinocerebellar ataxia with motor neuron involvement (Asidan). *Neurology*, 79, 333–341 (2012).

278. McEachin ZT, Gendron TF, Raj N, et al. Chimeric Peptide Species Contribute to Divergent Dipeptide Repeat Pathology in c9ALS/FTD and SCA36. *Neuron*, 107, 292-305.e6 (2020).

279. Arias M, García-Murias M, Sobrido MJ. Spinocerebellar ataxia 36 (SCA36): "Costa da Morte ataxia."

*Neurología*, 32, 386–393 (2017).

280. Liu W, Ikeda Y, Hishikawa N, et al. Characteristic RNA foci of the abnormal hexanucleotide GGCCUG repeat expansion in spinocerebellar ataxia type 36 (Asidan). *Eur J Neurol*, 21, 1377–1386 (2014).

281. Serrano-Munuera C, Corral-Juan M, Stevanin G, et al. New subtype of spinocerebellar ataxia with altered vertical eye movements mapping to chromosome 1p32. *JAMA Neurol*, 70, 764–71 (2013).

282. Di Gregorio E, Borroni B, Giorgio E, et al. ELOVL5 Mutations Cause Spinocerebellar Ataxia 38. *Am J Hum Genet*, 95, 209–217 (2014).

283. Borroni B, Di Gregorio E, Orsi L, et al. Clinical and neuroradiological features of spinocerebellar ataxia 38 (SCA38). *Parkinsonism Relat Disord*, 28, 80–86 (2016).

284. Gazulla J, Orduna-Hospital E, Benavente I, et al. Contributions to the study of spinocerebellar ataxia type 38 (SCA38). *J Neurol*, 267, 2288–2295 (2020).

285. Johnson JO, Stevanin G, van de Leemput J, et al. A 7.5-Mb duplication at chromosome 11q21-11q22.3 is associated with a novel spastic ataxia syndrome. *Mov Disord*, 30, 262–266 (2015).

286. Tsoi H, Yu ACS, Chen ZS, et al. A novel missense mutation in CCDC88C activates the JNK pathway and causes a dominant form of spinocerebellar ataxia. *J Med Genet*, 51, 590–595 (2014).

287. Leńska-Mieciek M, Charzewska A, Królicki L, et al. Familial ataxia, tremor, and dementia in a polish family with a novel mutation in the CCDC88C gene. *Mov Disord*, 34, 142–144 (2019).

288. Fogel BL, Hanson SM, Becker EBE. Do mutations in the murine ataxia gene TRPC3 cause cerebellar ataxia in humans? *Mov Disord*, 30, 284–286 (2015).

289. Martin-Trujillo A, Iglesias-Platas I, Coto E, et al. Genotype of an individual single nucleotide polymorphism regulates DNA methylation at the TRPC3 alternative promoter. *Epigenetics*, 6, 1236–1241 (2011).

290. Coutelier M, Blesneac I, Monteil A, et al. A Recurrent Mutation in CACNA1G Alters Cav3.1 T-Type Calcium-Channel Conduction and Causes Autosomal-Dominant Cerebellar Ataxia. *Am J Hum Genet*, 97, 726–737 (2015).

291. Morino H, Matsuda Y, Muguruma K, et al. A mutation in the low voltage-gated calcium channel CACNA1G alters the physiological properties of the channel, causing spinocerebellar ataxia. *Mol Brain*, 8, 89 (2015).

292. Barresi S, Dentici ML, Manzoni F, et al. Infantile-Onset Syndromic Cerebellar Ataxia and CACNA1G Mutations. *Pediatr Neurol*, 104, 40–45 (2020).

293. Depondt C, Donatello S, Rai M, et al. MME mutation in dominant spinocerebellar ataxia with neuropathy (SCA43). *Neurol Genet*, 2, e94 (2016).

294. Davarniya B, Hu H, Kahrizi K, et al. The Role of a Novel TRMT1 Gene Mutation and Rare GRM1

Gene Defect in Intellectual Disability in Two Azeri Families. *PLoS One*, 10, e0129631 (2015).

295. Nibbeling EAR, Duarri A, Verschuuren-Bemelmans CC, et al. Exome sequencing and network analysis identifies shared mechanisms underlying spinocerebellar ataxia. *Brain*, 140, 2860–2878 (2017).

296. Dijk GW van, Wokke JHJ, Oey PL, et al. A new variant of sensory ataxic neuropathy with autosomal dominant inheritance. *Brain*, 118, 1557–1563 (1995).

297. Gennarino VA, Palmer EE, McDonell LM, et al. A Mild PUM1 Mutation Is Associated with Adult-Onset Ataxia, whereas Haploinsufficiency Causes Developmental Delay and Seizures. *Cell*, 172, 924-936.e11 (2018).

298. Genis D, Ortega-Cubero S, San Nicolás H, et al. Heterozygous STUB1 mutation causes familial ataxia with cognitive affective syndrome (SCA48). *Neurology*, 91, e1988–e1998 (2018).

299. Carroll LS, Massey TH, Wardle M, et al. Dentatorubral-pallidoluysian Atrophy: An Update. *Tremor Other Hyperkinet Mov (N Y)*, 8, 577 (2018).

300. Nagafuchi S, Yanagisawa H, Sato K, et al. Dentatorubral and pallidoluysian atrophy expansion of an unstable CAG trinucleotide on chromosome 12p. *Nat Genet*, 6, 14–18 (1994).

301. Koide R, Ikeuchi T, Onodera O, et al. Unstable expansion of CAG repeat in hereditary dentatorubral–pallidoluysian atrophy (DRPLA). *Nat Genet*, 6, 9–13 (1994).

302. Burke JR, Wingfield MS, Lewis KE, et al. The Haw River Syndrome: Dentatorubropallidoluysian atrophy (DRPLA) in an African–American family. *Nat Genet*, 7, 521–524 (1994).

303. Yamada M. Dentatorubral-pallidoluysian atrophy (DRPLA): The 50th Anniversary of Japanese Society of Neuropathology. *Neuropathology*, 30, 453–7 (2010).

304. Charroux B, Fanto M. The fine line between waste disposal and recycling: DRPLA fly models illustrate the importance of completing the autophagy cycle for rescuing neurodegeneration. *Autophagy*, 6, 667–669 (2010).

305. Suzuki Y, Jin C, Yazawa I. Increased aggregation of polyleucine compared with that of polyglutamine in dentatorubral-pallidoluysian atrophy protein. *Neurosci Lett*, 552, 156–161 (2013).

306. Suzuki Y, Nakayama K, Hashimoto N, et al. Proteolytic processing regulates pathological accumulation in dentatorubral-pallidoluysian atrophy. *FEBS J*, 277, 4873–4887 (2010).

307. D'Adamo MC, Hasan S, Guglielmi L, et al. New insights into the pathogenesis and therapeutics of episodic ataxia type 1. *Front Cell Neurosci*, 9 (2015).

308. Paulhus K, Ammerman L, Glasscock E. Clinical Spectrum of KCNA1 Mutations: New Insights into Episodic Ataxia and Epilepsy Comorbidity. *Int J Mol Sci*, 21, 2802 (2020).

309. Litt M, Kramer P, Browne D, et al. A gene for episodic ataxia/myokymia maps to chromosome 12p13. *Am J Hum Genet*, 55, 702–9 (1994).

310. Browne DL, Gancher ST, Nutt JG, et al. Episodic ataxia/myokymia syndrome is associated with point mutations in the human potassium channel gene, KCNA1. *Nat Genet*, 8, 136–140 (1994).

311. Jen JC, Wan J. Episodic ataxias. *Handb Clin Neurol*, 205–215 (2018).

312. Eunson LH, Rea R, Zuberi SM, et al. Clinical, genetic, and expression studies of mutations in the potassium channel gene KCNA1 reveal new phenotypic variability. *Ann Neurol*, 48, 647–656 (2000).

313. Klein A, Boltshauser E, Jen J, et al. Episodic Ataxia Type 1 with Distal Weakness: A Novel Manifestation of a Potassium Channelopathy. *Neuropediatrics*, 35, 147–149 (2004).

314. Mantuano E, Romano S, Veneziano L, et al. Identification of novel and recurrent CACNA1A gene mutations in fifteen patients with episodic ataxia type 2. *J Neurol Sci*, 291, 30–36 (2010).

315. Kramer PL, Yue Q, Gancher ST, et al. A locus for the nystagmus-associated form of episodic ataxia maps to an 11-cM region on chromosome 19p. *Am J Hum Genet*, 57, 182–5 (1995).

316. Brederlow B Von, Hahn AF, Koopman WJ, et al. Mapping the gene for acetazolamide responsive hereditary paryoxysmal cerebellar ataxia to chromosome 19p. *Hum Mol Genet*, 4, 279–284 (1995).

317. Ophoff RA, Terwindt GM, Vergouwe MN, et al. Familial Hemiplegic Migraine and Episodic Ataxia Type-2 Are Caused by Mutations in the Ca2+ Channel Gene CACNL1A4. *Cell*, 87, 543–552 (1996).

318. Jacobi H, du Montcel ST, Bauer P, et al. Long-term disease progression in spinocerebellar ataxia types 1, 2, 3, and 6: a longitudinal cohort study. *Lancet Neurol*, 14, 1101–1108 (2015).

319. Spacey SD, Materek LA, Szczygielski BI, et al. Two Novel CACNA1A Gene Mutations Associated With Episodic Ataxia Type 2 and Interictal Dystonia. *Arch Neurol*, 62, 314 (2005).

320. Guterman EL, Yurgionas B, Nelson AB. Pearls & Oy-sters: Episodic ataxia type 2. *Neurology*, 86, e239–e241 (2016).

321. Mori Y, Friedrich T, Kim M-S, et al. Primary structure and functional expression from complementary DNA of a brain calcium channel. *Nature*, 350, 398–402 (1991).

322. Strupp M, Kalla R, Glasauer S, et al. Aminopyridines for the treatment of cerebellar and ocular motor disorders. *Prog Brain Res*, 535–541 (2008).

323. Alvina K, Khodakhah K. KCa Channels as Therapeutic Targets in Episodic Ataxia Type-2. *J Neurosci*, 30, 7249–7257 (2010).

324. Jen J, Kim GW, Baloh RW. Clinical spectrum of episodic ataxia type 2. *Neurology*, 62, 17–22 (2004).

325. Steckley JL, Ebers GC, Cader MZ, et al. An autosomal dominant disorder with episodic ataxia, vertigo, and tinnitus. *Neurology*, 57, 1499–1502 (2001).

326. Cader MZ, Steckley JL, Dyment DA, et al. A genome-wide screen and linkage mapping for a large pedigree with episodic ataxia. *Neurology*, 65, 156–158 (2005).

327. Farmer TW. Vestibulocerebellar Ataxia. *Arch Neurol*, 8, 471 (1963).

328. Damji KF, Allingham RR, Pollock SC, et al. Periodic Vestibulocerebellar Ataxia, an Autosomal Dominant Ataxia With Defective Smooth Pursuit, Is Genetically Distinct From Other Autosomal Dominant Ataxias. *Arch Neurol*, 53, 338–344 (1996).

329. Merrill MJ, Nai D, Ghosh P, et al. Neuropathology in a case of episodic ataxia type 4. *Neuropathol Appl Neurobiol*, 42, 296–300 (2016).

330. Escayg A, De Waard M, Lee DD, et al. Coding and Noncoding Variation of the Human Calcium-Channel β4-Subunit Gene CACNB4 in Patients with Idiopathic Generalized Epilepsy and Episodic Ataxia. *Am J Hum Genet*, 66, 1531–1539 (2000).

331. Jen JC, Wan J, Palos TP, et al. Mutation in the glutamate transporter EAAT1 causes episodic ataxia, hemiplegia, and seizures. *Neurology*, 65, 529–534 (2005).

332. de Vries B, Mamsa H, Stam AH, et al. Episodic Ataxia Associated With EAAT1 Mutation C186S Affecting Glutamate Reuptake. *Arch Neurol*, 66 (2009).

333. Kerber KA, Jen JC, Lee H, et al. A New Episodic Ataxia Syndrome With Linkage to Chromosome 19q13. *Arch Neurol*, 64, 749 (2007).

334. Conroy J, McGettigan P, Murphy R, et al. A novel locus for episodic ataxia:UBR4 the likely candidate. *Eur J Hum Genet*, 22, 505–510 (2014).

335. Schwarz N, Bast T, Gaily E, et al. Clinical and genetic spectrum of SCN2A-associated episodic ataxia. *Eur J Paediatr Neurol*, 23, 438–447 (2019).

336. Fazeli W, Becker K, Herkenrath P, et al. Dominant SCN2A Mutation Causes Familial Episodic Ataxia and Impairment of Speech Development. *Neuropediatrics*, 49, 379–384 (2018).

337. Schwarz N, Hahn A, Bast T, et al. Mutations in the sodium channel gene SCN2A cause neonatal epilepsy with late-onset episodic ataxia. *J Neurol*, 263, 334–343 (2016).

338. Liao Y, Anttonen AK, Liukkonen E, et al. SCN2A mutation associated with neonatal epilepsy, late-onset episodic ataxia, myoclonus, and pain. *Neurology*, 75, 1454–1458 (2010).

339. Piarroux J, Riant F, Humbertclaude V, et al. FGF14 -related episodic ataxia: delineating the phenotype of Episodic Ataxia type 9. *Ann Clin Transl Neurol*, 7, 565–572 (2020).

340. Matilla-Dueñas A, Infante J, Serrano-Munuera C, et al. Novel Therapeutic Challenges in Cerebellar Diseases. *Handb Cerebellum Cerebellar Disord*, 1–33 (2020).

341. Nakamura K, Yoshida K, Miyazaki D, et al. Spinocerebellar ataxia type 6 (SCA6): Clinical pilot trial with gabapentin. *J Neurol Sci*, 278, 107–111 (2009).

342. Ristori G, Romano S, Visconti A, et al. Riluzole in cerebellar ataxia: A randomized, double-blind, placebo-controlled pilot trial. *Neurology*, 74, 839–845 (2010).

343. Romano S, Coarelli G, Marcotulli C, et al. Riluzole in patients with hereditary cerebellar ataxia: a

randomised, double-blind, placebo-controlled trial. *Lancet Neurol*, 14, 985–991 (2015).

344. Lei L-F, Yang G-P, Wang J-L, et al. Safety and efficacy of valproic acid treatment in SCA3/MJD patients. *Parkinsonism Relat Disord*, 26, 55–61 (2016).

345. Zesiewicz TA, Greenstein PE, Sullivan KL, et al. A randomized trial of varenicline (Chantix) for the treatment of spinocerebellar ataxia type 3. *Neurology*, 78, 545–550 (2012).

346. Freeman W, Wszolek Z. Botulinum toxin type A for treatment of spasticity in spinocerebellar ataxia type 3 (Machado-Joseph disease). *Mov Disord*, 20, 644–644 (2005).

347. Botez MI, Young SN, Botez T, et al. Treatment of Heredo-Degenerative Ataxias with Amantadine Hydrochloride. *Can J Neurol Sci*, 18, 307–311 (1991).

348. Tuite PJ, Rogaeva EA, St George-Hyslop PH, et al. Dopa-responsive parkinsonism phenotype of Machado-Joseph disease: Confirmation of 14q CAG expansion. *Ann Neurol*, 38, 684–687 (1995).

349. Buhmann C, Bussopulos A, Oechsner M. Dopaminergic response in Parkinsonian phenotype of Machado-Joseph disease. *Mov Disord*, 18, 219–221 (2003).

350. Schols L, Haan J, Riess O, et al. Sleep disturbance in spinocerebellar ataxias: Is the SCA3 mutation a cause of restless legs syndrome? *Neurology*, 51, 1603–1607 (1998).

351. Hening WA, Allen RP, Ondo WG, et al. Rotigotine improves restless legs syndrome: A 6-month randomized, double-blind, placebo-controlled trial in the United States. *Mov Disord*, 25, 1675–1683 (2010).

352. Zintzaras E, Kitsios GD, Papathanasiou AA, et al. Randomized trials of dopamine agonists in restless legs syndrome: A systematic review, quality assessment, and meta-analysis. *Clin Ther*, 32, 221–237 (2010).

353. Lo RY, Figueroa KP, Pulst SM, et al. Coenzyme Q10 and spinocerebellar ataxias. *Mov Disord*, 30, 214–220 (2015).

354. Watase K, Gatchel JR, Sun Y, et al. Lithium Therapy Improves Neurological Function and Hippocampal Dendritic Arborization in a Spinocerebellar Ataxia Type 1 Mouse Model. *PLoS Med*, 4, e182 (2007).

355. Saccà F, Puorro G, Brunetti A, et al. A randomized controlled pilot trial of lithium in spinocerebellar ataxia type 2. *J Neurol*, 262, 149–153 (2015).

356. Manes M, Alberici A, Di Gregorio E, et al. Docosahexaenoic acid is a beneficial replacement treatment for spinocerebellar ataxia 38. *Ann Neurol*, 82, 615–621 (2017).

357. Kanai K. Muscle cramp in Machado-Joseph disease: Altered motor axonal excitability properties and mexiletine treatment. *Brain*, 126, 965–973 (2003).

358. De Rosa A, Striano P, Barbieri F, et al. Suppression of myoclonus in SCA2 by piracetam. *Mov Disord*,

21, 116–118 (2006).

359. Kanai K, Sakakibara R, Uchiyama T, et al. Sporadic case of spinocerebellar ataxia type 17: Treatment observations for managing urinary and psychotic symptoms. *Mov Disord*, 22, 441–443 (2007).

360. Ince Gunal D, Agan K, Afsar N, et al. The effect of piracetam on ataxia: clinical observations in a group of autosomal dominant cerebellar ataxia patients. *J Clin Pharm Ther*, 33, 175–178 (2008).

361. Teixeira-Castro A, Jalles A, Esteves S, et al. Serotonergic signalling suppresses ataxin 3 aggregation and neurotoxicity in animal models of Machado-Joseph disease. *Brain*, 138, 3221–3237 (2015).

362. Scoles DR, Meera P, Schneider MD, et al. Antisense oligonucleotide therapy for spinocerebellar ataxia type 2. *Nature*, 544, 362–366 (2017).

363. Friedrich J, Kordasiewicz HB, O'Callaghan B, et al. Antisense oligonucleotide–mediated ataxin-1 reduction prolongs survival in SCA1 mice and reveals disease-associated transcriptome profiles. *JCI Insight*, 3 (2018).

364. Toonen LJA, Rigo F, van Attikum H, et al. Antisense Oligonucleotide-Mediated Removal of the Polyglutamine Repeat in Spinocerebellar Ataxia Type 3 Mice. *Mol Ther - Nucleic Acids*, 8, 232–242 (2017).

365. Nóbrega C, Nascimento-Ferreira I, Onofre I, et al. Silencing Mutant Ataxin-3 Rescues Motor Deficits and Neuropathology in Machado-Joseph Disease Transgenic Mice. *PLoS One*, 8, e52396 (2013).

366. Miyazaki Y, Du X, Muramatsu S, et al. An miRNA-mediated therapy for SCA6 blocks IRES-driven translation of the CACNA1A second cistron. *Sci Transl Med*, 8, 347ra94 (2016).

367. Griggs RC, Moxley RT, Lafrance RA, et al. Hereditary paroxysmal ataxia: Response to acetazolamide. *Neurology*, 28, 1259–1259 (1978).

368. Glasauer S. 4-aminopyridine restores visual ocular motor function in upbeat nystagmus. *J Neurol Neurosurg Psychiatry*, 76, 451–453 (2005).

369. Ilg W, Synofzik M, Brotz D, et al. Intensive coordinative training improves motor performance in degenerative cerebellar disease. *Neurology*, 73, 1823–1830 (2009).

370. Ilg W, Brötz D, Burkard S, et al. Long-term effects of coordinative training in degenerative cerebellar disease. *Mov Disord*, 25, 2239–2246 (2010).

371. Song Y-G, Ryu Y-U, Im S-J, et al. Effects of dance-based movement therapy on balance, gait, and psychological functions in severe cerebellar ataxia: A case study. *Physiother Theory Pract*, 35, 756–763 (2019).

372. Keller JL, Bastian AJ. A Home Balance Exercise Program Improves Walking in People With Cerebellar Ataxia. *Neurorehabil Neural Repair*, 28, 770–778 (2014).

373. Namikawa K, Dorigo A, Köster RW. Neurological Disease Modelling for Spinocerebellar Ataxia Using

Zebrafish. *J Exp Neurosci*, 13, 1179069519880515 (2019).

374. Namikawa K, Dorigo A, Zagrebelsky M, et al. Modeling Neurodegenerative Spinocerebellar Ataxia Type 13 in Zebrafish Using a Purkinje Neuron Specific Tunable Coexpression System. *J Neurosci*, 39, 3948–3969 (2019).

375. Carlson KM, Melcher L, Lai S, et al. Characterization of the Zebrafish atxn1/axh Gene Family. *J Neurogenet*, 23, 313–323 (2009).

376. Watchon M, Yuan KC, Mackovski N, et al. Calpain Inhibition Is Protective in Machado–Joseph Disease Zebrafish Due to Induction of Autophagy. *J Neurosci*, 37, 7782–7794 (2017).

377. Carrillo-Rosas S, Weber C, Fievet L, et al. Loss of zebrafish Ataxin-7, a SAGA subunit responsible for SCA7 retinopathy, causes ocular coloboma and malformation of photoreceptors. *Hum Mol Genet*, 28, 912–927 (2019).

378. Manjón J V., Coupé P. volBrain: An Online MRI Brain Volumetry System. *Front Neuroinform*, 10, 30 (2016).

379. Abecasis GR, Cherny SS, Cookson WO, et al. Merlin--rapid analysis of dense genetic maps using sparse gene flow trees. *Nat Genet*, 30, 97–101 (2002).

380. Jablecki CK, Andary MT, Di Benedetto M, et al. American Association of Electrodiagnostic Medicine guidelines for outcome studies in electrodiagnostic medicine. *Muscle Nerve*, 19, 1626–35 (1996).

381. Cagnoli C, Michielotto C, Matsuura T, et al. Detection of Large Pathogenic Expansions in FRDA1, SCA10, and SCA12 Genes Using a Simple Fluorescent Repeat-Primed PCR Assay. *J Mol Diagnostics*, 6, 96–100 (2004).

382. Ewing B, Green P. Base-Calling of Automated Sequencer Traces Using Phred. II. Error Probabilities. *Genome Res*, 8, 186–194 (1998).

383. Li H, Durbin R. Fast and accurate short read alignment with Burrows-Wheeler transform. *Bioinformatics*, 25, 1754–1760 (2009).

384. Koboldt DC, Chen K, Wylie T, et al. VarScan: variant detection in massively parallel sequencing of individual and pooled samples. *Bioinformatics*, 25, 2283–2285 (2009).

385. McKenna A, Hanna M, Banks E, et al. The Genome Analysis Toolkit: A MapReduce framework for analyzing next-generation DNA sequencing data. *Genome Res*, 20, 1297–1303 (2010).

386. Kersey PJ, Allen JE, Armean I, et al. Ensembl Genomes 2016: more genomes, more complexity. *Nucleic Acids Res*, 44, D574–D580 (2016).

387. Karczewski KJ, Francioli LC, Tiao G, et al. The mutational constraint spectrum quantified from variation in 141,456 humans. *Nature*, 581, 434–443 (2020).

388. González-Pérez A, López-Bigas N. Improving the Assessment of the Outcome of Nonsynonymous

SNVs with a Consensus Deleteriousness Score, Condel. *Am J Hum Genet*, 88, 440–449 (2011).

389. Kumar P, Henikoff S, Ng PC. Predicting the effects of coding non-synonymous variants on protein function using the SIFT algorithm. *Nat Protoc*, 4, 1073–1081 (2009).

390. Adzhubei IA, Schmidt S, Peshkin L, et al. A method and server for predicting damaging missense mutations. *Nat Methods*, 7, 248–249 (2010).

391. Schwarz JM, Cooper DN, Schuelke M, et al. MutationTaster2: mutation prediction for the deep-sequencing age. *Nat Methods*, 11, 361–362 (2014).

392. Coutelier M, Coarelli G, Monin M-L, et al. A panel study on patients with dominant cerebellar ataxia highlights the frequency of channelopathies. *Brain*, 140, 1579–1594 (2017).

393. Richards S, Aziz N, Bale S, et al. Standards and guidelines for the interpretation of sequence variants: a joint consensus recommendation of the American College of Medical Genetics and Genomics and the Association for Molecular Pathology. *Genet Med*, 17, 405–423 (2015).

394. Abecasis GR, Cherny SS, Cookson WO, et al. Merlin—rapid analysis of dense genetic maps using sparse gene flow trees. *Nat Genet*, 30, 97–101 (2002).

395. Cottingham RW, Idury RM, Schäffer AA. Faster sequential genetic linkage computations. *Am J Hum Genet*, 53, 252–63 (1993).

396. Broman KW, Murray JC, Sheffield VC, et al. Comprehensive Human Genetic Maps: Individual and Sex-Specific Variation in Recombination. *Am J Hum Genet*, 63, 861–869 (1998).

397. Kong A, Gudbjartsson DF, Sainz J, et al. A high-resolution recombination map of the human genome. *Nat Genet*, 31, 241–247 (2002).

398. Dib C, Fauré S, Fizames C, et al. A comprehensive genetic map of the human genome based on 5,264 microsatellites. *Nature*, 380, 152–154 (1996).

399. Schäffer AA, Gupta SK, Shriram K, et al. Avoiding Recomputation in Linkage Analysis. *Hum Hered*, 44, 225–237 (1994).

400. Ott J. Computer-simulation methods in human linkage analysis. *Proc Natl Acad Sci U S A*, 86, 4175–8 (1989).

401. Li H, Handsaker B, Wysoker A, et al. The Sequence Alignment/Map format and SAMtools. *Bioinformatics*, 25, 2078–2079 (2009).

402. Flicek P, Amode MR, Barrell D, et al. Ensembl 2012. *Nucleic Acids Res*, 40, D84–D90 (2012).

403. Ng SB, Buckingham KJ, Lee C, et al. Exome sequencing identifies the cause of a mendelian disorder. *Nat Genet*, 42, 30–35 (2010).

404. Marco-Sola S, Sammeth M, Guigó R, et al. The GEM mapper: fast, accurate and versatile alignment by filtration. *Nat Methods*, 9, 1185–1188 (2012).

405. Cingolani P, Platts A, Wang LL, et al. A program for annotating and predicting the effects of single nucleotide polymorphisms, SnpEff. *Fly (Austin)*, 6, 80–92 (2012).

406. Wang K, Li M, Hakonarson H. ANNOVAR: functional annotation of genetic variants from high-throughput sequencing data. *Nucleic Acids Res*, 38, e164–e164 (2010).

407. Liu X, Wu C, Li C, et al. dbNSFP v3.0: A One-Stop Database of Functional Predictions and Annotations for Human Nonsynonymous and Splice-Site SNVs. *Hum Mutat*, 37, 235–241 (2016).

408. Vaser R, Adusumalli S, Leng SN, et al. SIFT missense predictions for genomes. *Nat Protoc*, 11, 1–9 (2016).

409. Adzhubei I, Jordan DM, Sunyaev SR. Predicting functional effect of human missense mutations using PolyPhen-2. *Curr Protoc Hum Genet* (2013).

410. Shihab HA, Gough J, Cooper DN, et al. Predicting the functional consequences of cancer-associated amino acid substitutions. *Bioinformatics*, 29, 1504–1510 (2013).

411. Reva B, Antipin Y, Sander C. Predicting the functional impact of protein mutations: application to cancer genomics. *Nucleic Acids Res*, 39, e118–e118 (2011).

412. Choi Y, Sims GE, Murphy S, et al. Predicting the Functional Effect of Amino Acid Substitutions and Indels. *PLoS One*, 7, e46688 (2012).

413. Rentzsch P, Witten D, Cooper GM, et al. CADD: predicting the deleteriousness of variants throughout the human genome. *Nucleic Acids Res*, 47, D886–D894 (2019).

414. Barnett DW, Garrison EK, Quinlan AR, et al. BamTools: a C++ API and toolkit for analyzing and managing BAM files. *Bioinformatics*, 27, 1691–1692 (2011).

415. Zerbino DR, Birney E. Velvet: Algorithms for de novo short read assembly using de Bruijn graphs. *Genome Res*, 18, 821–829 (2008).

416. Fan X, Abbott TE, Larson D, et al. BreakDancer: Identification of Genomic Structural Variation from Paired-End Read Mapping. *Curr Protoc Bioinforma*, 45, 15.6.1–11 (2014).

417. Zhang J, Wang J, Wu Y. An improved approach for accurate and efficient calling of structural variations with low-coverage sequence data. *BMC Bioinformatics*, 13, S6 (2012).

418. Sindi S, Helman E, Bashir A, et al. A geometric approach for classification and comparison of structural variants. *Bioinformatics*, 25, i222–i230 (2009).

419. Tempel S. Using and understanding RepeatMasker. *Methods Mol Biol*, 859, 29–51 (2012).

420. Zerbino DR, Achuthan P, Akanni W, et al. Ensembl 2018. *Nucleic Acids Res*, 46, D754–D761 (2018).

421. Lennon G, Auffray C, Polymeropoulos M, et al. The I.M.A.G.E. Consortium: An Integrated Molecular Analysis of Genomes and Their Expression. *Genomics*, 33, 151–152 (1996).

422. Kovacs GG. Invited review: Neuropathology of tauopathies: principles and practice. *Neuropathol Appl*

*Neurobiol*, 41, 3–23 (2015).

423. Moms JC, Heyman A, Mohs RC, et al. The Consortium to Establish a Registry for Alzheimer's Disease (CERAD). Part I. Clinical and neuropsychological assesment of Alzheimer's disease. *Neurology*, 39, 1159–1159 (1989).

424. Mirra SS, Heyman A, McKeel D, et al. The Consortium to Establish a Registry for Alzheimer's Disease (CERAD): Part II. Standardization of the neuropathologic assessment of Alzheimer's disease. *Neurology*, 41, 479–479 (1991).

425. Braak H, Alafuzoff I, Arzberger T, et al. Staging of Alzheimer disease-associated neurofibrillary pathology using paraffin sections and immunocytochemistry. *Acta Neuropathol*, 112, 389–404 (2006).

426. Thal DR, Rüb U, Orantes M, et al. Phases of Aβ-deposition in the human brain and its relevance for the development of AD. *Neurology*, 58, 1791–1800 (2002).

427. Jackson JF, Currier RD, Morton NE. Dominant Spinocerebellar Ataxia: Genetic Counseling. *J Neurogenet*, 1, 87–90 (1983).

428. Braak H, Rüb U, Del Tredici K. Involvement of precerebellar nuclei in multiple system atrophy. *Neuropathol Appl Neurobiol*, 29, 60–76 (2003).

429. Schindelin J, Rueden CT, Hiner MC, et al. The ImageJ ecosystem: An open platform for biomedical image analysis. *Mol Reprod Dev*, 82, 518–529 (2015).

430. Livak KJ, Schmittgen TD. Analysis of Relative Gene Expression Data Using Real-Time Quantitative PCR and the 2−ΔΔCT Method. *Methods*, 25, 402–408 (2001).

431. Dunham I, Kundaje A, Aldred SF, et al. An integrated encyclopedia of DNA elements in the human genome. *Nature*, 489, 57–74 (2012).

432. Anders S, Pyl PT, Huber W. HTSeq--a Python framework to work with high-throughput sequencing data. *Bioinformatics*, 31, 166–169 (2015).

433. Paz I, Kosti I, Ares M, et al. RBPmap: a web server for mapping binding sites of RNA-binding proteins. *Nucleic Acids Res*, 42, W361–W367 (2014).

434. Messeguer X, Escudero R, Farre D, et al. PROMO: detection of known transcription regulatory elements using species-tailored searches. *Bioinformatics*, 18, 333–334 (2002).

435. Hu B, Jin J, Guo A-Y, et al. GSDS 2.0: an upgraded gene feature visualization server. *Bioinformatics*, 31, 1296–1297 (2015).

436. Lehle S, Hildebrand DG, Merz B, et al. LORD-Q: a long-run real-time PCR-based DNA-damage quantification method for nuclear and mitochondrial genome analysis. *Nucleic Acids Res*, 42, e41–e41 (2014).

437. Hildebrand A, Remmert M, Biegert A, et al. Fast and accurate automatic structure prediction with

HHpred. *Proteins Struct Funct Bioinforma*, 77, 128–132 (2009).

438. Zhou Y, Yang S, Mao T, et al. MAPanalyzer: a novel online tool for analyzing microtubule-associated proteins. *Database*, 2015, bav108 (2015).

439. Yachdav G, Kloppmann E, Kajan L, et al. PredictProtein—an open resource for online prediction of protein structural and functional features. *Nucleic Acids Res*, 42, W337–W343 (2014).

440. Linding R, Jensen LJ, Diella F, et al. Protein Disorder Prediction. *Structure*, 11, 1453–1459 (2003).

441. Mitchell AL, Attwood TK, Babbitt PC, et al. InterPro in 2019: improving coverage, classification and access to protein sequence annotations. *Nucleic Acids Res*, 47, D351–D360 (2019).

442. Necci M, Piovesan D, Dosztányi Z, et al. MobiDB-lite: fast and highly specific consensus prediction of intrinsic disorder in proteins. *Bioinformatics*, 33, 1402–1404 (2017).

443. Blom N, Gammeltoft S, Brunak S. Sequence and structure-based prediction of eukaryotic protein phosphorylation sites. *J Mol Biol*, 294, 1351–1362 (1999).

444. Horn H, Schoof EM, Kim J, et al. KinomeXplorer: an integrated platform for kinome biology studies. *Nat Methods*, 11, 603–604 (2014).

445. Szklarczyk D, Gable AL, Lyon D, et al. STRING v11: protein–protein association networks with increased coverage, supporting functional discovery in genome-wide experimental datasets. *Nucleic Acids Res*, 47, D607–D613 (2019).

446. Parodi L, Coarelli G, Stevanin G, et al. Hereditary ataxias and paraparesias. *Curr Opin Neurol*, 31, 462–471 (2018).

447. Duarri A, Nibbeling EAR, Fokkens MR, et al. Functional Analysis Helps to Define KCNC3 Mutational Spectrum in Dutch Ataxia Cases. *PLoS One*, 10, e0116599 (2015).

448. Iwaki A, Kawano Y, Miura S, et al. Heterozygous deletion of ITPR1, but not SUMF1, in spinocerebellar ataxia type 16. *J Med Genet*, 45, 32–35 (2007).

449. Echeveste B, Covarrubias E, Cabello JP, et al. Isolated palatal tremor as unique clinical manifestation of SCA 18 due to a new mutation of IFRD1. *Parkinsonism Relat Disord*, 42, 100–101 (2017).

450. Löbbe AM, Kang J-S, Hilker R, et al. A Novel Missense Mutation in AFG3L2 Associated with Late Onset and Slow Progression of Spinocerebellar Ataxia Type 28. *J Mol Neurosci*, 52, 493–496 (2014).

451. Szpisjak L, Nemeth VL, Szepfalusi N, et al. Neurocognitive Characterization of an SCA28 Family Caused by a Novel AFG3L2 Gene Mutation. *The Cerebellum*, 16, 979–985 (2017).

452. Musova Z, Kaiserova M, Kriegova E, et al. A Novel Frameshift Mutation in the AFG3L2 Gene in a Patient with Spinocerebellar Ataxia. *The Cerebellum*, 13, 331–337 (2014).

453. Lin C-C, Gan S-R, Gupta D, et al. Hispanic Spinocerebellar Ataxia Type 35 (SCA35) with a Novel Frameshift Mutation. *The Cerebellum*, 18, 291–294 (2019).

454. Yang Z, Shi M, Liu Y, et al. TGM6 gene mutations in undiagnosed cerebellar ataxia patients. *Parkinsonism Relat Disord*, 46, 84–86 (2018).

455. Graves TD, Imbrici P, Kors EE, et al. Premature stop codons in a facilitating EF-hand splice variant of CaV2.1 cause episodic ataxia type 2. *Neurobiol Dis*, 32, 10–15 (2008).

456. Balck A, Tunc S, Schmitz J, et al. A Novel Frameshift CACNA1A Mutation Causing Episodic Ataxia Type 2. *The Cerebellum*, 17, 504–506 (2018).

457. Condliffe SB, Fratangeli A, Munasinghe NR, et al. The E1015K Variant in the Synprint Region of the Ca V 2.1 Channel Alters Channel Function and Is Associated with Different Migraine Phenotypes. *J Biol Chem*, 288, 33873–33883 (2013).

458. Grieco GS, Gagliardi S, Ricca I, et al. New CACNA1A deletions are associated to migraine phenotypes. *J Headache Pain*, 19, 75 (2018).

459. Bonifert T, Karle KN, Tonagel F, et al. Pure and syndromic optic atrophy explained by deep intronic OPA1 mutations and an intralocus modifier. *Brain*, 137, 2164–2177 (2014).

460. Sitarz KS, Yu-Wai-Man P, Pyle A, et al. MFN2 mutations cause compensatory mitochondrial DNA proliferation. *Brain*, 135, e219–e219 (2012).

461. Peretti A, Perie M, Vincent D, et al. LRSAM1 variants and founder effect in French families with ataxic form of Charcot-Marie-Tooth type 2. *Eur J Hum Genet*, 27, 1406–1418 (2019).

462. Engelfried K, Vorgerd M, Hagedorn M, et al. Charcot-Marie-Tooth neuropathy type 2A: novel mutations in the mitofusin 2 gene (MFN2). *BMC Med Genet*, 7, 53 (2006).

463. Synofzik M, Schüle R. Overcoming the divide between ataxias and spastic paraplegias: Shared phenotypes, genes, and pathways. *Mov Disord*, 32, 332–345 (2017).

464. Megahed H, Nicouleau M, Barcia G, et al. Utility of whole exome sequencing for the early diagnosis of pediatric-onset cerebellar atrophy associated with developmental delay in an inbred population. *Orphanet J Rare Dis*, 11, 57 (2016).

465. Ohba C, Haginoya K, Osaka H, et al. De novo KIF1A mutations cause intellectual deficit, cerebellar atrophy, lower limb spasticity and visual disturbance. *J Hum Genet*, 60, 739–742 (2015).

466. Mancini C, Giorgio E, Rubegni A, et al. Prevalence and phenotype of the c.1529C>T SPG7 variant in adult-onset cerebellar ataxia in Italy. *Eur J Neurol*, 26, 80–86 (2019).

467. Sánchez-Ferrero E, Coto E, Beetz C, et al. SPG7 mutational screening in spastic paraplegia patients supports a dominant effect for some mutations and a pathogenic role for p.A510V. *Clin Genet*, 83, 257–262 (2013).

468. Van Damme P, Veldink JH, van Blitterswijk M, et al. Expanded ATXN2 CAG repeat size in ALS identifies genetic overlap between ALS and SCA2. *Neurology*, 76, 2066–2072 (2011).

469. Meloni M, Farris R, Solla P, et al. C9ORF72 Intermediate Repeat Expansion in a Patient With Psychiatric Disorders and Progressive Cerebellar Ataxia. *Neurologist*, 22, 245–246 (2017).

470. Hirano M, Quinzii CM, Mitsumoto H, et al. Senataxin mutations and amyotrophic lateral sclerosis. *Amyotroph Lateral Scler*, 12, 223–227 (2011).

471. Ticozzi N, Vance C, LeClerc AL, et al. Mutational analysis reveals the FUS homolog TAF15 as a candidate gene for familial amyotrophic lateral sclerosis. *Am J Med Genet Part B Neuropsychiatr Genet*, 156, 285–290 (2011).

472. Kim H-J, Oh K-W, Kwon M-J, et al. Identification of mutations in Korean patients with amyotrophic lateral sclerosis using multigene panel testing. *Neurobiol Aging*, 37, 209.e9-209.e16 (2016).

473. Rossi M, Balint B, Millar Vernetti P, et al. Genetic Dystonia-ataxia Syndromes: Clinical Spectrum, Diagnostic Approach, and Treatment Options. *Mov Disord Clin Pract*, 5, 373–382 (2018).

474. Xiao J, Uitti RJ, Zhao Y, et al. Mutations in CIZ1 cause adult onset primary cervical dystonia. *Ann Neurol*, 71, 458–469 (2012).

475. Chelban V, Wiethoff S, Fabian-Jessing BK, et al. Genotype-phenotype correlations, dystonia and disease progression in spinocerebellar ataxia type 14. *Mov Disord*, 33, 1119–1129 (2018).

476. Lynch DS, Rodrigues Brandão de Paiva A, Zhang WJ, et al. Clinical and genetic characterization of leukoencephalopathies in adults. *Brain*, 140, 1204–1211 (2017).

477. Rademakers R, Baker M, Nicholson AM, et al. Mutations in the colony stimulating factor 1 receptor (CSF1R) gene cause hereditary diffuse leukoencephalopathy with spheroids. *Nat Genet*, 44, 200–205 (2012).

478. Konno T, Tada M, Tada M, et al. Haploinsufficiency of CSF-1R and clinicopathologic characterization in patients with HDLS. *Neurology*, 82, 139–148 (2014).

479. Moskowitz AM, Belnap N, Siniard AL, et al. A de novo missense mutation in ZMYND11 is associated with global developmental delay, seizures, and hypotonia. *Mol Case Stud*, 2, a000851 (2016).

480. Zanni G, Bertini ES. X-linked disorders with cerebellar dysgenesis. *Orphanet J Rare Dis*, 6, 24 (2011).

481. Viollet L, Glusman G, Murphy KJ, et al. Alternating Hemiplegia of Childhood: Retrospective Genetic Study and Genotype-Phenotype Correlations in 187 Subjects from the US AHCF Registry. *PLoS One*, 10, e0127045 (2015).

482. Baets J, Duan X, Wu Y, et al. Defects of mutant DNMT1 are linked to a spectrum of neurological disorders. *Brain*, 138, 845–861 (2015).

483. Coutelier M, Burglen L, Mundwiller E, et al. GRID2 mutations span from congenital to mild adult-onset cerebellar ataxia. *Neurology*, 84, 1751–1759 (2015).

484. Seixas AI, Loureiro JR, Costa C, et al. A Pentanucleotide ATTTC Repeat Insertion in the Non-coding

Region of DAB1 , Mapping to SCA37 , Causes Spinocerebellar Ataxia. *Am J Hum Genet*, 101, 87–103 (2017).

485. Corral-Juan M, Serrano-Munuera C, Rábano A, et al. Clinical, genetic and neuropathological characterization of spinocerebellar ataxia type 37. *Brain*, 141, 1981–1997 (2018).

486. Jacobi H, Bauer P, Giunti P, et al. The natural history of spinocerebellar ataxia type 1, 2, 3, and 6: A 2-year follow-up study. *Neurology*, 77, 1035–1041 (2011).

487. Kohno S, Kohno T, Nakano Y, et al. Mechanism and significance of specific proteolytic cleavage of Reelin. *Biochem Biophys Res Commun*, 380, 93–97 (2009).

488. Bar I, Tissir F, Lambert de Rouvroit C, et al. The Gene Encoding Disabled-1 (DAB1), the Intracellular Adaptor of the Reelin Pathway, Reveals Unusual Complexity in Human and Mouse. *J Biol Chem*, 278, 5802–5812 (2003).

489. Yano M, Hayakawa-Yano Y, Mele A, et al. Nova2 Regulates Neuronal Migration through an RNA Switch in Disabled-1 Signaling. *Neuron*, 66, 848–858 (2010).

490. Robertson AD. Intramolecular interactions at protein surfaces and their impact on protein function. *Trends Biochem Sci*, 27, 521–6 (2002).

491. Nagamachi A, Matsui H, Asou H, et al. Haploinsufficiency of SAMD9L, an Endosome Fusion Facilitator, Causes Myeloid Malignancies in Mice Mimicking Human Diseases with Monosomy 7. *Cancer Cell*, 24, 305–317 (2013).

492. Nissanka N, Moraes CT. Mitochondrial DNA damage and reactive oxygen species in neurodegenerative disease. *FEBS Lett*, 592, 728–742 (2018).

493. Itoh K, Adachi Y, Yamada T, et al. A brain-enriched drp1 isoform associates with lysosomes, late endosomes, and the plasma membrane. *J Biol Chem*, 293, 11809–11822 (2018).

494. Fukumitsu K, Hatsukano T, Yoshimura A, et al. Mitochondrial fission protein Drp1 regulates mitochondrial transport and dendritic arborization in cerebellar Purkinje cells. *Mol Cell Neurosci*, 71, 56–65 (2016).

495. Sun M, Johnson AK, Nelakuditi V, et al. Targeted exome analysis identifies the genetic basis of disease in over 50% of patients with a wide range of ataxia-related phenotypes. *Genet Med*, 21, 195–206 (2019).

496. Ngo KJ, Rexach JE, Lee H, et al. A diagnostic ceiling for exome sequencing in cerebellar ataxia and related neurological disorders. *Hum Mutat*, 41, 487–501 (2020).

497. Németh AH, Kwasniewska AC, Lise S, et al. Next generation sequencing for molecular diagnosis of neurological disorders using ataxias as a model. *Brain*, 136, 3106–3118 (2013).

498. Lee H, Deignan JL, Dorrani N, et al. Clinical Exome Sequencing for Genetic Identification of Rare Mendelian Disorders. *JAMA*, 312, 1880 (2014).

499. Farwell KD, Shahmirzadi L, El-Khechen D, et al. Enhanced utility of family-centered diagnostic exome sequencing with inheritance model–based analysis: results from 500 unselected families with undiagnosed genetic conditions. *Genet Med*, 17, 578–586 (2015).

500. Keogh MJ, Steele H, Douroudis K, et al. Frequency of rare recessive mutations in unexplained late onset cerebellar ataxia. *J Neurol*, 262, 1822–1827 (2015).

501. Pyle A, Smertenko T, Bargiela D, et al. Exome sequencing in undiagnosed inherited and sporadic ataxias. *Brain*, 138, 276–283 (2015).

502. Marelli C, Guissart C, Hubsch C, et al. Mini-Exome Coupled to Read-Depth Based Copy Number Variation Analysis in Patients with Inherited Ataxias. *Hum Mutat*, 37, 1340–1353 (2016).

503. van de Warrenburg BP, Schouten MI, de Bot ST, et al. Clinical exome sequencing for cerebellar ataxia and spastic paraplegia uncovers novel gene–disease associations and unanticipated rare disorders. *Eur J Hum Genet*, 24, 1460–1466 (2016).

504. Montaut S, Tranchant C, Drouot N, et al. Assessment of a Targeted Gene Panel for Identification of Genes Associated With Movement Disorders. *JAMA Neurol*, 75, 1234 (2018).

505. Kim M, Kim AR, Kim JS, et al. Clarification of undiagnosed ataxia using whole-exome sequencing with clinical implications. *Parkinsonism Relat Disord*, 80, 58–64 (2020).

506. Amarasinghe SL, Su S, Dong X, et al. Opportunities and challenges in long-read sequencing data analysis. *Genome Biol*, 21, 30 (2020).

507. Duque KR, Marsili L, Sturchio A, et al. Progressive Ataxia with Hemiplegic Migraines: a Phenotype of CACNA1A Missense Mutations, Not CAG Repeat Expansions. *The Cerebellum* (2020).

508. Gerber S, Alzayady KJ, Burglen L, et al. Recessive and Dominant De Novo ITPR1 Mutations Cause Gillespie Syndrome. *Am J Hum Genet*, 98, 971–980 (2016).

509. Zambonin JL, Bellomo A, Ben-Pazi H, et al. Spinocerebellar ataxia type 29 due to mutations in ITPR1: a case series and review of this emerging congenital ataxia. *Orphanet J Rare Dis*, 12, 121 (2017).

510. Tipton PW, Guthrie K, Strongosky A, et al. Spinocerebellar ataxia 15: A phenotypic review and expansion. *Neurol Neurochir Pol*, 51, 86–91 (2017).

511. Almajan ER, Richter R, Paeger L, et al. AFG3L2 supports mitochondrial protein synthesis and Purkinje cell survival. *J Clin Invest*, 122, 4048–4058 (2012).

512. Kirwan AF, Bibby AC, Mvilongo T, et al. Inhibition of protein kinase C catalytic activity by additional regions within the human protein kinase Calpha-regulatory domain lying outside of the pseudosubstrate sequence. *Biochem J*, 373, 571–581 (2003).

513. Magri S, Fracasso V, Plumari M, et al. Concurrent AFG3L2 and SPG7 mutations associated with syndromic parkinsonism and optic atrophy with aberrant OPA1 processing and mitochondrial network fragmentation. *Hum Mutat*, 39, 2060–2071 (2018).

514. Figueroa KP, Coon H, Santos N, et al. Genetic analysis of age at onset variation in spinocerebellar ataxia type 2. *Neurol Genet*, 3, e155 (2017).

515. Nam SH, Kanwal S, Nam DE, et al. Association of miR-149 polymorphism with onset age and severity in Charcot–Marie–Tooth disease type 1A. *Neuromuscul Disord*, 28, 502–507 (2018).

516. Galatolo D, Tessa A, Filla A, et al. Clinical application of next generation sequencing in hereditary spinocerebellar ataxia: increasing the diagnostic yield and broadening the ataxia-spasticity spectrum. A retrospective analysis. *Neurogenetics*, 19, 1–8 (2018).

517. Nibbeling EAR, Delnooz CCS, de Koning TJ, et al. Using the shared genetics of dystonia and ataxia to unravel their pathogenesis. *Neurosci Biobehav Rev*, 75, 22–39 (2017).

518. Laurá M, Pipis M, Rossor AM, et al. Charcot–Marie–Tooth disease and related disorders. *Curr Opin Neurol*, 32, 641–650 (2019).

519. Nicita F, Ginevrino M, Travaglini L, et al. Heterozygous KIF1A variants underlie a wide spectrum of neurodevelopmental and neurodegenerative disorders. *J Med Genet*, jmedgenet-2020-107007 (2020).

520. Mathis S, Duval F, Soulages A, et al. The ataxic neuropathies. *J Neurol* (2020).

521. Verhoeven K, De Jonghe P, Van de Putte T, et al. Slowed Conduction and Thin Myelination of Peripheral Nerves Associated with Mutant Rho Guanine-Nucleotide Exchange Factor 10. *Am J Hum Genet*, 73, 926–932 (2003).

522. De Jonghe P, Timmerman V, Nelis E, et al. A Novel Type of Hereditary Motor and Sensory Neuropathy Characterized by a Mild Phenotype. *Arch Neurol*, 56, 1283 (1999).

523. Hu B, Arpag S, Zuchner S, et al. A novel missense mutation of CMT2P alters transcription machinery. *Ann Neurol*, 80, 834–845 (2016).

524. Rouzier C, Bannwarth S, Chaussenot A, et al. The MFN2 gene is responsible for mitochondrial DNA instability and optic atrophy “plus” phenotype. *Brain*, 135, 23–34 (2012).

525. Ahmad KE, Davis RL, Sue CM. A novel OPA1 mutation causing variable age of onset autosomal dominant optic atrophy plus in an Australian family. *J Neurol*, 262, 2323–2328 (2015).

526. Chakravorty S, Logan R, Elson MJ, et al. Expanding the genotype–phenotype correlation of childhood sensory polyneuropathy of genetic origin. *Sci Rep*, 10, 16184 (2020).

527. Van Hove JLK, Cunningham V, Rice C, et al. Finding twinkle in the eyes of a 71-year-old lady: A case report and review of the genotypic and phenotypic spectrum of TWINKLE-related dominant disease. *Am J Med Genet Part A*, 149A, 861–867 (2009).

528. Chen S, Sayana P, Zhang X, et al. Genetics of amyotrophic lateral sclerosis: an update. *Mol Neurodegener*, 8, 28 (2013).

529. Siddique N, Siddique T. Genetics of Amyotrophic Lateral Sclerosis. *Phys Med Rehabil Clin N Am*, 19,

429–439 (2008).

530. Brown JA, Min J, Staropoli JF, et al. SOD1, ANG, TARDBP and FUS mutations in amyotrophic lateral sclerosis: A United States clinical testing lab experience. *Amyotroph Lateral Scler*, 13, 217–222 (2012).

531. Niemann S. Familial ALS in Germany: origin of the R115G SOD1 mutation by a founder effect. *J Neurol Neurosurg Psychiatry*, 75, 1186–1188 (2004).

532. Felbecker A, Camu W, Valdmanis PN, et al. Four familial ALS pedigrees discordant for two SOD1 mutations: are all SOD1 mutations pathogenic? *J Neurol Neurosurg Psychiatry*, 81, 572–577 (2010).

533. Park JH, Elpers C, Reunert J, et al. SOD1 deficiency: a novel syndrome distinct from amyotrophic lateral sclerosis. *Brain*, 142, 2230–2237 (2019).

534. Koeppen AH. The neuropathology of the adult cerebellum. *Handb Clin Neurol*, 129–149 (2018).

535. Sassi C, Nalls MA, Ridge PG, et al. Mendelian adult-onset leukodystrophy genes in Alzheimer's disease: critical influence of CSF1R and NOTCH3. *Neurobiol Aging*, 66, 179.e17-179.e29 (2018).

536. Konno T, Kasanuki K, Ikeuchi T, et al. CSF1R -related leukoencephalopathy. *Neurology*, 91, 1092–1104 (2018).

537. Bereznyakova O, Dupré N. Spastic ataxias. *Handb Clin Neurol*, 191–203 (2018).

538. Finsterer J, Löscher W, Quasthoff S, et al. Hereditary spastic paraplegias with autosomal dominant, recessive, X-linked, or maternal trait of inheritance. *J Neurol Sci*, 318, 1–18 (2012).

539. Pfeffer G, Pyle A, Griffin H, et al. SPG7 mutations are a common cause of undiagnosed ataxia. *Neurology*, 84, 1174–1176 (2015).

540. Casari G, De Fusco M, Ciarmatori S, et al. Spastic Paraplegia and OXPHOS Impairment Caused by Mutations in Paraplegin, a Nuclear-Encoded Mitochondrial Metalloprotease. *Cell*, 93, 973–983 (1998).

541. Klebe S, Depienne C, Gerber S, et al. Spastic paraplegia gene 7 in patients with spasticity and/or optic neuropathy. *Brain*, 135, 2980–2993 (2012).

542. Bot ST, Vermeer S, Buijsman W, et al. Pure adult-onset Spastic Paraplegia caused by a novel mutation in the KIAA0196 (SPG8) gene. *J Neurol*, 260, 1765–1769 (2013).

543. Lin P, Li J, Liu Q, et al. A Missense Mutation in SLC33A1, which Encodes the Acetyl-CoA Transporter, Causes Autosomal-Dominant Spastic Paraplegia (SPG42). *Am J Hum Genet*, 83, 752–759 (2008).

544. Bremova-Ertl T, Schiffmann R, Patterson MC, et al. Oculomotor and Vestibular Findings in Gaucher Disease Type 3 and Their Correlation with Neurological Findings. *Front Neurol*, 8 (2018).

545. Fogel BL, Lee H, Deignan JL, et al. Exome Sequencing in the Clinical Diagnosis of Sporadic or Familial Cerebellar Ataxia. *JAMA Neurol*, 71, 1237 (2014).

546. Hills LB, Masri A, Konno K, et al. Deletions in GRID2 lead to a recessive syndrome of cerebellar ataxia and tonic upgaze in humans. *Neurology*, 81, 1378–1386 (2013).

547. Sweadner KJ, Toro C, Whitlow CT, et al. ATP1A3 Mutation in Adult Rapid-Onset Ataxia. *PLoS One*, 11, e0151429 (2016).

548. Winkelmann J, Lin L, Schormair B, et al. Mutations in DNMT1 cause autosomal dominant cerebellar ataxia, deafness and narcolepsy. *Hum Mol Genet*, 21, 2205–2210 (2012).

549. Algahtani H, Shirah B. A novel mutation in the DNMT1 gene in a patient presenting with pure cerebellar ataxia. *J Genet Med*, 14, 71–74 (2017).

550. Bi H, Hojo K, Watanabe M, et al. Expanded genetic insight and clinical experience of DNMT1-complex disorder. *Neurol Genet*, 6, e456 (2020).

551. Teive HAG, Arruda WO. Cognitive dysfunction in spinocerebellar ataxias. *Dement Neuropsychol*, 3, 180–187 (2009).

552. Kraus K, Kleene R, Braren I, et al. A fragment of adhesion molecule L1 is imported into mitochondria, and regulates mitochondrial metabolism and trafficking. *J Cell Sci*, 131, jcs210500 (2018).

553. Paulson H. Repeat expansion diseases. *Handbook of Clinical Neurology* (2018).

554. Groh M, Silva LM, Gromak N. Mechanisms of transcriptional dysregulation in repeat expansion disorders. *Biochem Soc Trans*, 42, 1123–1128 (2014).

555. Lin CH, Chen CM, Hou YT, et al. The CAG repeat in SCA12 functions as a cis element to up-regulate PPP2R2B expression. *Hum Genet*, 128, 205–212 (2010).

556. Naumann A, Hochstein N, Weber S, et al. A Distinct DNA-Methylation Boundary in the 5′- Upstream Sequence of the FMR1 Promoter Binds Nuclear Proteins and Is Lost in Fragile X Syndrome. *Am J Hum Genet*, 85, 606–616 (2009).

557. Zu T, Gibbens B, Doty NS, et al. Non-ATG-initiated translation directed by microsatellite expansions. *Proc Natl Acad Sci U S A*, 108, 260–5 (2011).

558. Donnelly CJ, Zhang P-W, Pham JT, et al. RNA Toxicity from the ALS/FTD C9ORF72 Expansion Is Mitigated by Antisense Intervention. *Neuron*, 80, 415–428 (2013).

559. Ishiguro T, Sato N, Ueyama M, et al. Regulatory Role of RNA Chaperone TDP-43 for RNA Misfolding and Repeat-Associated Translation in SCA31. *Neuron*, 94, 108-124.e7 (2017).

560. Bañez-Coronel M, Ayhan F, Tarabochia AD, et al. RAN Translation in Huntington Disease. *Neuron*, 88, 667–677 (2015).

561. Gourdon G, Meola G. Myotonic Dystrophies: State of the Art of New Therapeutic Developments for the CNS. *Front Cell Neurosci*, 11 (2017).

562. Kong HE, Zhao J, Xu S, et al. Fragile X-Associated Tremor/Ataxia Syndrome: From Molecular Pathogenesis to Development of Therapeutics. *Front Cell Neurosci*, 11 (2017).

563. Antonellis A, Ellsworth RE, Sambuughin N, et al. Glycyl tRNA Synthetase Mutations in Charcot-

Marie-Tooth Disease Type 2D and Distal Spinal Muscular Atrophy Type V. *Am J Hum Genet*, 72, 1293–1299 (2003).

564. Jordanova A, Irobi J, Thomas FP, et al. Disrupted function and axonal distribution of mutant tyrosyl-tRNA synthetase in dominant intermediate Charcot-Marie-Tooth neuropathy. *Nat Genet*, 38, 197–202 (2006).

565. Calado A, Tome FMS, Brais B, et al. Nuclear inclusions in oculopharyngeal muscular dystrophy consist of poly(A) binding protein 2 aggregates which sequester poly(A) RNA. *Hum Mol Genet*, 9, 2321–2328 (2000).

566. Gabanella F, Butchbach MER, Saieva L, et al. Ribonucleoprotein Assembly Defects Correlate with Spinal Muscular Atrophy Severity and Preferentially Affect a Subset of Spliceosomal snRNPs. *PLoS One*, 2, e921 (2007).

567. Galka-Marciniak P, Urbanek MO, Krzyzosiak WJ. Triplet repeats in transcripts: structural insights into RNA toxicity. *Biol Chem*, 393, 1299–315 (2012).

568. Barker H V., Niblock M, Lee Y-B, et al. RNA Misprocessing in C9orf72-Linked Neurodegeneration. *Front Cell Neurosci*, 11, 195 (2017).

569. Palladino G, Nicolia V, Kovacs GG, et al. Sexually Dimorphic Expression of Reelin in the Brain of a Mouse Model of Alzheimer Disease. *J Mol Neurosci*, 61, 359–367 (2017).

570. Magliaro C, Cocito C, Bagatella S, et al. The number of Purkinje neurons and their topology in the cerebellar vermis of normal and reln haplodeficient mouse. *Ann Anat*, 207, 68–75 (2016).

571. HadjSahraoui N, Frederic F, DelhayeBouchaud N, et al. Gender effect on Purkinje cell loss in the cerebellum of the heterozygous reeler mouse. *J Neurogenet*, 11, 45–58 (1996).

572. Gross CM, Flubacher A, Tinnes S, et al. Early life stress stimulates hippocampal reelin gene expression in a sex-specific manner: Evidence for corticosterone-mediated action. *Hippocampus*, 22, 409–420 (2012).

573. Velázquez-Pérez L, Seifried C, Santos-Falcón N, et al. Saccade velocity is controlled by polyglutamine size in spinocerebellar ataxia 2. *Ann Neurol*, 56, 444–7 (2004).

574. Wadia N, Pang J, Desai J, et al. A clinicogenetic analysis of six Indian spinocerebellar ataxia (SCA2) pedigrees. The significance of slow saccades in diagnosis. *Brain*, 121 Pt 1, 2341–55 (1998).

575. Seifried C, Velázquez-Pérez L, Santos-Falcón N, et al. Saccade velocity as a surrogate disease marker in spinocerebellar ataxia type 2. *Ann N Y Acad Sci*, 1039, 524–7 (2005).

576. Bürk K, Fetter M, Abele M, et al. Autosomal dominant cerebellar ataxia type I: oculomotor abnormalities in families with SCA1, SCA2, and SCA3. *J Neurol*, 246, 789–97 (1999).

577. Christova P, Anderson JH, Gomez CM. Impaired Eye Movements in Presymptomatic Spinocerebellar Ataxia Type 6. *Arch Neurol*, 65, 530 (2008).

578. Day JW, Schut LJ, Moseley ML, et al. Spinocerebellar ataxia type 8: clinical features in a large family. *Neurology*, 55, 649–57 (2000).

579. Velázquez-Pérez L, Seifried C, Abele M, et al. Saccade velocity is reduced in presymptomatic spinocerebellar ataxia type 2. *Clin Neurophysiol*, 120, 632–5 (2009).

580. Raposo M, Vasconcelos J, Bettencourt C, et al. Nystagmus as an early ocular alteration in Machado-Joseph disease (MJD/SCA3). *BMC Neurol*, 14, 17 (2014).

581. Wessel K, Moschner C, Wandinger KP, et al. Oculomotor testing in the differential diagnosis of degenerative ataxic disorders. *Arch Neurol*, 55, 949–56 (1998).

582. Henn V, Hepp K, Buttner-Ennever JA. The primate oculomotor system. II. Premotor system. A synthesis of anatomical, physiological, and clinical data. *Hum Neurobiol*, 1, 87–95 (1982).

583. Voogd J, Schraa-Tam CKL, van der Geest JN, et al. Visuomotor cerebellum in human and nonhuman primates. *Cerebellum*, 11, 392–410 (2012).

584. Kheradmand A, Zee DS. Cerebellum and ocular motor control. *Front Neurol*, Sep 1;2, 5, 1–15 (2011).

585. Duarri A, Jezierska J, Fokkens M, et al. Mutations in potassium channel kcnd3 cause spinocerebellar ataxia type 19. *Ann Neurol*, 72, 870–80 (2012).

586. Verbeek DS. Spinocerebellar ataxia type 23: a genetic update. *Cerebellum*, 8, 104–7 (2009).

587. Niimi Y, Takahashi M, Sugawara E, et al. Abnormal RNA structures (RNA foci) containing a penta-nucleotide repeat (UGGAA) n in the Purkinje cell nucleus is associated with spinocerebellar ataxia type 31 pathogenesis. *Neuropathology*, 33, 600–611 (2013).

588. Obayashi M, Stevanin G, Synofzik M, et al. Spinocerebellar ataxia type 36 exists in diverse populations and can be caused by a short hexanucleotide GGCCTG repeat expansion. *J Neurol Neurosurg Psychiatry*, 86, 986–95 (2015).

589. Chen D-H, Latimer C, Yagi M, et al. Heterozygous STUB1 missense variants cause ataxia, cognitive decline, and STUB1 mislocalization. *Neurol Genet*, 6, 1–13 (2020).

590. Miyata T, Ono Y, Okamoto M, et al. Migration, early axonogenesis, and Reelin-dependent layer-forming behavior of early/posterior-born Purkinje cells in the developing mouse lateral cerebellum. *Neural Dev*, 5, 23 (2010).

591. Hirota Y, Nakajima K. Control of Neuronal Migration and Aggregation by Reelin Signaling in the Developing Cerebral Cortex. 5, 1–8 (2017).

592. Goffinet AM, So KF, Yamamoto M, et al. Architectonic and hodological organization of the cerebellum in reeler mutant mice. *Brain Res*, 318, 263–76 (1984).

593. Goldowitz D, Cushing RC, Laywell E, et al. Cerebellar disorganization characteristic of reeler in scrambler mutant mice despite presence of reelin. *J Neurosci*, 17, 8767–8777 (1997).

594. Morimura T, Hattori M, Ogawa M, et al. Disabled1 regulates the intracellular trafficking of reelin receptors. *J Biol Chem*, 280, 16901–16908 (2005).

595. Jossin Y, Goffinet AM. Reelin Signals through Phosphatidylinositol 3-Kinase and Akt To Control Cortical Development and through mTor To Regulate Dendritic Growth. *Mol Cell Biol*, 27, 7113–7124 (2007).

596. Lee A-H, Iwakoshi NN, Glimcher LH. XBP-1 Regulates a Subset of Endoplasmic Reticulum Resident Chaperone Genes in the Unfolded Protein Response. *Mol Cell Biol*, 23, 7448–7459 (2003).

597. Yang S, Huang S, Gaertig MA, et al. Age-dependent decrease in chaperone activity impairs MANF expression, leading to Purkinje Cell degeneration in inducible SCA17 Mice. *Neuron*, 81, 349–365 (2014).

598. Strupp M, Hüfner K, Sandmann R, et al. Central oculomotor disturbances and nystagmus: a window into the brainstem and cerebellum. *Dtsch Arztebl Int*, 108, 197–204 (2011).

599. Jacobi H, Reetz K, du Montcel ST, et al. Biological and clinical characteristics of individuals at risk for spinocerebellar ataxia types 1, 2, 3, and 6 in the longitudinal RISCA study: analysis of baseline data. *Lancet Neurol*, 12, 650–658 (2013).

600. Gomez CM, Thompson RM, Gammack JT, et al. Spinocerebellar ataxia type 6: Gaze-evoked and vertical nystagmus, Purkinje cell degeneration, and variable age of onset. *Ann Neurol*, 42, 933–950 (1997).

601. Teive HAG, Munhoz RP, Raskin S, et al. Spinocerebellar ataxia type 10: Frequency of epilepsy in a large sample of Brazilian patients. *Mov Disord*, 25, 2875–2878 (2010).

602. Nick JM. Deep tendon reflexes, magnesium, and calcium: assessments and implications. *J Obstet Gynecol neonatal Nurs*, 33, 221–30 (1990).

603. Bürk K, Abele M, Fetter M, et al. Autosomal dominant cerebellar ataxia type I Clinical features and MRI in families with SCA1, SCA2 and SCA3. *Brain*, 119, 1497–1505 (1996).

604. Teive H, Munhoz R, Arruda W, et al. Spinocerebellar ataxias – genotype-phenotype correlations in 104 Brazilian families. *Clinics*, 67, 443–449 (2012).

605. Infante J, Combarros O, Volpini V, et al. Autosomal dominant cerebellar ataxias in Spain: molecular and clinical correlations, prevalence estimation and survival analysis. *Acta Neurol Scand*, 111, 391–399 (2005).

606. Day JW, Schut LJ, Moseley ML, et al. Spinocerebellar ataxia type 8: Clinical features in a large family. *Neurology*, 55, 649–657 (2000).

607. Paulson HL. The Spinocerebellar Ataxias. *J Neuro-Ophthalmology*, 29, 227–237 (2009).

608. van de Warrenburg BPC, Verbeek DS, Piersma SJ, et al. Identification of a novel SCA14 mutation in a Dutch autosomal dominant cerebellar ataxia family. *Neurology*, 61, 1760–1765 (2003).

609. Hara K, Fukushima T, Suzuki T, et al. Japanese SCA families with an unusual phenotype linked to a locus overlapping with SCA15 locus. *Neurology*, 62, 648–651 (2004).

610. Stevanin G. Huntington's disease-like phenotype due to trinucleotide repeat expansions in the TBP and JPH3 genes. *Brain*, 126, 1599–1603 (2003).

611. Indelicato E, Fanciulli A, Ndayisaba JP, et al. Autonomic function testing in spinocerebellar ataxia type 2. *Clin Auton Res*, 28, 341–346 (2018).

612. Yeh T-H, Lu C-S, Chou Y-HW, et al. Autonomic Dysfunction in Machado-Joseph Disease. *Arch Neurol*, 62, 630 (2005).

613. González-Salazar C, Takazaki KAG, Martinez ARM, et al. Autonomic dysfunction in hereditary spastic paraplegia type 4. *Eur J Neurol*, 26, 687–693 (2019).

614. Nielsen JE, Johnsen B, Koefoed P, et al. Hereditary spastic paraplegia with cerebellar ataxia: a complex phenotype associated with a new SPG4 gene mutation. *Eur J Neurol*, 11, 817–824 (2004).

615. Allison R, Edgar JR, Reid E. Spastin MIT Domain Disease-Associated Mutations Disrupt Lysosomal Function. *Front Neurosci* (2019).

616. Sahoo SS, Kozyra EJ, Wlodarski MW. Germline predisposition in myeloid neoplasms: Unique genetic and clinical features of GATA2 deficiency and SAMD9/SAMD9L syndromes. *Best Pract Res Clin Haematol*, 33, 101197 (2020).

617. de Jesus AA, Hou Y, Brooks S, et al. Distinct interferon signatures and cytokine patterns define additional systemic autoinflammatory diseases. *J Clin Invest* (2020).

618. Chen D-H, Below JE, Shimamura A, et al. Ataxia-Pancytopenia Syndrome Is Caused by Missense Mutations in SAMD9L. *Am J Hum Genet*, 98, 1146–1158 (2016).

619. Tesi B, Davidsson J, Voss M, et al. Gain-of-function SAMD9L mutations cause a syndrome of cytopenia, immunodeficiency, MDS, and neurological symptoms. *Blood*, 129, 2266–2279 (2017).

620. Asou H, Matsui H, Ozaki Y, et al. Identification of a common microdeletion cluster in 7q21.3 subband among patients with myeloid leukemia and myelodysplastic syndrome. *Biochem Biophys Res Commun* (2009).

621. Narumi S, Amano N, Ishii T, et al. SAMD9 mutations cause a novel multisystem disorder, MIRAGE syndrome, and are associated with loss of chromosome 7. *Nat Genet*, 48, 792–7 (2016).

622. Schwartz JR, Ma J, Lamprecht T, et al. The genomic landscape of pediatric myelodysplastic syndromes. *Nat Commun*, 8, 1557 (2017).

623. Wong JC, Bryant V, Lamprecht T, et al. Germline SAMD9 and SAMD9L mutations are associated with extensive genetic evolution and diverse hematologic outcomes. *JCI Insight*, 3, e121086 (2018).

624. Thunström S, Axelsson M. Leukoencephalopathia, demyelinating peripheral neuropathy and dural

ectasia explained by a not formerly described de novo mutation in the SAMD9L gene, ends 27 years of investigations - a case report. *BMC Neurol*, 19, 89 (2019).

625. Cheah JJC, Brown AL, Schreiber AW, et al. A novel germline SAMD9L mutation in a family with ataxia-pancytopenia syndrome and pediatric acute lymphoblastic leukemia. *Haematologica*, 104, e318–e321 (2019).

626. Pastor VB, Sahoo SS, Boklan J, et al. Constitutional SAMD9L mutations cause familial myelodysplastic syndrome and transient monosomy 7. *Haematologica*, 103, 427–437 (2018).

627. Babu MM. The contribution of intrinsically disordered regions to protein function, cellular complexity, and human disease. *Biochem Soc Trans*, 44, 1185–1200 (2016).

628. Meyer K, Kirchner M, Uyar B, et al. Mutations in Disordered Regions Can Cause Disease by Creating Dileucine Motifs. *Cell*, 175, 239-253.e17 (2018).

629. Lucero M, Suarez AE, Chambers JW. Phosphoregulation on mitochondria: Integration of cell and organelle responses. *CNS Neurosci Ther*, 25, 837–858 (2019).

630. Zaja I, Bai X, Liu Y, et al. Cdk1, PKCδ and calcineurin-mediated Drp1 pathway contributes to mitochondrial fission-induced cardiomyocyte death. *Biochem Biophys Res Commun*, 453, 710–721 (2014).

631. Hazan J, Fonknechten N, Mavel D, et al. Spastin, a new AAA protein, is altered in the most frequent form of autosomal dominant spastic paraplegia. *Nat Genet*, 23, 296–303 (1999).

632. Allison R, Edgar JR, Reid E. Spastin MIT Domain Disease-Associated Mutations Disrupt Lysosomal Function. *Front Neurosci*, 13 (2019).

633. McDermott CJ, Grierson AJ, Wood JD, et al. Hereditary Spastic Paraparesis: Disrupted Intracellular Transport Associated with Spastin Mutation. *Ann Neurol*, 54, 748–759 (2003).

634. Matamoros AJ, Baas PW. Microtubules in health and degenerative disease of the nervous system. *Brain Res Bull*, 126, 217–225 (2016).

635. Beyer A, Scheuring S, Müller S, et al. Comparative sequence and expression analyses of four mammalian VPS4 genes. *Gene*, 305, 47–59 (2003).

636. Eskelinen E-L. Maturation of autophagic vacuoles in Mammalian cells. *Autophagy*, 1, 1–10 (2005).

637. Guerra F, Bucci C. Multiple Roles of the Small GTPase Rab7. *Cells*, 5, 34 (2016).

638. Kiral FR, Kohrs FE, Jin EJ, et al. Rab GTPases and Membrane Trafficking in Neurodegeneration. *Curr Biol*, 28, R471–R486 (2018).

639. Liu J, Lamb D, Chou MM, et al. Nerve growth factor-mediated neurite outgrowth via regulation of Rab5. *Mol Biol Cell*, 18, 1375–1384 (2007).

640. Deinhardt K, Salinas S, Verastegui C, et al. Rab5 and Rab7 Control Endocytic Sorting along the Axonal

Retrograde Transport Pathway. *Neuron*, 52, 293–305 (2006).

641. Nielsen E, Severin F, Backer JM, et al. Rab5 regulates motility of early endosomes on microtubules. *Nat Cell Biol*, 1, 376–382 (1999).

642. Sittler A, Muriel MP, Marinello M, et al. Deregulation of autophagy in postmortem brains of Machado-Joseph disease patients. *Neuropathology*, 38, 113–124 (2018).

643. Watase K, Unno T, Koike M, et al. Lysosomal contribution to the Purkinje cell degeneration in mouse models of spinocerebellar ataxia type 6. *J Neurochem*, 125, 194–280 (2013).

644. Alves S, Cormier-Dequaire F, Marinello M, et al. The autophagy/lysosome pathway is impaired in SCA7 patients and SCA7 knock-in mice. *Acta Neuropathol*, 128, 705–722 (2014).

645. Seki T, Sato M, Kibe Y, et al. Lysosomal dysfunction and early glial activation are involved in the pathogenesis of spinocerebellar ataxia type 21 caused by mutant transmembrane protein 240. *Neurobiol Dis*, 120, 34–50 (2018).

646. Cornelius N, Wardman JH, Hargreaves IP, et al. Evidence of oxidative stress and mitochondrial dysfunction in spinocerebellar ataxia type 2 (SCA2) patient fibroblasts: Effect of coenzyme Q10 supplementation on these parameters. *Mitochondrion*, 34, 103–114 (2017).

647. Hsu J-Y, Jhang Y-L, Cheng P-H, et al. The Truncated C-terminal Fragment of Mutant ATXN3 Disrupts Mitochondria Dynamics in Spinocerebellar Ataxia Type 3 Models. *Front Mol Neurosci*, 10, 196 (2017).

648. Ward JM, Stoyas CA, Switonski PM, et al. Metabolic and Organelle Morphology Defects in Mice and Human Patients Define Spinocerebellar Ataxia Type 7 as a Mitochondrial Disease. *Cell Rep*, 26, 1189-1202.e6 (2019).

649. Wang Y-C, Lee C-M, Lee L-C, et al. Mitochondrial Dysfunction and Oxidative Stress Contribute to the Pathogenesis of Spinocerebellar Ataxia Type 12 (SCA12). *J Biol Chem*, 286, 21742–21754 (2011).

650. Crespo-Barreto J, Fryer JD, Shaw CA, et al. Partial Loss of Ataxin-1 Function Contributes to Transcriptional Dysregulation in Spinocerebellar Ataxia Type 1 Pathogenesis. *PLoS Genet*, 6, e1001021 (2010).

651. Ramani B, Panwar B, Moore LR, et al. Comparison of spinocerebellar ataxia type 3 mouse models identifies early gain-of-function, cell-autonomous transcriptional changes in oligodendrocytes. *Hum Mol Genet*, 26, 3362–3374 (2017).

652. Robinson KJ, Yuan KC, Don EK, et al. Motor Neuron Abnormalities Correlate with Impaired Movement in Zebrafish that Express Mutant Superoxide Dismutase 1. *Zebrafish*, 16, 8–14 (2019).

653. Cooper-Knock J, Moll T, Ramesh T, et al. Mutations in the Glycosyltransferase Domain of GLT8D1 Are Associated with Familial Amyotrophic Lateral Sclerosis. *Cell Rep*, 26, 2298-2306.e5 (2019).

654. Lissouba A, Liao M, Kabashi E, et al. Transcriptomic Analysis of Zebrafish TDP-43 Transgenic Lines. *Front Mol Neurosci*, 11, 463 (2018).

655. Roberts R, Elsner J, Bagnall MW. Delayed Otolith Development Does Not Impair Vestibular Circuit Formation in Zebrafish. *J Assoc Res Otolaryngol*, 18, 415–425 (2017).

656. Granato M, van Eeden FJ, Schach U, et al. Genes controlling and mediating locomotion behavior of the zebrafish embryo and larva. *Development*, 123, 399–413 (1996).

657. Takahashi M, Narushima M, Oda Y. In Vivo Imaging of Functional Inhibitory Networks on the Mauthner Cell of Larval Zebrafish. *J Neurosci*, 22, 3929–3938 (2002).

658. Lorent K, Liu KS, Fetcho JR, et al. The zebrafish space cadet gene controls axonal pathfinding of neurons that modulate fast turning movements. *Development*, 128, 2131–42 (2001).

659. Jontes JD, Buchanan J, Smith SJ. Growth cone and dendrite dynamics in zebrafish embryos: early events in synaptogenesis imaged in vivo. *Nat Neurosci*, 3, 231–237 (2000).

660. Umeda K, Shoji W. From neuron to behavior: Sensory-motor coordination of zebrafish turning behavior. *Dev Growth Differ*, 59, 107–114 (2017).

661. Dunn TW, Mu Y, Narayan S, et al. Brain-wide mapping of neural activity controlling zebrafish exploratory locomotion. *Elife*, 5, e12741 (2016).

662. Umeda K, Ishizuka T, Yawo H, et al. Position- and quantity-dependent responses in zebrafish turning behavior. *Sci Rep*, 6, 27888 (2016).

663. Kent WJ, Sugnet CW, Furey TS, et al. The Human Genome Browser at UCSC. *Genome Res*, 12, 996–1006 (2002).

664. Google. (n.d.). [Google Maps south of Spain]. Retrieved October 11, 2020, from https://www.google.com/maps/d/u/0/viewer?hl=es&mid=1CbwU4N0CSh-GVy-rzY5lYtEiz0lzx4T2&ll=37.27522489058714%2C-7.122866896874999&z=8).

# SUPPLEMENTARY DATA

**Supplementary Table 1. Oligonucleotide primer sequences used and PCR conditions for SCA repeat expansion detection.**

| Oligonucleotide Primer ID | Sequence (5'-3') | Annealing Temp. |
|---|---|---|
| **SCA1 Genotyping** | | |
| hATXN1_EX8_EXP_FW | [6FAM]AGCTGGAGGCCTATTCCACTC | 58 ºC |
| hATXN1_EX8_EXP_RV | TGGAAATGTGGACGTACTGGTTC | |
| **SCA2 Genotyping** | | |
| hATXN2_EX1_EXP_FW | [6FAM]TATGGGCCCCTCACCATGT | 62 ºC |
| hATXN2_EX1_EXP_RV | ACGAGGAGACCGAGGACGA | |
| **SCA3 Genotyping** | | |
| hATXN3_EX10_EXP_FW | [6FAM]TCACTTTTGAATGTTTCAGACAGCA | 58 ºC |
| hATXN3_EX10_EXP_RV | GAGCAGGCCTTACCTAGATCACTC | |
| **SCA6 Genotyping** | | |
| hCACNA1A_EXP_FW | [6FAM]TATTCCCCTGTGATCCGTAAGG | 60 ºC |
| hCACNA1A _EXP_RV | ATCTCCGGCCAGAGGCTC | |
| **SCA7 Genotyping** | | |
| hATXN7_EX3_EXP_FW | [6FAM]GAGCGGAAAGAATGTCGGAG | 58 ºC |
| hATXN7_EX3_EXP_FW | CATCACTTCAGGACTGGGCA | |
| hATXN8_EXP_RV | GGTCCTTCATGTTAGAAAACCTGGCT | |
| **SCA10 Genotyping** | | |
| hATXN10_repeats_FW | [6FAM]AATGGCTTAAATATCCAACTAAAAGACTAC | 57 ºC |
| hATXN10_repeats_RV | GGCAACATAGAGAGACTTCATCTCA | |
| **SCA10 TP-PCR** | | |
| hATXN10_repeats_FW | [6FAM]AATGGCTTAAATATCCAACTAAAAGACTAC | 55 ºC |
| hATXN10_RP_RV | TACGCATCCCAGTTTGAGACGAGAATAGAATAGAA TAGAATAGAAT | |
| hATXN10_FLAG | TACGCATCCCAGTTTGAGACG | |
| **SCA12** | | |
| hPPP2R2B_Prom_EXP_FW | [6FAM]CTGCTGGGAAAGAGTCGTGG | 56 ºC |
| hPPP2R2B_Prom_EXP_RV | TAGGGAAGCTGGCGGGG | |
| **SCA17** | | |
| hTBP_EX3_EXP_FW | [6FAM]TGACCCCACAGCCTATTCAGA | 58 ºC |
| hTBP_EX3_EXP_RV | CTGGGACGTTGACTGCTGAAC | |
| **SCA36** | | |
| hNOP56_int1_EXP_FW | [6FAM]CGACGGTGGGGGTTTC | 58 ºC |
| hNOP56_int1_EXP_RV | AACGCAACCTCAGCGTCT | |

| | | |
|---|---|---|
| **SCA36 TP-PCR** | | |
| hNOP56_int1_RP_FW | [6FAM]TTTCGGCCTGCGTTCGGG | 58 ºC |
| hNOP56_int1_RP_RV | TACGCATCCCAGTTTGAGACGCAGGCCCA GGCCCAGGCCCAGGCC | |
| hNOP56_FLAG | TACGCATCCCAGTTTGAGACG | |
| **DRPLA** | | |
| hATN1_EXP_FW | [6FAM]CCCAGTCCACCGCCCACCCACCA | 68 ºC |
| hATN1_EXP_RV | TGCTCCAGGAGGAGGGGGCCCAGA | |

One-hundred ng of DNA were included in a 20 µl reaction. PCR conditions were as follows: initial denaturation at 95 ºC for 5 min with a Taq DNA Polymerase, recombinant (ThermoFisher Scientific) followed by 35 cycles (95 ºC for 30 sec, specific annealing temperature 40 sec, 72 ºC for 50 sec), and a final denaturation at 72 ºC for 10 min.

**Supplementary Table 2. Custom NGS Ataxia panels.**

| Version (Number of genes) years | Genes |
|---|---|
| Version 1 (119 genes) 2015-2017 | ABCB7, ABHD12, ADCK3, AFG3L2, AIMP1, ANO10, APTX, ARSA, ATCAY, ATM, ATP1A3, ATP7B, ATP8A2, ATR, BEAN1, C10ORF2, CA8, CACNA1A, CACNB4, CEP290, CLCN2, COQ2, COQ9, COX20, CP, CYP27A1, CYP7B1, DDHD2, DNAJC19, DNMT1, EEF2, EIF2B1, EIF2B2, EIF2B3, EIF2B4, EIF2B5, ELOVL4, FAM126A, FGF14, FLVCR1, FMR1, FUS, FTL, FXN, GALC, GBA2, GOSR2, GRID2, GRM1, HEXA, HSD17B4, IFRD1, ITM2B, ITPR1, KCNA1, KCNC3, KCND3, KCNJ10, KIAA0226, KIF1C, LYST, MRE11A, MTPAP, MTTP, NKX2-1, NPHP1, OPA1, PAX6, PC, PDGFB, PDHA1, PDSS1, PDSS2, PDYN, PHYH, PIK3R5, PLEKHG4, PLP1, POLG, POLR3A, POLR3B, PRKCG, PRNP, PRPS1, PSAP, PTS, RPGRIP1L, SACS, SCARB2, SCN8A, SCP2, SETX, SIL1, SLC1A3, SLC20A2, SLC2A1, SLC9A6, SOD1, SPG7, SPTBN2, STUB1, SYNE1, SYT14, TARDBP, TDP1, TGM6, TMEM67, TPP1, TTBK2, TTC19, TTPA, TUBB4A, TYROBP, VAMP1, VAPB, VLDLR, WDR45, WWOX, ZNF592. |
| Version 2 (133 genes) 2017-2019 | ABCB7, ABHD12, AFG3L2, AIFM1, AIMP1, ANO10, APTX, AP5Z1, ARSA, ATCAY, ATM, ATP1A3, ATP7B, ATP8A2, ATR, BEAN1, B4GALNT1, CA8, CACNA1A, CACNB4, CEP290, CLCN2, COQ2, COQ8A, COQ9, COX20, CP, CSF1R, CYP2U1, CYP27A1, CYP7B1, DDHD2, DNAJC19, DNMT1, EEF2, EIF2B1, EIF2B2, EIF2B3, EIF2B4, EIF2B5, ELOVL4, FAM126A, FGF14, FLVCR1, FMR1, FUS, FTL, FXN, GALC, GBA2, GOSR2, GRID2, GRM1, HEXA, HSD17B4, IFRD1, ITM2B, ITPR1, KCNA1, KCNC3, KCND3, KCNJ10, KIF1A, KIF1C, LYST, MAG, MRE11, MTPAP, MTTP, NKX2-1, NPHP1, NOTCH3, OPA1, PAX6, PC, PDGFB, PDHA1, PDSS1, PDSS2, PDYN, PHYH, PIK3R5, PLA2G6, PLEKHG4, PLP1, PNPLA6, POLG, POLR3A, POLR3B, PRKCG, PRNP, PRPS1, PRRT2, PSAP, PTS, RPGRIP1L, RUBCN, SACS, SCARB2, SCN8A, SCP2, SETX, SIL1, SLC1A3, SLC20A2, SLC2A1, SLC9A6, SOD1, SPG7, SPTBN2, SQSTM1, STUB1, SURF1, SYNE1, SYT14, TARDBP, TDP1, TGM6, TMEM67, TPP1, TTBK2, TTC19, TTPA, TUBB4A, TWNK, UCHL1, TYROBP, VAMP1, VAPB, VLDLR, WDR45, WWOX, ZNF592. |
| Version 3 (347 genes) 2019-2020 | AAAS, AARS2, ABCB7, ABCD1, ABHD12, ABHD5, ACO2, AFG3L2, AHI1, AIFM1, AIMP1, ALDH5A1, ALG6, AMACR, ANO10, AP1S2, AP5Z1, APTX, ARL13B, ARL6, ARSA, ASS1, ATAD3A, ATCAY, ATM, ATP13A2, ATP1A2, ATP1A3, ATP2B3, ATP7A, ATP7B, ATP8A2, ATR, B4GALNT1, B9D1, BBS1, BBS12, BEAN1, BRAT1, BSCL2, BTD, C12orf65, C19orf12, C5ORF42, CA8, CACNA1A, CACNA1C, CACNA1G, CACNB4, CAMTA1, CAPN1, CASK, CC2D2A, CCDC88C, CEP104, CEP120, CEP290, CEP41, CLCN2, CLN5, CLN6, CLPP, CNTNAP2, COASY, COG5, COQ2, COQ8A, COQ9, COX10, COX14, COX15, COX20, COX6B1, COX8A, CP, CSF1R, CSPP1, CTBP1, CTSA, CTSD, CTSF, CWF19L1, CYP27A1, CYP2U1, CYP7B1, DARS2, DDHD2, DLAT, DNAJC19, DNAJC3, DNAJC5, DNMT1, DPM1, EBF3, EEF2, EIF2B1, EIF2B2, EIF2B3, EIF2B4, EIF2B5, ELOVL4, ELOVL5, EPM2A, ERCC4, ERCC8, EXOSC3, FA2H, FAM126A, FASTKD2, FBXL4, FGF12, FGF14, FLVCR1, FMR1, FOLR1, FOXRED1, FTL, FUS, FXN, GALC, GAN, GBA, GBA2, GFAP, GJB1, GJC2, GLDC, GOSR2, GRID2, GRM1, GSS, HARS, HEPACAM, HEXA, HEXB, HIBCH, HSD17B4, HTRA1, IFRD1, INPP5E, IQSEC2, ITM2B, ITPR1, KARS, KCNA1, KCNA2, KCNC1, KCNC3, KCND3, KCNJ10, KCNMA1, KCTD7, KIAA0556, KIAA0586, KIF1A, KIF1C, KIF5A, KIF7, L2HGDH, LAMA1, LMNB1, LMNB2, LRP4, LRPPRC, LRSAM1, LYST, MAG, MARS2, MECP2, MECR, MED13L, MFSD8, MKS1, MLC1, MME, MPV17, MPZ, MRE11, MTFMT, MTPAP, MTTP, NAGLU, NDUFAF6, NDUFS1, NDUFS2, NDUFS4, NDUFS7, NDUFV1, NEU1, NKX2-1, NLRP3, NOTCH3, NPC1, NPC2, NPHP1, NUBPL, NUP93, OFD1, OPA1, OPA3, OPHN1, OTX2, PABPC4L, PANK2, PAX6, PC, PCNA, PDE6D, PDGFB, PDHA1, PDHX, PDSS1, PDSS2, PDYN, PET100, PEX10, PEX16, PEX2, PEX6, PEX7, PGK1, PHYH, PIBF1, PIK3R5, PITRM1, PLA2G6, PLD3, PLEKHG4, PLP1, |

| | |
|---|---|
| | PMM2, PMPCA, PNKD, PNKP, PNPLA6, POLG, POLR1C, POLR3A, POLR3B, PRICKLE1, PRKCG, PRNP, PRPS1, PRRT2, PRX, PSAP, PSEN1, PTRH2, PTS, RARS2, RNF170, RNF216, RPGRIP1L, RPL10, RRM2B, RTN4IP1, RUBCN, SACS, SAMD9L, SCARB2, SCN2A, SCN8A, SCO1, SCP2, SCYL1, SETX, SIL1, SLC16A2, SLC17A5, SLC1A3, SLC20A2, SLC25A46, SLC2A1, SLC52A2, SLC52A3, SLC6A1, SLC9A1, SLC9A6, SNAP25, SNX14, SOD1, SOX10, SPG11, SPG7, SPR, SPTBN2, SQSTM1, STUB1, SUFU, SUMF1, SURF1, SVBP, SYNE1, SYT14, TACO1, TANGO2, TARDBP, TBC1D24, TBCE, TCTN1, TCTN2, TCTN3, TDP1, TDP2, TGM6, THG1L, TMEM138, TMEM216, TMEM231, TMEM237, TMEM240, TMEM67, TPK1, TPP1, TRAPPC11, TRPC3, TSEN2, TSEN34, TSEN54, TSFM, TTBK2, TTC19, TTPA, TTR, TUBB4A, TWNK, TYROBP, UBA5, UCHL1, VAMP1, VAPB, VARS2, VLDLR, VPS13D, VRK1, VWA3B, WARS2, WDR45, WDR73, WDR81, WFS1, WWOX, XPA, ZBTB18, ZFYVE26, ZMYND11, ZNF423, ZNF592 |

**Supplementary Table 3. Oligonucleotide primer sequences used and PCR conditions for SCA37 studies.**

| Oligonucleotide Primer ID | Sequence (5'-3') |
|---|---|
| **Genetic Polymorphic Markers on 1p32 PCR amplification** | |
| D1S2867_FW | [6FAM]GTTCAGTGCATCTGACAGG |
| D1S2867_RV | GCTGCCAACCGTGTGT |
| D1S2665_FW | [6FAM]TAGATAAGGAGCAACAGAGAATGAC |
| D1S2665_RV | TGAAGTGGAAGGCTCGC |
| rs79992829&rs146472695_FW | CCAGTGCTCCTTTCACTAGACCA |
| rs79992829&rs146472695_RV | AGCTTGCAATTTCTTTCCAATAGAA |
| D1S1150_FW | [6FAM]AGAGGCTGCATTGAGCTAAGATCT |
| D1S1150_RV | CTCTAGTTCCATACTCTACAGTCATACCAG |
| rs145097803_FW | TCTAGAGAATAAAATCAATGGGATGTAAAG |
| rs145097803_RV | ATCTCAGTCTTCCTATGTAGCCCAA |
| D1S2650_FW | [6FAM]GGAAGATCCAGAATCCATGTGAA |
| D1S2650_RV | GGTGAACCAAACATCAGTGCC |
| **ATTTC expanded repeat mutation PCR amplification** | |
| ALU24F | ATTTGCCCTTTGCTGATTGA |
| ALU24R | TGAAACTGAGGCTCAAAATGA |
| **ATTTC expanded repeat mutation sequencing** | |
| ATTTC_FW_seq | CACAGCTTACTGCAGCCTCA |
| ATTTC_RV_seq | GACCACTTTAGCCCAGGAGTT |
| **5' UTR DAB1 transcripts analysis and Real Time qRT-PCR** | |
| EXON1_DAB1_cDNA_FW (1 FW) | TAGGAGTGAGCATCCCCTCTC |
| EXON2_DAB1_cDNA_FW (2 FW) | AGACCTCAGGGACACAGATAA |
| EXON3_DAB1_cDNA_FW (3 FW) | AAGATCAAGGCACCATCTGAT |
| EXON4_DAB1_cDNA_FW (4 FW) | GCCTGGACACATTGACTGAA |
| EXON5_DAB1_cDNA_FW (5 FW) | TCCTTGGCAGTGGATAGCAT |
| EXON6_DAB1_cDNA_FW (6 FW) | GGATTGGTTTCAATTTTCTCCT |
| EXON7_DAB1_cDNA_FW (7 FW) | CTGACTCTCAGTCTTCATGATTG |
| EXON8_DAB1_cDNA_FW (8 FW) | CCCTTCCTGGCACTCCATATA |
| EXON9_DAB1_cDNA_FW (9 FW) | ACTCGGCTAAGCTCTCGG |
| EXON10_DAB1_cDNA_FW (10 FW) | AGGATGCTCTGGGCTAGGC |
| EXON11_DAB1_cDNA_FW (11 FW) | CACACAAGAGGGTGTCAACC |
| EXON12_DAB1_cDNA_RV (12 RV) | TTTCTTTCTGGAGTCTTTCTTGG |

| Coding DAB1 transcript analysis | |
|---|---|
| EXON12_DAB1_cDNA_FW (12 FW) | CCAGCGCCAAGAAAGACTCC |
| EXON14.19_hDAB1_cDNA_FW (14.19 RV) | GGCTGGTGGGAACCCCTGTC |
| EXON17alt_DAB1_cDNA_RV (17alt RV) | CCAGGTTTTGCAGTCAGTGGA |
| EXON20_hDAB1_cDNA_FW (20 FW) | AATGGCTATTCGTTTGAGGATTTTGAAG |
| EXON20_hDAB1_cDNA_RV (20 RV) | GGTGGCTGCAGCAAACCGTTC |
| EXON26_DAB1_cDNA_RV (26 RV) | CACTGGGCTCACCAAATGGA |
| **Coding DAB1 transcript Real Time qRT-PCR** | |
| EXON14_DAB1_cDNA_FW (14 FW) | TCGTTCCAAAGGAGAACACAAA |
| EXON17alt_DAB1_cDNA_RV (17alt RV) | CCAGGTTTTGCAGTCAGTGGA |
| EXON17_18_DAB1_cDNA_RV (17.18 RV) | GCCTCAAACACAATGTACTGG |
| **GAPDH Real Time qRT-PCR** | |
| GAPDH_FW | CTTGTCATCAATGGAAATCCCA |
| GAPDH_RV | CAGTGGACTCCACGACGTACTC |

One-hundred ng of DNA were included in a 20 µl reaction. PCR conditions were as follows: initial denaturation at 95 ºC for 5 min with a Taq DNA Polymerase, recombinant (ThermoFisher Scientific) followed by 35 cycles (95 ºC for 30 sec, 58 ºC for 40 sec, 72 ºC for 50 sec), and a final denaturation at 72 ºC for 10 min. The ATTTC repeat expanded mutation was amplified as previously described (Seixas et al., 2017). cDNA *DAB1* transcripts were amplified with an initial denaturation at 95 ºC for 15 min with a HotStarTaq Master Mix (Qiagen) followed by 35-45 cycles (95 ºC for 30 sec, 58 ºC for 40 sec, 72 ºC for 60 sec), and a final denaturation at 72 ºC for 10 min.

**Supplementary Table 4. Oligonucleotide primer sequences used and PCR conditions for M-SCA studies.**

| Oligonucleotide Primer ID | Sequence (5'-3') |
|---|---|
| ***hSAMD9L* c.1877C>T (p.Ser626Leu) Sanger Sequencing** | |
| hSAMD9L.S626L_FW | GAAAAATAGAAGTTCCACCAGGA |
| hSAMD9L.S626L_RV | TTTCTATTACTCTCTTCAGTGGAAAGC |
| ***hSAMD9L* transcript Real Time qRT-PCR** | |
| hSAMD9L_cDNA_Exon4_FW | GGCACGGAAAGTGAGTGAGT |
| hSAMD9L_cDNA_Exon5 _RV | AGAATTTGCCCGTATTGCTCATT |
| ***hGAPDH* Real Time qRT-PCR** | |
| GAPDH_FW | CTTGTCATCAATGGAAATCCCA |
| GAPDH_RV | CAGTGGACTCCACGACGTACTC |
| ***hSAMD9L* CDS cloning** | |
| hSAMD9L.cloning.ATG.FW | ATGAGTAAACAAGTATCTCTACCTGAAA |
| hSAMD9L.cloning.TAA.RV | TTAAATTACTTCTATATCATATGCCAGAG |

One-hundred ng of DNA were included in a 20 µl reaction. PCR conditions were as follows: initial denaturation at 95 ºC for 5 min with a Taq DNA Polymerase, recombinant (ThermoFisher Scientific) followed by 35 cycles (95 ºC for 30 sec, 58 ºC for 40 sec, 72 ºC for 50 sec), and a final denaturation at 72 ºC for 10 min. Real Time qRT-PCR were performed using TB Green Premix Ex Taq II (Takara Bio) and PCR conditions were as follows: 95 ºC for 2 min, and 40 cycles (95 ºC for 5 sec, 60 ºC for 20 sec, 72 ºC for 20 sec). The $2^{-\Delta\Delta Ct}$ method (430) was used to analyse the relative cDNA levels data obtained by Real Time qRT-PCR.

**Supplementary Table 5. Oligonucleotide primer sequences used and PCR conditions for mtDNA amplification.**

| Oligonucleotide Primer ID | Sequence (5'-3') |
|---|---|
| **mtDNA PCR amplification** | |
| hMT_15058_Frag1_FW | CGGATCATTTCTCTACTCAGAAA |
| hMT_208_Frag1_RV | ACACACTTTAGTAAGTATGTTCGCC |
| hMT_16516_Frag2_FW | GGGTCATAAAGCCTAAATAGC |
| hMT_1751_Frag2_RV | TCGCCTATACTTTATTTGGGTA |
| hMT_1404_Frag3_FW | ACTTAAGGGTCGAAGGTGGATT |
| hMT_3947_Frag3_RV | TCGATGTTGAAGCCTGAGACTA |
| hMT_3734_Frag4_FW | AAGTCACCCTAGCCATCATTCTAC |
| hMT_6739_Frag4_RV | GATATCATAGCTCAGACCATACCTATG |
| hMT_6364_Frag5_FW | GTGTCTCCTCTATCTTAGGGGCCAT |
| hMT_9785_Frag5_RV | GTAGATGCCGTCGGAAATGGTG |
| hMT_8655_Frag6_FW | GTACGTAGTCTAGGCCATATGTGT |
| hMT_10740_Frag6_RV | CACCACCCAACAATGACT |
| hMT_10361_Frag7_FW | TCTGGCCTATGAGTGACTACAAAAAGG |
| hMT_12373_Frag7_RV | TCAGGGTTAGGGTGGTTATAGTAGTGTGC |
| hMT_11977_Frag8_FW | CTCCCTCTACATATTTACCACAACACA |
| hMT_13830_Frag8_RV | AAGTCCTAGGAAAGTGACAGCGA |
| hMT_13469_Frag9_FW | TAGCATTAGCAGGAATACCTTTCC |
| hMT_15347_Frag9_RV | GCAAGAATAGGAGGTGGAGTGTT |
| **mtDNA qRT-PCR** | |
| hMT_DLOOP_FW | CAGGCGAACATACTTACTAAAGTGTGTTA |
| hMT_DLOOP_RV | GTGACTGTTAAAAGTGCATACCGC |
| hMT_MT-CO3_FW | ATCAGGAGTATCAATCACCTGAGCTCA |
| hMT_MT-CO3_RV | GTAGATGCCGTCGGAAATGGTG |
| hGAPDH_DNA_FW | ACGTAGCTCAGGCCTCAAGACCT |
| hGAPDH_DNA_ RV | TTCTCTCCGCCCGTCTTCAC |
| **LORD-Q method for mitochondrial genome damage** | |
| AS2.F_mtDNA | GGCCACAGCACTTAAACACA |
| AS2.R_mtDNA | TGGTTAGGCTGGTGTTAGGG |
| CL5.F_mtDNA | ATCGTAGCCTTCTCCACTTC |

For mtDNA amplification one-hundred ng of DNA were included in a 20 µl reaction. PCR conditions were as follows: initial denaturation at 94 ºC for 3 min with a LA Taq DNA Polymerase with GC Buffer I (Takara) followed by 35 cycles (94 ºC for 30 sec, 58 ºC for 30 sec, 72 ºC for 4 min), and a final denaturation at 72 ºC for 10 min. mtDNA Real Time qRT-PCR were performed using TB Green Premix Ex Taq II (Takara Bio) and PCR conditions were as follows: 95 ºC for 2 min, and 40 cycles (95 ºC for 5 sec, 60 ºC for 20 sec, 72 ºC for 20

sec). The $2^{-\Delta\Delta Ct}$ method (430) was used to analyse the relative cDNA levels data obtained by Real Time qRT-PCR. Adapted LORD-Q (long-run real-time PCR-based DNA-damage quantification) method amplified a long 3,723 bp mtDNA fragment using only one reagent, TB Green Premix Ex Taq II (Takara Bio) instead of an independent fluorescent dye in combination with a Hot Start Taq. Data analysis was based on the amplification efficiencies of long (EL) and short (ES) probes, number of base pairs of the long fragment (a), number of quantification cycles (Cp) and the number of reference samples (n) (436).

**Supplementary Table 6. SAMD9L domains and motifs identified by Hhpred for protein homology detection and structure prediction.**

| Hit | Name | Probability | E-value | Position in the query sequence | Target Length | Conclusion |
|---|---|---|---|---|---|---|
| 4PZO_A | Polyhomeotic-like protein 3; SAM domain {Homo sapiens} | 97.23 | 0.000047 | 6-85 | 82 | SAM |
| 1Z6T_B | Apoptotic protease activating factor 1; Apaf-1, caspase activation, ADP, nucleotide; {Homo sapiens}; | 97.2 | 0.0014 | 716-1018 | 591 | Apaf-1 ADP |
| 2DKZ_A | hypothetical protein LOC64762; CELL-FREE PROTEIN SYNTHESIS, PROTEIN REGULATION; NMR {Homo sapiens} | 96.97 | 0.00015 | 2-79 | 84 | SAM_PNT-domain |
| 5UJ7_E | Origin recognition complex subunit 1; Replication, DNA-binding, AAA+ ATPase, DNA; {Homo sapiens}; | 96.77 | 0.0025 | 716-872 | 284 | DNA-binding, AAA+ ATPase, |
| 5UJ7_B | Origin recognition complex subunit 1; Replication, DNA-binding, AAA+ ATPase, DNA; {Homo sapiens}; | 96.55 | 0.0052 | 711-873 | 391 | AAA+ ATP-ase |
| 3UK6_B | RuvB-like 2 (E.C.3.6.4.12); Hexameric AAA+ ATP-ase, DNA unwinding; {Homo sapiens}; | 96.54 | 0.0048 | 711-873 | 368 | AAA+ ATP-ase |
| 2XSZ_B | RUVB-LIKE 1 (E.C.3.6.4.12), RUVB-LIKE 2; HYDROLASE, AAA+ PROTEINS, HELICASE, CHROMATIN; 0A {HOMO SAPIENS}; | 96.52 | 0.042 | 708-946 | 367 | HYDROLASE |
| 6BLB_A | Adenosylhomocysteinase {Pseudomonas aeruginosa }; | 96.51 | 0.0031 | 711-873 | 355 | HYDROLASE |
| 5VHO_A | 26S proteasome non-ATPase regulatory subunit; p28, 26S proteasome, regulatory particle;{Homo sapiens}; | 96.43 | 0.0062 | 715-910 | 267 | HYDROLASE |
| 6P07_B | **Spastin (E.C.5.6.1.1), polyglutamate peptide; AAA+ ATPase, Homohexamer, Microtubule Severing; {Drosophila melanogaster};** | 96.38 | 0.019 | 689-904 | 494 | AAA+ ATPase |
| 5UJ7_C | Origin recognition complex subunit 1; Replication, DNA-binding, AAA+ ATPase, DNA; {Homo sapiens}; | 96.35 | 0.0096 | 708-873 | 436 | DNA-binding, AAA+ ATPase |
| 1XWI_A | **SKD1 protein; VPS4B, SKD1, AAA ATPase, PROTEIN; {Homo sapiens}** | 96.27 | 0.013 | 692-902 | 322 | AAA ATPase |
| 6B5C_A | **Katanin p60 ATPase-containing subunit A-like; Katanin, AAA ATPase, Microtubule severing; {Homo sapiens};** | 96.23 | 0.0083 | 715-873 | 307 | AAA ATPase |
| 2X8A_A | NUCLEAR VALOSIN-CONTAINING PROTEIN-LIKE; NUCLEAR PROTEIN; {HOMO SAPIENS} | 96.22 | 0.018 | 690-873 | 274 | HYDROLASE |
| 5J1S_A | **Torsin-1A (E.C.3.6.4.-), Torsin-1A-interacting protein 2; AAA+ ATPase, Torsin, endoplasmic reticulum; {Homo sapiens};** | 96.2 | 0.019 | 711-873 | 284 | AAA+ ATPase |
| 6MSB_E | 26S proteasome; Proteosome, HYDROLASE; {Homo sapiens}; | 96.19 | 0.03 | 713-909 | 403 | |
| 5VHN_F | 26S proteasome non-ATPase regulatory subunit; p28, 26S proteasome, regulatory particle; {Homo sapiens}; | 96.19 | 0.025 | 716-910 | 267 | HYDROLASE |
| 5UJM_A | Origin recognition complex subunit 1; ORC, replication, ATPase; {Homo sapiens} | 96.17 | 0.022 | 713-873 | 522 | ATPase |
| 6G2Z_A | Transitional endoplasmic reticulum ATPase (E.C.3.6.4.6); ATPase, p97, protein degradation, hydrolase; HET: ADP, MPD, EJW; 1.923A {Homo sapiens}; | 96.03 | 0.024 | 708-873 | 306 | ATPase |

hSAMD9L NCBI Reference Sequence: NP_001290425.1; HHpred – default parameters with HHblits, against NCBI_Conserved_Domains(CD)_v3.16, PDB_mmCIF70_4_Feb, Pfam-A_v32.0 and SMART_V6.0 databases. Sequence similarity results obtained with E-Value < 0.05. In bold proteins found functionally associated with SAMD9L mentioned in chapter III.

**Supplementary Table 7. Microtubule associated motifs significantly present in microtubule associated proteins identified in hSAMD9L.**

| Motif | Start | End | p-value * for significantly motif presence in microtubule interaction sites/domains |
|---|---|---|---|
| **S....LKS** | 619 | 626 | 0.009 |
| Q...KR | 1261 | 1266 | 0.023 |
| R..P...SS | 633 | 641 | 0.035 |
| SKPS | 93 | 96 | 0.036 |
| P.SKL | 1395 | 1399 | 0.042 |
| T..P..P | 508 | 514 | 0.047 |
| T..P..P | 951 | 957 | 0.047 |
| H..R....S | 686 | 694 | 0.048 |
| PK....K | 729 | 735 | 0.048 |
| KR....K | 711 | 717 | 0.048 |
| KR....K | 1464 | 1470 | 0.048 |
| K..SS...S | 1450 | 1458 | 0.048 |
| K....KPE | 152 | 159 | 0.048 |
| SSL....R | 1453 | 1460 | 0.049 |
| E...E.RK | 520 | 527 | 0.05 |

hSAMD9L NCBI Reference Sequence: NP_001290425.1; MAPanalyzer was set to moderate threshold with 90% of sensitivity obtaining a significant combined score of 0.014 which classified hSAMD9L as a microtubule associated protein. In bold, the motif where c.1877C>T (p.Ser626Leu) locates, highlighted in red.

**Supplementary Table 8. Intrinsic disorder region (IDR) predicted around WT SAMD9L Ser626 and mutated Leu626 SAMD9L.**

| Predictor algorithm | Ser626 SAMD9L Disorder region (DR) | Leu626 SAMD9L Disorder region (DR) |
|---|---|---|
| PredictProtein (PROFBval) | 622-634 | 622-634 |
| PredictProtein (Ucon) | 626-627 | 627 |
| DisEMBL (Hot loops) | 625-650 | 626-650 |
| InterPro (MobiDB-lite) | 626-645 | - |

PredictProtein (PROFBval and Ucon), DisEMBL (Hot loops) and InterPro (MobiDB-lite) identified an intrinsic disorder (IDR) around the SAMD9L amino acid Ser626. p.Ser626Leu change lead to a prediction change for Ucon and Hot loops and and abolish the identified prediction for InterPro (MobiDB-lite). hSAMD9L NCBI Reference Sequence: NP_001290425.1 was used except for InterPro (MobiDB-lite) where 626-645 region was analysed.

**Supplementary Table 9. Related diseases and protein function of genes associated with microtubules and endosomal/lysosomal pathway identified in SAMD9L PPi network.**

| Gene | Disease | Inheritance | Relevant clinical signs | Protein function |
|---|---|---|---|---|
| ***ATL1*** | Autosomal Dominant and Neuropathy, Hereditary Sensory, Type ID | AD | Hyperreflexia, Sensorimotor axonal neuropathy | Dynamin superfamily of large GTPases involved in cellular trafficking patterns |
| | Spastic Paraplegia 3 | AD | Hyperreflexia, Decreased vibratory sense in lower limbs | |
| ***SPAST*** | Spastic Paraplegia 4 | AD | Hyperreflexia, Decreased vibratory sense in the lower limbs | Activity in axonal transport and the maintenance of excitatory synapses of motor neurons in the brain cortex and the spinal cord |
| ***RAB7A*** | Charcot-Marie-Tooth disease, type 2B | AD | Hyporeflexia, marked distal sensory impairment | Key regulators of endosomal membrane traffic. functions in retrograde endosomal transport |
| ***KATNB1*** | Lissencephaly 6, with microcephaly | AR | Hyperreflexia | Required for the transport into neuronal processes by microtubule-dependent motor proteins. |
| ***IFI44*** | - | - | - | Aggregates to form microtubular structures |
| ***KATNA1*** | - | - | - | Required for the transport into neuronal processes by microtubule-dependent motor proteins. |
| ***KATNAL1*** | - | - | - | Katnal1 mutant mice revealed numerous morphological abnormalities and defects in neuronal migration and morphology. |
| ***KATNAL2*** | - | - | - | Severs microtubules in vitro in an ATP-dependent manner. |
| ***EEA1*** | - | - | - | Participates in endosomal trafficking |
| ***RAB7B*** | - | - | - | Mediate transport from endosomes to the TGN and/or Golgi, a step that is also needed to accomplish efficient delivery of lysosomal enzymes to the endocytic route |
| ***RAB5A*** | - | - | - | Involved in axonal and dendritic endocytosis, and participates in axonal endosome vesicles. |
| ***VPS4B*** | - | - | - | VPS4B belongs to the AAA (ATPases associated with diverse cellular activities) protein family and is involved in lysosomal/endosomal membrane trafficking |
| ***VTA1*** | - | - | - | Involved in trafficking of the multivesicular body, an endosomal compartment involved in sorting membrane proteins for degradation in lysosomes |
| ***CHMP2A*** | - | - | - | Probable core component of the endosomal sorting required for transport complex III (ESCRT-III) which is involved in multivesicular bodies (MVBs) formation and sorting of endosomal cargo proteins into MVBs. |

Mutations in *ATL1, SPAST, RAB7A and KATNB1* have been previously associated with diseases presenting hyperreflexia, sensory axonal neuropathy or sensory impairment among other signs, overlapping with signs identified in this new ataxia subtype. Proteins identified are mainly related to microtubules, cellular transport or to endosomal/lysosomal trafficking. Uniprot and GeneCards database were used for the protein function description.

**Supplementary Figure 1. GFAP up-regulation in the SCA37 cerebellum.**

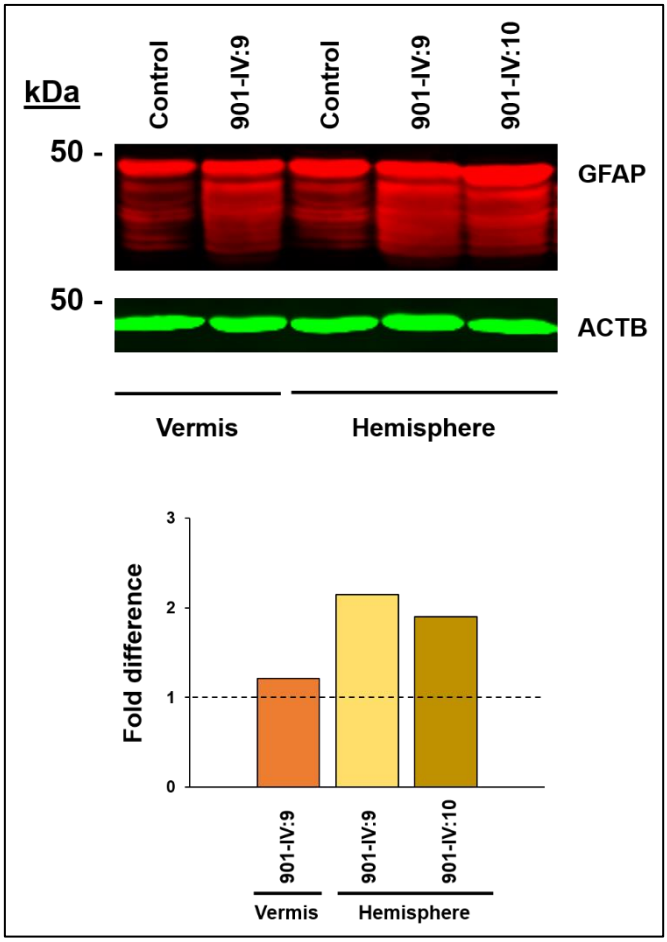


The GFAP protein was found up-regulated in the SCA37 cerebellum in agreement with reactive astrogliosis. The average levels of protein are shown as a ratio normalised to beta-actin. All values shown for patients 901-IV:9 and 901-IV:10 are relative to the obtained control value set to 1 (dotted line).

**Supplementary Figure 2. Characterisation of the cerebellar *DAB1-2* transcript.**

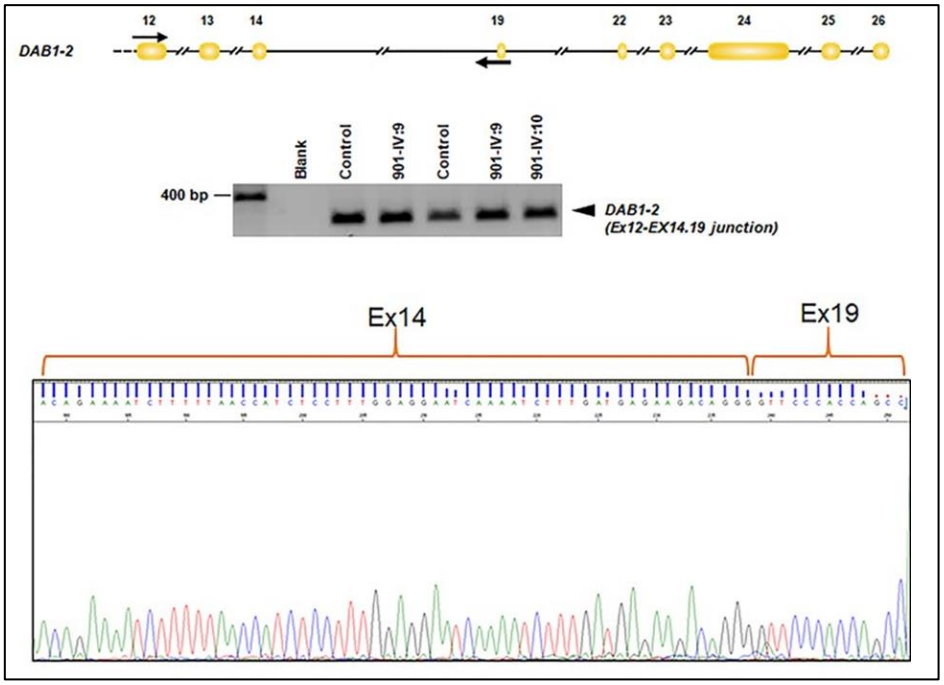


Characterisation of the cerebellar *DAB1-2* transcript in patients IV:9 and IV:10 from AT-901 family and control originated by alternative splicing of exons 15-18, which generates the shortest 63 kDa DAB1 isoform shown in Figure 20A. Extracted from (485)

**Supplementary Figure 3. Hematologic Evaluation and heterozygosity of *SAMD9L* c.1877C>T (p.Ser626Leu) Sanger sequencing.**

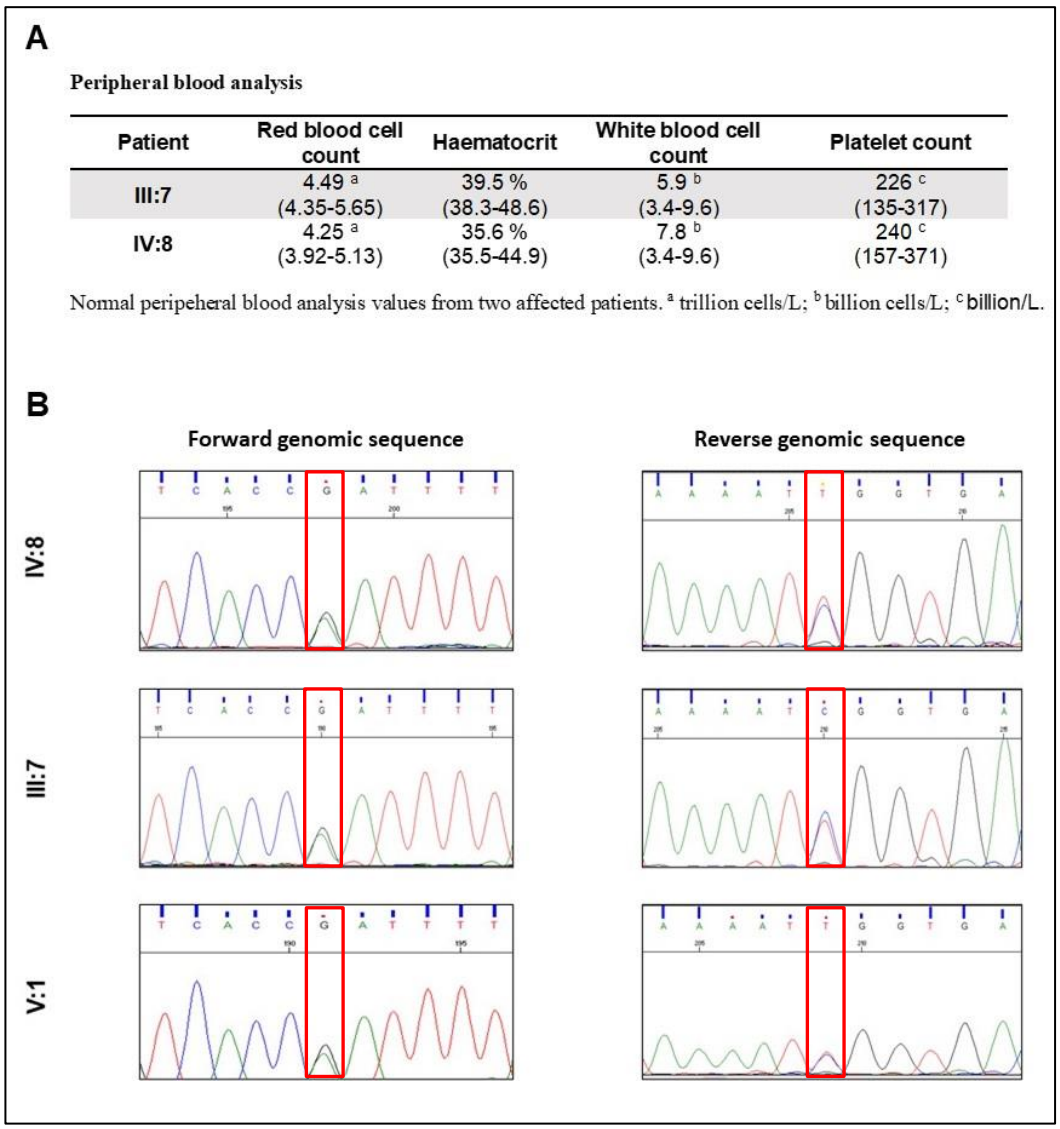


Complete blood counts and red cell indices were normal without hematologic manifestations (**A**). (**B**) DNA isolated from peripheral blood shows *SAMD9L* heterozygous c.1877C>T (p.Ser626Leu) mutation in affected patients IV:8, III:7 and V:1, discarding decrease of mutant allele in haematopoiesis.

**Supplementary Figure 4. No alteration in mtDNA mutation load and mtDNA damage in patient's fibroblasts.**

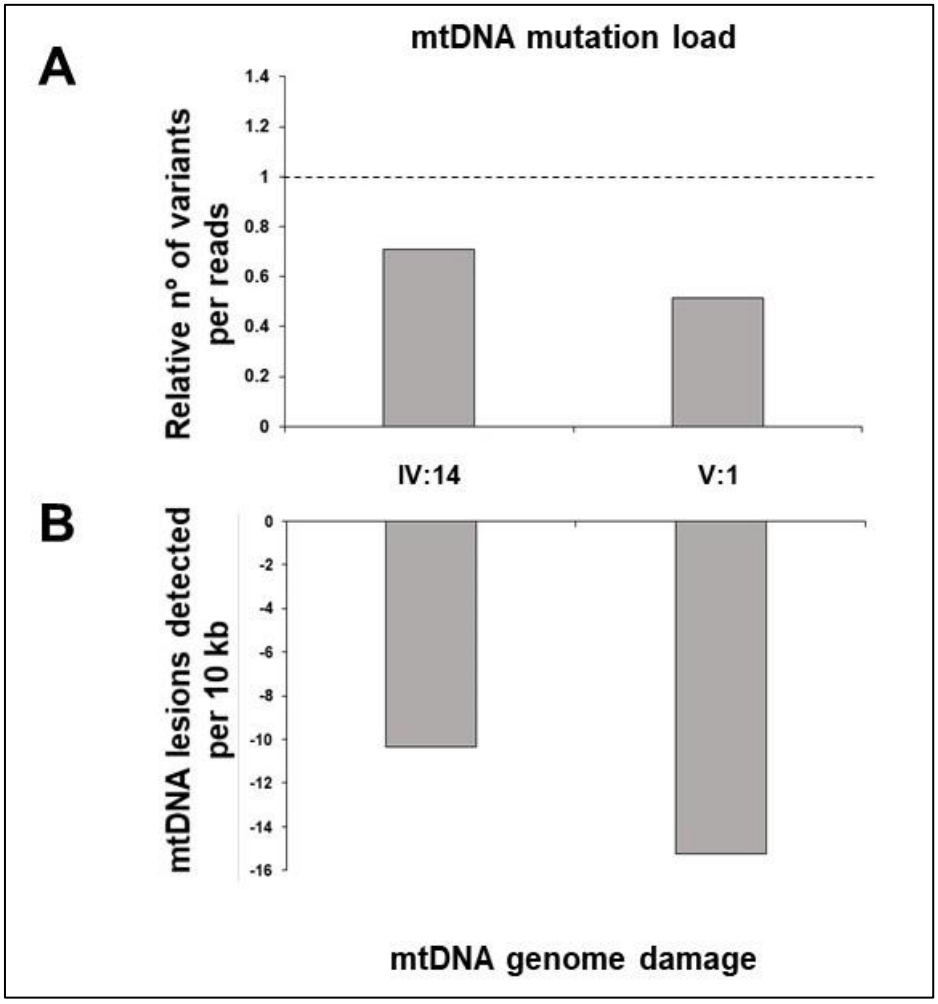


NGS analysis showed no alteration in variant frequency in affected patients' fibroblasts (variation frequency= 2.1x $10^{-2}$/ reads) compared to four age matched controls (variation frequency= 3.1x $10^{-2}$/ reads) (**A**) Values shown for patients IV:14 and V:1 are relative to the obtained control value set to 1 (dotted line). None of the identified variants were predicted to be pathogenic. (**B**) LORD-Q method denotes similar mitochondrial genome damage representing number of detected lesions per 10 kb in affected fibroblasts compared to controls, discarding a possible oxidative stress effect.

**Supplementary Figure 5. Characterisation of human *SAMD9L* ortholog gene in zebrafish, analysis RNA-seq zebrafish cerebellar expression in previously reported candidate regions.**

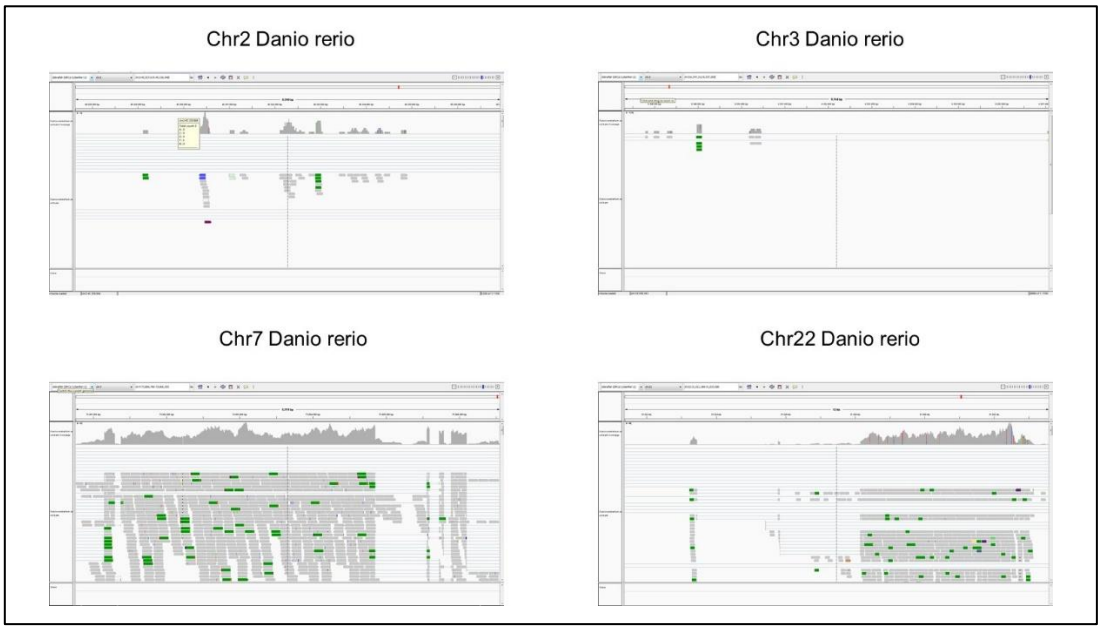


Candidate regions were selected regarding previously generated transgenic zebrafishes reported to be candidate for human *SAMD9L* orthologs (https://zmp.buschlab.org/). Zebrafish cerebellum RNA-seq data from SRA database (Accession: SRX4184229) was aligned using HISAT2 and candidate regions analysed.